Development of a methodology to exploit nuclear data in the unresolved resonance range and the impact on criticality safety and reactor applications

Clément Jeannesson

▶ To cite this version:

université
PARIS-SACLAY

Development of a methodology to exploit nuclear data in the unresolved resonance range and the impact on criticality safety and reactor applications

Thèse de doctorat de l'université Paris-Saclay

Thèse présentée et soutenue à Fontenay-aux-Roses, le 15/12/2020, par

Clément JEANNESSON

Composition du Jury

Frank GUNSING
Directeur de Recherche (HDR), CEA Paris-Saclay — Président

Oscar CABELLOS
Professeur, Universidad Politécnica de Madrid (Espagne) — Rapporteur & Examinateur

Cyrille DE SAINT JEAN
Directeur de Recherche (HDR), CEA DIF — Rapporteur & Examinateur

Tatiana IVANOVA
Chef de la Division des Sciences Nucléaires, OECD - NEA — Examinatrice

Vladimir SOBES
Professeur Associé, Oak Ridge National Laboratory (États-Unis) — Examinateur

Luiz LEAL
Ingénieur-Chercheur (HDR), IRSN — Directeur de thèse

Mireille COSTE-DELCLAUX
Ingénieur-Chercheur, CEA Paris-Saclay — Encadrante

Cédric JOUANNE
Ingénieur-Chercheur, CEA Paris-Saclay — Encadrant

Contents

Remerciements

Le présent manuscrit de thèse est l'aboutissement d'un parcours commencé en avril 2016, lorsque j'ai rejoint l'IRSN en tant que stagiaire au Service de Neutronique et Criticité[1]. C'était il y a presque cinq ans. Au cours de cette période, de nombreuses personnes m'ont très régulièrement soutenu, encouragé, aidé ; elles m'ont même parfois repêché. Je tiens à leur exprimer le plus justement possible ma gratitude dans ce paragraphe, même si je trouve que les mots manquent pour fidèlement exprimer mon ressenti.

Je tiens en premier lieu à remercier les personnes à l'origine de la thèse, qui m'ont donné la chance de travailler sur un domaine de la physique à l'interface entre sciences fondamentales et applications pratiques. Je commencerai donc évidemment par mentionner Luiz Leal, mon directeur de thèse, que je ne pouvais imaginer si qualifié, si motivé, et si réactif. Dans le même temps, la liberté qu'il m'a accordée m'a permis de réellement progresser dans nombre de domaines, et, je crois, de réellement m'approprier le sujet. Merci Luiz pour ces cinq années ! Un grand merci doit également être destiné à Sophie Pignet, cheffe de laboratoire à mon arrivée et cheffe de service lors de mon départ, qui a toujours observé avec attention les évolutions de ma situation tout en m'apportant son soutien confiant, ce qui m'a été d'une grande aide. Je tiens aussi à remercier Eric Dumonteil pour ses conseils avisés, et Aurélie Bardelay pour sa prise en main rapide et efficace des problématiques administratives de ma thèse, ce qui a grandement contribué à ce que celle-ci se termine dans de bonnes conditions.

Le doctorat a fait l'objet d'une collaboration avec le CEA, et j'ai été amené à aller régulièrement à Saclay, surtout vers la fin de la seconde année et le début de la troisième année. Cette période a été une des plus fécondes de ma thèse, et nul doute que je dois beaucoup à l'encadrement de Mireille Coste-Delclaux et Cédric Jouanne. Ces derniers ont pris le temps de me débloquer "en mettant les mains dans le cambouis", de me poser les bonnes questions, et de me faire remarquer certains points importants que je n'aurais pas relevé seul. Leur disponibilité était un réel plaisir, et n'avait d'égal que leur grande compétence. Mes venues au CEA resteront comme un moment fort de cette thèse. Merci pour tout.

Je voudrais à présent remercier les membres du jury d'avoir accepté d'évaluer la qualité de mon doctorat, et pour leur lecture attentive du manuscrit. Merci à M. Frank Gunsing d'avoir présidé le jury, à M. Cyrille de Saint Jean et M. Oscar Caballos qui ont été les rapporteurs de la thèse, et à Mme Tatiana Ivanova et M. Vladimir Sobes qui en ont été les examinateurs.

Ce travail de thèse doit beaucoup à Wim Haeck, qui a développé de nombreux composants du logiciel GAIA. Ce dernier m'a aidé à prendre en main le code lors de mon année à l'IRSN avant la thèse, et a toujours été disponible pour répondre à mes questions sur le traitement des

---

[1]La thèse devait initialement se dérouler à la suite du stage. Pour des raisons indépendantes de la volonté des acteurs en jeu, son début a été repoussé d'un an, ce qui m'a permis de parfaire mes capacités en programmation C++ au sein du laboratoire. Je ne peux m'empêcher de préciser ce fait au sein d'une note de bas de page - dont j'abuse peut-être dans la suite du document - car cette expérience très positive a eu un impact assez fort sur la suite de mes activités.

données nucléaires. Son style de programmation clair et précis m'a permis de faire de grands progrès, et de réaliser qu'un programme bien structuré pouvait aider à comprendre la physique. Je l'en remercie sincèrement.

A l'IRSN, j'ai quotidiennement bénéficié de l'intérêt et du soutien constant de l'équipe IN-SIDER, dédiée à l'étude des données nucléaires. Merci aux membres de l'équipe, et plus précisément à Nicolas, qui m'a énormément aidé avec les benchmarks, à Raphaëlle avec qui je m'occupais du processing, à Fred pour la cogestion de GAIA-2, à Alexis pour mes questions relatives à MORET, et à Amine avec qui j'ai partagé avec plaisir un bureau pendant un an, et avec qui j'ai pu entrevoir la réalité du métier d'évaluateur.

Ceux qui exercent des métiers transverses sont plus à même d'être souvent sollicités. C'est le cas de Yann que j'ai parfois harcelé pour qu'il réponde à mes diverses questions de statistique, de Grégory qui m'a souvent aidé lorsque je voulais optimiser mes développements, et de Catherine, qui a régulièrement dû gérer des tâches administratives me concernant. Merci à vous ! Je ne suis plus là, mais les autres si, donc courage.

De manière générale, j'ai réellement apprécié l'ambiance au SNC, où régnait la bonne humeur. Les pauses cafés et les matches de frisbee ont toujours été des moments extrêmement agréables. Merci dans le désordre à tous ceux qui ont fait que l'IRSN soit plus qu'un lieu de travail, Mathieu, Julien, Mariya, Benjamin, JB, Johann, Frank, Florian, Paul, Nicolas, Arthur, Wilfried, Nadège, Geoffrey, Guénaël, Roland, et les autres. Un grand merci à mes copains thésards, qui ont partagé avec moi les galères et les bons moments liés à notre condition, Léa, Romain, Kévin (courage aux deux derniers !). Enfin, j'en profite pour adresser des remerciements spéciaux à Vivian, qui a relu de lui-même ma thèse et a corrigé les dernières fautes qui s'y trouvaient.

J'ai été très bien accueilli au CEA, et les doctorants du SERMA ont formé un groupe soudé, avec lequel il était plaisant de manger le midi. Mes pensées vont aussi a Camillo et Laura qui m'ont partagé leur bureau lorsque je débarquais un peu à l'improviste, et avec qui j'ai toujours aimé prendre un café !

Enfin, je tiens à remercier Vaibhav, avec qui j'ai partagé un bureau pendant deux ans et demi, avant de le retrouver au CEA, et de nouveau à l'IRSN. Les journées sont tout de suite apparues moins longues lorsqu'il était présent ; merci pour tous ces bons moments, et pour tout ce que j'ai appris de lui, au et hors du travail.

La thèse a été plus facile avec le soutien de mes amis et de ma famille, à qui j'aurais aimé exposer mon travail au cours d'une soutenance en présentiel, avant que l'actualité ne nous rattrape[2]. Même si ces derniers n'ont pas forcément interagi directement avec la thèse elle-même, ils ont eu une influence forte sur mon moral pendant ces années. Merci Gauthier, Adrien et Aurélien ; il était rigolo que je puisse voir l'un d'entre vous quelque soit mon lieu de travail la journée, pour une pause toujours méritée - IRSN, CEA, Paris, et évidemment au 51. Delphine, Camille, Juliette, les déjeuners du midi à Saint-Lazare sont toujours un super moment, hâte qu'on en fasse d'autres ! Merci à Paul pour les apéros à Châtillon, et pour les futurs à Maisons-Alfort. Merci aux membres du PUC pour les entraînements de frisbee du lundi, mardi, jeudi, les tournois, et les soirées au Fleurus ! Vivement que les entraînements reprennent réellement, ça me manque. Dédicace au sous-groupe de "déménagements bordel", Valentin, Fabien, Alex, Léo, Gaëtan, Gabi, même si on a fait plus de jeux et de soutenances de thèse que de déménagements. Un grand merci à tout Maxi Format, avec qui c'est toujours simple et cool. Pensée aux copains du lycée, je suis bien content quand on se retrouve à chaque fois. Merci aussi aux autres copains de l'ENSTA, et à ceux que je n'ai pas encore mis dans une case, Benoît, Aurélien, Laura, Camille... Merci finalement à ma famille de toujours être là pour moi, à mon Papa, ma Maman, Etienne, Marthe, Ariane, mes cousin(e)s, mes oncles et tantes ; je pense fort à mes grand-parents, Papy Mamie, Pépé Mémé. Je vous aime. Enfin, merci Thelma pour tous ces moments passés ensemble, pour ton aide, ta patience, ton courage, ton amour. Merci de m'avoir accompagné jusqu'ici, et pour la suite !

---

[2]Pour le moi du futur, je précise au cas où j'oublierais que nous étions alors en pleine pandémie de covid-19, et que la soutenance s'est tenue en visioconférence.

Introduction

Nuclear physics is the study of the atomic nuclei which aims at describing their structure, their interactions with other particles, and their radioactive decays. Its fields of application are numerous, including the design of nuclear power plants, radiotherapy, astrophysics, weaponry, or archaeology and geology. In this work, the applications of interest are more specifically related to neutronics which is the study of the motion and interactions of neutrons in matter. Neutronics is a crucial component of the nuclear industry, whereby it serves as a basis for the operation of nuclear reactors in power plants. Neutronics calculations are also necessary to estimate the risks of a criticality accident due to a self-sustained uncontrolled chain reaction.

An interaction between a neutron and a nucleus can lead to several kinds of nuclear reactions, such as the capture of the neutron by the nucleus followed by a fission for instance. Basic data about the nature of these reactions are required to perform quantitative neutronics calculations, which are called nuclear data. Among them, one may quote the reaction cross sections which indicate the probability for a particular reaction to occur, the angular distributions of secondary emitted particles, or radioactive decay rates such as half-lives of unstable nuclei. Nuclear data are essential ingredients required by neutronics codes to model the motion of neutrons in any nuclear facility.

Although many achievements have been accomplished in the nuclear arena, to this day, full knowledge of the fundamental properties of matter is still a challenge. The precise description of the behavior of a neutron in the inner parts of a nucleus remains out of reach of theoretical developments. The current methods rely on experimental approaches to measure relevant quantities about the neutron-nuclei interactions. These latter are then completed and corrected during an evaluation process to produce nuclear data libraries, which contain sufficient information to reproduce the experimental data. At this stage, nuclear data libraries must undergo an additional processing step to be turned into forms suitable for applications. This is the goal of the so-called processing codes, among which the NJOY code developed at Los Alamos National Laboratory in the United States is the most frequently used. Once processed, the nuclear data can be used as an input for nuclear applications by computer neutronics codes. Their quality is tested in *benchmarks*, that are simple experiments representative of practical cases, and for which several quantities have been measured like the neutron flux or the effective multiplication factor k_{eff} which expresses the intensity of the chain reactions.

The *Institut de Radioprotection et de Sûreté Nucléaire*[3] (IRSN) is the public institute responsible for the nuclear safety in France. Its role is to provide a safety expertise for any nuclear activity in France, from the medical sphere to nuclear power plants. Many research activities are undertaken at IRSN to support its expertise missions. This is for instance the role of the Neutronics Laboratory, part of the Criticality and Neutronics Service (SNC), which develops tools and monitors experimental programs to improve the quality of the criticality safety and

---

[3]Institute for Radiological Protection and Nuclear Safety.

reactor physics analyses performed at IRSN. Due to their importance, assessing the quality of nuclear data used by neutronics codes is also part of the laboratory activities.

The present work has been achieved in collaboration with the *Commissariat à l'énergie atomique et aux énergies alternatives*[4] (CEA), the main public organization in France which performs research in the field of nuclear science. The collaboration arose between the IRSN SNC and the CEA *Service d'Études des Réacteurs et de Mathématiques Appliquées*[5] (SERMA), in charge of the development of the nuclear data processing codes and the generation of libraries for neutronics applications, among many other things.

In the last few years, IRSN has expanded its capability to test and validate nuclear data and associated uncertainties. In particular the development of an independent nuclear data processing tool, GAIA-2, was initiated in 2012 during a PhD carried by M. Ghislain Ferran [1]. The development of this code was motivated by the urge to implement new independent methods to handle the modeling steps carried out during the nuclear data processing in existing software. The development of independent methods serves to cross-check existing codes outputs, and is thus relevant for a safety institute. In 2014, the code was able to handle all the formalisms derived from the general R-Matrix theory and several methods to Doppler-broaden the cross sections in the so-called resolved resonance range. In addition, both operations were performed in a single step without relying on an intermediate linearization of the 0K cross sections. Cross-checking GAIA-2 with NJOY results proved that the methods implemented in the resolved resonance range led to equivalent results, which validated the first developments of GAIA-2.

In the processing step of nuclear data, another important objective is to handle the cross sections calculations for another domain of the incident neutron energies, called the unresolved resonance range. This energy range, adjacent to the resolved resonance range, is characterized by resonance parameters given as average values due to experimental resolution constraints. Cross section calculations have to be adapted to manage this new situation, and additional models are required compared to the resolved resonance range. In this context, the objectives of the present PhD are to examine the existing procedures of nuclear data treatment in the unresolved resonance range, develop new methods to improve the quality of the processed data, and implement them in GAIA-2. The present thesis is thus a straight continuation of the work carried out in GAIA-2 until now.

The usual practice in the unresolved resonance range is to compute cross sections as *probability tables*. These tables are discrete versions of the probability distributions of the cross section values at tabulated reference energies. Their computation relies on a Monte-Carlo procedure called the ladder method, based on the sampling of several statistical acceptable sets of resolved resonances across the unresolved resonance range. The resonance sampling requires evaluated average resonance parameters and the knowledge of the theoretical statistical laws they follow. One of the main objectives of this work is to develop a methodology to compute these probability tables. All the hypotheses made at any step of their calculation will be presented in this dissertation and several methods and results will be compared to those obtained with existing cross section processing codes.

The present document is divided into three main parts, each of them composed of two chapters. The first part deals with the global aspect of the nuclear data processing in the unresolved resonance range. In the first chapter, the basics of the neutron-induced nuclear reactions theory is presented. The scope in which this work has been carried out is briefly presented, along with a more detailed section related to the R-Matrix theory that structures the entire nuclear data representation in the resonance ranges. In a second chapter the practical challenges of the nuclear data processing in the unresolved resonance range are exposed. The format of the input evaluated nuclear data is described and the two principal manners of data processing are exhibited. The first one is a direct computation of the average cross section values

---

[4]Alternative Energies and Atomic Energy Commission.
[5]Service for the Study of Reactors and Applied Mathematics.

using the so-called Hauser-Feschbach formalism. The second route is the aforementioned ladder method. In particular all the hypotheses and potential sources of disagreement between possible implementations of the ladder method are listed.

The second part is focused on the cornerstone of the ladder method, which is the statistical sampling of resonances from their average parameters. The statistical sampling of resonances is an important exercise in nuclear physics, which also occurs during the exploitation of experimental data to create nuclear data evaluations. In the framework of the ladder method, several questions arise among which the sampling starting point, the number of resonances to sample, and the number of Monte-Carlo iterations to run. Some developments performed in this work to answer these questions notably introduce the definition of a finer set of input resonance parameters, referred as *elementary spingroups*, which turn out to be very useful in many applications. The fourth chapter tackles a slightly more complex topic which introduces elements of the random matrix theory in the resonance sampling. The main idea of the chapter is to abandon the usual law of the spacing between resonances to adopt a more physical approach that takes into account correlations between resonances. A variant of the Hauser-Feschbach formalism to compute average cross sections is also shown, and compared to the usual practice.

The third part is dedicated to the use of probability tables in the unresolved resonance range for practical applications. In the fifth chapter, the construction of probability tables from the resulting sampling of the ladder method is investigated. The existing methods are presented as well as two innovative approaches, based on k-clustering algorithms. The sixth and final chapter of this thesis deals with the integration of probability tables in the workflow of processing codes. In particular, the question of the choice of the reference energy mesh on which to compute the probability tables is examined. Then, probability tables are used in benchmark calculations to estimate the quality of the developed methods to handle the unresolved resonance range all along the thesis, and implemented in the IRSN nuclear data processing code GAIA-2.

Part I

State of the art and unresolved resonance range processing

Fundamentals of the neutron-induced nuclear reactions theory in the resonance ranges

1.1 Generalities about nuclear reactions

A particular field of interest in nuclear physics is the study of the interactions between an incident particle and a target nucleus. The interaction is likely to produce a nuclear reaction, after which the state of the system may have changed. Several kinds of reactions may occur in the process. For instance, the incident particle may be absorbed, scattered, or even create a fission. Being able to model in detail the possible nuclear reactions is essential, as their outputs are used in various physics and engineering simulations at the macroscopic scale. For the applications which motivated this work such as nuclear reactor physics, radioprotection, and criticality safety, the incident particle is a neutron[1]. The target nuclei however depend on the applications. In the case of a PWR reactor for example, important targets are the uranium isotopes present in the fuel, many actinides which are created through the irradiation process, oxygen and hydrogen isotopes which compose water, metallic nuclei in the vessel and the structure around the fuel, and a few other nuclei as for instance boron isotopes which can be poured in water to decrease reactivity. These isotopes are quite well studied as they are vital for the nuclear energy industry. For other applications such as criticality safety or astrophysics the range of nuclides of interest is much wider.

In this section, the basics of neutron-induced nuclear reactions will be presented, along with the key-concept of cross section. Then, a subdivision of the incident neutron energy in ranges of interest will be introduced.

1.1.1 Nuclear reactions modeling

In the following, we will consider the paired system composed of a neutron n, interacting with a target nucleus $^Z_A X$ composed of A nucleons, among which Z protons and $N = A - Z$ neutrons. The interaction between the neutron and the nucleus may induce a nuclear reaction, and let the system in a new state, as depicted on Figure 1.1. Reachable states must follow some conservation rules as:

- System total energy conservation

---

[1]This is not necessarily the case in radiotherapy for instance, where the incident particle may be a proton.

- System total linear momentum conservation

- System angular kinetic momentum conservation

- Conservation of the total number of nucleons A. It should be emphasized that the number of neutrons and protons are not necessarily conserved, as $\beta^{+/-}$ radioactivity is able to turn a proton into a neutron and vice versa. In most nuclear reaction models however, such radioactive decays are neglected and the number of neutrons and protons is conserved.
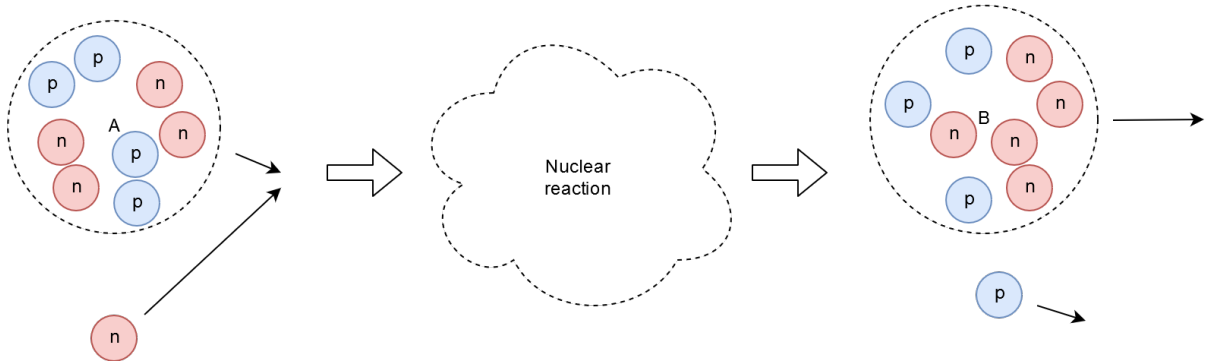
Figure 1.1: Example of a reaction (n,p)

Types of nuclear reactions

A typical notation for a nuclear reaction is

$$A(a, b)B \tag{1.1}$$

where A is the target nucleus, a the incident particle (in our case a neutron n), B the residual nucleus, and b the outgoing particle. When there is no ambiguity, or when the detail of the reaction is not required, A and B may be dropped. In the same way, b is sometimes replaced by a more general expression, so that most common reactions are written:

- (n,n): elastic scattering

- (n,n'): inelastic scattering

- (n, γ): radiative capture

- (n, f): fission

- (n, p): emission of a proton

- (n, α): emission of an α-particle

- (n, xn): emission of several neutrons

In all cases the output state of the system (characterized by the number and type of nucleons in B and b along with their excitation energy) defines a reaction. Let us describe more in detail these reactions.

A scattering corresponds to the case where a neutron is emitted and the residual nucleus is $_A^Z X$. If the residual nucleus is at ground level, the scattering is said to be elastic. In case the target nucleus is left in an excited state, the scattering is referred to as an inelastic scattering. Mechanisms leading to these reactions may be very different.

A capture occurs when the incident neutron is captured by the target nucleus to form a resulting nucleus with $A + 1$ nucleons. In such a case, B is equivalent to $_Z^{A+1} X$. Such a system

is usually unstable, and decays by emitting photons (γ-rays), so that the reaction is said to be radiative.

Sometimes, the neutron influence is able to break the target nucleus into several nuclides, producing a fission reaction. Fission typically occurs for large mass nuclides ($A > 230$) which have more chances to be cut in two under the neutron influence.

Many other reactions are possible, such as the emission of a proton, the emission of an alpha particle, the emission of several neutrons[2], and so on. For an incident neutron, up to several hundreds of reactions may be defined in practice.

From a terminology point of view, the nature of the reactions actually differs. If the state of the resulting nuclides (ie. their nature and their excitation energy) is well defined after a reaction, this reaction is said to be *fundamental*. This is the case of elastic scattering: resulting nuclides are well defined, as well as their energies. On the other hand, only mentioning a fission reaction does not suffice to indicate the nature of the reaction, as nuclides do not always break up into the same components. In the same way, during an inelastic scattering the nuclide can be left in different excited levels. The same goes for radiative capture, as there are many possible ways of decay for the remaining nucleus. Actually, in all those cases the reactions are said to be *composed*, as they group many sub-reactions, which are themselves fundamental. It is sometimes more convenient to deal with composed reactions in practice. A crucial case is the *total reaction*, which regroups all the possible reactions. Total reaction is usually subdivided into scattering reaction and absorption reaction. The latter notably groups fission reactions and radiative captures. Figure 1.2 summarizes the usual grouping of the most common reactions. Section 1.3.2 shows that considering the real quantum state of the remaining nuclides (instead of just their nature and excitation levels) leads to the notion of channel, which plays a major role in the mathematical framework used to describe the nuclear reactions.
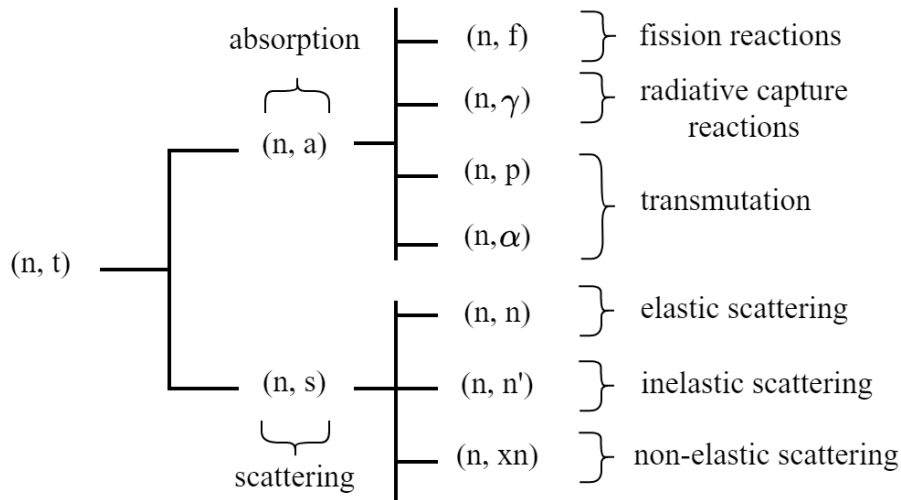
Figure 1.2: Main reactions hierarchy

To each reaction it is possible to associate a Q-value, the energy produced by the reaction. It corresponds to the mass balance before and after the reaction, multiplied by the square of the light speed c. The Q-value is an intrinsic quantity of any reaction.

$$Q = c^2[m_{initial} - m_{final}] \tag{1.2}$$

Some reactions are said to be *threshold reactions* when energy must be provided so that the reaction happens. This is the case of some fission reactions for example. In particular, a reaction is always a threshold reaction if its associated Q-value is negative: a negative Q-value means

---

[2](n, xn) is sometimes considered as a kind of inelastic scattering, but this definition is not the one adopted in the nuclear data formats [2]. (n, xn) reaction contributes along with inelastic scattering and others to the non-elastic reaction (which is a composed reaction).

that the reaction is possible only when the neutron kinetic energy is greater than $-Q$. This is the case of the inelastic scattering, for example.

Nuclear reaction mechanisms

An interaction between a neutron and a nucleus can occur in several ways which depend on many factors. The simplest case is a kind of elastic scattering often called *potential elastic scattering*: the neutron is deflected by the nucleus, exactly like two billiard balls from a classical mechanics point of view[3] [3]. In this very particular type of interaction, everything appears as if the neutron does not penetrate in the nucleus. For this reason, this reaction is sometime refereed to as nuclear scattering.

On the contrary, when the neutron penetrates the nucleus, it mixes with the nucleus' nucleons. Three different mechanisms are usually differentiated, according to the characteristics of the interaction: direct, compound nucleus and pre-equilibrium nuclear reactions. Each one is preponderant for a particular energy range of the incident neutron. As they exhibit quite different features, several theoretical or empirical models have been developed to represent each mechanism properly. Among the features used to distinguish these mechanisms one can notice the reaction time, which is closely related to the number of collisions between the neutron and the target's nucleons, and the residual nucleus angular distributions shape.

Below 20 MeV, which actually corresponds to the nuclear reactors operating conditions, the neutron-nucleus collision is more likely to lead to the formation of a *compound nucleus*. Such a formation is a slow reaction ($\sim 10^{-18}$ s), which indicates many intra-nucleus collisions due to the low energy of the neutron. During the process, the incident neutron energy (equal to the sum of the neutron kinetic energy and its binding energy within the nucleus) is shared among the $A+1$ nucleons and subsequently the composed system forgets the conditions under which it has been created. This memory loss of the compound nucleus is referred to as Bohr's amnesia hypothesis [4]. As a result, the states of the system before and after the reaction are mainly uncorrelated. It is then relevant to consider the compound nucleus formation as a two-step process. Once the neutron enters the nucleus, an excited system composed of $A+1$ nucleons is formed, in which the incident neutron has shared its energy. Such a system being highly unstable, the compound nucleus then decays by emitting nuclides or/and radiations. The angular distributions of these remaining nuclides is mainly isotropic. The compound nucleus reactions are preponderant in the formalism used to treat the energy range of interest in this document. Details will be given in Section 1.1.3.

At higher energies (> 20 MeV), direct[4] reactions become the dominant reaction scheme. They are characterized by a short duration length ($< 10^{-22}$ s), which features only a few intra-nucleus collisions. In this case, things appear as the neutron traverses the nucleus. The very short laps of time during which the reaction occurs does not enable the incident neutron energy to be shared by the nucleons uniformly. As a result, there is a strong correlation between the system states before and after the reaction. For instance, the angular distribution of the residual nuclides is strongly peaked in the incident neutron direction, and exhibits a strong oscillatory behavior.

Between the compound nucleus and the direct reactions models lies an intermediate category of mechanisms, which embodies features from both. They are referred to as *pre-equilibrium*, *pre-compound* or *multi-step* processes. They are sometimes themselves distinguished between *multi-step compound* (MSC) and *multi-step direct* (MSD) reactions, according to the weight of each mechanism to describe the characteristics of the reaction. In these models, the composed

---

[3]From a quantum mechanics point of view, the nucleus can be seen as a potential well, and the neutron wave does not have enough energy to break through the potential barrier.

[4]About the terminology in use, some references use the term "direct" when an output particle turns out to be the incident neutron (for instance potential elastic scattering can be featured as a direct reaction for this reason, as in [3]). Such uses must not be confused, but for direct reaction mechanism, the incoming neutron is often part of the output particles. In particular, capture reactions mainly follow the compound nucleus scheme.

system decays without losing its memory.

In this document, we will mainly discuss about the compound nucleus model which best describes the nuclear reactions mechanism in the energy range of interest for this study, the so-called unresolved resonance range.

1.1.2 The concept of cross section

Let us imagine a neutron traveling through a material, composed of nuclei of the same type. The neutron trajectory resembles its course in the void, straight ahead at constant speed, until it encounters a nucleus[5]. A very important idea is to state that the probability for a neutron to provoke a nuclear reaction is proportional to its chances to meet a nucleus. Accordingly this probability can be expressed as a "characteristic area", called a *cross section*. The larger the cross section the higher the probability of interaction. Cross sections are expressed in barns, a surface unit so that $1b = 10^{-24}$ cm^2, which is the square of the typical nucleus radius order of magnitude, 10^{-12} cm. In a broader approach, cross sections can be defined for all reactions as the probability of a particular reaction to occur. It is related to the joint probability to meet a nucleus and provoke a reaction of a certain type.

Two very different kinds of cross sections can be defined. *Microscopic cross sections*, usually written σ, are intrinsic properties of nuclei. They can roughly be assimilated to the nuclei characteristic "size", as seen by the incoming neutron. They depend on the nucleus and the reaction considered, but also depend on the temperature and on the incident neutron speed, or equivalently, on the incident neutron kinetic energy[6]. They can be quite complex functions. As an example Figure 1.3 displays some reactions cross sections of ^{140}Ba at 0K.
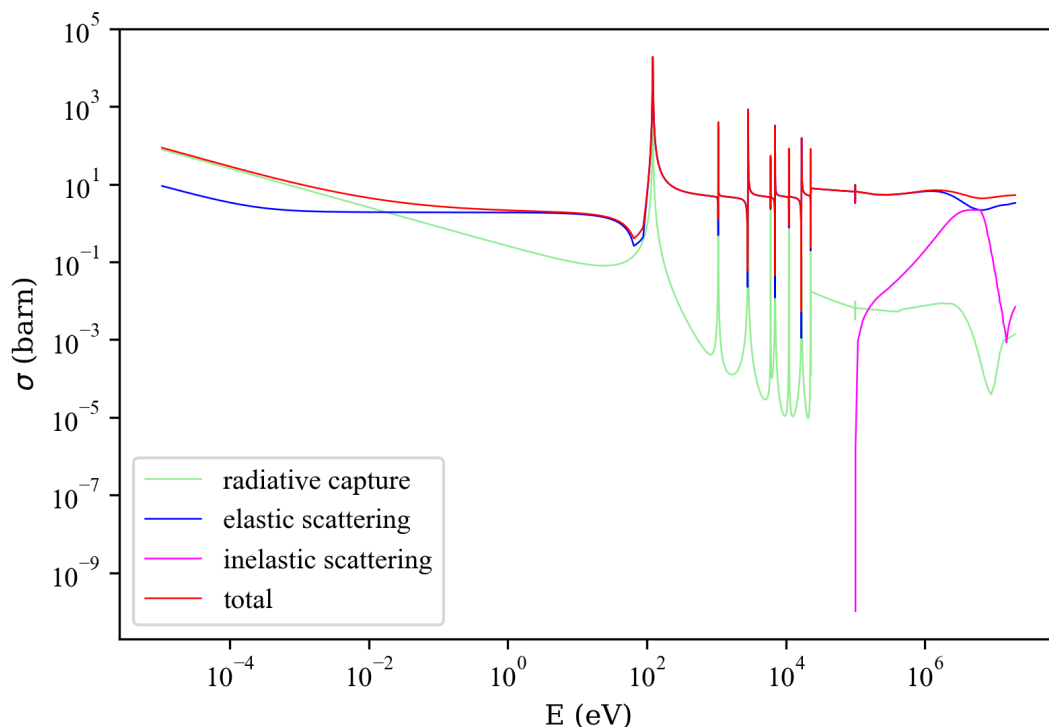
Figure 1.3: ^{140}Ba cross sections

Microscopic cross sections must not be confounded with *macroscopic cross sections*, usually written Σ, which are used to describe a neutron probability of interaction within an applied

---

[5]The neutron "ignores" the electrons.

[6]For practical use, microscopic cross sections are provided in the center of mass of the paired system referential.

geometry[7] at the macroscopic level (for instance a nuclear reactor fuel assembly, large of several meters and composed of many nuclei of different types). The inverse of the macroscopic cross section $\Lambda = 1/\Sigma$ is the mean free path of the neutron in the material. The link between the macroscopic and microscopic cross sections is quite straightforward. Let us imagine a material composed of M nuclides, with densities $n_i(\vec{r}, t)$ ($[m^{-3}]$) respectively. For a particular reaction x, the macroscopic cross section is the sum of the product of the density with the cross section for each nuclide:

$$\Sigma_x(\vec{r}, E, t) = \sum_{i=1}^{M} n_i(\vec{r}, t)\sigma_{x,i}(E) \tag{1.3}$$

From this definition, it is clear that macroscopic cross sections depend on the geometry of the problem, and are susceptible to be time-dependent.

Cross sections are one of the most important data encountered in the field of nuclear physics and neutronics, as they are required to solve the well-known Boltzmann equation which expresses the neutron transport. This equation serves in nuclear reactor physics, radioprotection, critical-ity safety, etc., to calculate the *neutron flux* in a real geometry, which is one the main objective in neutronics. The neutron flux ϕ is defined as the product of the neutron density with speed. For instance, taking a mono-energetic[8] beam of neutrons with density n_p, the neutron flux is simply defined as $\phi = n_p v$. In the most general case, the neutron flux is a function of the neutron beam energy, the geometry, the time, and the neutron flux direction $\vec{\Omega}$. When the neutrons flux is angle-integrated, one may talk of the scalar flux. The Boltzmann equation is established by balancing the number of neutrons in a tiny element of the configuration space and brings into play macroscopic cross sections. It is usually relevant to use the lethargy $u = \ln\left(\dfrac{E}{E_0}\right)$ instead of the energy to write the Boltzmann equation. For an isotropic and homogeneous region of space, the stationary Boltzmann equation becomes:

$$-\vec{\Omega}\vec{\nabla}\phi(\vec{r}, \vec{\Omega}, u) - \Sigma_t(u)\phi(\vec{r}, \vec{\Omega}, u) + S(\vec{r}, \vec{\Omega}, u) = 0 \tag{1.4}$$

where S is a source term, $\vec{\Omega}$ the neutron direction, u the lethargy. Solving this equation is the role of neutronics transport codes which can use Monte-Carlo techniques to simulate neutrons histories, or deterministic methods often based on finite elements to determine the flux.

It is possible to deduce various quantities from the neutron flux, such as reaction rates for instance, which quantify the number of reactions by second in a volume element. Reaction rates are very important in criticality safety where the goal is to apprehend the evolution of chain reactions. Formally one could define the reaction rate as the number of reactions of a certain type per unit of time, volume, speed (ie. energy), and solid angle, but useful quantities are often angle-integrated and energy-integrated. It is the product of the macroscopic cross section and the neutron flux, and is expressed in $m^{-3}s^{-1}$.

$$\tau(\vec{r}, t) = \int_E \underbrace{\Sigma(\vec{r}, E, t)}_{n_t(\vec{r},t)\sigma(E)} \phi(\vec{r}, E, t)dE \tag{1.5}$$

Finally, let us underline that it is also possible to define *differential cross sections* (written $\frac{d\sigma}{d\Omega}$) as the occurrence probability of a reaction (actually a scattering) whose produced neutron arrives in a solid angle Ω. Formally, scattering cross sections are the angle-integrated differential scattering cross sections. It is even possible to define *double-differential cross sections* (written $\frac{d^2\sigma}{d\Omega dE}$), as the occurrence probability of a reaction whose a product neutron arrives in a solid

---

[7]All along this document, a geometry designates not only the proper geometric dimensions of all the materials which compose a structure of interest, but also the temperatures and isotopic compositions of its constituent parts.

[8]So that they all have the same speed.

angle $d\Omega$ with an energy dE.

$$\sigma(E) = \int \frac{d\sigma}{d\Omega}(E)d\Omega = \int \frac{d^2\sigma}{d\Omega dE'}(E)d\Omega dE' \tag{1.6}$$

The precise knowledge of microscopic cross sections, from which macroscopic cross sections can be computed, is of major importance to achieve properly any neutronics computations. The calculation of cross sections relies on the reaction model chosen; in practice, this choice depends on the considered energy range. In this work, the computation of cross sections for the compound nucleus reactions is of particular interest. Before dealing with the mathematical background to establish the analytic expression of cross sections (which will be done in Section 1.3.2), let us have a look at some qualitative characteristics of the compound nucleus itself.

1.1.3 The compound nucleus model

Quantum numbers conservation

During a nuclear reaction, the total angular momentum $\vec{J}$ of the paired system is conserved. It can be defined as:

$$\vec{J} = \vec{I} + \vec{i} + \vec{L} \tag{1.7}$$

where $\vec{I}$ is the target nucleus spin, $\vec{i}$ the neutron spin, and $\vec{L}$ the relative angular orbital momentum of the pair neutron-nucleus in the center of mass. In a quantum context, spins are usually considered to be equivalent to intrinsic angular momenta of the nuclides, even if they are actually quantum quantities without any real equivalent in classical mechanics. As many quantum quantities, spins and angular momenta are defined entirely by their norm and their projection on a single axis only, instead of three in classical mechanics[9]. Furthermore, spins and angular momenta are quantized values, which means they can only take discrete values separated by quantum leaps. In particular the neutron spin value is $\|\vec{i}\| = i = \hbar/2$. For the angular orbital momentum for instance,

$$\left\| \vec{L} \right\| = \sqrt{l(l+1)}\hbar \tag{1.8}$$

where l is the angular orbital quantum number, a positive integer. The first possible values for l usually denote "waves". This is the case for $l = 0$ (s-waves), $l = 1$ (p-waves), $l = 2$ (d-waves), $l = 3$ (f-waves). Greater values of l are very scarce, although possible. Often these quantities are normalized, and the Planck constant is dropped ($\hbar = 1$).

Another quantity of interest appears in the quantum context, and does not have any classical equivalent: the *parity* π of the system. Parity is equal to +1 or -1, and indicates some symmetry properties of the system's wavefunction. Usually, quantum quantities are associated to a parity. Next relation holds for parities:

$$J^\pi = I^\pi i^\pi (-1)^l \tag{1.9}$$

Actually, only weak interaction does not conserve the parity. As weak interaction is usually neglected in nuclear reactions models, parity is always conserved, and π is not necessarily precised.

Without loss of generality, the spin of the pair $\vec{s} = \vec{I} + \vec{i}$ (referred as channel spin) is usually introduced so that $\vec{J} = \vec{s} + \vec{L}$. Introducing the channel spin $\vec{s}$ is useful in the compound nucleus model as only a few values of l usually contribute to a reaction. It is no longer the case at higher energies where the spin-orbit coupling becomes strong, and $\vec{j} = \vec{i} + \vec{L}$ is rather introduced so that $\vec{J} = \vec{I} + \vec{j}$. We talk of "l-s" and "j-j" couplings. Quantization leads to the next inequalities:

$$|I - i| < s < |I + i| \tag{1.10}$$

---

[9]This is due to the quantum uncertainty principle and non-commutation between the spin components.

$$|l - s| < J < |l + s| \tag{1.11}$$
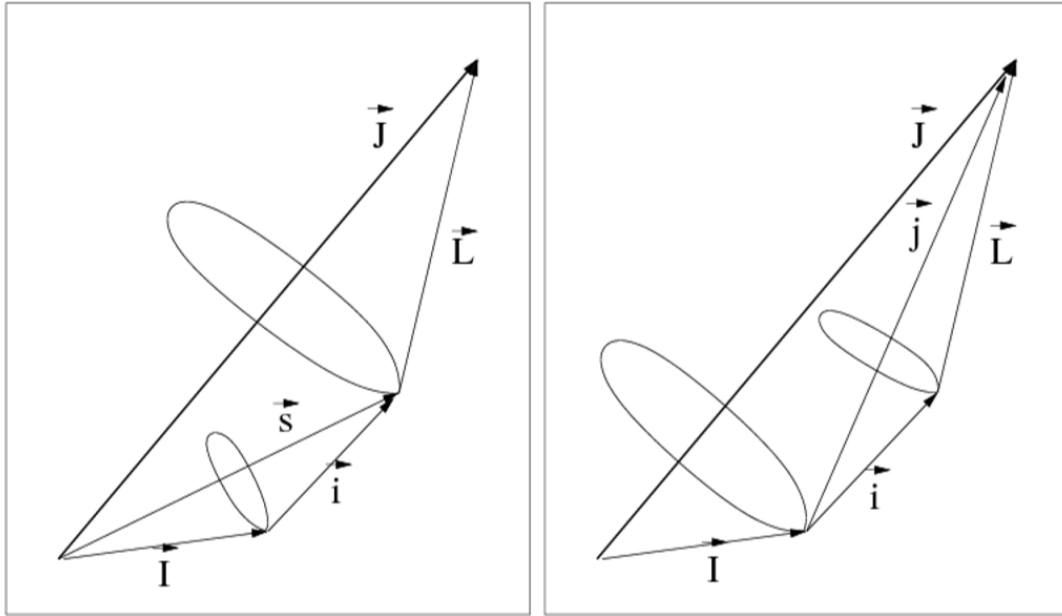
Figure 1.4: "l-s" and "j-j" couplings [5]

As an example for ^{235}U, $I = 7/2^-$ and for a neutron $i = 1/2^+$ (the sign indicates the parity). The spin of the compound nucleus is a function of the angular orbital momentum as summarized in Table 1.1.

l	s^π	J^π					Spectroscopic notation
0	3^-	3^-					s
	4^-	4^-					
1^+	3^+	2^+	3^+	4^+			p
	4^+	3^+	4^+	5^+			
2^-	3^-	1^-	2^-	3^-	4^-	5^-	d
	4^-	2^-	3^-	4^-	5^-	6^-	

Table 1.1: Spin of the compound nucleus $n + ^{235}_{92}$U

Nuclear shell model and resonance phenomenon

An useful description of an atomic nucleus is the nuclear shell model, derived from the well-established model of the atom. In this model nucleons, both neutron and protons are considered as independent subgroups, and are allocated on "levels" following the Pauli exclusion principle. Accordingly only three quantum numbers (n, J, m) serve to define a nucleon state. n defines the level on which is the nucleon ($n \in \mathbb{N}^*$), J is the norm of $\vec{J}$, the total angular momentum of the nucleus, and M its projection on an arbitrary axis. For a nucleon on level n, J can take n values, all positive half-integers. Regarding M, it can take half-integer values under the condition $-M \leq J \leq M$, so that M can only take $2J + 1$ values. Pauli exclusion principle states that nucleons cannot be in the same state (n, J, M). As a direct consequence, each level can only contain $n(n + 1)$ nucleons[10].

---

[10] Of the same type, as neutrons and protons are considered independently.

Let us assume that the nucleus is spherical, and that each nucleon is moving in a spherical potential of the type $V = V(r) + f(r)\vec{L}\vec{s}$. Such a simplified potential[11] is the sum of a harmonic oscillator, and a spin-orbit coupling, which means the potential depends on the nucleon spin and momentum orientation. Combining this potential with the shell nuclear model enables us to draw some conclusions. First, the higher the level, the higher the nucleon energy. Then, within the same level, nucleons having the same orbital moment l have decreasing energies in function of J; we may talk of sublevels (l, J). Finally, the nucleon energy does not depend on M.

Nuclides energy levels are defined as the possible sums of the nucleons energies: together, their distribution on the several levels defines the so-called energy levels (or excitation energies) of the nucleus. For instance, the situation in which all nucleons are distributed in increasing order on the levels define the ground state of the nucleus. Energy levels of the nucleus correspond to situations in which excited nucleons changed levels or spin, always according to the Pauli exclusion principle. In a nutshell:

- Nucleus energy levels are discrete. They correspond to stationary solutions of the Schrödinger equation. In other words, they are eigenvalues of the Hamiltonian, as explained in Section 1.3.2.

- To each energy level corresponds a particular value of the total angular momentum J and a particular value of the orbital angular momentum l. When energy levels of nuclei are determined experimentally, it is usually necessary to give them a spin value, which is a complex task.

- Since the number of nucleons available on each level increases with n, the nucleus energy levels tend to get closer when the energy increases. This has a strong influence on the cross section shape.

When the neutron enters the nucleus at a sufficient low energy, a compound nucleus system of $A + 1$ nucleons is formed. Except for the recoil energy of the neutron, the excited states of this system more or less correspond to the energy levels of the isotope $^{A+1}_{Z}X$. These energy levels are discrete, whereas the kinetic energy of the incident neutron is continuous. When the neutron comes up with an energy corresponding to a transition toward a compound nucleus with $A + 1$ nucleons, the reaction probability increases sharply, which corresponds to a peak in the cross section. This phenomenon is called a *resonance*, and is one of the major feature of the cross sections at low and intermediate energies. Such peaks have a very strong influence on any neutronics macroscopic calculation, as they multiply the probability for a neutron to undergo a reaction. It is quite interesting to notice that all reaction cross sections increase at resonance energies, as a resonance only corresponds to the likelihood of the compound nucleus formation, which only results from the coupling between the incident neutron energy and the energy levels of the compound nucleus.

Compound nucleus reaction

The resonance theory enables to give a more detailed insight of the compound nucleus reaction scheme. Figure 1.5 which comes from [3] represents well the compound nucleus mechanism in case of a large mass nuclide. Once the neutron enters the target nucleus, the excitation energy of the compound nucleus E^* is equal to the system nucleus-neutron kinetic energy e_{exc} in the center of mass plus the binding energy $S_n(A+1, Z)$ of the new neutron in the compound nucleus. Calling $M(A, Z)$ the mass of the target nucleus $^{A}_{Z}X$, $M(A + 1, Z)$ the mass of the compound nucleus $^{A+1}_{Z}X$, c the light speed, and m_n the neutron mass,

$$S_n(A + 1, Z) = c^2[(M(A, Z) + m_n) - M(A + 1, Z)] \tag{1.12}$$

---

[11]A more complete potential would be for instance Wood-Saxon potential.

$$E^* = e_{exc} + S_n(A + 1, Z) \tag{1.13}$$
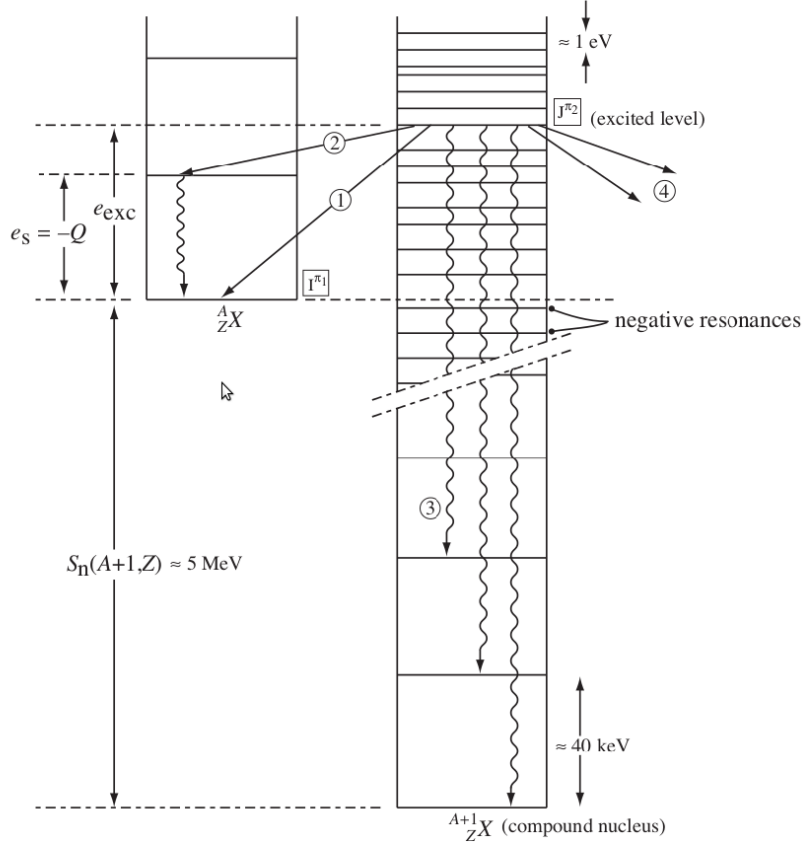
Figure 1.5: Compound nucleus mechanism [3]

Actually, even if E^* is not strictly equal to a level energy, there is a resonance phenomenon. Indeed, each level e_i has an energy width ΔE_i due to the Heisenberg uncertainty principle: the compound nucleus at level i has an average lifetime $\Delta \tau_i = 1/\lambda_i$, before decaying[12] and Heisenberg principle states that $\Delta E_i \Delta \tau_i \geq \hbar$, so that we can define Γ_i the level width (in eV, defined in the center of mass):

$$\Gamma_i = \Delta E_i = \frac{\hbar}{\Delta \tau_i} = \hbar \lambda_i \tag{1.14}$$

The width Γ_i of an energy level is related to the probability of formation of a compound nucleus at level i. As a consequence, all resonances of the compound nucleus contribute to the cross section for a particular energy. This is a very important feature, even if in practice the influence of a resonance on the cross section decreases when the energy is far from e_i.

Once a compound nucleus is formed, it usually decays; some possibilities for the compound nucleus to decay are represented by arrows on Figure 1.5. ① corresponds to an elastic scattering, ② to an inelastic scattering followed by a radiative decay, ③ to a radiative capture, and finally ④ to the compound nucleus fissionning into two fragments.

These decay modes are the several observed nuclear reactions. To each of these reactions one can attribute a partial reaction width Γ_{ix} so that each width is proportional to the probability of decay into this reaction. The sum of all partial widths equals the level width.

$$\Gamma_i = \sum_x \Gamma_{ix} \tag{1.15}$$

---

[12]λ_i is the radioactive constant

These widths, along with the level energies, are the so-called *resonance parameters* which serve to define the resonances of the compound nucleus. These parameters are the key-data from which cross sections can be computed in the compound nucleus model. The mathematical framework which connects the cross sections to these parameters is known as the *R-Matrix theory* and will be developed in Section 1.3.
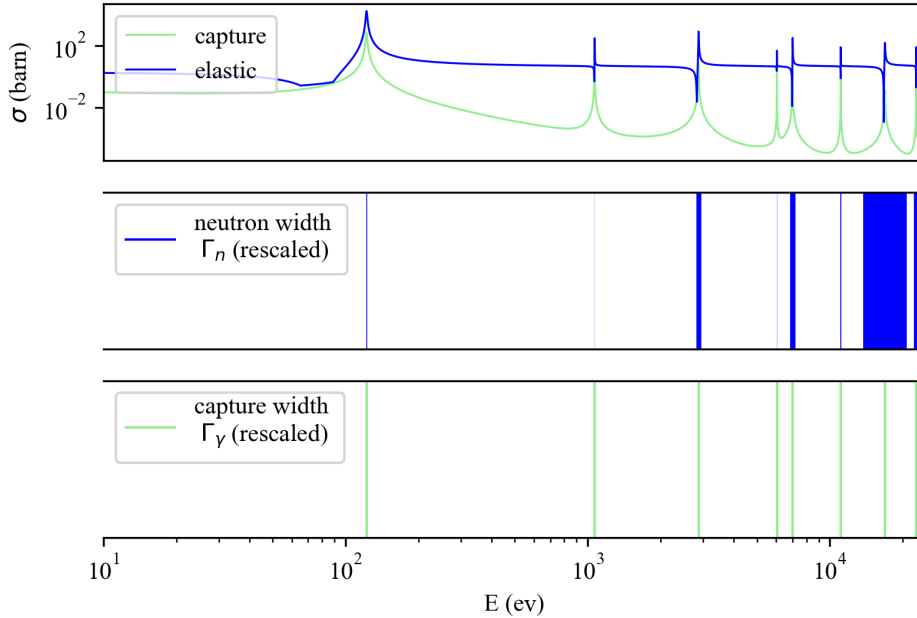
Figure 1.6: Compound nucleus resonances for ^{140}Ba and corresponding elastic and capture cross sections. The larger the shading on the two subplots, the larger the resonance widths.

Figure 1.6 shows ^{140}Ba neutron and capture resonance widths along with the shape of cross sections. The elastic cross section presents a combination of a successive minimum off-peaks and maximum peaks at resonance energies. This phenomenon is typical to elastic cross sections for s-waves ($l = 0$). It is due to an interference term between levels for the scattering cross section.

1.1.4 Temperature dependence of cross sections

Temperature effects have to be considered in the computation of cross sections, especially around resonances. Cross sections are a function of the neutron incident energy in the center of mass, which is equivalent to state that they are a function of the neutron relative speed to the target nucleus. If the nucleus is up to some temperature different from 0K (which is obviously the case in most applications), the nucleus is subjected to thermal agitation, and has a certain speed, which impacts calculations.

Actually, the situation is similar to the one found in acoustics. If the nucleus is going in its direction, a neutron with a slightly higher energy than a resonance energy might catch up with the nucleus with a relative speed corresponding to the resonance. And inversely, for a nucleus going in the opposite direction, the relative speed corresponding to a resonance would be reached for neutron with an incident energy slightly lower than the resonance energy at 0K. This phenomenon is called Doppler effect. The main consequences are a flattening and a broadening of the resonance peaks, as more energies of the incoming neutron are susceptible to provoke a reaction. Figure 1.7 exhibits this phenomenon for the second resonance of ^{140}Ba. The flattening and broadening are clearly visible, both for the capture and elastic cross sections. Note that elastic scattering cross section reversed peaks are flattened as well as peaks.
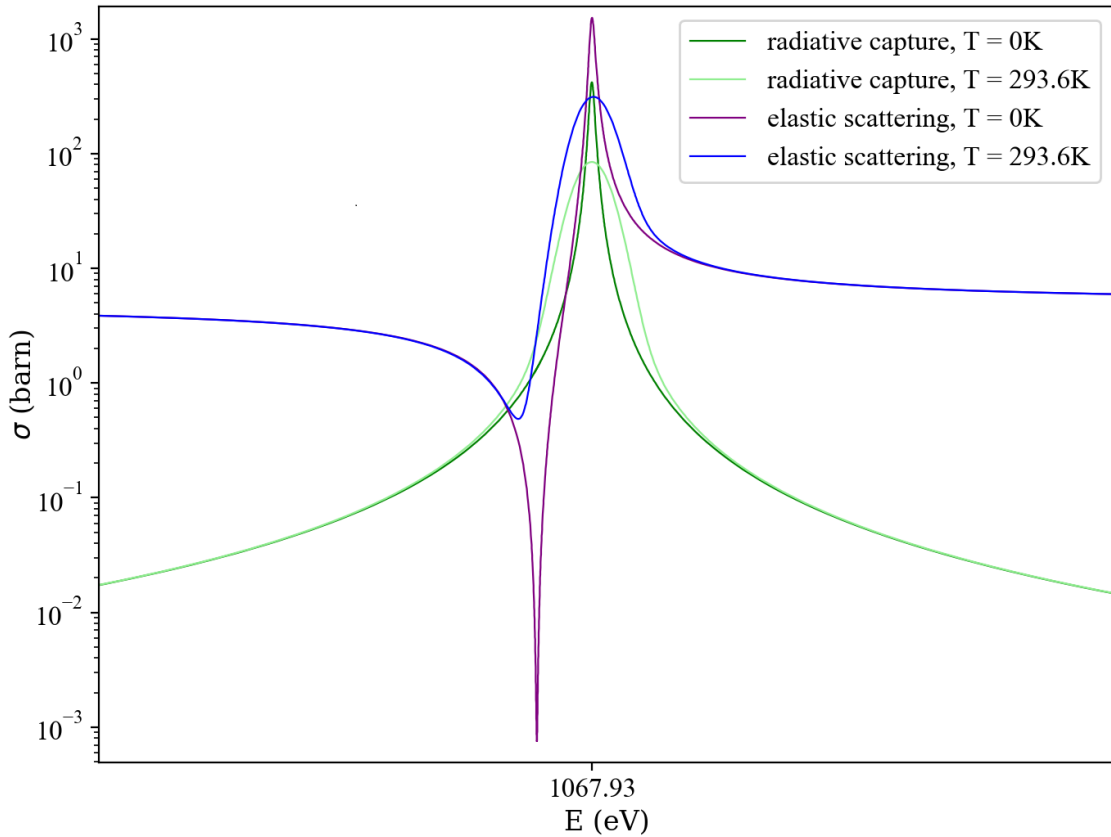
Figure 1.7: ^{140}Ba cross sections around the second resonance for different temperatures

Computations of the Doppler effect are an important step, as it has a clear effect on the reaction rate in the resonances region. The wider the resonances, the higher the capture rate for instance, and the weaker the reactivity in a nuclear reactor. Mathematical calculations can be achieved through a convolution between the cross section at 0K with the target's velocity field. Equations and several methods of Doppler-broadening are presented in Section 1.3.4.

1.1.5 Separation in energy ranges

In practice, the resonant structure of the cross sections motivates the separation of the energy domain for each material into several ranges. Before the first resonance of the considered material the energy range is sometimes called the thermal range. While the capture cross section decreases in $\frac{1}{v}$ the elastic cross section is almost constant. Around the first resonance of the material the *resolved resonance range* (RRR) begins[13]. This energy range corresponds to all the successive resonances of the compound nucleus, and the cross sections exhibit many peaks.

When the energy increases, the compound nucleus lifetime gets shorter, and its energy levels tend to be wider. In the same time, the energy levels get closer to each other as the possible states of nucleons on high energy levels increase (cf. Section 1.1.3). At some point resonances recover each other and the resonance phenomenon disappears. Above this energy the range extending up to infinity is called *continuum*, where cross sections are smoothly-varying functions of energy.

For heavy nuclei with many resonances an additional energy range may be defined, the so-called *unresolved resonance range* (URR), located between the resolved resonance range and the continuum. It corresponds to the situation in which resonances still exist, but are so close they cannot be distinguished experimentally. The unresolved resonance range is thus an artificial range whose underlying physics corresponds to the resolved resonance range, but individual

---

[13]The thermal range may be part of the resolved range according to some terminologies.

resonances cannot be resolved due to experimental limitations[14]. The end of the unresolved range and the beginning of the continuum is often chosen to be the threshold of the first inelastic scattering, but there is no physical meaning behind that choice. Figure 1.8 displays ^{235}U cross sections and the corresponding separation between energy ranges.
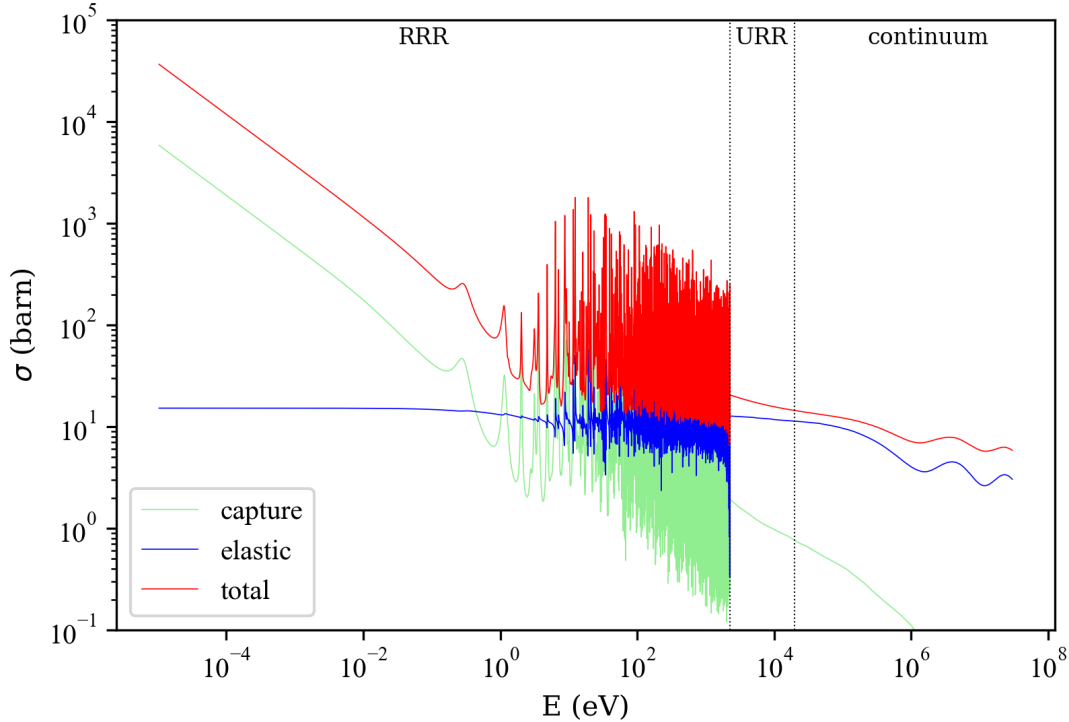
Figure 1.8: ^{235}U cross sections

There is a strong link between this subdivision and the choice of a nuclear model to use. The nucleus-nuclide interactions in the resolved resonance range are mainly compound nucleus reactions. Cross section calculations in the resolved resonance range are achieved through a semi-empirical mathematical model called the R-Matrix theory, addressed in detail in Section 1.3. In the continuum however, direct reactions play a dominant role, and optical and statistical models are used to compute cross sections. These models rely on the description of the nuclear scattering on the basis of the S-Matrix theory [6] and consider the nucleons within the target as a mean field interacting with a high-speed neutron. The unresolved resonance range underlying physics corresponds to the resolved resonance range, and the mathematical framework used to handle computations is the R-Matrix theory as well. This subdivision is not perfect; in particular, some direct reactions may occur at each energy and contribute to the cross section. This is the case of the direct inelastic scattering whose threshold may be located below the continuum. In that case, corrections must be taken into account to accurately represent the cross sections.

1.1.6 Cross sections representations, probability tables and self-shielding

An analytical form of the cross section as a function of the incident neutron energy is hard to obtain, and model-dependent: computations rely on R-Matrix theory and experimental parameters in the resolved resonance range whereas they rely on optical models in the continuum. In the unresolved resonance range average cross sections in a closed form may be derived from

---

[14]For instance, it is a common practice to plot cross sections in this range as regular curves. However in that case, only average cross sections are represented instead of the actual fluctuating sections. It is the case on Figure 1.8.

average experimental parameters. In any case, all these expressions are usually not suitable to be used directly in neutronics-oriented applications[15]. In order to be used, cross sections are usually pre-computed and provided into one of the next forms to neutronics codes:

- **Tabulated linearized cross sections**

  The simplest representation of cross sections is a tabulated function of energy (E_i, σ_i). This is the most common representation used by continuous energy codes, such as Monte-Carlo codes, except for the unresolved resonance range. An accurate representation of cross sections requires the energy grid to be thin enough in the resolved resonance range notably. In order to ensure that no resonance is missed during tabulation, cross sections are *linearized*. This means the resulting energy grid must be thin enough so that any value of the cross section $\sigma(E)$ at some energy $E_i < E < E_{i+1}$ can be obtained through linear interpolation, without huge approximation. Typically, a tolerance level of the order of 0.1% is imposed during the linearization procedure, so that interpolating on the resulting grid leads to a relative error compared to the real value inferior to 0.1%:

  $$\left| \sigma(E) - \left[\sigma_i + \frac{\sigma_{i+1} - \sigma_i}{E_{i+1} - E_i} \left(E - E_i \right) \right] \right| < 0.1\% \tag{1.16}$$

  Linearized grids for all reactions can be fused, in order to ensure a proper representation of all reaction cross sections on a single common energy grid.

- **Multigroup cross sections**

  Tabulated cross sections may represent a huge amount of data, which is uneasy to deal with in some formalism. In particular, deterministic codes use as an input *flux-weighted* average cross sections on successive energy intervals called groups, instead of the proper tabulated cross sections. These successive average cross sections are called *multigroup* cross sections. In practice, the definition of the groups limits depends on the code and the application scope. There might be up to several hundreds groups. In order to take into account a phenomenon known as self-shielding (that is presented in next paragraph), these average cross sections must be weighted by the neutron flux. As the neutron flux depends on the geometry of the considered problem, the multigroup cross sections are actually problem-dependent, and their computation is crucial for deterministic codes.

- **Probability tables**

  A third representation of calculated cross sections may be used as an intermediary between tabulated and multigroup forms, which is the so-called probability tables approach. This representation may be used in place of the average cross sections in multigroup codes, and in the unresolved resonance range where tabulated cross sections are not available. The main idea is to describe cross sections over energy groups, as in the multigroup approach, but providing probability distributions $p(\sigma)$ of the cross section values instead of (weighted) average values. Doing so the precise energy dependence of the cross section is lost but its variability is conserved over the interval. Actually when cross sections are used they are often used in integral quantities (eg. in the Boltzmann equation or in reaction rates), and it is possible to replace a Riemann integral with an equivalent Lebesgue integral. Calling E_g and E_{g+1} the energy limits of group g,

  $$\frac{1}{E_{g+1} - E_g} \int_{E_g}^{E_{g+1}} f(\sigma(E)) dE = \int_0^{+\infty} p(\sigma) f(\sigma) d\sigma \tag{1.17}$$

---

[15]A very interesting exception is the analytical representation of cross sections as a sum of rational functions, known as multipole representation. Such analytical form (which relies on some strong assumptions in the form of the cross section though) can be easily Doppler-broadened [7], and attempts to use it directly in Monte-Carlo codes to apply the temperature effect "on the fly" have been developed with some success [8].

and in particular

$$\langle \sigma \rangle_g = \frac{1}{E_{g+1} - E_g} \int_{E_g}^{E_{g+1}} \sigma(E)dE = \int_0^{+\infty} \sigma p(\sigma)d\sigma \qquad (1.18)$$

Integrals over σ do not extend down to $-\infty$ as a cross section must be positive.

In practice, only a discretization of the probability distribution is provided to neutronics codes which is frequently referred as a *probability table*. Instead of the real knowledge of the probability density, a set of *discrete* couples (σ_k, p_k) is provided so that

$$\sum_k p_k = 1 \qquad \text{and} \qquad p(\sigma) = \sum_k p_k \delta(\sigma - \sigma_k) \qquad (1.19)$$

where δ is the Dirac function. Formally, the probability density function (pdf) is replaced with a probability mass function (pmf), which is the equivalent probability distribution function for discrete probabilities. The probability tables approach is thus an approximation of the real continuous density function as a sum of Dirac. This is equivalent to defining some "bands" along the cross section dimension, meant to match the total cross section with appropriate weights p_k, as shown in Figure 1.9. A probability table is not unique, as several sets of weights p_k and base-points σ_k may correspond to a same cross section shape. The construction of such discrete probability tables in the unresolved resonance range is the whole topic of Chapter 5.

To be even more accurate, the previous definitions concern the total cross section. Indeed, the transformation of partial reaction cross sections into probability tables needs to be achieved under the condition that their sum remains equal to the total cross section. In order to obtain coherent tables, each reaction weight $p_{r,k}$ is set equal to p_k, and their base-points $\sigma_{r,k}$ are defined under the condition that the kth base-point of the total cross section is σ_k (cf Chapter 5).

A probability table contains much more information than just an average value. In particular it efficiently takes into account the *self-shielding* effect [9].

A brief point about self-shielding

The self-shielding is a major phenomenon which must be considered when dealing with neutronics computations. In a material, the neutron flux ϕ actually decreases around a resonance, mainly because the number of neutron decreases around this energy due to higher absorption reactions. As a consequence, the reaction rates, defined as the product of flux with cross sections, are slowly-varying around resonances. This compensating phenomenon between the neutron flux and the resonance shapes is called self-shielding. A main concern arises when the cross section resonant structure is replaced with average values, because the self-shielding cannot be considered in that case. This occurs in two cases: when multigroup cross sections are defined, and in the unresolved resonance range where the exact resonant shape is not available. Multigroup codes must use weighted (self-shielded) average cross sections over a group. Such self-shielded average reaction cross sections can be computed as

$$\langle \sigma_r(E) \rangle_g^{ss} = \frac{\int_{E_g}^{E_{g+1}} \sigma_r(E)\phi(E,\vec{r})dE}{\int_{E_g}^{E_{g+1}} \phi(E,\vec{r})dE} \qquad (1.20)$$

where $\phi(E,\vec{r})$ is the real flux, which remains unknown as it is geometry-dependent. In the real treatment of the self-shielding, the flux is thus calculated by the neutronics codes.

Without the knowledge of the nature of the system, a typical assumption is to replace the unknown flux with a theoretical flux. This enables to compute "theoretical" average self-shielded
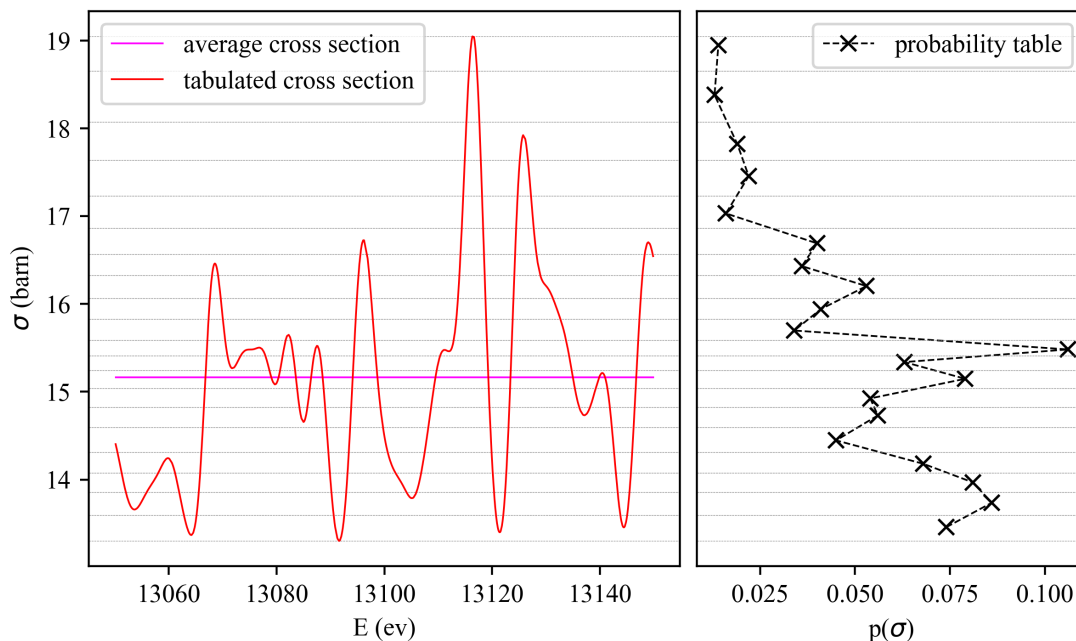
Figure 1.9: Cross sections representations. Left picture is an example of a tabulated cross section around 1.31e4 eV, superimposed to its average value. Right picture is a corresponding probability table with 20 entries.

cross sections, which is the best one can do with no prior information about the real geometry of the system. The most emblematic example is the calculation of Bondarenko self-shielded cross sections. In that case, the flux is assumed to be a smoothly-varying function of energy $C(E)$, weighted with the sum of the total cross section reaction for the isotope and a scalar *dilution cross section* σ_0, representing the combined effect of other isotopes and leakage[16].

$$\phi(E) = \frac{\sigma_0 C(E)}{\sigma_0 + \sigma_t(E)} \tag{1.21}$$

Peaks in the cross section tend to create inflections in the flux. If $\sigma_0 \gg \sigma_t$, the self-shielded average cross sections equals the unshielded ones. In that case, cross sections are said to be infinitely diluted. There are not enough nuclei of that type in the material so that peaks in their cross sections have almost no influence on the flux. This equation can be solved numerically for several values of σ_0 and a flux $C(E)$ provided by the user, for instance as a tabulated function. It can also be calculated from the probability table representation.

Assuming a normalized flat flux for simplicity[17] (a tabulated flux would require to cut the group in subgroups) Equation (1.21) becomes in the Lebesgue continuous formalism:

$$\langle \sigma_r \rangle_g^{\sigma_0} = \frac{\int_0^\infty \sigma_r(\sigma_t) \frac{p(\sigma_t)}{\sigma_0 + \sigma_t} d\sigma_t}{\int_0^\infty \frac{p(\sigma_t)}{\sigma_0 + \sigma_t} d\sigma_t} \tag{1.22}$$

When probability tables are used instead of the continuous probability density functions, the average self-shielded average cross section for a particular reaction r at dilution σ_0 is:

---

[16]A more realistic theoretical flux could be for instance a Maxwellian spectra in the thermal range combined with a $1/v$ contribution, and a fission flux at higher energies.
[17]This assumption is taken from NJOY [10].

$$\langle \sigma_r \rangle_g^{\sigma_0} = \left(\sum_{k=0}^{N-1} \sigma_{r,k} \frac{p_k}{\sigma_0 + \sigma_{t,k}} \right) \times \left(\sum_{k=0}^{N-1} \frac{p_k}{\sigma_0 + \sigma_{t,k}} \right)^{-1} \quad (1.23)$$

And for the total cross-section, the previous expression can be worked to become [11]:

$$\langle \sigma_t \rangle_g^{\sigma_0} = \left(\sum_{k=0}^{N-1} \frac{p_k}{\sigma_0 + \sigma_{t,k}} \right) \times \left(\sum_{k=0}^{N-1} \frac{p_k}{(\sigma_0 + \sigma_{t,k})^2} \right)^{-1} - \sigma_0 \quad (1.24)$$

Probability tables are thus an effective mean to compute self-shielded cross sections [12]. The previous formulas for the Bondarenko self-shielding have been notably implemented in this work (cf Section 6.1.1).

1.2 From nuclear data to nuclear safety applications

Some definitions and important aspects of the neutron-nucleus interaction have been presented in the previous section. It is now of interest to devote some time to describe the actual requirements of nuclear data, in the scope of the nuclear industry and associated applications.

1.2.1 Suitable nuclear data at stake

The general denomination "nuclear data" applies to all the information related to the atomic nucleus which are used as input data for calculations by applications-oriented codes. Cross sections and resonance parameters are for instance certain types of nuclear data. They are of course not the only ones[18], but are of particular importance in this work. Nuclear data are usually compiled in large files called *evaluations* that constitute *nuclear data libraries*. These files are usually the results of many experimental measurements along with many steps of modeling and evaluation process. The complex chain of operations required to produce a suitable library is displayed on Figure 1.10.

Nuclear data evaluations are produced by evaluators. These latter ones can rely on experiments results or theoretical models. Let us discuss the case of cross sections for instance. The atomic nucleus is composed of neutrons and protons bounded together because of the strong force. Dedicated quantum mechanics tools (and in particular quantum chromodynamic - QCD) could in principle lead to a quantitative description of the forces between neutrons and protons within the nucleus [13]. In such a context, computing cross sections from theoretical models[19] sounds appealing. In practice however, two main issues appear. First, the intensity of the strong force does not allow the use of the perturbation theory in the QCD framework, not to mention that the exact state of the forces within the nucleus is unknown. Secondly, this approach turns out to be a many-body problem, involving all the nucleons within the nucleus (around 230 for uranium isotopes for instance). In order to circumvent this issue it is a common practice to average all the interactions between the target nucleus nucleons into a large potential field. Rather than studying the interactions between an incident neutron and all the target nucleons, one studies the interaction between the projectile and a mean field. This approach is known as the *optical model*, first introduced by Bethe [14] in 1935. It has been the reference method used in the continuum for years. Recently, due to the ever-growing computational power of computers, these methods are expanding fast: recent codes such as TALYS [15] are now widely used to produce evaluations from optical calculations directly.

On the other hand optical model approaches are not suited for the study of well-defined resonances. In the resonance range, cross sections are rather obtained experimentally for each material with *Time-Of-Flight* (TOF) experiments. These methods measure a neutron time of

---

[18]For instance Table 1.2 summarizes the nuclear data contained in ENDF files.

[19]One talk about *ab initio* calculations.
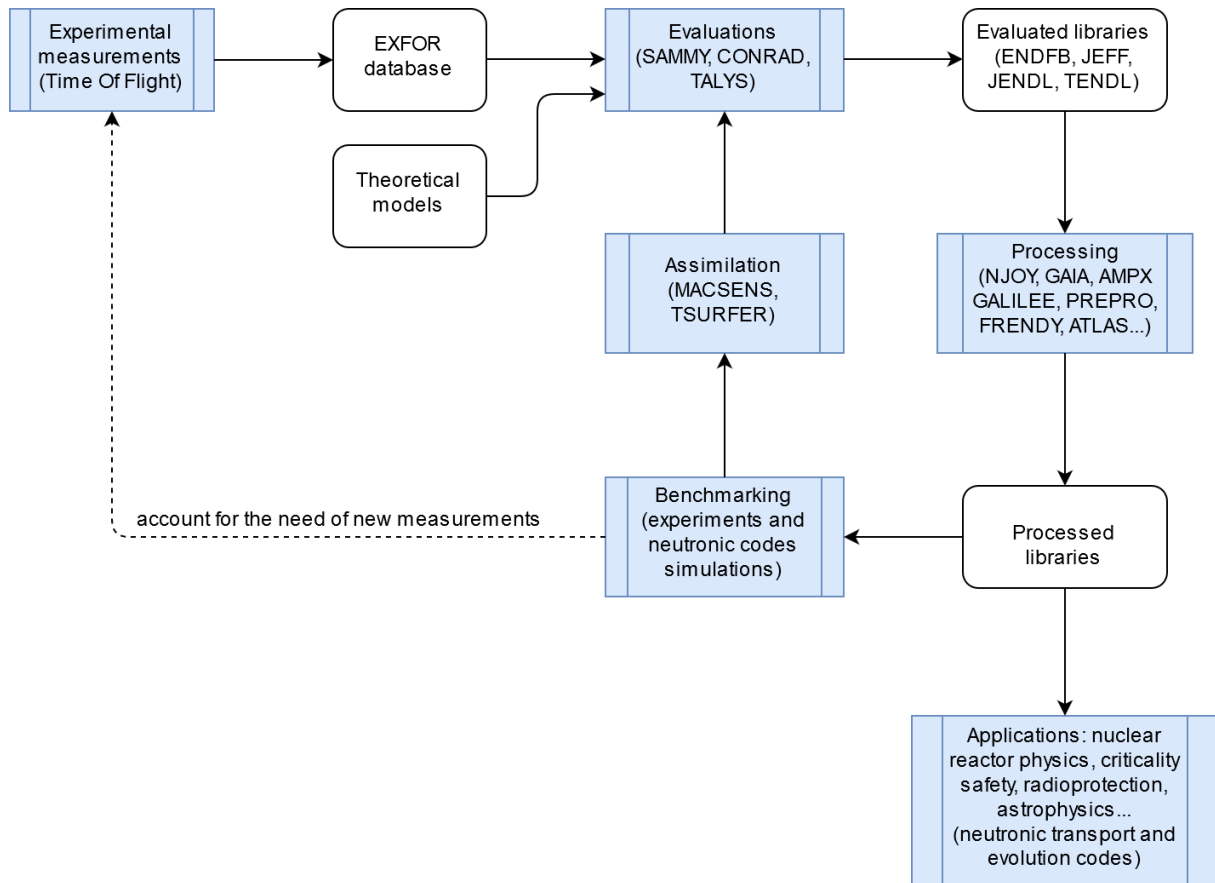
Figure 1.10: Nuclear data production path

travel to find its energy, related to its velocity. In the same time transmission and reaction measurements performed together enable measurements of the total and reaction cross sections [16]. Presently in Europe, experimental facilities that are able to perform data measurements are the GELINA linear accelerator in Geel (Belgium) and the n-TOF complex at CERN in Geneva. Experimental data are stored in the EXFOR database, a devoted international platform. Evaluators exploit these data with dedicated tools to produce evaluated nuclear data libraries. For instance, accurate resonance parameters are required in libraries. They can be obtained from the evaluation of measured cross sections[20]. Powerful codes enable the cross-compilation of several measurements together with complex iterative fitting procedures and correlations accounting to produce nuclear data evaluation files. Such codes are for example SAMMY [17] from the Oak Ridge National Laboratory, or CONRAD, developed at CEA Cadarache. Usually, an evaluation designates an evaluated file for a single isotope. Regularly, sets of evaluated files for all isotopes[21] are released in libraries by several groups. Most of them use the well-established *ENDF-6 format* presented in Section 1.2.2.

Once the nuclear data libraries are available, they still cannot be used by neutronics codes directly. They need to be processed by nuclear processing codes. This processing step is often referred as "turning the data in a form suitable for the different applications codes". In practice however, nuclear data processing is more than that. Processing codes do not only turn data from the ENDF format into other formats (which they do), but they undertake several modeling steps whose relevance is still under study. The most well-known task performed by processing codes

---

[20]It might sound surprising that resonance parameters are evaluated from experimental cross sections, as they are used afterwards to calculate the cross sections. The main reason is that they are more stable data than tabulated experimental cross sections. In particular, they enable the cross section calculations at any energy.

[21]"All" isotopes is an ambiguous denomination, as highly unstable isotopes may exist or get artificially created. Let us say that a typical library regroups several hundreds of isotopes evaluations.

is the calculation of temperature-dependent Doppler-broadened cross sections from resonance parameters in the resonance range. Another issue is the calculation of probability tables in the unresolved resonance range, which is the main object of this document. As processing is a topic of relevance in our concerns, Section 1.2.3 describes them in more detail.

Neutronics codes use the processed nuclear data libraries as an input to perform their calculations. For instance, some of them solve the Boltzman equation for the neutron transport in a provided geometry, with applications in nuclear reactor physics and criticality. Among transport codes, one distinguishes deterministic codes and Monte-Carlo codes. Deterministic codes are mainly used for nuclear reactor calculations, and make use of finite elements theory to solve the equation. Well-known codes of this family are for instance APOLLO (CEA), the chain DRAGON-DONJON (École Polytechnique de Montréal), or the chain CASMO-SIMULATE (Studsvik). Monte-Carlo codes on the other hand simulate thousands of random histories for neutrons in the provided configuration. Quantities of interest are obtained from averaging over the neutron histories, on the base of ergodic properties of the system. Such well-known Monte-Carlo codes are MCNP (Los Alamos National Laboratory), MORET (IRSN), TRIPOLI (CEA), KENO/SCALE (Oak Ridge National Laboratory), SERPENT (VTT Technical Center of Finland), OPEN-MC (MIT), etc. If they can be slower and less flexible than deterministic codes, their results are usually considered more trustworthy. Let us finally mention another important kind of application codes in the nuclear industry, the depletion codes. These codes are used to solve the Bateman equations (radioactive decay) to enable *burn-up* calculations to determine the isotopic composition of materials under irradiation. Let us quote SERPENT (VTT) and VESTA (IRSN) as example of depletion codes.

For most applications the main source of uncertainty in neutronics calculations comes from the input nuclear data [18]. Estimating the quality of evaluated nuclear data is thus a crucial concern. To reach this goal, simple experimental set-ups referred to as *benchmarks* are developed, and *integral data*[22] are measured. Very common measured data are for instance the effective neutron multiplicity factor k_{eff} (the ratio of the number of neutrons created and absorbed in a configuration, crucial in criticality safety assessment as it indicates the development of a chain reaction), shielding factors, two-groups cross sections, etc. These measured data are then compared to the results of calculations performed by neutronics codes, which make use of the processed nuclear data. The final objective is to adjust the nuclear data to match the benchmarks results. Recent evaluations systematically provide covariance matrices for energy-grouped cross sections and resonance parameters. Using these matrices and the perturbation theory, Monte-Carlo neutronics codes are able to perform sensitivity computations. Such calculations are used to evaluate the influence of selected parameters on the final uncertainties, which is extremely useful. Then, in order to investigate susceptible modifications of the nuclear data, dedicated tools for data assimilation have been developed, such as MACSENS (IRSN) or TSURFER (Oak Ridge). These tools rely on the GLSM (global least square method) and the Bayes theorem to compile information from many sensitivity calculations and benchmark results with several codes and libraries, to incorporate the integral data results into evaluations (in particular, they aim at improving the covariance matrices in the evaluations). When necessary, it appears that new measurements are required, for both differential and integral data. For instance, benchmarks in the epithermal range (and in particular in the unresolved resonance range) are still scarce, and many evaluations for important isotopes which date from the 60s have been performed without covariance matrices.

---

[22]opposed to differential data, which are intrinsic measure of isotopes properties, like during time of flight experiments).

1.2.2 Nuclear data formats

ENDF-6 format

The most common nuclear data format used around the world is the Evaluated Nuclear Data Format (ENDF), which is currently up to its sixth revision. It has been introduced to manage the American nuclear data libraries, namely ENDF/B (whose version ENDF/B-VIII has been released in 2018) and adopted by most libraries around the world. Among them let us quote JEFF (Joint Evaluated Fission and Fusion) libraries[23] – whose version JEFF-3.3 has been released in 2018 –, the Japanese library JENDL (Japan Evaluated Nuclear Data Library, currently JENDL-4), the Chinese library CENDL (China Evaluated Nuclear Data Library, currently CENDL-3.2), the Russian library BROND (currently BROND-3.1), and TENDL (TALYS Evaluated Nuclear Data Library) which is produced by the TALYS code on the basis of theoretical models[24]. All these libraries use the well-known ENDF-6 format detailed in reference [2]. Most of the released libraries are freely available on the Internet, distributed by the Nuclear Energy Agency. They usually gather several sub-libraries, such as incident neutron libraries, photo-atomic libraries, thermal scattering data libraries, decay libraries, etc. In this work, we focus on incident neutron libraries.

In practice an ENDF-6 format evaluation is a huge ASCII file, written on 80 columns originally to match the capabilities of FORTRAN-based processing codes, and up to several hundred of thousands lines. An ENDF tape may contain information relative to several isotopes (referred as MAT in the ENDF context), even if the usual practice is to write a single isotope by tape. An ENDF tape is then divided into special-formatted sections called *files*, referred as MF. Table 1.2 summarizes the nuclear data gathered in an incident neutron evaluation. MF files are sometimes divided into MT numbers. In particular for File MF3 (reaction cross sections), MT numbers correspond to reaction identifiers. For instance, "MAT 9228 MF3 MT2" refers to the elastic scattering cross section of ^{235}U.

The ENDF format introduces some limitations, which become more and more problematic as experimental and simulations capabilities increase. For instance, some resonance parameters are not provided for all reactions and spingroups. For our concerns, the format-related limitations will be discussed in Section 2.1.2. For this reason, a new nuclear data format known as General Nuclear Data Structure (GNDS) is under development at the Lawrence Livermore National Laboratory [19], which should enable to alleviate some limitations of the ENDF format. GNDS should be released in the upcoming years, so that evaluators may issue evaluations in this format.

PENDF format

PENDF (Pointwise ENDF) is a derivation of the ENDF format used in most processing codes to transmit information between the different steps of calculation (cf. Section 1.2.3). The main idea is to keep the original ENDF format to write processed data along the calculations pipe. Some parts of the ENDF files are rewritten, or unused MT sections are filled to be internally used afterwards. For instance, initial ENDF files may contain tabulated cross sections in File MF3, or background cross sections to be added to cross sections calculated from resonance parameters[25]. Once cross sections have been calculated they might be written on a File MF3 in a PENDF file as tabulated values, so that a linear interpolation can be used. All the limitations of the ENDF format are embedded in the processing codes outputs when they rely on PENDF files.

---

[23]A common mistake is to think that "E" in JEFF means European, while the JEFF project is actually an international project, hosted by the National Energy Agency, part of OECD. Countries such as Japan and Canada are involved in the project, along with most European countries.

[24]Important isotopes resonance parameters still rely on experimental-based evaluations, taken from JEFF or ENDF/B for instance.

[25]Dedicated flags in the evaluations systematically indicate the nature of the contents.

MF number	Nuclear data
1	General information (comments, evaluation type and materials, raw data flag . . .)
2	Resonance parameters
3	Reaction cross sections
4	Angular distributions for emitted particles
5	Energy distributions for emitted particles
6	Energy-angle distributions for emitted particles
7	Thermal neutron scattering law data
8	Radioactivity and fission-product yield data
9	Multiplicities for radioactive nuclide production
10	Cross sections for radioactive nuclide production
12-15	Photon production related data
19-22	Electron production related data
23-27	Photo-atomic related data
31	Covariance matrices for neutron multiplicities
32	Covariance matrices for resonance parameters
33	Covariance matrices for reaction cross sections
34	Covariance matrices for angular distribution
35	Covariance matrices for energy distribution
40	Covariance matrices for radioactive nuclide production cross sections

Table 1.2: Nuclear data and corresponding MF files in an ENDF-6 library

MT number	Reaction
1	Total reaction (composed)
2	Elastic scattering
3	Non-elastic reactions (composed)
4	Production of one neutron (composed, sum of MT=50-91)
5	Anything: sum of all reactions not identified by a MT number
18	Fission (composed, sum of 19-21 and 38)
19	First chance neutron-induced fission
20	Second chance neutron-induced fission
21	Third chance neutron-induced fission
27	Total absorption (composed)
50	Production of a neutron leaving the nucleus in its ground state
51	Production of a neutron leaving the nucleus in its first excited state state
. . .	
90	Production of a neutron leaving the nucleus in its 40th excited state state
102	Radiative capture
103	(n,p) reaction
107	(n,α) reaction
. . .	

Table 1.3: Some available reactions and corresponding MT numbers in ENDF-6 format

ACE format

Monte-Carlo codes such as MCNP and MORET use processed data in ASCII-based ACE (A Compact ENDF) files. An ACE file contains processed data for a single isotope and a single temperature. Data are gathered in a compact manner, often hard to decipher.

1.2.3 Processing codes

Processing codes are meant to turn the evaluated nuclear data libraries into processed libraries suitable for applications into neutronics codes. They often adopt a modular design, on the model of the software NJOY [10] first developed at Los Alamos National Laboratory in the 60s, which is still the most-used processing code in the world. Such a design is mainly motivated by the fact that the successive transformations of an evaluation are not necessarily identical according to the final use of the nuclear data. Some steps may not be required, formats usually differ, and the nuclear data calculations themselves may be different. As stated, Monte-Carlo neutronics transport codes use tabulated cross sections on a thin energy mesh, whereas deterministic codes often require cross sections and other quantities to be averaged and self-shielded in groups on a predefined energy mesh. From a practical point of view, a modular design is easier to develop and maintain, and enables the piping of several modules from different codes. The latter is of relative importance to investigate the impacts due to a change in a particular module only, and will be exploited in this document.

Except NJOY whose most recent update dates from 2016 [10], many other processing codes have been developed in several institutes. In the US let us quote AMPX, which is a module of the SCALE system developed in Oak Ridge National Laboratory, and FUDGE, currently under development at Lawrence Livermore National Laboratory. In France, the code GALILEE-1 is being developed at CEA on the basis of the code CALENDF. Other important codes are PREPRO (International Atomic Energy Agency), ATLAS (China), and FRENDY (Japan). Recently, IRSN devoted efforts to develop its own processing code, GAIA-2, in order to cross-check the results obtained with other codes for safety purposes. One of the objectives of this PhD work is to develop a module equivalent to the "PURR" module of NJOY in order to compute probability tables in the unresolved resonance range. All developments summarized in this document have been implemented in GAIA-2, in a module named "TOP" ("Tables Of Probability").

Figure 1.11 details the successive operations required to produce ACE files for Monte-Carlo codes and multigroup libraries for deterministic codes. In this figure, NJOY modules and GAIA-2 modules have been named altogether along their purpose.

First step is to perform the reconstruction of cross sections from resonance parameters, using formulas detailed further in Section 1.3.2, on a *linearized* energy grid; at the end of the procedure all reaction cross sections are furnished as tabulated functions on a grid thin enough so that a linear interpolation can be carried out between the tabulated values. Computation of cross sections from resonance parameters is not carried on all reactions (often, it is only achieved for elastic scattering, fission, and radiative capture), nor on all energy ranges (for instance cross sections are given as already tabulated values in the continuum). The linearization operation requires to connect all cross section functions together.

Then, cross sections must be broadened to take into account the Doppler effect. This is usually achieved with the SIGMA1 algorithm [20] which takes as an input the thinned linearized cross section at 0K. In GAIA-2 however, the Doppler-broadening takes place at the same time as the reconstruction of cross sections, so that the error due to the linearization does not propagate to the temperature broadening. An original method relying on Fourier transforms was implemented in the module DOP [1] to achieve this goal, whose results have been proved to be very satisfying.

After these steps, the chaining of modules is more flexible, and depends on the needs of the users. It might be of interest to compute radiation damage cross sections to simulate the aging of materials under irradiation, which is achieved by the module HEATR of NJOY. It might also be sometimes useful to compute the gas production[26] cross sections (MT=203-207). This is done in NJOY in the GASPR module.

It is also important to correct the scattering cross sections in the thermal range to take into

---

[26]Gas corresponds to light products such as proton, deuterium, tritium, α which can accumulate as gas.
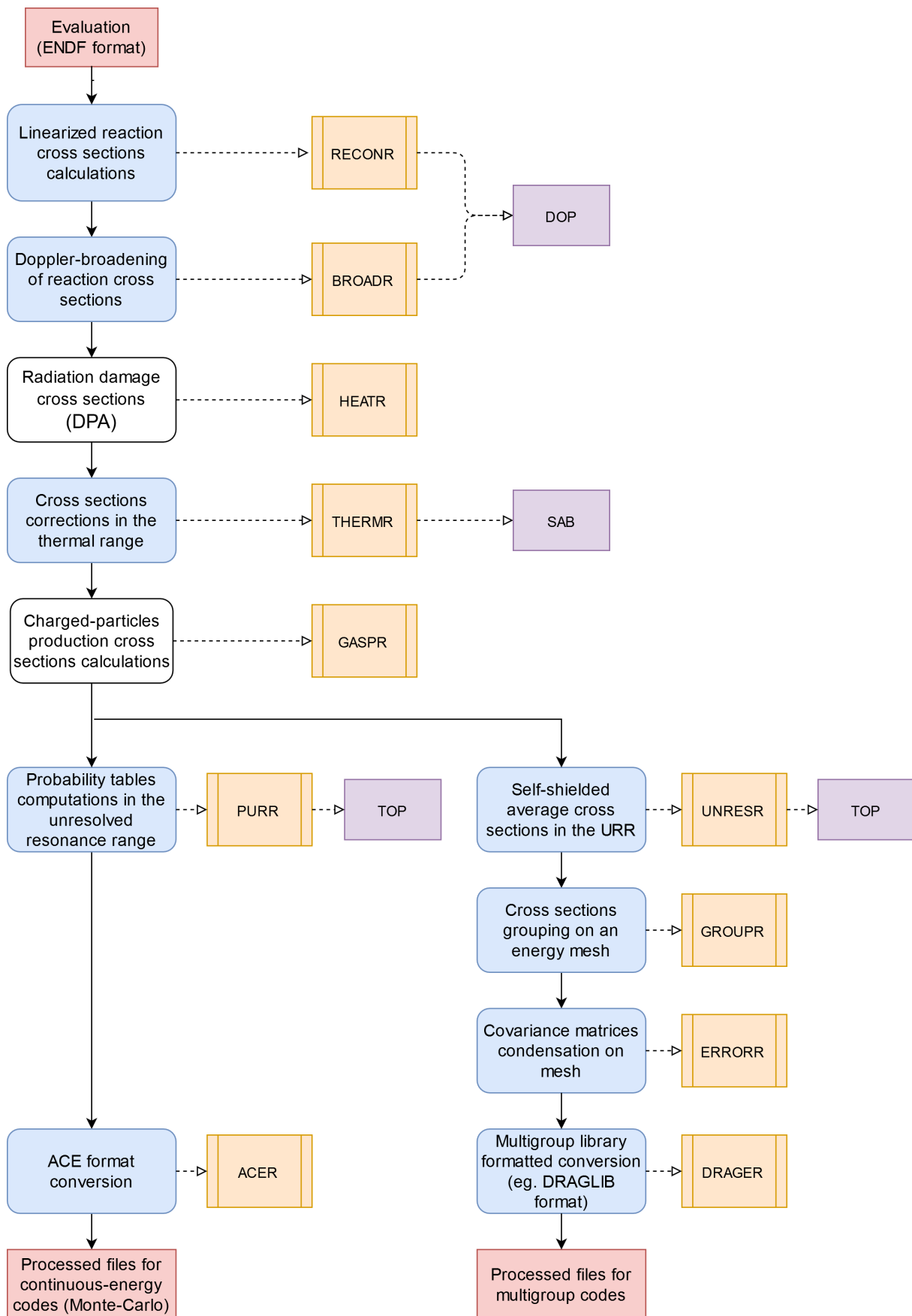
Figure 1.11: Processing of an ENDF file. Blue steps are mandatory to obtain a suitable file for criticality applications. Orange modules refer to NJOY, purple ones to GAIA-2.

account the effect of molecular bounding. This is of particular importance for nuclear reactors such as PWR or BWR in which water plays a major role as moderator. At low energy the hydrogen cross section is not the same when the hydrogen is free or bounded within a water molecule, which is the case in PWR. The module THERMR of NJOY is able to take into account cross section corrections for these applications. In GAIA-2, this is performed by the SAB module, developed in 2018 [21].

At this point, the path followed by continuous-energy and multigroup codes starts to differ. First comes the unresolved resonance range (URR) particular processing. As a reminder, only average resonance parameters are provided in this range. One may calculate average cross sections, but as there is still an underlying resonant structure, it is very important to consider self-shielding. UNRESR computes Bondarenko self-shielded average cross sections in the URR to consider the resonant structure. Then, the main step for multigroup codes is to average the reconstructed cross sections on an energy mesh provided by the user (GROUPR), taking into account the self-shielding in the resonance region too. Then the evaluation's covariance matrices must be adapted to the mesh (ERRORR) accordingly.

For Monte-Carlo codes, the processing of the unresolved resonance range is quite different. They do not rely on average cross sections, but make use of probability tables to capture the resonant structure of the underlying cross sections. In NJOY, probability tables are computed by the module PURR. These probability tables enable Monte-Carlo codes to take into account the self-shielding effect in the URR. The topic of this document is the production of such probability tables.

Finally, processed data are converted into suitable forms such as ACE files (using the NJOY module ACER) for Monte-Carlo codes MCNP and MORET, or other modules for other codes. For instance DRAGR is a NJOY module meant to convert multigroup processed libraries in DRAGLIB files for the deterministic code DRAGON.

In this section, some important details about the nuclear data were discussed. Next section will provide a more quantitative description of the mathematical framework used in the resonance range to calculate cross sections, known as the R-Matrix theory. Resonance parameters are provided in respect with this theory in the ENDF-6 evaluations.

1.3 R-Matrix theory of nuclear reactions

The R-Matrix theory is a very general and powerful formalism, used to compute cross sections in the resonance range. It has been developed by Lane and Thomas [22] who worked on an original idea of Wigner and Eisenbud [23]. R-Matrix main idea is to describe the cross sections as a function of the eigenvalues and eigenvectors of the system's Hamiltonian. These values correspond to the energy states of the system, and turn out to be the resonance parameters already mentioned. The process to compute cross sections in the resonance range is thus a two-step process. Experimental measurements are performed from which it is possible to obtain experimental resonance parameters. These parameters are then used as input to compute cross sections at any energy with the R-Matrix formulas. The very core of the neutron-nucleus interaction is thus considered as a black box. The R-Matrix parametrization is very convenient in the resonance range but could be used to process direct reactions too.

The presentation made here aims at describing the origin of the equations used in the following to compute cross sections in the resonance range. In this section, the hypotheses of the R-Matrix theory and the configuration space of the problem are introduced. In particular, a formal definition of the notion of channel is given. For the sake of consistency, the complex equations of the R-Matrix are presented, even if steps of calculation are often skipped. More details are provided for the approximations of the R-Matrix theory known as Single-Level and Multi-Level Breit-Wigner formalisms, as they are of particular importance for the unresolved resonance range processing. The presentation makes a great use of materials from Ghislain Ferran's PhD thesis [1], from a course given by Luiz Leal at MIT [24], from the ENDF-6 format

manual [2], and from the Oak Ridge evaluation code SAMMY manual [17]. For a complete description of the R-Matrix theory, these documents provide a good reference, as well as the original and exhaustive article of Lane and Thomas.

1.3.1 Hypotheses and configuration space definition

The theory provides a very rigorous and large framework which only relies on a small amount of hypotheses:

1. **Non-relativist quantum mechanics apply**

   This implies that if Φ is the system's wavefunction and H its Hamiltonian, for any point of space the Schrödinger equation holds.

   $$H\Phi = i\hbar \frac{d\Phi}{dt} \tag{1.25}$$

   In particular, the non-relativistic hypothesis is coherent with the reactor physics energy range where neutrons have energies up to 20 MeV only.

2. **A reaction does not produce more than two products**

   This is quite restrictive considering that a three-products reaction may occur. This hypothesis assumes that this phenomenon is way scarcer than a two-products fission, which is legitimate in the resonance range. In some cases such a reaction can be approximated successfully with two successive two-products reactions.

3. **Creation and destruction processes are negligible**

   This hypothesis is actually related to the system's Hamiltonian structure and is used to neglect the weak interaction. It implies that there is no creation or destruction operator in the Hamiltonian. As a consequence β^+ and β^- radioactive decays are not handled by the theory, as they produce or destroy a photon and a neutron. They were the main consequence of the weak interaction, which is thus neglected. Only the strong force and the electromagnetic interaction are considered during a nuclear interaction.

   More generally, this hypothesis would lead to discard any reaction involving photons as input particles. These reactions can be treated yet adding some more hypotheses, but that is not a matter here.

4. **For each pair of nuclei c, a finite radial distance of separation a_c exists**

   Calling c a pair of nuclei (in our case an incident neutron and a target nucleus), it is assumed that a finite distance a_c exists, beyond which there is no longer any polarizing action between the nuclei. Thus, a central force can describe the interaction between the nuclei. As any distance greater than a_c must be a separation distance too, a_c denotes the minimal distance beyond which there is no interaction.

   If the pair of nuclei does not contain any charged nucleus, a_c is the sum of the two nuclear radii (which mark the end of the strong interaction). If one or more is charged, electromagnetism will affect the nuclei and a_c will be slightly higher.

   This distance a_c is called *the channel radius* associated to the pair c.

   This hypothesis leads to the distinction between two distinct regions of the phase space, known as *inner region* ($r < a_c$) and *outer region* ($r > a_c$). During a nuclear reaction which implies a compound nucleus formation, the inner region corresponds to the compound nucleus, while the outer region corresponds to the situation where the nuclei are well separated.

As stated, these hypotheses are quite simple. In particular, hypotheses 1 and 4 are very important. The objective will be to exploit the system equation (the Schrödinger equation according to the first hypothesis) in the outer and inner regions, before connecting them.

These considerations require to properly define a pair of nuclides c. Let us imagine a system composed of A nucleons, divided in two subgroups of A_1 and A_2 nucleons. For instance, if the second subgroup is a neutron alone, $A_2 = 1$. Both are in the quantum state α_1 and α_2, which characterize the type and the excitation level of each nucleon in the subgroups. In the following the notation $\alpha = (\alpha_1\alpha_2)$ will be used. These subgroups have a spin $\vec{I_1}$ and $\vec{I_2}$. In case the second subgroup is a neutron, $\vec{I_2} = \vec{i}$ and so $\vec{I_1} = \vec{I}$. Their projections on a given axis are called i_1 and i_2. Finally, it is necessary to introduce the orbital angular momentum $\vec{l}$ and its projection m in order to provide information about the relative motion of the nuclides in the pair. A pair of nuclides as defined in the hypothesis 4 of the R-Matrix theory is thus entirely defined by the set of quantum numbers $c = \{\alpha i_1 i_2 lm\}$[27]. The projections i_1 and i_2 can be replaced by an equivalent characterization with the spin of the pair $\vec{s}$ and its projection ν. Likewise, it is possible to obtain an equivalent characterization with the total angular momentum $\vec{J}$ and its projection M. An accurate definition of a pair of nuclides is thus

$$c = \{\alpha l s J M\} \tag{1.26}$$

Each nucleon in the paired system has 5 degrees of freedom (three spatial and two for their intrinsic spin) so the configuration space of the system is a 5A-dimensions space. When the radial distance between the nuclides is greater than the radius a_c (which actually only depends on the quantum state of the system $\alpha = (\alpha_1\alpha_2)$ so that a_c could be rewritten a_α), the pair of nuclides is well separated and the system occupies a part of the outer region. In the outer region, each element of the configuration space of the pair c is called a *channel*. It corresponds to a characterization of the total system in a separated pair, in the state $\{\alpha l s J M\}$. In such a context, a channel defines a pair of nuclides[28]. Because the nucleons in each subgroup are indistinguishable, there are actually $\left(\frac{N_1}{N}\right)\left(\frac{Z_1}{Z}\right)$ corresponding channels for a single pair c (N and Z are the numbers of neutrons and protons in the total system, N_1 and Z_1 the number of neutrons and protons in A_1). A channel associated to the pair c is actually defined as the sum of these $\left(\frac{N_1}{N}\right)\left(\frac{Z_1}{Z}\right)$ channels. The region of the configuration space such that $r_c = a_c$ is called the *channel surfaces* $\mathcal{S}_c$. The union of all these surfaces forms the *inner region surface* $\mathcal{S}$ which is the border of the configuration space between the inner and outer regions.

Using this formalism a nuclear reaction in the compound model can be understood as follows: the system occupies an *entrance* (or input) *channel* ($r_\alpha > a_\alpha$) in the outer region, then enters the inner region when it forms a compound nucleus ($r_\alpha < a_\alpha$), and occupies a *decay* (or output) *channel* ($r_\alpha < a_\alpha$) in the outer region when the compound nucleus decays in a pair of nuclides. Note that in the case of a fission or a capture, the resulting nuclides are no more a neutron and the initial target nucleus. The decay channel identifies the type of the reaction. Actually, a reaction is the sum of all the decay channels whose α corresponds to the reaction. In the case of an elastic scattering, the resulting pair is the same than the entrance pair. In that case, this means the output channel of the reaction corresponds to the input channel. Input channels can thus only correspond to an elastic scattering reaction. However, there can be several different entrance channels for a nuclear reaction, as they rely on the quantum state of the system α and the quantum numbers s and l.

All channels with the same quantum numbers J and π (parity) form a *spingroup* J^π. As J and π are conserved during a reaction, entrance and decay channels in a reaction must belong to the same spingroup: a decay channel is open only if it belongs to the same spingroup than the entrance channel.

---

[27]The norms of intrinsic spins I_1 and I_2 can be deduced from α, and are not necessarily integrated int the channel definition.

[28]This justifies the notation "c" used to define a pair.

1.3.2 Brief derivation of the R-Matrix theory

In the outer region

Let us consider a system in the outer region with an excitation energy E. The system is in the channel defined by $c = \{\alpha s l J M\}$. The wavefunction describing the state of the system is an eigenvector of the Hamiltonian:

$$H\Psi = E\Psi \tag{1.27}$$

This Hamiltonian can be rewritten $H = T + V$ where T is the kinetic energy operator and V the potential energy operator. Supposing that the center of mass of the system is at rest (this hypothesis will be discarded in Section 2.1.2, with minor changes to take into account the change of referential from the center of mass to the laboratory referential), and defining μ_c the reduced mass of the pair, T and V can be rewritten in the outer region as

$$T = -\frac{\hbar}{2\mu_\alpha}\nabla_r^2 + T_{int,\alpha_1} + T_{int,\alpha_2} \tag{1.28}$$

$$V = V_c(r_\alpha) + V_{int,\alpha_1} + V_{int,\alpha_2} \tag{1.29}$$

T_{int} and V_{int} are the kinetic energy operator and intern potential of the nuclides respectively. The form of V_c is due to the hypotheses of the R-Matrix theory, which ensure that the potential of the system can be described by a central force in the outer region. The Hamiltonian can be rewritten $H = H_c + H_{\alpha_1} + H_{\alpha_2}$. H_c describes the relative motion of the nuclides within the pair and H_{α_i} the intrinsic state of the nuclides. The wavefunction can be decomposed in the outer region:

$$\Psi = \psi_c \psi_{\alpha_1} \psi_{\alpha_2} \tag{1.30}$$

so that

$$\begin{aligned} H_c\psi_c &= E_c\psi_c \\ H_{\alpha_1}\psi_{\alpha_1} &= E_{\alpha_1}\psi_{\alpha_1} \\ H_{\alpha_2}\psi_{\alpha_2} &= E_{\alpha_2}\psi_{\alpha_2} \end{aligned} \tag{1.31}$$

$$E = E_c + E_{\alpha_1} + E_{\alpha_2} \tag{1.32}$$

The product $\psi_{\alpha_1}\psi_{\alpha_2}$ in Equation (1.30) can be replaced by an expression $\psi_{\alpha s\nu}$ or equivalently $\psi_{\alpha J M}$. $\psi_{\alpha J M}$ describe the system intern states in the channel, and are called the spin channel wavefunctions.

The equation $H_c\psi_c = E_c\psi_c$ can be developed on a spherical harmonic base. Defining r_α and Ω_α the norm and direction of the radial vector between the nuclides of the pair,

$$\psi_c = \frac{1}{r_\alpha}u_c(r_\alpha)i^l Y_m^l(\Omega_\alpha) \tag{1.33}$$

where Y_m^l are the usual spherical functions, and u_c is a solution of the radial Schrödinger equation (c marks the channel here):

$$\left[\frac{d^2}{dr_\alpha^2} + \frac{2\mu_\alpha}{\hbar^2}\left(E_c - V_c(r_\alpha) - \frac{l(l+1)\hbar^2}{2\mu_\alpha r_\alpha^2}\right)\right]u_c(r_\alpha) = 0 \tag{1.34}$$

As V_c can be null or expressed as a Coulomb potential (for instance in the case of a reaction (n,p)), it is possible to solve this equation. Two cases are actually possible, as E_c can be positive or negative. In the first case the channel is said to be a positive energy channel. In that case, Equation (1.34) has two independent solutions corresponding to incident and emitted waves,

$I_c = I_{\alpha l}$ and $O_c = O_{\alpha l}$. In particular these waves are complex conjugates. In the second case only a real emitted wave vanishes in infinity and has a physical meaning.

Grouping these results in Equation (1.30), the two linearly independent solutions of the Hamiltonian equation are an emitted and incoming waves such that

$$\Psi_c^{inc} = \frac{I_c}{v_\alpha^1/2 r_\alpha} \psi_{\alpha JM} i^l Y_m^l \tag{1.35}$$

$$\Psi_c^{out} = \frac{O_c}{v_\alpha^{1/2} r_\alpha} \psi_{\alpha JM} i^l Y_m^l \tag{1.36}$$

It is now relevant to introduce several quantities of interest. In particular we can introduce the logarithmic derivative of the waves for the channel c:

$$\mathcal{L}_c = \left[\frac{r_c}{I_c}\frac{dI_c}{dr_c}\right]_{r_c=a_c} \text{ and } L_c = \left[\frac{r_c}{O_c}\frac{dO_c}{dr_c}\right]_{r_c=a_c} = S_c + iP_c \tag{1.37}$$

S_c is called *shift factor* as it shifts the resonance energies from the compound nucleus levels in the cross sections expression, as seen later. P_c is called the *penetrability factor* as it appears as a factor in the expression of the resonance widths. It is also useful to introduce the *surface waves* as the product of $\psi_{\alpha JM}$ and the multiplicative factor of the radial part of ψ_c (cf. Equation (1.33)):

$$\zeta_c = \frac{1}{r_\alpha}\psi_{\alpha JM} i^l Y_m^l \tag{1.38}$$

These functions form an orthonormal family on the inner region surface $\mathcal{S}$ (which is the union of all the channel surfaces, ie. the regions of the configuration space such that $r_c = a_c$). With this formalism the radial part of the complete wavefunction (ie. $u_{\alpha JM}$, written u_c) on the surface $\mathcal{S}$ can be rewritten as $u_c(a_c) = \int_{\mathcal{S}} \zeta_c^* \Psi dS$ using the properties of the scalar product in a Hilbert space. It is useful to introduce the quantity V_c and D_c such that

$$V_c = \sqrt{\frac{\hbar^2}{2\mu_c a_c}} u_c(a_c) = \sqrt{\frac{\hbar^2}{2\mu_c a_c}} \int_{\mathcal{S}} \zeta_c^* \Psi dS \tag{1.39}$$

$$D_c = \sqrt{\frac{a_c \hbar^2}{2\mu_c}} \left(\frac{du_c}{dr_c}\right)_{r_c=a_c} = V_c + \sqrt{\frac{a_c \hbar^2}{2\mu_c}} \int_{\mathcal{S}} \zeta_c^* \nabla_n \Psi dS \tag{1.40}$$

In the inner region

In the inner region the potential is unknown and the Schrödinger equation cannot be solved. That means the behavior of the system's inner wave function of the pair of nuclei is unknown. The wavefunction is composed of several wavefunctions Φ_{JM} which correspond to the to the same energy but for different values of J and M.

$$H\Phi_{JM} = E\Phi_{JM} \tag{1.41}$$

The Hamiltonian of the system is real, which ensures the existence of an orthonormal base of eigenfunctions $(\phi_{\lambda JM})_{\lambda \in N}$ on which Φ_{JM} can be decomposed.

$$\Phi_{JM} = \sum_\lambda A_{\lambda J} \phi_{\lambda JM} \tag{1.42}$$

Using the properties of the scalar product in a Hilbert space, the coefficients $A_{\lambda J}$ can be expressed as an integral over the whole inner region τ:

$$A_{\lambda J} = \int_\tau \phi_{\lambda JM}^* \Phi_{JM} d\tau \tag{1.43}$$

The defined $\phi_{\lambda JM}$ are associated to real energies $E_{\lambda J}$ which are eigenvalues of the Hamiltonian, which do not depend on M. As a consequence, $A_{\lambda J}$ do not depend on M either.

$$H\phi_{\lambda JM} = E_{\lambda J}\phi_{\lambda JM} \tag{1.44}$$

Exactly like in the outer region, it is possible to define the radial projection on the surface $\mathcal{S}$ of these functions.

$$\gamma_{\lambda c} = \sqrt{\frac{\hbar^2}{2\mu_c a_c}} \int_{\mathcal{S}} \zeta_c^* \phi_{\lambda JM} dS \tag{1.45}$$

$$\delta_{\lambda c} = \gamma_{\lambda c} + \sqrt{\frac{a_c \hbar^2}{2\mu_c}} \int_{\mathcal{S}} \zeta_c^* \nabla_n \phi_{\lambda JM} dS \tag{1.46}$$

c in the index defines the corresponding channel $\{\alpha s l J M\}$ on the vicinity of the surface (ie on $\mathcal{S}_c$). This projection on the radial surface around channel c is called the *reduced width* of the level $E_{\lambda J}$ for channel c, usually written $\gamma_{\lambda c}$. It is directly related to the probability to get in the channel c around $E_{\lambda J}$.

An important fact is the necessity to fix a boundary condition on $\mathcal{S}$ to solve the radial Schrödinger equation. It is possible to achieve it and ensure the orthonormality of the $(\phi_{\lambda JM})$. This is achieved by setting the ratio $\gamma_{\lambda c}/\delta_{\lambda c}$ to a constant B_c, independent of the levels $E_{\lambda J}$.

$$\frac{\gamma_{\lambda c}}{\delta_{\lambda c}} = B_c \tag{1.47}$$

Several parametrizations of the theory are possible according to the chosen value of B_c. In particular, the Wigner-Eisenbud choice consists in setting $B_c = S_c$[29], which is often convenient[30]. It is now relevant to formally introduce the *resonance widths* (or level widths) used in Section 1.1 as a function of the reduced level widths such that:

$$\Gamma_{\lambda c} = 2P_c \gamma_{\lambda c}^2 \tag{1.48}$$

In this equation, P_c is the penetrability factor already mentioned, whose name comes from the fact it appears in this relation. $\Gamma_{\lambda c}$ has the dimension of an energy and is linked to the probability that the compound nucleus decays in channel c. It must be underlined that $\Gamma_{\lambda c}$ may depend on the energy through P_c, while $\gamma_{\lambda c}$ is energy-independent. The level widths and energies are the *resonance parameters*.

Connecting the inner and outer region

It is now possible to connect the wavefunctions between the inner and the outer regions on the surface $\mathcal{S}$. Φ_{JM} describes the whole system with quantum numbers J and M in the inner region. Its "value" V_c and derivative D_c on the surface must connect to the total wavefunction in the outer region, ie. to Equation (1.39) and Equation (1.40). Reminding that $E_{\lambda J}$ is an eigenvalue of the Hamiltonian corresponding to $\phi_{\lambda JM}$ and E an eigenvalue corresponding to Φ_{JM}, and using the Green theorem, the scalar product of Φ_{JM} and $\phi_{\lambda JM}$ gives:

$$(E_{\lambda J} - E) \int_\tau \phi_{\lambda JM}^* \Phi_{JM} d\tau = \sum_{c \in J^\pi} (\gamma_{\lambda c} D_c - V_c \delta_{\lambda c}) \tag{1.49}$$

so that we can reformulate the coefficients $A_{\lambda J}$ of the decomposition of Φ_{JM} and then Φ_{JM} itself, the total wavefunction in the inner region in function of its value and derivative on the surface $\mathcal{S}$.

---

[29]In the limit $k_c a_c \to 0$, $B_c = -l$, which is sometimes the provided definition in the literature.

[30]Another well-known possibility consists to set $B_c = L_c$, which is the Kapur-Peirls parametrization. Matrix inversions are easier but resonance parameters depend on the energy implicitly.

$$A_{\lambda J} = \frac{1}{E_{\lambda J} - E} \sum_{c \in J^\pi} (D_c - B_c V_c) \gamma_{\lambda c} \tag{1.50}$$

$$\Phi_{JM} = \sum_{c \in J^\pi} \sum_\lambda \frac{\gamma_{\lambda c} \phi_{\lambda JM}}{E_{\lambda J} - E} (D_c - B_c V_c) \tag{1.51}$$

A last step is necessary to express the information related to the inner region (the reduced widths and the energy levels) as functions of the quantities of the outer region. Let us consider another channel $c' = \{\alpha' s' l' J' M'\}$. Multiplying Equation (1.51) with the surface wave $\zeta_{c'}^*$ and integrating over S yields the final equation defining the R-Matrix:

$$V_{c'} = \sum_{c \in J^\pi} \underbrace{\left(\sum_\lambda \frac{\gamma_{\lambda c} \gamma_{\lambda c'}}{E_{\lambda J} - E} \delta_{JJ'} \right)}_{R_{cc'}} (D_c - B_c V_c) \tag{1.52}$$

The large matrix whose coefficients are $R_{cc'}$ is called the R matrix. Its dimension matches the number of channels (which can reach numbers up to several thousands). As the $\gamma_{\lambda c}$ are real, this matrix is real symmetric. The Kronecker symbol appears as J is conserved during a nuclear reaction, and so the reference to J in the level energies is usually dropped in the R matrix expression.

The performed manipulations enable to express some inner region related quantities of interest (reduced widths and energy levels) as functions of components of the outer region. The concept of the R-Matrix theory is to calibrate the outer region behavior (ie. the cross sections) as a function of these parameters which can be determined experimentally. In the following part, the link with the cross sections will be briefly exposed.

Collision matrix and link to the cross sections

A general solution of the Schrödinger equation in the outer region can be formulated as a combination of incoming and emitted waves.

$$\Psi = \sum_c (y_c \Psi_c^{out} + x_c \Psi_c^{inc}) \tag{1.53}$$

Actually, there must exist a relation between the amplitudes of the incoming and emitted waves, that is formulated as a matrix relation introducing the so-called *collision matrix* U:

$$y_c = -\sum_{c'} U_{cc'} x_{c'} \tag{1.54}$$

After manipulations, it is possible to connect the collision matrix to the values V_c and D_c on the surface $\mathcal{S}$, and then to the R matrix. Calculations are not detailed there, but the final matrix relation between the collision matrix and the R matrix is:

$$U = \Omega_c W_{cc'} \Omega_{c'} \tag{1.55}$$

$$\text{with } \Omega_c = \left(\frac{I_c}{O_c} \right)^{\frac{1}{2}}_{r_c = a_c} = e^{i(w_c - \phi_c)} \tag{1.56}$$

$$\text{and } W = P^{1/2} \left[I - R(L - B) \right]^{-1} \left[I - R(\mathcal{L} - B) \right] P^{-1/2} \tag{1.57}$$

in which only the R matrix is not diagonal. w_c is the *Coulomb-phase shift difference*, null for non-Coulomb channels, and ϕ_c is the *hard-sphere scattering phase shift*, sometimes named potential scattering shift. Hard-sphere phase shift is the phase shift due to the scattering on a sphere with radius a_c, which is a well-known problem in quantum physics. Phase shifts expressions can be

computed from the channel radius for different l-values; when there is no ambiguity ϕ_c can be replaced with ϕ_l, even if they depend on α through a_c.

Cross sections can be expressed as functions of the collision matrix. The key-point is to remark that the amplitude of the emitted wave can be connected to the differential cross sections, and then cross sections by integrating over all the solid angles, like for instance in [1] or [17]. Let us introduce $k_c = k_\alpha$ the channel wave number and g_J the statistical spin factor[31]:

$$k_\alpha = \sqrt{\frac{2\mu_\alpha |E|}{\hbar^2}} \tag{1.58}$$

$$g_J = \frac{2J + 1}{(2I_1 + 1)(2I_2 + 1)} \tag{1.59}$$

$$= \frac{2J + 1}{2(2I_1 + 1)} \text{ for a neutron} \tag{1.60}$$

If the incident particle is a neutron, cross section from a channel c to a channel c' is given as

$$\sigma_{cc'} = \frac{\pi}{k_\alpha^2} g_J |\delta_{cc'} - U_{cc'}|^2 \delta_{JJ'} \tag{1.61}$$

This expression is assumed in this document. To obtain the expression of the cross section for the total reaction, elastic scattering reaction and other reactions, $\sigma_{cc'}$ must be summed over the right channels. Total cross section is a sum over all incident channels and all exit channels for all spingroups. As exit channels can be incident channels, summing over all exit channels is equivalent to summing over all channels:

$$\sigma_{tot}(E) = \sum_J \sum_{\substack{c \in J^\pi \\ \text{incident} \\ \text{channels}}} \sum_{\substack{c' \in J^\pi \\ \text{all} \\ \text{channels}}} \frac{\pi}{k_\alpha^2} g_J |\delta_{cc'} - U_{cc'}|^2 \tag{1.62}$$

$$= \frac{2\pi}{k_\alpha^2} \sum_J g_J \sum_{l,s} \left[1 - \text{Re}(U^J_{\alpha ls, \alpha ls}) \right] \tag{1.63}$$

In the last expression, U^J is the submatrix of U with channels belonging to spingroup J^π. Elastic cross section and reaction cross section ("reaction" is any reaction other than elastic scattering) can be derived too:

$$\sigma_{el}(E) = \sigma_{\alpha,\alpha}(E) = \frac{\pi}{k_\alpha^2} \sum_J g_J \sum_{\substack{c \in J^\pi \\ \text{incident} \\ \text{channels}}} \left(1 - 2\text{Re}(U_{cc}) + \sum_{\substack{c' \in J^\pi \\ \text{incident} \\ \text{channels}}} |U_{cc'}|^2 \right) \tag{1.64}$$

$$= \frac{\pi}{k_\alpha^2} \sum_J g_J \sum_{s,l} \left(1 - 2\text{Re}(U^J_{\alpha sl, \alpha sl}) + \sum_{s',l'} |U^J_{\alpha sl, \alpha s'l'}|^2 \right) \tag{1.65}$$

$$\sigma_r(E) = \sigma_{\alpha \neq \alpha'}(E) = \sum_J \sum_{\substack{c \in J^\pi \\ \text{incident} \\ \text{channels}}} \sum_{\substack{c' \in J^\pi \\ \text{reaction} \\ \text{channels}}} \frac{\pi}{k_\alpha^2} g_J |U_{cc'}|^2 \tag{1.66}$$

$$= \frac{\pi}{k_\alpha^2} \sum_J g_J \sum_{l,s,l',s'} |U^J_{\alpha ls, \alpha' l' s'}|^2 \tag{1.67}$$

---

[31]g_J indirectly depends on α through I_1 and I_2.

The indication "reaction channel" designates all channels which contribute to the reaction. Note that in both cases α' is well defined ($\alpha' = \alpha$ for elastic scattering) and the sum over channel c and c' is actually a sum over quantum numbers l and s.

Theoretically, the derivation presented here enables the calculation of cross sections as functions of the resonance parameters $\Gamma_{\lambda c}$ and E_λ. However in practice, computations remain uneasy. Indeed, the R matrix has a very large dimension and is hard to invert. Moreover, the resonance parameters must be determined for each channel, which is often not possible experimentally. Some approximations are thus used in the R-Matrix theory, known as *formalisms*. Next part will briefly present the most common approximations of the R-Matrix theory, and the consequences on the cross sections.

1.3.3 Formalisms of the R-Matrix theory

Introducing the level matrix

First of all let us introduce another matrix, known as the *level matrix*, which has as many entries as the number of levels in the compound nucleus. Again, the demonstration of the relation between the level matrix $A_{\lambda\mu}$ and the collision matrix is not detailed here. Let us just say we have the next relations:

$$U_{cc'} = e^{-i(\phi_c + \phi_{c'})} \left[\delta_{cc'} + 2iP_c^{1/2} \left(\sum_{\lambda\mu} \gamma_{\lambda c} A_{\lambda\mu} \gamma_{\mu c} \right) P_{c'}^{1/2} \right] \tag{1.68}$$

$$A_{\lambda\mu}^{-1} = (E_\lambda - E)\delta_{\lambda\mu} - \sum_c \left[\gamma_{\lambda c}(L_c - B_c)\gamma_{\mu c} \right] \tag{1.69}$$

The formalisms of the R-Matrix theory are understandable in terms of the level matrix. First two formalisms are known as Breit-Wigner formalisms. They are not recommended in the resolved resonance range anymore, as they give poor results in some cases (for instance with fissile nuclei [25]) and should be replaced with the third one presented here known as Reich-Moore formalism, or even with the Limited R-Matrix formalism which is very close to the general R-Matrix theory. However, Breit-Wigner formalisms are of particular interest in this document as they are the only formalisms for which parameters are provided in the evaluations for the unresolved resonance range (cf Section 2.1.2).

It must be underlined that ENDF evaluations themselves add several constraints due to the format. This is the case for Multi-Level Breit-Wigner and Reich-Moore formalisms, whose implementations in evaluations are very restrained compared to their theoretical frames.

Multi-Level Breit Wigner formalism

In the Multi-Level Breit Wigner formalism (MLBW), the level matrix is considered as a diagonal matrix. This means the off-diagonal elements of the second term in Equation (1.69) are neglected. Coefficients of the level matrix become:

$$A_{\lambda\mu} = \frac{\delta_{\lambda\mu}}{E_\lambda - E - \Delta_\lambda - \frac{i}{2}\Gamma_\lambda} \tag{1.70}$$

where the level shift Δ_λ and the total width Γ_λ have been introduced so that[32]

$$\Delta_\lambda = \sum_c (S_c - B_c)\gamma_{\lambda c}^2 \tag{1.71}$$

$$\Gamma_\lambda = \sum_c \Gamma_{\lambda c} \tag{1.72}$$

---

[32]As a reminder, the definition of $L_c = S_c + iP_c$ has been used, as well as the relation between the reduced resonance widths and resonance widths. The total width is the same as the one introduced in Section 1.1.3.

The shifted energy level is often introduced as $E'_\lambda = E_\lambda - \Delta_\lambda$. The expression of the cross section for a reaction other than elastic scattering thus becomes:

$$\sigma_{\alpha' \neq \alpha}(E) = \sum_J \underbrace{\sum_{c \in J^\pi}}_{\substack{\text{incident} \\ \text{channels}}} \underbrace{\sum_{c' \in J^\pi}}_{\substack{\text{reaction} \\ \text{channels}}} \frac{\pi}{k_\alpha^2} g_J \sum_{\lambda,\mu} \frac{\Gamma_{\lambda c}^{1/2} \Gamma_{\lambda c'}^{1/2} \Gamma_{\mu c}^{1/2} \Gamma_{\mu c'}^{1/2}}{\left(E'_\lambda - E - \frac{i}{2} \Gamma_\lambda \right) \left(E'_\mu - E + \frac{i}{2} \Gamma_\mu \right)} \tag{1.73}$$

Expanding the summation over μ as in [24], one obtains

$$\sigma_{\alpha' \neq \alpha}(E) = \sum_J \underbrace{\sum_{c \in J^\pi}}_{\substack{\text{incident} \\ \text{channels}}} \underbrace{\sum_{c' \in J^\pi}}_{\substack{\text{reaction} \\ \text{channels}}} \frac{4\pi}{k_\alpha^2} g_J \sum_\lambda \frac{\Gamma_{\lambda,c} \Gamma_{\lambda c'}}{\Gamma_\lambda^2} \left[\text{Re}(C_\lambda^{cc'}) \psi_\lambda + \text{Im}(C_\lambda^{cc'}) \chi_\lambda \right] \tag{1.74}$$

where ψ_λ and χ_λ are the Voigt profiles of the reduced variable $x = \frac{2\left(E'_\lambda - E \right)}{\Gamma_\lambda}$.

$$\psi_\lambda = \frac{1}{1 + x^2} \qquad \chi_\lambda = \frac{x}{1 + x^2} \tag{1.75}$$

$$\text{and} \qquad C_\lambda^{cc'} = 1 + \sum_{\mu \neq \lambda} \frac{\Gamma_{\mu c}}{\Gamma_{\lambda c}} \frac{i \Gamma_\lambda}{\left(E'_\mu - E'_\lambda \right) + \frac{i}{2} \left(\Gamma_\mu + \Gamma_\lambda \right)} \frac{\Gamma_{\mu c'}}{\Gamma_{\lambda c'}} \tag{1.76}$$

For the elastic scattering, a similar equation can be deduced from Equation (1.64):

$$
\begin{aligned}
\sigma_{el}(E) =\ & \frac{4\pi}{k_\alpha^2} \sum_l (2l + 1) \sin^2 \phi_l \\
& + \frac{\pi}{k_\alpha^2} \sum_J g_J \underbrace{\sum_{c \in J^\pi}}_{\substack{\text{incident} \\ \text{channels}}} \left[\sum_\lambda \frac{2(E - E'_\lambda) \Gamma_{\lambda c} \sin(2\phi_l) - 2\sin^2(\phi_l) \Gamma_{\lambda c} \Gamma_\lambda}{\left(E'_\lambda - E \right)^2 + \frac{\Gamma_\lambda^2}{4}} \right] \\
& + \frac{\pi}{k_\alpha^2} \sum_J g_J \underbrace{\sum_{c \in J^\pi}}_{\substack{\text{incident} \\ \text{channels}}} \left[\underbrace{\sum_{c' \in J^\pi}}_{\substack{\text{incident} \\ \text{channels}}} \sum_{\lambda,\mu} \frac{\Gamma_{\lambda c}^{1/2} \Gamma_{\lambda c'}^{1/2} \Gamma_{\mu c}^{1/2} \Gamma_{\mu c'}^{1/2}}{\left(E'_\lambda - E - \frac{i}{2} \Gamma_\lambda \right) \left(E'_\mu - E + \frac{i}{2} \Gamma_\mu \right)} \right]
\end{aligned} \tag{1.77}
$$

The first term of the sum is the *potential elastic scattering*, while the second and third ones are the resonant components of the elastic cross section. It is possible to rewrite this equation as a function of the Voigt profile, using the previous notation $C_\lambda^{cc'}$:

$$
\sigma_{el}(E) = \frac{4\pi}{k_\alpha^2} \sum_l (2l + 1) \sin^2 \phi_l + \frac{4\pi}{k_\alpha^2} \sum_J g_J \underbrace{\sum_{c \in J^\pi}}_{\substack{\text{incident} \\ \text{channels}}} \sum_\lambda \frac{\Gamma_{\lambda c}}{\Gamma_\lambda}.
$$

$$
\left\{ \psi_\lambda \left[(\cos(2\phi_c) - 1) + \underbrace{\sum_{c' \in J^\pi}}_{\substack{\text{incident} \\ \text{channels}}} \frac{\Gamma_{\lambda c'}}{\Gamma_\lambda} \text{Re}(C_\lambda^{cc'}) \right] + \chi_\lambda \left[-\sin(2\phi_c) + \underbrace{\sum_{c' \in J^\pi}}_{\substack{\text{incident} \\ \text{channels}}} \frac{\Gamma_{\lambda c'}}{\Gamma_\lambda} \text{Im}(C_\lambda^{cc'}) \right] \right\} \tag{1.78}
$$

Single-Level Breit Wigner formalism

The simplest approximation of the R-Matrix theory is known as the Single Level Breit Wigner (SLBW) formalism. In this approximation, interferences between the energy levels are

neglected. Each level is considered as it was alone. Mathematically, applying this formalism is equivalent to considering that the level matrix is a scalar. Equation (1.69) simply becomes

$$\frac{1}{A} = E_\lambda - E - \Delta_\lambda - \frac{i}{2}\Gamma_\lambda \tag{1.79}$$

The expression of the cross sections for the SLBW formalism are the same than in the MLBW case, with $C_\lambda^{cc'} = 1$.

Reich-Moore formalism

The Reich-Moore formalism is the most often used in evaluations in the resolved resonance range. It consists in neglecting the off-diagonal elements of the second term in Equation (1.69), but only for channels with photons. These channels correspond to a radiative capture. This might be understood as follows: during a radiative capture, there are many possibilities for the compound nucleus to decay releasing a photon and so, many radiative capture channels. As there are many channels it is possible to assume that their resonance widths are small compared to the level width. Moreover it is possible to suppose (following an hypothesis from Bethe) that the reduced widths have uncorrelated signs. Statistically, the contribution of the photon channels is on the diagonal only. The expression of the level matrix coefficients becomes:

$$A_{\lambda\mu}^{-1} = (E'_\lambda - E - i\frac{\Gamma_{\lambda c}}{2})\delta_{\lambda\mu} - \sum_{c\notin\gamma}[\gamma_{\lambda c}(L_c - B_c)\gamma_{\mu c}] \tag{1.80}$$

$$E'_\lambda = E_\lambda - \Delta_\lambda \quad \text{and} \quad \Delta_\lambda = \sum_{c\in\gamma}\left[\gamma_{\lambda c}^2(L_c - B_c)\right] \tag{1.81}$$

The computation of cross sections requires now a matrix inversion, which is slightly[33] more expensive than a sum like in the MLBW formulas. However Reich-Moore formalism handles channels interference, which is very useful for fission reactions[34].

1.3.4 Doppler-broadening methods

Cross sections usually need to be Doppler-broadened to take into account the temperature effects as presented in Section 1.1.4. The equation dealing with the Doppler effect is well-known and has been established for instance in [26]. The main idea is to perform a convolution product between the target nucleus velocity field and the cross section at 0K. In the resonance range, it is possible to neglect the binding of the target nucleus within the structure it belongs to (a crystal or a molecule for instance), and consider that we are faced to a perfect gas. These effects cannot be ignored at lower energies [21] where the neutron energy is comparable to the chemical binding energies. Lamb [27] showed that the velocity field $p(\vec{V})$ of a huge number of target nuclei at temperature T follows a Boltzmann distribution with an effective temperature:

$$p(\vec{V}) = \left(\frac{\beta}{\pi}\right)^{\frac{3}{2}} e^{-\beta V^2} \tag{1.82}$$

with $\beta = \frac{M}{2kT}$, M the mass of the target nucleus, k the Boltzmann constant. With such an hypothesis, the computation of the cross section at temperature T, σ_T, can be performed from the cross section at 0K. Calling E_r the energy in the center of mass and E the energy in the lab referential,

$$\sigma_T(E) = \frac{1}{E}\sqrt{\frac{\alpha}{4\pi}} \int_0^\infty \sqrt{E_r}\sigma_0(E_r)\left[e^{-\alpha(\sqrt{E}-\sqrt{E_r})^2} - e^{-\alpha(\sqrt{E}+\sqrt{E_r})^2}\right] dE_r \tag{1.83}$$

---

[33]In practice the matrix to invert has only three entries due to the ENDF limitations.

[34]Fission reactions happen usually through two or three intermediary channels.

$$\text{using} \quad \alpha = \frac{A}{kT} \quad \text{and} \quad A = \frac{M}{m} \tag{1.84}$$

This equation is known as the Solbrig equation. Several methods to solve this equation have been developed.

Method SIGMA1

The most well-known approach is the SIGMA1 method [20], used by NJOY in its module BROADR (cf Section 1.2.3). It uses the linearized reconstructed cross sections at 0K. A linearized cross section is tabulated as a set of (E_i, σ_i) values on a grid thin enough so that each value of the cross sections between the tabulated points can be approximated with a linear interpolation. If $E_i < E < E_{i+1}$, $\sigma_0(E)$ can be calculated as:

$$\sigma_0(E) = \sigma_0(E_i) + \frac{\sigma_0(E_{i+1}) - \sigma_0(E_i)}{E_{i+1} - E_i}(E - E_i) = A_i + B_i E \tag{1.85}$$

Introducing this expression of the cross section at 0K in Equation (1.83), one obtains:

$$\sigma_T(E) = \frac{1}{E}\sqrt{\frac{\alpha}{4\pi}} \sum_i \int_{E_i}^{E_{i+1}} \sqrt{E_r}(A_i + B_i E_r) \left[e^{-\alpha(\sqrt{E}-\sqrt{E_r})^2} - e^{-\alpha(\sqrt{E}+\sqrt{E_r})^2} \right] dE_r \tag{1.86}$$

It is then possible to solve this equation analytically, expressing this integral as a linear combination of simple error functions. The error achieved with this method is due to the linearization of the cross section, but does not impact much the results if the cross section has been properly linearized, as proved in [28].

Method $\psi - \chi$

This method is of particular importance for our purposes. It is only applicable when σ_0 is computed with the Breit-Wigner formalism, and assumes that only the energies around the point of calculation contribute to the integral in Equation (1.83). Latter hypothesis can be formalized with the next three assumptions:

- The second exponential term in Equation (1.83) is neglected, ie. $\alpha\sqrt{EE_r} \gg 1$. It cannot be applied at low energies where it tends to underestimate the contribution of small E_r, but rapidly becomes acceptable at higher energies. Actually, this hypothesis is not so restrictive.

- It is possible to develop $\sqrt{E_r}$ as a Taylor series around E, so that

$$\alpha(\sqrt{E} - \sqrt{E_r})^2 \approx \left(\frac{E - E_r}{\Delta}\right)^2 \quad \text{with} \quad \Delta = \sqrt{\frac{4E}{\alpha}} = \sqrt{\frac{4EM}{kT}} \tag{1.87}$$

  Δ is referred to as the Doppler width. This approximation is acceptable at high energies. For instance, reference [29] provides a table of comparison between $e^{-\alpha(\sqrt{E}-\sqrt{E_r})^2}$ and $e^{-\left(\frac{E-E_r}{\Delta}\right)^2}$ as a function of αE. It appears that the error is less than 1% when $\alpha E > 10^6$, which for instance corresponds to $E = 100$ eV for ^{238}U at room temperature.

- Negative E_r contribution to the integral is neglected, so that $\int_0^\infty dE_r = \int_{-\infty}^\infty dE_r$. Accordingly, this hypothesis is less restrictive than the second one.

With all these hypotheses Equation (1.83) becomes:

$$\sigma_T(E) = \frac{1}{E}\sqrt{\frac{\alpha}{4\pi}}\int_{-\infty}^{\infty}\sqrt{E_r}\sigma_0(E_r)e^{-\left(\frac{\sqrt{E}-\sqrt{E_r}}{\Delta}\right)^2}dE_r \tag{1.88}$$

The main idea of the $\psi - \chi$ method is to use this approximated kernel with a Breit-Wigner shaped cross section in which the Voigt profiles $\psi = \frac{1}{1+x^2}$ and $\chi = \frac{x}{1+x^2}$ appear, such as in the formulas of Section 1.3.3. Assuming that $\Gamma_{\lambda c}$, ϕ_c, P_c and S_c are slowly-varying functions of the energy so that they can be considered constant for the integration, the Doppler broadening is only applied to the ψ and χ functions. The broadened $\tilde{\psi}_\lambda$-$\tilde{\chi}_\lambda$ functions can be rewritten as the real and imaginary part of the Faddeeva function w [30]:

$$w(z) = e^{-z^2}\text{erfc}(-iz) = e^{-z^2}\left(1 + \frac{2i}{\sqrt{\pi}}\int_0^z e^{t^2}dt\right) \tag{1.89}$$

$$\tilde{\psi}_\lambda = \frac{\sqrt{\pi}}{2\zeta}\text{Re}\left[w\left(\frac{x}{2\zeta}, \frac{1}{2\zeta}\right)\right] \tag{1.90}$$

$$\tilde{\chi}_\lambda = \frac{\sqrt{\pi}}{2\zeta}\text{Im}\left[w\left(\frac{x}{2\zeta}, \frac{1}{2\zeta}\right)\right] \tag{1.91}$$

$$\text{using} \quad x = \frac{2(E'_\lambda - E)}{\Gamma_\lambda} \quad \text{and} \quad \zeta = \frac{\Delta}{\Gamma_\lambda} \tag{1.92}$$

The Faddeeva function belongs to the large family of the error functions, and many available libraries enable its precise calculation at high speed. The $\psi - \chi$ method is of particular importance for this work, as it enables the fast computation of the Doppler effect at a single energy (while the SIGMA1 requires to use a tabulated cross section on an energy grid) from Breit-Wigner analytical forms. In particular, its main defaults (weak precision at low energies, Breit-Wigner formalism only) are not as critical in the unresolved resonance range which starts at relatively high energies (for instance it starts at $E = 20$ keV for ^{238}U in the JEFF-3.2 library, to be compared with $E = 100$ eV evoked previously), and still relies on the Breit-Wigner formulas.

1.3.5 Referential of the laboratory

All R-Matrix formulas have been established as functions of the energy in the center of mass referential. In practice, resonance parameters are provided in ENDF evaluations in the laboratory referential where cross sections must be computed as well. As a consequence, previous formulas have to be converted in the lab referential. In the center of mass referential, the kinetic energy of the system neutron is $E^{cdm} = \frac{1}{2}\mu v_r$, μ being the reduced mass of the system and v_r the relative speed between the neutron and the target nucleus. In the lab referential, nucleus is at rest for now (T = 0K) so that $E^{lab} = \frac{1}{2}mv_r$, and so:

$$E^{lab} = \frac{m+M}{M}E^{cdm} \tag{1.93}$$

All formulas remain true when the energy in the lab referential is used (by now marked E) under condition that the resonance parameters and channel wavenumber k_α are replaced with the next formulas:

$$E_\lambda^{lab} = \frac{m+M}{M}E_\lambda^{cdm} \tag{1.94}$$

$$\gamma_{\lambda c}^{lab} = \sqrt{\frac{M}{m+M}}\gamma_{\lambda c}^{cdm} \tag{1.95}$$

$$k_\alpha = \frac{M}{m+M}\sqrt{\frac{2m|E|}{\hbar}} \tag{1.96}$$

Unresolved resonance range processing

As seen in previous chapter, it is observed that as the energy increases, resonances get closer and closer until experimental resolution is insufficient to separate them (unresolved resonance range), and until they finally overlap (continuum). In the unresolved resonance range, resonances can no longer be experimentally distinguished but a resonance structure can still be observed in the cross section. Evaluators can no longer access the particular detail of each resonance. On the other hand, they are still able to access their statistical behavior. More precisely, for resonances belonging to a same spingroup J^π, the individual knowledge of resonance energies E_λ is replaced by average values, in particular the *average level spacing* between resonances often noted $\langle D_J \rangle_\lambda$. In the same way, resonance widths are given as averaged values. These information characterize ensembles of resonances, and are thus provided at arbitrary tabulated reference energies along the unresolved resonance range. Average level spacings and average widths are energy-dependent; it is the role of the evaluator to estimate a proper energy mesh on which tabulated average parameters can reproduce the average cross sections.

In practice, average resonance parameters are often obtained using a combination of information from the resolved resonances and tools mainly used in the continuum, such as averages from optical models. The approach in use in the unresolved resonance range is based on the compound nucleus model though: resonance parameters are given in the R-Matrix formalism. Formulas and methods developed in this chapter to compute cross sections stem from the theoretical developments exhibited in the previous chapter.

Experimentally-obtained average resonance parameters are not the only available knowledge at our disposal in the unresolved resonance range. Indeed, assumptions based on experimental observations first, and then theoretical developments have led to a complete statistical theory of resonances, and in particular to a relevant description of the statistical distribution laws followed by the resonance parameters. For now, let us assume the next results:

- The spacing between resonances from the same spingroup follows a distribution known as the *Wigner surmise* [31], defined by:

$$p(x)dx = \frac{\pi}{2}xe^{-\frac{\pi}{4}x^2}dx \tag{2.1}$$

  which is actually a Rayleigh distribution with parameter $\sigma = \sqrt{\frac{2}{\pi}}$. This law was first introduced by Wigner, who modified a Poisson process to introduce a level repulsion to match experimental observations[1]. Almost surprisingly, it turned out to match the

---

[1]This point is addressed in more detail in Section 4.1.1.

experimental data admirably.

- The reduced widths $\gamma_{\lambda c}$ follow a normal centered law. This hypothesis has been first introduced by Porter and Thomas [32]. The $\gamma_{\lambda c}$ are values of the internal radial eigenfunction on the channel surface, as defined in Equation (1.45). The integrands in Equation (1.45) are supposed to be strongly oscillating with random signs [14], so that the integral is supposed to be close to 0, with finite variance $\langle \gamma_{\lambda c}^2 \rangle$. With so little information available on the system, supposing that $\gamma_{\lambda c}$ follow a normal centered law sounded like a reasonable guess[2]. Resonance widths are related in quadratic manner to the reduced widths $\Gamma_{\lambda c} = 2P_c \gamma_{\lambda c}^2$ with penetrability supposed to be a slowly-varying function of energy. Summing over the channels contributing to a reaction, the reaction width is a sum of squares of normal centered laws. As a consequence, the reaction widths follow χ^2-law whose degree of freedom ν is the number of open channels for the reactions:

$$\chi_\nu^2(x)dx = \frac{\nu}{2\Gamma\left(\frac{\nu}{2}\right)} \left(\frac{\nu x}{2}\right)^{\nu/2-1} e^{-\nu x/2} dx \tag{2.2}$$

In this expression, Γ designates the classical Γ special function[3]. In case a single channel is open for the reaction ($\nu = 1$), the expression of the χ^2-law is sometimes referred as the Porter-Thomas distribution:

$$p(x)dx = \frac{e^{-x/2}}{\sqrt{2\pi x}} dx \tag{2.3}$$

The Wigner and χ^2 distributions are displayed on Figure 2.1. Actually, they proved to be derived from a more general theoretical framework, the random matrix theory (RMT), a rich mathematical field which was pioneered notably by Wigner before being applied to many other domains. The main idea is to replace the unknown Hamiltonian of the system by a very large (infinite) matrix with random coefficients, to explore its statistical spectral properties. Mandatory symmetries of the Hamiltonian enabled to define a remarkable ensemble of random matrices, the Gaussian Orthogonal Ensemble (GOE) whose spectral distributions matched the resonance parameters behavior. In particular, the Wigner law appeared as the statistical distribution of the spacing between eigenvalues of random matrices of the GOE of size 2x2. This particular topic will be addressed in more detail in Chapter 4.

In brief, even if the individual resonance parameters are not provided in the unresolved resonance range, knowledge of average values and statistical distributions have proven to be a turning point in the processing capabilities based on the R-Matrix formalism. Admittedly, cross sections cannot be computed as pointwise functions of energy, but other representations remain available. First, the R-Matrix theory has been adapted to compute mean cross sections in the unresolved resonance range. Secondly, fluctuations of the cross sections can be captured by the *ladder method*, whose main point is to sample sets of resonances from their known statistical distributions. Resolved R-Matrix formulas can then be applied to obtain samples of cross sections values, from which probability tables can be computed.

The main goal of this document is to describe and estimate the relevance of these techniques. In the next part, we will present the ENDF-6 format in which resonance parameters are stored, and most of the matters to consider when processing evaluated data. Then, details of the mean R-Matrix theory to compute average cross sections in the unresolved resonance range will be briefly exposed. Finally, the ladder method and its related sources of uncertainty will be listed. Let us already underline that the validity of the ladder method will be the main topic of the next chapters.

---

[2]Actually, it is the most conservative choice following the maximum entropy principle of probability theory [30].
[3]It must not be confused with the resonance width.
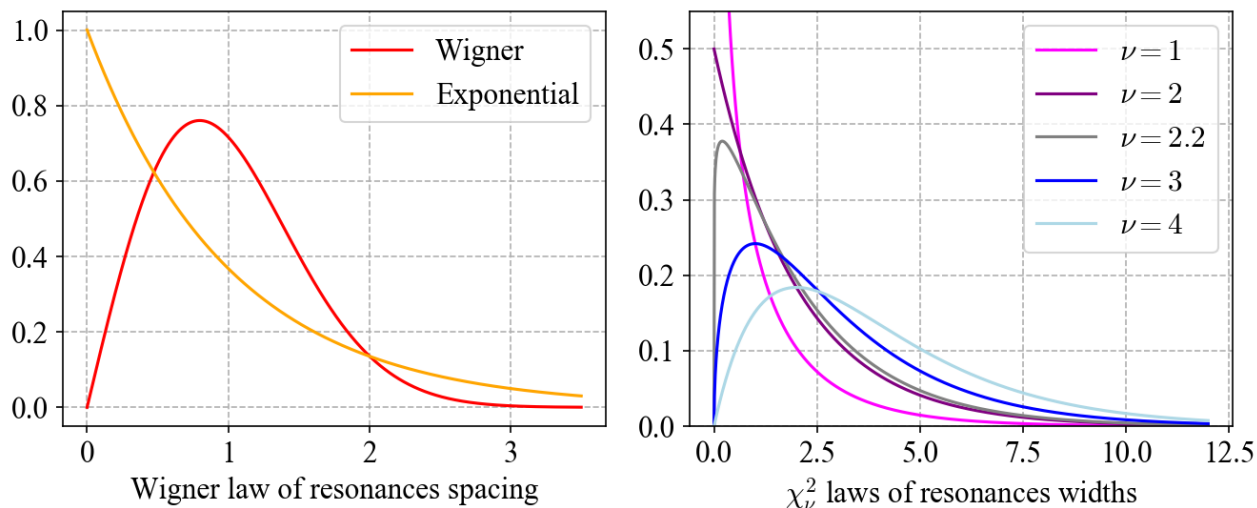
Figure 2.1: On left, the Wigner probability distribution for the resonances spacing, superposed to the exponential distribution (Poisson process) for comparison. On the right, several χ^2-distributions with various degrees of freedom, that are used to sample resonance reaction widths.

2.1 From theoretical framework to ENDF evaluations representation

Evaluated nuclear data are usually stored in Evaluated Nuclear Data Format (ENDF) files. These data are meant to be processed before any use in neutronics codes. The ENDF format was developed at times when computer resources were scarce. It does not permit a full representation of the underlying physics of the neutron-nucleus interaction process. The structure of an ENDF tape has already been shortly introduced in Section 1.2.2. In particular, for cross sections computations in the resonance ranges[4] only two ENDF files are required, MF2 and MF3. Resonance parameters (resonance widths and energies, or spacings for the unresolved range case) are provided in MF2, along with the target spin, and channel radii. File MF3 contains energy-tabulated cross sections whose interpretation relies on the nature of the considered range and flags in MF2.

MF2 file is separated into special formatted subsections, each defining a particular energy range. They start with a "header", typically three or four dedicated lines. These headers contain two float values to define the energy range limits, and several flags to indicate the nature and the format of the data it stores. In particular the flag LRU=1 is used to mark the beginning of a resolved resonance range, and LRU=2 marks the start of an unresolved resonance range[5].

Resonance parameters are always provided with an indication on the formalism meant to be employed to compute cross sections[6], and corresponding formulas must be used. Indeed, evaluators actually provide resonance parameters in adequacy with a suggested formalism. Care must be taken when generating cross sections from resonance parameters. The processing must follow the resonance formalism indicated by the evaluation.

The range of applications of the ENDF-formatted resonance parameters may be quite limited compared to what the R-Matrix theory actually enables, both for resolved and unresolved parameters. It should be noticed that these limitations are not due to the format only but also to an evaluator's lack of abilities to properly characterize each resonance.

---

[4]Both resolved and unresolved.

[5]Nothing forbids successive ranges of the same type (for instance several ranges defined with different formalism) but usually there is a single resolved resonance range possibly followed by an unresolved resonance range

[6]For instance for resolved ranges, the LRF flag indicates the formalism in use.

In the unresolved resonance range, the only formalism permitted in ENDF evaluations is the SLBW formalism. This formalism is not very powerful, and is even more weakened by the ENDF formatting. Next section details the resolved Breit-Wigner formalism (actually both SLBW and MLBW, which share the same ENDF format) and their ENDF interpretation.

2.1.1 ENDF resolved range Single-Level Breit-Wigner format

Open channels

In a Breit-Wigner-formatted resolved resonance range, only three reaction channels are open for each (l, J, s), which constitutes a first limitation. There is one for elastic scattering (which is thus the input channel), one for fission, and one for radiative capture. Cross sections can be computed from resonance parameters for these three reactions only, each being described with only a single partial width. In order to take into account the influence of all other reactions and channels, a competitive width may be provided to be added to other partial reaction widths to retrieve the total width. Note that there is no cross section computed for this competitive reaction, as it is not a proper reaction in itself.

A second main restriction concerns the quantum numbers. The ENDF format first considers that the l quantum number is conserved during a reaction. Moreover, as it is often very hard to distinguish between resonances with different channel spin s, widths are actually summed over s. This is a turning point in the way calculations are performed, and in the manner resonance parameters are defined. Notably, resonances are no longer classified into spingroups J^π, but are allocated to a spin sequence (J^π, l). As a consequence, $\sum_{l,l',s,s'} = \sum_l$, and resonance parameters are provided according to (l, J^π) sequences. Usually, the parity is dropped, and such spin sequences are called spingroups as well, for convenience.

A common practice in ENDF is to work with reaction resonances: channel c is replaced with reaction y and level λ with resonance r so that:

$$\Gamma_{\lambda c} \to \Gamma_{yr} \quad \text{defined for each } (l, J) \text{ spin sequence.} \tag{2.4}$$

The adopted notations for the widths are $\Gamma_{\gamma r}$ for the radiative capture, Γ_{fr} for the fission, and Γ_{nr} for the elastic scattering reaction. Γ_{nr} may be called the neutron width as it is the only width associated to entrance channels. The total width is written Γ_r, and is the sum of these three reaction widths plus the competitive width Γ_{xr}, if provided. The resolved range SLBW formulas[7] described in Section 1.3.3 simply become with these notations:

$$\sigma_\gamma(E) = \frac{\pi}{k_\alpha^2} \sum_J g_J \sum_l \sum_r \frac{\Gamma_{\gamma r}\Gamma_{nr}}{\Gamma_r^2}\psi_r \tag{2.5}$$

$$\sigma_f(E) = \frac{\pi}{k_\alpha^2} \sum_J g_J \sum_l \sum_r \frac{\Gamma_{fr}\Gamma_{nr}}{\Gamma_r^2}\psi_r \tag{2.6}$$

$$\sigma_{el}(E) = \frac{4\pi}{k_\alpha^2} \sum_l (2l+1)\sin^2(\phi_l) + \frac{4\pi}{k_\alpha^2} \sum_J g_J \sum_l \sum_r \frac{\Gamma_{nr}}{\Gamma_r}\left[\left(\cos(2\phi_l) - 1 + \frac{\Gamma_{nr}}{\Gamma_r}\right)\psi_r - \sin(2\phi_l)\chi_r\right] \tag{2.7}$$

where ψ_r and χ_r are the Voigt profiles, whose expression shall be adapted according to the temperature value.

As a reminder, in the previous expression the reaction widths are supposedly energy dependent through penetrability. Penetrabilities in the ENDF format however, are chosen to

---

[7]MLBW formulas could be adapted in the same manner. Let us underline that this format is even more gutted in practice, as MLBW ENDF files indicate that only the elastic scattering cross section must be reconstructed using the MLBW formula, while fission and capture must be computed with SLBW formulas.

be constant equal to 1 for capture and fission widths, so that resonance widths are energy-independent for these reactions. The ENDF format provides resonance widths at the resonance energies, GN_r, GG_r and GF_r, so that[8]:

$$\begin{aligned}
GN_r &= \Gamma_{nr}(|E_r|) = 2P_l(|E_r|)\gamma_{nr}^2 \\
GG_r &= \Gamma_{\gamma r}(|E_r|) = 2\gamma_{\gamma r}^2 \\
GF_r &= \Gamma_{fr}(|E_r|) = 2\gamma_{fr}^2
\end{aligned} \tag{2.8}$$

As a consequence, only the neutron width and total width are energy-dependent in Equations (2.5)–(2.7). The next relation holds:

$$\Gamma_{nr} = \Gamma_{nr}(|E_r|)\frac{P_l(|E|)}{P_l(|E_r|)} \tag{2.9}$$

The explicit dependence in E for the neutron width is usually dropped, and precised when the neutron width is computed at a resonance energy.

Neutron penetration factor and shifts factors

In previous equations, the hard-sphere penetration factor P_c has been indexed with l instead of c for neutron elastic scattering. Actually, although it depends on α through the channel radius and the channel wavenumber, its expression can be established as a function of $\rho = k_c a_c = k_\alpha a_\alpha$ for successive l values, which justifies this notation. The same applies for level shift S_c and hard-sphere phase shift ϕ_c. Table 2.1 summarizes the expressions of penetrabilities and shifts as functions of ρ.

l	$P_l(\rho)$	$S_l(\rho)$	$\phi_l(\rho)$
0	ρ	0	ρ
1	$\dfrac{\rho^3}{\rho^2+1}$	$\dfrac{-1}{\rho^2+1}$	$\rho - \arctan(\rho)$
2	$\dfrac{\rho^5}{\rho^4+3\rho^2+9}$	$\dfrac{-3\rho^2-18}{\rho^4+3\rho^2+9}$	$\rho - \arctan(\frac{3\rho}{3-\rho^2})$
$l+1$	$\dfrac{\rho^2 P_l(\rho)}{P_l^2(\rho)+(l+1-S_l(\rho))^2}$	$\dfrac{\rho^2(l+1-S_l(\rho))}{P_l^2(\rho)+(l+1-S_l(\rho))^2} - (l+1)$	

Table 2.1: Penetrabilities, shifts and phase shifts for several l-values. Here, $\rho = k_c a_c$.

Channel radius

Calculating the channel radius is possible from the information contained in the evaluations, with some restrictions in the SLBW format. Actually, two radii may be used, namely the "true" radius and the "effective" (or scattering) radius, in order to compensate for the effect of distant resonances. The true radius is meant to be used in the calculation of penetrability and shift factors P_c and S_c, while the scattering radius is used in the phase shift ϕ_c calculations. In the Breit-Wigner formatted values, the ENDF evaluation does not provide a value for both radii. Instead, it provides a single value AP, and relies on flags NRO and NAPS to detail its use in calculations. In the most common case (NAPS=0), AP corresponds to the scattering radius,

---

[8]The absolute value takes into account the possible negative resonance energies (bound levels), which are unreachable resonances of the compound nucleus. They structure the cross sections, but their energy is below the kinetic neutron energy, and thus negative.

and the true radius is computed from a formula from Lynn [33], so that the channel is slightly larger than the compound nucleus radius[9]:

$$a_c = 0.123A^{1/3} + 0.08 \qquad (2.10)$$

where A is the mass of the target nucleus in atomic mass unit[10]. Sometimes, the AP value provided in the evaluation is supposed to be used for both true and effective radius (NAPS=1). It must be highlighted that for both cases the radii provided are not channel-dependent. This is not the case for all ENDF formalisms[11].

In practice, both these methods are well used. Anticipating a little bit, one can already precise that the same flags and values are in use in the unresolved resonance range, and for example Figure 2.2 displays for all the isotopes of JEFF-3.2 with an unresolved resonance range, the mass against the channel radius. All values out of the $a_c \approx M^{1/3}$ line correspond to cases for which the channel radius is directly provided in the evaluation.
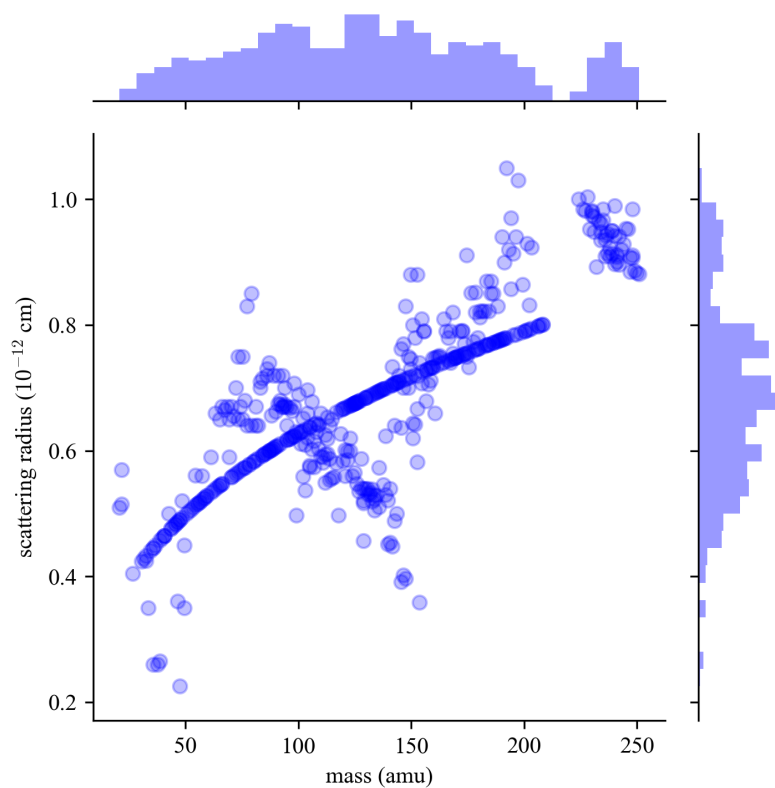
Figure 2.2: Mass and scattering radius for isotopes with an unresolved range in JEFF-3.2

To be slightly more flexible, an additional radius as a tabulated function of energy may be provided, even if it is very rare. For instance in library JEFF-3.2, only one isotope out of 307[12] was evaluated using this feature (^{197}Au). If such a tabulated function is provided, the AP(E) value replaces the provided scalar AP value except for the special case NAPS=2, where the scalar AP defines the true radius and AP(E) the scattering radius.

---

[9]As stated in Section 1.3.2, the R-Matrix theory defines the channel radius as a distance above which interacting nuclei can be clearly differentiated (and the interaction is only a central force). Once a radius value a_c is determined, any value greater than a_c could be an acceptable channel radius. Of course once a channel radius has been set, the associated resonance parameters depend on it.

[10]ie. it is the ratio of the target mass to the neutron mass

[11]In particular ENDF LRF=7 (R-Matrix Limited) format enables the use of a radius for each channel.

[12]In this library, an unresolved resonance range was defined for 307 isotopes out of 473.

Boundary condition

In the ENDF files SLBW-formatted data the boundary condition $B_c = S_c$ has been chosen, in agreement with the Wigner-Eisenbud R-Matrix parametrization, but this choice is particular to each resonance. For resonance r, the choice is made to set $B_c = S_l(|E_r|)$. This is a calculation artifact, which enables the resonance shift to be null for s-wave resonances. This choice implies that the resonance energy shift E'_r depends on E in the following manner:

$$E'_r - E_r = (S_l(|E|) - S_l(|E_r|)) \frac{\Gamma_{nr}}{2P_l(|E|)} \tag{2.11}$$

As a reminder, only the elastic scattering (associated to the neutron width Γ_{nr}) is an input channel, which explains this formula. Moreover, it is clear from the expressions of S_l in Table 2.1 that the resonance shift will be null for s-wave ($l = 0$) at any energy.

Competitive width

In order to take into account the influence of all other reactions and channels, a competitive width GX_r may be provided in ENDF evaluations for resonance r and spin sequence (l, J), to be added to other partial reaction widths to compute the total width. With explicit dependence on energy, the total resonance width must be computed as

$$\Gamma_r(E) = \Gamma_{nr}(E) + \Gamma_{\gamma r} + \Gamma_{fr} + \Gamma_{xr}(E) \tag{2.12}$$

Note that there is no cross section computed for the competitive reaction. This width is irrelevant for formalism different from SLBW or MLBW. In practice, it is meant to represent a possibly open decay channel for the inelastic scattering to the first level only (reaction MT51 in ENDF format). It depends on the energy through the penetrability in the same way than the elastic scattering, except for the inelastic scattering threshold energy E^*:

$$\Gamma_{xr}(E) = \Gamma_{xr}(|E_r|) \frac{P_l(|E - E^*|)}{P_l(|E_r - E^*|)} \qquad \text{if} \quad E \geq E^* \tag{2.13}$$
$$= 0 \qquad \text{otherwise}$$

The inelastic threshold energy E^* can be computed from the excitation energy QX provided in File MF2, so that $E^* = \frac{M+m}{M} QX$. Strictly speaking, competitive widths are rarely used in the resolved range (there is not a single one in JEFF-3.2), where the inelastic scattering channel is rarely open. However, it will be useful for our applications in the unresolved resonance range.

Background cross sections

Evaluators may provide "background cross sections" in the ENDF File MF3, to be added to the reconstructed cross sections from resonance parameters, for total, elastic, capture, and fission reactions. Background cross sections play a role to correct the resonant cross sections obtained from Equations (2.5)–(2.7) in order to match the experimental data. They are supposed to hold only a tiny fraction of the cross sections. In particular, they are used along calculations performed at 0K, while their values derive from comparisons with experimental measurements at room temperatures. The error is assumed to be unimportant if the background is small and does not structure the shape of the cross section.

Before describing the ENDF format in use for the unresolved resonance range, let us briefly mention that not only Breit-Wigner formalisms suffer from the ENDF limitations: Reich-Moore formalism, which is the most-used formalism in the resolved resonance range, is only used to compute capture, fission, and elastic scattering cross sections as well. The conservation of l is also assumed, along with the conservation of s. Two channels are open for fission, one for capture

and one for elastic scattering. The main advantage of this formalism is a better description of the fission channels, as two widths are provided. The calculation of cross sections from resonance parameters for more reactions require the use of a more developed formalism, the R-Matrix Limited Formalism, which enables the evaluator to provide more resonance parameters.

2.1.2 The unresolved resonance range in the ENDF format

Energy-tabulated values

In the unresolved resonance range, the well-defined resonance parameters are replaced with average values, provided at *reference energies*. It must be stressed that these energies do not correspond to resonances, but to arbitrary tabulated values chosen in the range by evaluators in order to describe the statistics of surrounding resonances. Ideally, evaluators aim at choosing an energy mesh thin enough so that computed quantities are accurate along the whole interval. Parameters can be furnished on a grid in three manners in the ENDF format, according to the values taken by flags LRF and LFW:

- LRF = 1 and LFW = 0: parameters are supposed to be energy-independent, and a single set is provided for the whole energy range. No fission width is provided.

- LRF = 1 and LFW = 1: same as previously, except for average fission widths, which are given at several tabulated energies.

- LRF = 2: all parameters are energy-dependent tabulated quantities. In that case, an interpolation scheme is also provided.

As it will be described in Section 2.2, the calculations of average cross sections can be achieved at these reference energies. In order to perform calculations between the tabulated energies, two interpolations may be considered: an interpolation between computed cross sections, or more physically, an interpolation on resonance parameters prior to the cross sections calculations. For a long time, the ENDF manual [2] recommended the interpolation to be performed on cross sections. It turned out that this prescription was a mistake, and led to differences up to 10% between processing codes, for instance between NJOY and PREPRO [34]. Such differences arise when the energy mesh chosen by the evaluator is too loose. It is now widely accepted that interpolation should be performed on parameters rather than cross sections, and codes which followed the former ENDF recommendation have changed their practice.

Average parameters

In the ENDF evaluations, a single data formatting is available to describe the unresolved resonance parameters at designated reference energies, which obeys the same limitations than the resolved Breit-Wigner formalisms. For this reason it is said quite often that SLBW is the only formalism allowed in the unresolved resonance range, even if Equations (2.5)–(2.7) do not apply directly. The form of the parameters resemble a lot the resolved Breit-Wigner formalism: only four (average) widths are provided, corresponding to elastic scattering, capture, fission, plus an average competitive width to take into account other channels effects. As a consequence, only elastic, capture, fission and so total cross sections can be computed. The computation of penetration and shifts factors, as well as the calculation of channel radius follows the same procedures than the resolved range Breit-Wigner format. For instance, the same flags NRO and NAPS rule the calculation of the channel radius. Moreover, conservation of l is assumed, and averages are summed over s-values, so that average parameters are given as (l, J) sequences[13].

---

[13]The number of values l (increasing integers from 0) is provided in the evaluation with flag NLS, and for each l-value, the associated J values to consider are provided too.

The main difference lies in the statistical nature of the provided data. Experimentally, averaging over many levels is a complex task, which leads to a definition of resonance parameters not exactly alike the previous resolved Breit-Wigner formats. In the following, an average over many levels with same quantum numbers is marked with a bar. For example, an average over (l, J) instances is noted $\overline{X}^{lJ} = \langle X \rangle_\lambda^{lJ}$. For each reference energies in the unresolved range and (l, J) spingroups are given:

- $\overline{D}^{lJ}$, the average spacing between resonances. As l is conserved in a reaction, each resonance is associated to a single J and l value. As a consequence, the spacing between resonances of the same (l, J) sequence follows a Wigner distribution.

- $\overline{\Gamma_n^0}^{lJ}$, an average *reduced* neutron width. Providing an average reduced width instead of an average neutron width is justified, as the neutron width depends on the energy through the penetration factor (which is not the case for capture and fission in the ENDF format), while the reduced neutron width does not.

- $\overline{\Gamma_\gamma}^{lJ}$, an average γ width;

- $\overline{\Gamma_f}^{lJ}$, an average fission width;

- $\overline{\Gamma_x}^{lJ}$, an average competitive width. As in the resolved Breit-Wigner formalism, the competitive width corresponds to an inelastic scattering to the first excited level. Unlike the resolved case, the competitive width is quite frequent in the unresolved resonance range, where the inelastic scattering becomes an important reaction. Its associated penetrability is defined as in Equation (2.13), but there, no threshold value QX is given in the ENDF file for the unresolved resonance range. Thus, it is assumed that the corresponding QX value is to be looked at File MF3 section MT51, which corresponds to the first inelastic scattering. If another reaction such as (n, p) or (n, α) had a threshold below the inelastic scattering, it is expected that its contribution is not taken into account in $\overline{\Gamma_x}^{lJ}$. The missing QX entry in the URR-format is a defect of the ENDF standard, due to the lack of space in files.

Unlike the resolved Breit-Wigner case, in the unresolved resonance range the *reduced* neutron width is rather provided than the neutron width, and its relationship with the neutron width follows the experimental definition instead of the theoretical one $\Gamma = 2P_c\gamma^2$:

$$\Gamma_{\lambda,n,lJs}(E) = \Gamma_{\lambda,n,lJs}^0 \sqrt{E} \frac{P_l(E)}{\rho} \tag{2.14}$$

Let us establish the relationship between the average reduced neutron width and the average neutron width. Like in the resolved case, we can suppose that entrance channels for same (l, J) values may contribute incoherently, so that [35]:

$$\Gamma_{n,lJ}^0 = \sum_s \Gamma_{n,lJs}^0 = \mu_{lJ} \Gamma_{n,lJs}^0 \tag{2.15}$$

where μ_{lJ} is the neutron multiplicity, which corresponds to the number of open channels for the (l, J) couple, ie. to the number of possible s values. Reachable s values must follow the rule $\vec{J} = \vec{s} + \vec{l}$. In practice μ_{lJ} is equal to 1 or 2. Inserting Equation (2.15) in Equation (2.14) one obtains the next expression for average neutron width:

$$\overline{\Gamma_n}^{lJ}(E) = \mu_{lJ} \overline{\Gamma_n^0}^{lJ} \sqrt{E} \frac{P_l(E)}{\rho} \tag{2.16}$$

Degrees of freedom

The multiplicity μ_{lJ} is provided in the ENDF evaluation as the AMUN number, where it is described as the number of degrees of freedom for the neutron width. As said previously, one of the hypotheses of the compound nucleus statistics is that reduced widths follow normal centered law. Reaction widths are then a sum of square of normal laws, so they follow a χ^2-law, whose degree of freedom relates to the number of open channels. In our case, reaction widths are given for (l, J) sequences, so that the number of open channels for neutron width only corresponds to the number of possible s-values under condition $\vec{J} = \vec{l} + \vec{s}$, which is μ_{lJ}. The degrees of freedom for other widths is also provided in the ENDF evaluation for each (l, J) sequence: AMUG, AMUF and AMUX obviously correspond to capture, fission, and competitive widths, respectively. They remain the same for all tabulated energies.

The case of fission and capture is different from elastic scattering as they are composed reactions. The provided degree of freedom rather correspond to an effective number of decays instead of the exact number of open channels. For fission, AMUF may take floating values between 1 and 4. This surprisingly small number compared to the many possible fission decay channels is explained as fission mechanisms actually undergo fission barrier tunneling effects: the various fission decays all go through a small number of intermediate open channels, known as Bohr-channels, before other fission mechanisms intervene to lead to the observed various fission reactions. From the compound nucleus point of view, the reaction appears as a decay into one of these intermediate channels which are not numerous. For capture, there is in practice a huge number of open channels (> 30) corresponding to the various radiative decays. As a χ^2-law with a high degree of freedom looks like a Dirac function, the average capture widths $\overline{\Gamma_\gamma}^{lJ}$ are supposed to be constant over the whole unresolved range. AMUG is then set equal to 0, which actually marks the limit AMUG $= +\infty$. For competitive widths, only the inelastic scattering channel is open. The degree of freedom is thus $\mu_{l'J} = \mu_{lJ}$ in our case as $l' = l$.

Background cross sections and LSSF flag

A last important difference with the resolved case shall be highlighted. We mentioned that the file MF3 of ENDF evaluations contains background cross sections in the resolved range. In the unresolved resonance range however, two possibilities are available according to the value of a flag called LSSF[14]:

- LSSF $= 0$: In that case, File MF3 for total, elastic scattering, capture, and fission contains average background cross sections to add to the cross sections computed from resonance parameters. Everything appears alike the resolved case.

- LSSF $= 1$. In that case, File MF3 for total, elastic scattering, capture, and fission contains average cross sections directly[15]. The ENDF-6 manual then indicates that File MF2 data are meant to be used to compute self-shielding factors in the unresolved resonance range. This actually only means that probability tables calculations have to be normalized to the average data provided in File MF3. This matter will be more detailed in Section 2.3.

The cross sections processing techniques in the unresolved resonance range are twofold. The first class of method consists in derivation of analytic formulas to compute average cross sections from the average resonance parameters directly. It will be tackled in the upcoming part. The second model aims at computing cross sections as probability tables from a Monte-Carlo

---

[14]Which is stored in File MF2.

[15]This means that cross sections data contained in File MF3 for total, elastic, capture, and fission reactions drastically change at the limit between the resolved and unresolved ranges. Tabulated cross sections turn from tiny background values to real average cross sections. The limit is marked with a repeated tabulating energy value.

sampling of resonances, which provide more information. There, problems related to the right ways of sampling emerge, and will be presented in the last section of this chapter before being dealt with in more detail in the next chapters of this document.

2.2 Average cross section calculations in the unresolved resonance range

In this section, the average cross sections calculations in the unresolved resonance range from average parameters will be derived. This exercise is closely related to the problematic encountered by evaluators in their journey to obtain accurate parameters. Average cross sections calculation has been a field of interest for decades to obtain correct average values as a function of experimental data such as transmission ratios. In the unresolved resonance range, average calculations can be performed on an interval δ centered on a reference energy of calculation E, large enough to contain many resonances so that $\delta \gg \Gamma_{\lambda c}$ and $\delta \gg \langle D_J \rangle_\lambda$[16], and at the same time small enough so that secular variations of level statistics can be neglected as well as other slowly-varying energy quantities. S_c, P_c and k_α are supposed to be constant over δ, as well as average reduced widths and average spacings. An average cross section over δ is written $\langle \sigma \rangle_E = \overline{\sigma}$[17], so that:

$$\langle \sigma \rangle_E = \overline{\sigma} = \frac{1}{\delta} \int_{E-\delta/2}^{E+\delta/2} \sigma(E') dE' \tag{2.17}$$

2.2.1 Direct approach

Let us suppose for now that cross sections are described with the SLBW formalism. Under these conditions, the energy average over the cross section for channel c to reaction channel c' (c' is not an input channel) belonging to spingroup J^π is[18]:

$$
\begin{aligned}
\langle \sigma_{cc'} \rangle_E &= \left\langle \frac{\pi}{k_\alpha^2} g_J \sum_\lambda \frac{\Gamma_{\lambda c} \Gamma_{\lambda c'}}{(E - E_\lambda)^2 + \frac{\Gamma_\lambda^2}{4}} \right\rangle_E \\
&= \frac{\pi}{k_\alpha^2} g_J \sum_\lambda \left[\frac{\Gamma_{\lambda c} \Gamma_{\lambda c'}}{\delta} \int_{E-\delta/2}^{E+\delta/2} \frac{dE}{(E - E_\lambda)^2 + \frac{\Gamma_\lambda^2}{4}} \right] \\
&= \frac{\pi}{k_\alpha^2} g_J \sum_\lambda \frac{2 \Gamma_{\lambda c} \Gamma_{\lambda c'}}{\delta \Gamma_\lambda} \left[\arctan\left(\frac{2(E - E_\lambda) + \delta}{\Gamma_\lambda} \right) - \arctan\left(\frac{2(E - E_\lambda) - \delta}{\Gamma_\lambda} \right) \right] \\
&= \frac{2\pi}{k_\alpha^2} \frac{g_J}{\langle D_J \rangle_\lambda} \left\langle \frac{\Gamma_{\lambda c} \Gamma_{\lambda c'}}{\Gamma_\lambda} \left[\arctan\left(\frac{2(E - E_\lambda) + \delta}{\Gamma_\lambda} \right) - \arctan\left(\frac{2(E - E_\lambda) - \delta}{\Gamma_\lambda} \right) \right] \right\rangle_\lambda
\end{aligned}
\tag{2.18}
$$

where it has been assumed that a sum of any quantity X over the levels within δ is the mean value of X times the number of levels in δ, which is just δ divided by the average number of levels:

$$\sum_{\lambda \in \delta} X \approx \langle X \rangle_\lambda \frac{\delta}{\langle D_J \rangle_\lambda} \tag{2.19}$$

This approximation is a crude *ensemble average* procedure, in which the energy average is replaced by an average over the levels without even considering their possible fluctuations.

---

[16]Average notations over many levels from previous chapter are used again.

[17]Which technically, should not be confused with $\langle . \rangle_\lambda$ the average over many levels around E.

[18]Let us remind that and $B_c = S_c$ and thus $\Delta_\lambda = 0$.

Similarly, it is possible to obtain an average expression for the elastic scattering. Without considering the potential cross section, the average scattering cross section is the sum of a resonant and interference terms:

$$\langle \sigma_{cc} \rangle_E = \left\langle \frac{\pi}{k_\alpha^2} g_J \sum_\lambda \left[\frac{\Gamma_{\lambda c}^2 - \Gamma_{\lambda c}\Gamma_\lambda \sin^2(\phi_c)}{(E-E_\lambda)^2 + \frac{\Gamma_\lambda^2}{4}} + \frac{2\Gamma_{\lambda c}(E-E_\lambda)\sin(2\phi_c)}{(E-E_\lambda)^2 + \frac{\Gamma_\lambda^2}{4}} \right] \right\rangle_E \tag{2.20}$$

The first term can be averaged in an equivalent manner as previously. On the other hand, the interference term leads to a different expression:

$$
\begin{aligned}
\left\langle \sum_\lambda \frac{2\Gamma_{\lambda c}(E-E_\lambda)\sin(2\phi_c)}{(E-E'_\lambda)^2 + \frac{\Gamma_\lambda^2}{4}} \right\rangle_E &= \sum_\lambda \frac{2\Gamma_{\lambda c}\sin(2\phi_c)}{\delta} \int_{E-\delta/2}^{E+\delta/2} \frac{(E-E_\lambda)}{(E-E_\lambda)^2 + \frac{\Gamma_\lambda^2}{4}} dE \\
&= \sum_\lambda \frac{\Gamma_{\lambda c}\sin(2\phi_c)}{\delta} \ln \frac{(E-E_\lambda+\delta/2)^2 + \Gamma_\lambda^2/4}{(E-E_\lambda-\delta/2)^2 + \Gamma_\lambda^2/4} \\
&= \frac{\sin(2\phi_c)}{\langle D_J\rangle_\lambda} \left\langle \Gamma_{\lambda c} \ln \frac{(E-E_\lambda+\delta/2)^2 + \Gamma_\lambda^2/4}{(E-E_\lambda-\delta/2)^2 + \Gamma_\lambda^2/4} \right\rangle_\lambda
\end{aligned}
\tag{2.21}
$$

These expressions can be simplified. Given N levels in δ, neglecting the level fluctuations is equivalent to considering equidistant levels around E, $E_k = E + k\langle D_J\rangle_\lambda$, with k an integer varying between $-\frac{N}{2}$ and $\frac{N}{2}$. Then we can use the square formula to obtain:

$$\langle (E-E_\lambda)^2 \rangle_\lambda = \frac{1}{N} \sum_{k=-\frac{N}{2}}^{k=\frac{N}{2}} k^2 \langle D_J\rangle_\lambda^2 \approx \frac{\langle D_J\rangle_\lambda \delta}{12} \tag{2.22}$$

As $\delta \gg \langle D_J\rangle_\lambda$, we can neglect $E-E_\lambda$ compared to δ in the previous formulas. Reminding that we have supposed that $\delta \gg \Gamma_\lambda$ as well, and that arctan is an impair function whose limit in infinity equals $\frac{\pi}{2}$:

$$\left\langle \frac{\Gamma_{\lambda c}\Gamma_{\lambda c'}}{(E-E_\lambda)^2 + \frac{\Gamma_\lambda^2}{4}} \right\rangle_E \approx \frac{2\pi}{\langle D_J\rangle_\lambda} \left\langle \frac{\Gamma_{\lambda c}\Gamma_{\lambda c'}}{\Gamma_\lambda} \right\rangle_\lambda \tag{2.23}$$

$$\left\langle \sum_\lambda \frac{2\Gamma_{\lambda c}(E-E_\lambda)\sin(2\phi_c)}{(E-E_\lambda)^2 + \frac{\Gamma_\lambda^2}{4}} \right\rangle_E \approx 0 \tag{2.24}$$

Inserting these expressions in the average cross section formulations with the limitations introduced by the ENDF format, we get for elastic scattering, radiative capture, and fission:

$$\langle \sigma_\gamma \rangle_E (E) = \frac{2\pi}{k_\alpha^2} \sum_l \sum_J \frac{g_J}{\overline{D}^{lJ}} \left\langle \frac{\Gamma_{\lambda\gamma}\Gamma_{\lambda n}}{\Gamma_\lambda} \right\rangle_\lambda^{lJ} \tag{2.25}$$

$$\langle \sigma_f \rangle_E (E) = \frac{2\pi}{k_\alpha^2} \sum_l \sum_J \frac{g_J}{\overline{D}^{lJ}} \left\langle \frac{\Gamma_{\lambda f}\Gamma_{\lambda n}}{\Gamma_\lambda} \right\rangle_\lambda^{lJ} \tag{2.26}$$

$$\langle \sigma_{el} \rangle_E (E) = \frac{4\pi}{k_\alpha^2} \sum_l (2l+1)\sin^2\phi_l + \frac{2\pi^2}{k_\alpha^2} \sum_l \sum_J \frac{g_J}{\overline{D}^{lJ}} \left[\left\langle \frac{\Gamma_{\lambda n}^2}{\Gamma_\lambda} \right\rangle_\lambda^{lJ} + 2\sin^2(\phi_l)\overline{\Gamma_n}^{lJ} \right] \tag{2.27}$$

These formulas are the recommended formulas to be used in the ENDF manual [2]. They are implemented in most processing codes, such as NJOY and PREPRO. The trickiest part is now to compute the averages $\left\langle \frac{\Gamma_{\lambda c}\Gamma_{\lambda c'}}{\Gamma_\lambda} \right\rangle_\lambda$. Neglecting the χ^2 widths fluctuations leads to blatant

incorrect results. The SAMMY manual [17] provides an insight of an exact analytical solution. The main idea is to notice that $\frac{1}{\Gamma} = \int_0^{+\infty} e^{-q\Gamma} dq$. Then for capture for instance

$$
\begin{aligned}
\left\langle \frac{\Gamma_{\lambda\gamma}\Gamma_{\lambda n}}{\Gamma_\lambda} \right\rangle_\lambda^{lJ} &= \int_0^{+\infty} \left\langle \Gamma_{\lambda\gamma}\Gamma_{\lambda n} e^{-q\Gamma_\lambda} \right\rangle_\lambda^{lJ} dq \\
&= \int_0^{+\infty} \left\langle \Gamma_{\lambda n} e^{-q\Gamma_{\lambda n}} \right\rangle_\lambda^{lJ} \left\langle \Gamma_{\lambda\gamma} e^{-q\Gamma_{\lambda\gamma}} \right\rangle_\lambda^{lJ} \left\langle e^{-q\Gamma_{\lambda f}} \right\rangle_\lambda^{lJ} \left\langle e^{-q\Gamma_{\lambda x}} \right\rangle_\lambda^{lJ} dq
\end{aligned}
\tag{2.28}
$$

where we have decomposed the total width into partial widths, considered as independent random values, and used the linearity of the mean. In order to compute each of these averages, one needs to use the probability distribution of the reaction widths. They follow a χ^2-distribution with $\nu_{r,lJ}$ degrees of freedom provided in the evaluation. Thus, these averaged exponentials may be simply rewritten:

$$
\left\langle e^{-q\Gamma_{\lambda r}} \right\rangle_\lambda^{lJ} = \int_0^{+\infty} \chi^2_{\nu_{r,lJ}}(x) e^{-qx\overline{\Gamma}_r^{lJ}} dx = \left(1 + q\frac{2\overline{\Gamma}_r^{lJ}}{\nu_{r,lJ}} \right)^{-\nu_{r,lJ}/2}
\tag{2.29}
$$

$$
\left\langle \Gamma_{\lambda r} e^{-q\Gamma_{\lambda r}} \right\rangle_\lambda^{lJ} = \int_0^{+\infty} \chi^2_{\nu_{r,lJ}}(x) x\overline{\Gamma}_r^{lJ} e^{-qx\overline{\Gamma}_r^{lJ}} dx = \overline{\Gamma}_r^{lJ} \left(1 + q\frac{2\overline{\Gamma}_r^{lJ}}{\nu_{r,lJ}} \right)^{-\nu_{r,lJ}/2-1}
\tag{2.30}
$$

Note that for capture, $\overline{\Gamma}_\gamma^{lJ}$ is supposed to be constant as many channels are open, so that

$$
\left\langle e^{-q\Gamma_{\lambda\gamma}} \right\rangle_\lambda^{lJ} = e^{-q\overline{\Gamma}_\gamma^{lJ}} \quad \text{and equivalently} \quad \left\langle \Gamma_{\lambda\gamma} e^{-q\Gamma_{\lambda\gamma}} \right\rangle_\lambda^{lJ} = \overline{\Gamma}_\gamma^{lJ} e^{-q\overline{\Gamma}_\gamma^{lJ}}
\tag{2.31}
$$

It is possible to insert these terms in equations of the type 2.28 to express the average cross sections as integrals from 0 to $+\infty$ over a product of terms 2.29 and 2.30. Taking advantage of the fact $\overline{\Gamma}_\gamma^{lJ}$ is constant, the change of variable $u = e^{-q\overline{\Gamma}_\gamma^{lJ}}$ enables to bring the integrals limits over]0,1[. Then, the integrals and the average cross section values can be easily computed with an adaptive Gauss-Legendre algorithm.

In a nutshell, the detailed formula used the next assumptions:

- δ is big enough so that $\delta \gg \Gamma_{\lambda c}$ and $\delta \gg D_J$, and small enough, so that P_c, S_c and ϕ_c are constant over δ.

- SLBW shape of the cross sections.

- The partial widths follow χ^2-distributions with ν degrees of freedom. The levels are not fluctuating too much. The spacings distribution has not been taken into account, and approximated by a picket fence in the ensemble average in Equation (2.19).

2.2.2 Reformulation as a Hauser-Feschbach problem

The computation of average cross sections was an early problem in nuclear physics. Average partial cross sections are related to the collision matrix (cf. Equation (1.61)):

$$
\overline{\sigma_{cc'}} = \overline{\frac{\pi}{k_\alpha^2} g_J |\delta_{cc'} - U_{cc'}|^2} = \frac{\pi}{k_\alpha^2} g_J \overline{|\delta_{cc'} - U_{cc'}|^2}
\tag{2.32}
$$

The computations of the average of squared elements of the collision matrix $\overline{|U_{cc'}|^2}$ are actually very hard to perform, as they require averaging over quadratic terms $\overline{U_{ab}^* U_{cd}}$. On the other hand, it appears that some cross sections only depend on $\overline{U_{cc}}$. More precisely, and as described in [36], the average elastic scattering cross section can be split up into a potential scattering and a resonant part:

$$\overline{\sigma_{cc}} = \underbrace{\frac{\pi}{k_\alpha^2} g_J \left(|1 - \overline{U_{cc}}|^2\right)}_{\overline{\sigma_{cc}^p}} + \underbrace{\frac{\pi}{k_\alpha^2} g_J \left(\overline{|U_{cc}|^2} - |\overline{U_{cc}}|^2\right)}_{\overline{\sigma_{cc}^r}} \tag{2.33}$$

Looking at the form of Equation (1.63), the average total cross section is simply obtained as:

$$\overline{\sigma_{c,T}} = \frac{2\pi}{k_\alpha^2} g_J (1 - \mathrm{Re}(\overline{U_{cc}})) \tag{2.34}$$

And we can define the probability of formation of a compound nucleus as the difference between the total reaction and the potential section:

$$\overline{\sigma_c} = \overline{\sigma_{c,T}} - \overline{\sigma_{cc}^p} = \frac{\pi}{k_\alpha^2} g_J \left(1 - |\overline{U_{cc}}|^2\right) \tag{2.35}$$

The diagonal entries of the collision matrix U_{cc} are related to an experimentally measurable quantity, known as the transmission ratio $T_c = 1 - |U_{cc}|^2$. Consequently, the average total cross section, the average probability of formation of a compound nucleus, and the average potential scattering cross section can be obtained from experimental measurements as they only depend on $\overline{U_{cc}}$ and not on the average over the *squared* elements of the collision matrix. Such average cross sections are thus very useful for evaluators as they are directly measurable quantities.

In order to obtain a global expression for the more general problem of the decay from channel c to channel c', the introduced transmission ratios are quite useful. Indeed, the cross section $\sigma_{cc'}$ can be rewritten as:

$$\sigma_{cc'} = \frac{\pi}{k_\alpha^2} g_J \frac{T_c T_{c'}}{\sum_i T_i} \tag{2.36}$$

Averaging over a small interval δ with many resonances like in the previous subsection and taking into account the potential cross section, a very general expression known as the Hauser-Feschbach formula for the average cross section can be derived[19]:

$$\overline{\sigma_{cc'}} = \sigma_{cc}^p \delta_{cc'} + \frac{\pi}{k_\alpha^2} \frac{T_c T_{c'}}{\sum_i T_i} W_{cc'} \tag{2.37}$$

where $W_{cc'}$ is the so-called *width fluctuation correction factor* (WFCF), which takes into account all the correlations between the ingoing and outgoing waves. The width fluctuation correction embeds most of the underlying physics of compound nucleus interaction. In the original work from Hauser and Feschbach, $W_{cc'} = 1$, which was proved wrong afterwards. Then, several models aimed at calculating the width fluctuation correction.

In particular, the expression of the average cross sections obtained in the previous subsection can be reinterpreted as a Hauser-Feschbach problem, and a width fluctuation correction factor can be deduced from it. The equations provided in the previous subsection have been first established by Moldauer [37], who linked the transmission ratios to the average resonance widths using the narrow resonance approximation:

$$T_c = 2\pi \frac{\overline{\Gamma_c}}{\overline{D}} \tag{2.38}$$

to rewrite as in the previous part the width fluctuation factor as:

$$W_{cc'} = \left\langle \frac{\Gamma_{\lambda c} \Gamma_{\lambda c'}}{\Gamma_\lambda} \right\rangle_\lambda \frac{\langle \Gamma_\lambda \rangle_\lambda}{\langle \Gamma_{\lambda c} \rangle_\lambda \langle \Gamma_{\lambda c'} \rangle_\lambda} \tag{2.39}$$

and then took advantage of the fact that reaction widths follow a χ_ν^2 distribution to avoid the crude approximation $W_{cc'} = 1$ used in the original work from Hauser and Feschbach, which

---

[19]We need to redefine the average transmission ratios as $T_c = 1 - |\overline{U_{cc}}|^2$.

has been proven wrong since. The average cross sections from previous part (Equations (2.25)–(2.27)) can thus be rewritten in the very general form of a Hauser-Feschbach problem 2.37, with the next width fluctuation correction factor, referred from now as the *Moldauer width fluctuation correction factor*:

$$W_{cc'} = \left(1 + \frac{2}{\nu_c}\delta_{cc'}\right) \int_0^\infty dq \prod_i \left(1 + q\frac{2\overline{\Gamma_i}}{\nu_i\overline{\Gamma}}\right)^{-\delta_{ac}-\delta_{bc}-\nu_c/2} \tag{2.40}$$

$$= \left(1 + \frac{2}{\nu_a}\delta_{ab}\right) \int_0^\infty dq \prod_i \left(1 + q\frac{2T_i}{\nu_i\sum_d T_d}\right)^{-\delta_{ac}-\delta_{bc}-\nu_c/2} \tag{2.41}$$

Note that in this equation, the hypothesis of many channels for the capture reaction has not been applied yet. In this expression, the elastic cross section is enhanced with a factor $\left(1 + \frac{2}{\nu_c}\right)$, and the other partial averages are reduced.

This expression of the width fluctuation correction factor is widely used in practice, and has been proven to be very accurate when compared to a more precise and much more complex expression obtained when elements of the collision matrix are calculated in the framework of the random matrix theory [38]. This more elaborate theory will be dealt with later in this thesis in Chapter 4. Finally, let us underline that for all models developed to compute the width fluctuation correction factor, the next relation, which is a direct consequence of the transmission conservation, holds [39]:

$$T_c = \sum_{c'} \frac{T_c T_{c'}}{\sum_d T_d} W_{cc'} \tag{2.42}$$

This equality is very useful to check the accuracy of the numerical WFCF calculations, and thus the average cross section values.

Average values can be computed for any energy in the unresolved resonance range, once resonance parameters have been properly interpolated. However, as it has been pointed out in Section 1.1.6, such average values are not sufficient to take into account some more subtle effects like self-shielding. These effects could be handled if cross sections were given in the unresolved resonance range as continuous energy functions – unreachable, as it is the main characteristic of the range –, or given as probability tables. It turns out that the knowledge of resonance parameters average values and probability distributions is enough to produce probability tables in the unresolved resonance range. This is achieved through a Monte-Carlo method called the ladder method.

2.3   The ladder method

2.3.1   General presentation

The ladder method was originally introduced by Levitt [9] to produce cross sections as probability tables[20]. The ladder method has been successfully adapted afterwards in several processing codes, among which the well-known NJOY (module PURR), PREPRO, and AMPX (module PURM) systems. All of them implemented different versions of the ladder method which will be compared in the following chapters.

The principle of the method is straightforward. Average resonance parameters for all spin sequences (considered independently) are provided at reference energies, and their distributions are known. In the vicinity of a reference energy, it is thus possible to sample successive resonances

---

[20]Probability tables are a discrete version of the cross sections probability distributions at a particular energy, or over a group. They have been firstly exposed in this document in Section 1.1.6.

to form a statistically acceptable set of resolved resonances. Such an ensemble of sampled resolved resonances is called a ladder. The detail of the sampling of suitable ladders of resonances is very important, and will be tackled in Chapter 3 and Chapter 4. Once sampled, it is possible to compute partial cross sections using the resolved R-Matrix formulas, combining the ladders for all the spin sequences. The obtained values are just a realization of the cross sections at the reference energy, based on the sampled ladder. As a consequence, it is relevant to repeat many times the full procedure to implement a Monte-Carlo method in which a single history is a ladder sampling, from which partial cross section values are retrieved. The cross sections realizations over the Monte-Carlo iterations form a cross sections sampling. From this sampling, probability distributions can be estimated, and probability tables derived as mentioned in Section 1.1.6. The construction of the probability tables from the sampling is the main topic of Chapter 5.

The successive steps of the method are summarized on Figure 2.3.
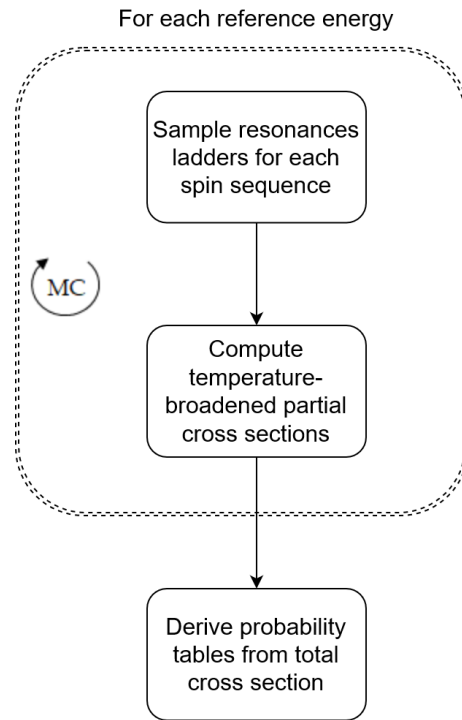
Figure 2.3: The ladder method steps

The main idea is thus very simple. However, even if this method enables the computation of probability tables, it includes many subtleties, and some implementation details often remain murky. In practice, it turns out that processing codes made some hypotheses and choices to develop Levitt's idea. Some crucial points will be discussed in this document, and a methodology to exploit the ladder method at best will be proposed.

2.3.2 Implementing the ladder method

Basically each step of the procedure can be questioned. The next paragraphs detail for all stages the issues which may arise.

Resonance ladders sampling

Probably the most important topic is the sampling of acceptable resonance ladders. Let us assume that we are using ENDF-formatted evaluated nuclear data, which is the case in practice, and so we are bound to the ENDF format limitations in the unresolved resonance range. In that case, resonances all belong to spin sequences (l, J), considered to be independent from each other. Moreover, only four average resonance widths are provided, using the Breit-Wigner

ENDF format. This means that the resolved ladders one can produce adopt the ENDF resolved Breit-Wigner formalism, and will be treated as such. Note that the general concepts in this subsection could be also applied to generate resonances suitable for other R-Matrix formalisms, which would be meaningful if corresponding input parameters were provided.

In general, the most common way to produce complete resonance ladders is to sample successive resonances. Assuming a resonance belonging to spin sequence (l, J)[21] is placed at energy $E_{r,i}$, the next resonance from the same spin sequence can be placed at energy $E_{r,i+1}$ so that $E_{r,i+1} = E_{r,i} + D_i$, where D_i is sampled from a Wigner distribution with average $\overline{D}^{lJ}$. It is easy to obtain a suitable D_i, using the inverse cumulative distribution function of the Wigner law, and sampling x_i from an uniform distribution over $[0, 1]$:

$$D_i = \overline{D}^{lJ} \sqrt{-\frac{4}{\pi} \ln x_i} \qquad (2.43)$$

Then, reaction widths need to be sampled from χ^2-distributions following a certain degree of freedom[22], supposing that each reaction width is independent from the other widths and other resonances. Obtaining random numbers following χ^2-distributions is a well-known issue, and many libraries perform that job properly. For instance, the BOOST library[23] enables χ^2-numbers generation on the basis of the calculation of inverse of incomplete gamma functions [40], using the fact that χ^2-distributions are a particular case of Gamma distributions.

Two main issues may be discussed, and will be investigated in Chapter 3 and Chapter 4:

- **The ladders limits.** The energy range spanned by the sampled resonances must be finite, which naturally leads to the next question: where should the ladder start and end ? Or alternatively, where should the ladder start, and what size should it be ? These questions are actually quite tricky. First, it seems reasonable that the energies of calculation should be far from the boundaries of the ladder in order to avoid side effects. When looking at the form of the partial cross sections then, one realizes that they turn out to be sums of rational terms whose $(E - E_r)$ component in the denominator gets higher as the resonance energy E_r is far from the energy of calculation E. To reach a physical meaning, one may expect these sums to converge as an addition of terms smaller and smaller in average. This convergence is displayed in Figure 2.4 which exhibits the contributions to the reaction cross sections of the 200 resonances closest to a reference energy of calculation E. This example corresponds to the resonant cross section values of a single spingroup of ^{235}U ($l = 0$, $J = 3$) at at $E = 2.25$ keV and T = 293.6K.

  From Figure 2.4, it appears clearly that the more the resonances are distant from the reference energy, the more their contribution is likely to be small, even if high values can still be obtained for some distant resonances due to the randomness of the ladder sampling. Another important aspect appears for the elastic scattering: resonances below the reference energy provide a positive contribution, whereas above ones bring a negative contribution, as mentioned in Section 1.3.4. This compensating phenomenon is typical of the elastic scattering reaction, which actually has important consequences as described in next chapter.

  In practice, the sampled resolved ladders must be large enough not to miss significant contributions of far resonances. And, even if this is a less important matter, it might be interesting not to have too big ladders in order to perform calculations in a manageable time.

---

[21] As both l and J are conserved during the reaction, the resonance ladders for each spin sequence (l, J) are considered to be independent.

[22] Again, this comes from the experimental and evaluation limitations, which define reaction widths rather than the widths of each channel, cf Section 2.1.

[23] BOOST is a powerful C++ library, sometimes considered as an extension of the STL library, which handles many aspects of programming, such as linear algebra, random number generation, threading, unit testing, etc. It is widely used in the GAIA-2 system.
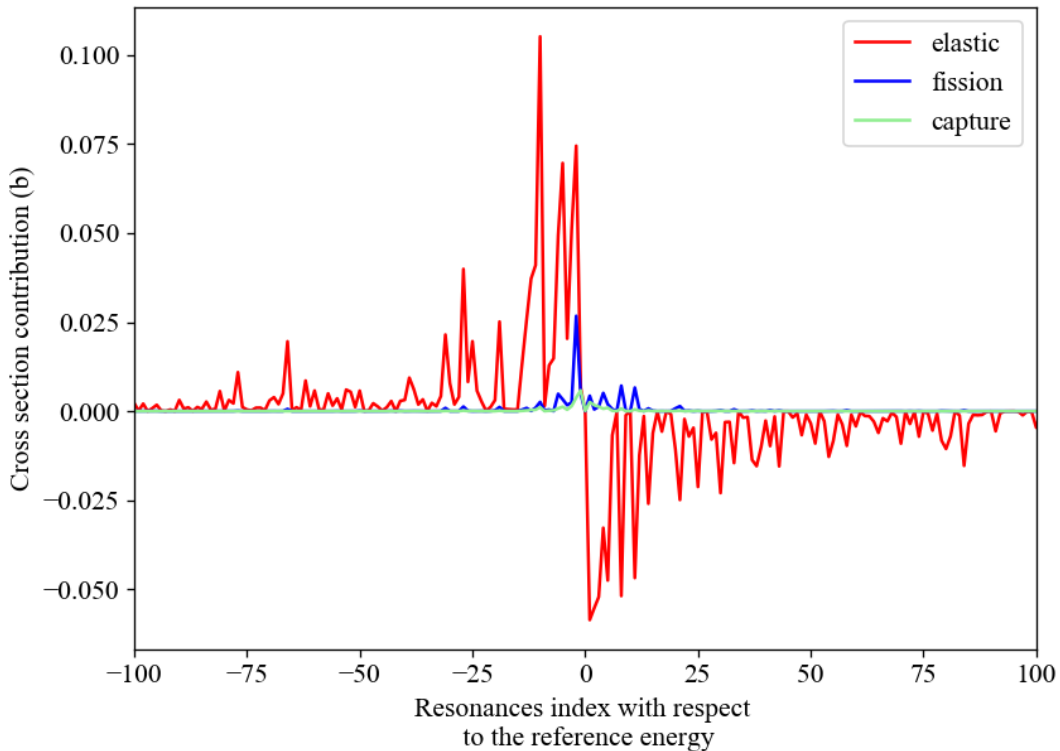
Figure 2.4: Contributions of resonances around a reference energy E to the cross sections calculated at E

- **Resonances correlations**. The described one by one sampling method results in uncorrelated sets of resonances, while experimental and theoretical results suggest that the nuclear levels are highly tied. For instance, the level spacings autocorrelation measure, $corr(D_\lambda, D_{\lambda+1})$, should equal -0.27. Thus, the resonance spectrum is in fact quite regular: a large spacing will have more chances to be followed by a small one, and so on. Such feature cannot be reproduced with the one by one sampling from a Wigner law, which then does not reproduce accurate sets of resonances. In fact, the Wigner law, initially postulated from an *ad hoc* "guess" and largely used, turns out to be a surprisingly good approximation of a more elaborated distribution law obtained from the random matrix theory, based on the properties of the so-called Gaussian Orthogonal Ensemble (GOE). Working with this more physical framework looks like a reasonable approach to improve the quality of the resonances sampling, which will be done in Chapter 4.

Cross sections computations

Once appropriate ladders have been sampled, partial cross sections can be computed using the R-Matrix formulas. There, the situation looks like the resolved case. The main issues are related to the performance and accuracy of the calculations, and whether full pointwise cross sections shall be computed on an energy grid. As often in Monte-Carlo applications, it is the trade-off between speed and precision which is of importance.

- **Accuracy of the calculations**

  In practice, ENDF limitations force us to generate Breit-Wigner shaped resonance ladders. Let us notice that some efforts to provide Reich-Moore compliant average resonance parameters in evaluations have been attempted recently with some success in a PhD dissertation by A. Holcomb at ORNL [41]. Moreover, the development of GNDS format is paving the way for a reinforced use of better formalisms in the future, even in the unresolved resonance range. This is even more appropriate as the use of SLBW formalism

in the ladder method sometimes leads to negative resonant elastic cross sections, which is of course highly nonphysical. Negative values may arise from the contributions of the asymmetric profile of resonances above the reference energy. If these resonances are much stronger than the resonances below, the positive contribution from these latter ones may not be sufficient to ensure a positive scattering resonant cross section at the interference minimum. Two possible ways to handle negative resonant scattering cross sections are thus possible:

- Discard the whole ladder. This approach may however bias the procedure, as situations in which above resonances are stronger than resonances below would be under-represented.
- Reset the elastic resonant scattering cross section to 0, and consider the total cross section to be the sum of the potential elastic scattering and other partials. This might be a correct approximation assuming the negative scattering values are close to 0.

It must be stressed that this defect of the SLBW formalism is enhanced in the ladder method, in which "unlucky" ladders (with respect to this feature) are potentially sampled. Using another formalism would remain the best practice, as MLBW for instance, for which level interferences correct the cross sections minima.

As in the resolved case, the choice of the Doppler-broadening method for temperature dependence may also have an impact. The Doppler effect is well understood, and using methods such as SIGMA1 or Leal-Hwang on linearized cross sections could be quite efficient. The use of $\psi - \chi$ Doppler is rather preferred in order to speed up calculations, as the approximations made by this method are reputed acceptable in the unresolved resonance range. In particular, its main disadvantages disappear in our situation (we are bound to use the Breit-Wigner formalism, and we are far from the low energies), while advantages seem tremendous (fast calculations, analytical form enabling computations at a single value, etc.).

- **Energy grid**

  In order to obtain a sampling of the cross section values at a reference energy from which we will be able to derive a probability table, the most rigorous way is to compute the cross sections at the reference energy only, for each Monte-Carlo iteration. This means that a single cross section value for each partial reaction can be obtained from a whole resonance ladder. This approach requires to sample many resonance ladders, which is time-consuming.

  In order to speed up the calculations, a common practice consists to reconstruct a "continuous" punctual cross section on an energy grid around the reference energy. Then, cross sections values can be exploited along the y-axis to obtain a probability distribution of the function on the range. Let us remark that the resulting sample can no longer be interpreted as statistical realizations of the cross section values at the reference energy precisely but over a whole range, which is ladder-dependent. The main advantage of this practice is to reduce the required number of ladders significantly, as much more information (in practice, much more sampled values) is grasped in a single round. However, the choice of the grid is a great additional source of uncertainty. There is no proper choice for such an energy grid which is highly connected to the resonance ladder. The definition of probability tables from the sampling is also less straightforward, as well as the convergence rate of the method.

Statistical aspects of the sampling

As any Monte-Carlo sampling, the statistical uncertainty associated to the cross section values decreases when the number of iterations increases. The question is whether enough

samples have been drawn. Some theoretical results can be useful in this kind of estimation. For instance, assuming the mean μ and variance σ^2 of the underlying cross section distribution exist, the Central Limit Theorem details the convergence of the empirical cross section mean $\overline{\sigma} = \frac{1}{n} \sum_{i=1}^{n} \sigma_i$ of independent realizations σ_i as a function of the number of iterations n:

$$\sqrt{n} \left(\overline{X_n} - \mu \right) \to \mathcal{N}(0, \sigma^2) \tag{2.44}$$

In our case we are not only interested in the cross sections means, but rather on the whole cross sections fluctuations, and then on the capacity of the sampling to approach the underlying cross sections distributions. The most useful theoretical support is the Givenko-Cantelli theorem, sometimes called the fundamental theorem of the statistics, which details the asymptotic behavior of the empirical distribution function as the number of independent observations increases. Let us call F the cumulative distribution function (cdf) of a random variable X. In case the random variable takes continuous values, the cumulative distribution function is the integral of the probability density function (pdf). From X_1, X_2, ..., X_n independent observations of the random variable X, one can define the empirical distribution function (ecdf) F_n as:

$$F_n(x) = \frac{1}{n} \sum_{i=1}^{n} \mathbb{1}_{\{X_i < x\}} \quad \text{for } x \in \mathbb{R} \tag{2.45}$$

where $\mathbb{1}_C$ is the indicator function of the set C. Actually, the empirical distribution is a step function, that jumps up by $\frac{1}{n}$ at each value taken by the observed X_i. The Glivenko-Cantelli theorem ensures that the empirical distribution converges toward the cumulative distribution in an *uniform* way, that is:

$$\mathbb{P}\left(||F_n - F||_\infty \xrightarrow[n \to \infty]{} 0 \right) = \mathbb{P}\left(\sup_{x \in \mathbb{R}} |F_n(x) - F(x)| \xrightarrow[n\infty]{} 0 \right) = 1 \tag{2.46}$$

To be even more precise, the Dvoretzky–Kiefer–Wolfowitz inequality (DKW) strengthens this theorem by specifying the rate of convergence as n increases, and bounds the probability that F_n differs from F more than a given constant ϵ for any $x \in \mathbb{R}$:

$$\mathbb{P}\left(\sup_{x \in \mathbb{R}} |F_n(x) - F(x)| > \epsilon \right) < 2e^{-2n\epsilon^2} \tag{2.47}$$

This inequality is closely related to the Kolmogorov-Smirnov test of adequacy to a distribution. It is possible to revert the inequality to draw a *simultaneous* band confidence around the cumulative distribution as a whole[24], which takes the form of a confidence envelope that contains the whole cdf at the same confidence level. For a tolerance level $1 - \alpha$, the interval that contains the true cdf is bounded with:

$$F_n(x) - \epsilon < F(x) < F_n(x) + \epsilon \quad \text{with} \quad \epsilon = \sqrt{\frac{\ln(2/\alpha)}{2n}} \tag{2.48}$$

For instance, if we want to have a simultaneous band confidence of $\epsilon = 1\%$ up to probability $1 - \alpha = 95\%$, the number of iterations to perform is then $n = \frac{\ln(2/\alpha)}{2\epsilon^2} = 18445$ iterations. For a fixed tolerance level α, the number of iterations is not a linear function of the simultaneous band confidence tightness. For instance, for 10000 iterations, the reached simultaneous band interval confidence approximately becomes 1.3% with probability 95%.

---

[24]Such a confidence interval is more demanding than a pointwise confidence interval, ie. a simple estimation of the confidence interval for each value of the cdf which allows for tighter level confidence at some individual points.

Probability tables computation

The definition of a probability table from a sampling is a step which requires questioning. It consists to turn a continuous density estimation into a discrete set of values possibly taken by the cross sections. This means artificially condensing a probability density function (pdf) into discrete equivalent values. This defines a probability mass function (pmf). A pmf is composed of a set of probability values p_k with associated base-points σ_k. These couples are called bin values. Of course, such a transformation is not unique, and the relevance of the selected method highly depends on the use of probability tables in Monte-Carlo codes afterwards. Are under study:

- **The number of bins to define**.

    More bins in the probability tables reduce the error due to the discretization of the continuous probability distribution, but slow down the Monte-Carlo codes. A relevant number of bins is closely related to the number of iterations and to the method used to build the probability tables.

- **The method to choose bin values**.

    Until now, several methods have been envisaged to build bins:

    - Regular binning
    - Equiprobable binning
    - Geometrical irregular procedures
    - The moment method, developed by P. Ribon and implemented in the CEA codes CALENDF and GALILEE.

    We present in Chapter 5 an investigation of these methods, along with original methods meant to compute reliable probability tables, based on a k-clustering algorithms.

Accurate energy mesh

This presentation of the ladder method described the generation of effective probability tables at a single reference energy, for which average resonance parameters are available. In the unresolved resonance range, the reference energies provided by the evaluator seem to be a default choice to produce energy-tabulated probability tables. However, nothing forbids processing codes to achieve calculations on a more refined mesh, taking advantage of resonance parameters interpolation. Investigating the impact of the determined energy mesh for probability tables in the unresolved resonance range sounds legitimate. In particular, there is almost no additional cost to produce extra probability tables in the unresolved resonance range. On the other hand, it provides more information to the Monte-Carlo neutronics codes, which sounds appealing.

In the following parts, these issues related to the ladder method will be tackled. The only question which will not be addressed is related to the cross sections computations step. In this work, for each sampled resonance ladder a single cross section value (for each partial reaction) is computed at the reference energy, relying on the SLBW formulas and $\psi - \chi$ Doppler effect. This seemed like the most conservative choice making use of the nature of the provided input parameters, and serves as a starting point to investigate the other issues. The chapters constitutive of the next part are focused on the quality of the resonance ladders sampling, but the question of the number of Monte-Carlo iterations will be also addressed. The quality of the ladder method sampling will also be tested against average Hauser-Feschbach calculations. In the final part of this document, the construction of probability tables from the sampled cross sections from the ladder method will be examined. Then, benchmarks calculations will be performed to investigate the quality of the methodology established to process nuclear data in the unresolved resonance range.

Part II

Statistical resonances sampling

Statistical resonance ladders sampling in the unresolved resonance range

The first critical step of the ladder method in the unresolved resonance range processing is to fill an energy region of interest with suitable sets of resonances. These sets are called *ladders*. Such sets are produced around a reference energy in the unresolved resonance range, at which cross sections can be computed using the R-Matrix formulas. This operation is repeated many times, resulting in Monte-Carlo sets of cross section values from which probability tables can be derived. This chapter aims at describing more in detail the sampling of resonance ladders in the unresolved resonance range.

The usual approach is to sample resonances one by one for each spin sequence, using the well-known Wigner and Porter-Thomas distributions of resonance parameters. This method may seem straightforward, but some questions still remain unanswered, in particular about the size and the choice of a reasonable starting point for the ladders. For both topics, existing codes do not clearly describe their strategy and the impact it may have on the cross sections computations. Moreover, the number of ladders to sample remains an open question as well.

In the following, the strategies adopted by reference codes for the ladder construction will be exposed, and proved to be equivalent under certain conditions. Afterwards, the question of the number of resonances to fill the ladders with will be tackled. In the course of our investigations, such problematic will be reformulated as an input-parameters problem. From this reformulation, a methodology will be proposed to estimate the proper size of the ladders to consider, along with the required number of Monte-Carlo iterations to run. At the end of this chapter, a reference methodology to sample resonances in the context of the ladder method will be set.

3.1 Resonance ladders sampling strategies

Let us focus for now on the usual practice to produce a resonance ladder, in which resonance energies are determined one by one. As described in Section 2.3, a resonance from the spin sequence (l, J) (indexed i) of a ladder is placed at distance D_i from the previous one, where D_i is the product of a random number from the Wigner distribution W, and the average spacing of the spingroup $\overline{D}^{lJ}$. Note that for now, only the immediate previous resonance serves to determine the position of the next one. Resonance widths for reactions α are then sampled from χ^2 distributions with appropriate degrees of freedom, and normalized on the average widths $\overline{\Gamma}_\alpha^{lJ}$. In practice however, ladders cannot extend to infinity: a first and a last resonance have

to be placed, and the range on which ladders extend must be defined. Two approaches can be envisaged, as it is possible to place first the farthest or the closest resonance from the reference energy. From another point of view, this choice is equivalent to building a ladder on a predefined energy range, or letting it grow until some stop criterion is met. Both methods have actually already been implemented in existing codes. The first approach is implemented in the PURR module from NJOY, while the latter is used in the PURM module of AMPX (part of the SCALE system). Both methods turn out to be equivalent under some conditions, which are about to be described.

3.1.1 PURR strategy: definition of an energy range

The first idea is to choose an energy interval $[E_1, E_2]$ for the ladder sampling directly. This method is implemented in the NJOY module PURR. In order to avoid the resonances to start at E_1 for all ladders, a random shift can be sampled. For instance, the first resonance for each spin sequence legitimately can be placed in $E_{r,1} = E_1 + \xi \overline{D}^{lJ}$ (ξ is sampled in an uniform distribution $\mathcal{U}[0,1]$). Then, resonances are sampled one by one until E_2 is reached.

E_1 and E_2 must be chosen to obtain ladders large enough so that enough resonances are sampled within it. Moreover, another important matter must be underlined: the starting point of the ladder must be far away from the energy of calculations in order to avoid the *waiting time paradox*, which will be presented in the next subsections.

Let us already mention that *ad hoc* practices are usually used to determine a sufficient range. For instance in PURR (NJOY), the choice of E_1 is fixed ($E_1 = 10$ eV), and E_2 is determined according to the following algorithm[1]:

```
E1 = 10                      # energies are in eV
nermax = 1000                # maximal number of resonances
erange = 0.9 * nermax * dmin # dmin is the smallest average
                             # spacing among all spin sequences
E2 = E1 + erange
```

This excerpt necessitates brief comments. Only the smallest average spacing among all spin sequences at the reference energy serves to determine the ladder range. This has several consequences. First, the resonance ladders are defined on the same energy range for all spin sequences. Secondly, the size of the ladders only depends on the average spacing values. More troubling, nothing seems to guarantee that the ladder spans the reference energy.

Actually, PURR circumvents this latter issue during the cross sections calculations step which comes afterwards. As mentioned in the description of the ladder method in Section 2.3, the sampled ladders of resonances serve to compute partial cross section values, that are stored to be turned into probability tables in the final step of the procedure. Two possibilities are practicable to choose the energy at which the cross sections are calculated. The first one is to compute the cross sections at the reference energy only, which provides probability tables representative of the cross sections at the reference energy exactly. The second option is to compute continuous cross sections on an energy grid around the reference energy. The first choice provides probability tables representative of the cross sections at the reference energy exactly, and is the default choice in this work. The second option provides probability tables representative of the cross sections in the vicinity of the reference energy. This latter method is the choice of PURR; the precise definition of the energy grid of calculation is presented in Listing 5.1, later in this document. The energy grid is chosen to be included in the limits of the ladders. This enables a correct calculations of the differences $(E - E_r)$ in the SLBW cross sections expressions Equation (2.7), and avoids the necessity for the ladder to really span the

---

[1]This code snippet has been extracted from NJOY 2016.35, which is open source.

reference energy. This second option presents the advantage to produce more than a single cross section value (for each reaction) for each sampled ladder[2], but introduces several additional questions about the choice of a relevant energy grid. In all the developments performed in this work, cross sections are only computed at the reference energy.

In any case, the definition of a ladder sampling from its energy limits seems cumbersome. Instead of choosing a ladder's edge as a starting point, it is possible to choose the center, as explained in next subsection.

3.1.2 AMPX strategy: paired sampling

A much more elegant idea than setting ladders boundaries consists to sampling resonances around the reference energy directly. This method has been initially implemented in the module PURM from AMPX. First, a central spacing D_0 between two resonances surrounding the reference energy must be sampled. As in the previous case, this central spacing may be randomly shifted for each ladder, in order to avoid a perfect symmetry between the first resonances. For example, the first resonances for each spin sequence can be placed at $E_{r,1} = E_{ref} + \xi D_0$ and $E_{r,-1} = E_{ref} + (1 - \xi)D_0$ ($\xi \sim \mathcal{U}[0, 1]$). Then, resonances can be drawn successively above and below the reference energy from these two first resonances. The problem is shifted from the definition of energy limits $[E_1, E_2]$ to a possible condition on the sufficient number of resonances to generate to compute cross sections, which looks more flexible. In order to avoid arbitrary asymmetric effects, the same number of resonances must be sampled on each side. In practice, resonances are then sampled as *pairs* around the reference energy.

Both sampling approaches are illustrated on Figure 3.1
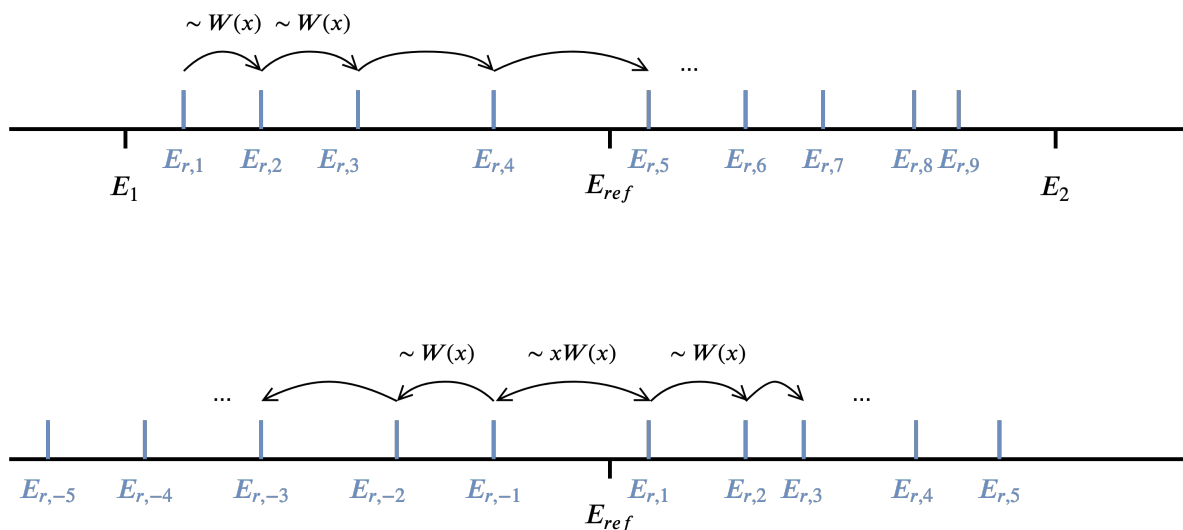
Figure 3.1: Successive samplings of resonances energies. The NJOY-like method determining $[E_1, E_2]$ is displayed on the upper figure. The bottom figure shows the AMPX-like method, where pairs of resonances are sampled around the reference energy.

3.1.3 The waiting time paradox

To our knowledge, there is a very important subtlety concerning the central spacing which has never been properly underlined. In order to be correct, the initial central spacing D_0 between $E_{r,-1}$ and $E_{r,1}$ must not be sampled from the Wigner distribution W, but using the slightly

---

[2]There are as many cross section values than there are energies in the chosen grid.

different $W^*(x) = xW(x)$ distribution instead. Indeed, the present situation turns out to be a variant of the well known *bus waiting time paradox*[3], which states that:

> *When someone arrives randomly at a bus stop, the elapsed time between the previous and the next bus is stochastically longer than the mean time between the buses.*

This paradox may be surprising at first sight. The main reason in the bus context lies in the fact buses do not reach the bus stop at equal time intervals due to the traffic conditions. Their arrival may be considered as a random variable. Intuitively, when a pedestrian reaches a bus stop at a random moment in a day, he is more likely to arrive at a time when previous and next buses are far from each other. The waiting time is susceptible to be greater than (half) the average elapsed time between the buses.

Going back to the resonance ladders, the first described method of sampling (NJOY-like) is equivalent to the bus problem. The reference energy of calculations plays the role of the bus stop, and sampled resonances are buses. The reference energy has thus more chances to be surrounded by distant resonances than close ones. In the second method, the fixed reference energy is chosen as the starting point, which creates a bias. This bias can be corrected taking into account the correct distribution of the first central spacing which surrounds the energy.

The distribution of the central spacing can be determined theoretically, which is done in Appendix A. More precisely, it is proved that if the spacing between resonances follows a distribution f with mean μ, then the *asymptotic* distribution followed by the spacing between the resonances *at a fixed energy* is $f^*(x) = \frac{x}{\mu}f(x)$. In the case of a Wigner distribution, $\mu = 1$, and so $W^*(x) = xW(x) = \frac{\pi}{2}x^2 e^{-\frac{\pi}{4}x^2}$. This corresponds (by chance) to a Maxwell distribution with parameter $\sqrt{\frac{2}{\pi}}$, which is easy to sample from. The mean of this distribution is $\frac{4}{\pi}$. The statistical average value of the spacing between the resonances that surround the reference energy is thus $\frac{4}{\pi}\overline{D}^{lJ}$, which is indeed larger than the mean spacing between resonances. As first resonances weight more than the others in the cross section calculations, this statistical detail is of importance, especially for light nuclei with large average resonance spacings.

It has been mentioned that W^*, the distribution followed by the central spacing, is an asymptotic result. This means it is valid in the limit of many sampled resonances, ie. when ladders extend to infinity. Accordingly, the AMPX-like method accurately simulates the asymptotic case, by construction. For the NJOY-like approach however, it seems relevant to investigate the central distribution behavior according to the number of sampled resonances.

To be slightly more precise, the demonstration presented in Appendix A deals with the central spacing[4] distribution in terms of the waiting time of a pedestrian that would walk by a bus stop at random time in the day. It is shown that the statistics of the time elapsed between the previous and next bus at his arrival converges toward a biased distribution T^* when the number of buses in the day becomes large.

For the NJOY-like method of sampling, the question would rather be: how far from the energy of calculation shall the starting point of the ladder be placed in order to avoid the central spacing to be biased ? Roughly speaking, if the starting point of the ladder is placed too close from the energy of calculations, the influence of the starting point is likely to bias the central spacing. On the other hand, if the starting point is far from the reference energy, many resonances have to be sampled before reaching it. This might be enough to dissipate the influence of the fixed starting point. The problem is thus similar than the situation in Appendix A, but instead of investigating the distribution of the waiting time of a pedestrian according to the number of possible time intervals one might come in, the question is about the required

---

[3]In the literature, this paradox is considered as a particular case of the *inspection paradox* which occurs whenever the probability of observing a quantity is related to the quantity itself.

[4]The spacing between resonances at the reference energy is still called as the central spacing, even though it might not be the central one in the first sampling method.

average distance between the starting point of the ladder (buses or resonances) and the point of interest (reference energy or arrival of the pedestrian).

A numerical simulation is quite easy to implement in order to estimate the minimum distance required between the starting point of the ladder and the energy of calculation so that the central spacing distribution reaches its asymptotic form. Figure 3.2 shows the result of such a numerical study, for which it appears that the starting point of the ladder in the first method must be taken at least four resonances away (in average) from the energy of calculation. If this condition is met, the central spacing roughly follows the asymptotic distribution $W^*(x) = xW(x)$, and both sampling methods behave equivalently. In practice, this condition is always met.
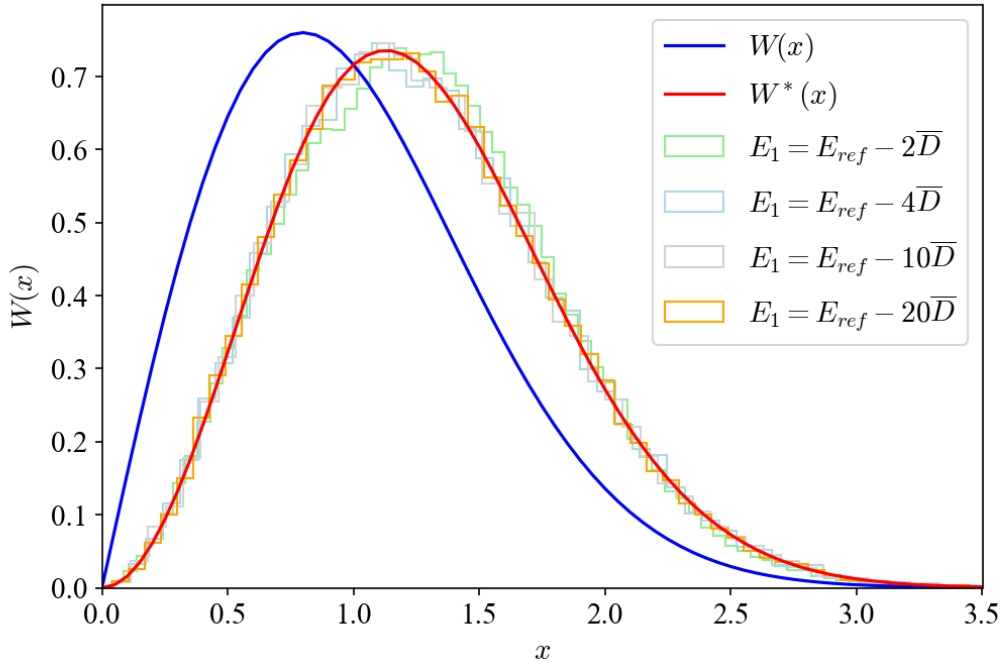
Figure 3.2: Convergence of the central spacing distribution to $W^*(x) = \frac{\pi}{2}x^2 e^{-\frac{\pi}{4}x^2}$ according to the starting point of the ladder.

Now that the choice of a ladder starting point has been examined, let us try to estimate the required size of the ladders to perform accurate cross section computations. It turns out that in the journey to achieve precise calculations, another internal parameter of the method can be tuned in the same way, namely the number of Monte-Carlo iterations to perform. Both these variables share common characteristics. Better results are achieved with more resonances and more Monte-Carlo iterations. Moreover, the minimum size of ladders, as well as the required number of ladders to sample, depend on the same input parameters. In the next section a methodology to estimate both these internal variables of the ladder method will be proposed.

3.2 A methodology to estimate the size and the number of ladders to sample

For a particular target nuclide, all resonances contribute to the reaction cross sections calculated at energy E. In practice, this contribution vanishes for distant resonances due to the $(E - E_r)$ term in the denominator in Equations (2.5)–(2.7). In the ladder method for producing probability tables, the objective is thus to produce resonance ladders wide enough so that all

"contributing" resonances are taken into account. However, the weight of each resonance cannot be apprehended analytically due to the random nature of the sampled resonance parameters. Moreover, the weight of each resonance is not the same for all partial reactions.

Two ways of dealing with this randomness seem practicable. The first one is to estimate on-the-fly quantities, which would indicate that the ladders are large enough. For example, the AMPX code makes use of its dynamic pair sampling approach to adopt this strategy. Resonances are added to the ladder as long as the cumulative number of levels does not approach a straight line satisfactorily[5]. The second option is to fix a ladder size *a priori*, based on the furnished average resonance parameters. This is for instance what the NJOY code does: it fixes the ladder limits based on the value of the smallest average spacing found among the target spingroups.

Our first goal is to estimate a sufficient size for the sampled resonance ladders to enable a proper calculation of cross sections at a reference energy, and thus probability tables. As mentioned in Section 3.1, defining a ladder over an energy range or with a number of pairs of resonances to be sampled is equivalent. The pair-based sampling was kept as a reference all along this thesis, as it seemed more practicable to work with one universal parameter (a number of pairs). As a consequence, the size of the ladders will be now expressed in terms of the *number of pairs of resonances to be sampled.*

Before dwelling into the inspection of the ladders size, let us now introduce an idea which will be useful to develop a methodology for the ladder method, that is the decomposition of libraries into *elementary spingroups.*

3.2.1 Decomposition of a library into elementary spingroups

Nuclear data are stored in libraries in terms of isotopes: a single file usually corresponds to a single nuclide in a particular isomeric state. In JEFF-3.2 for instance, out of 473 evaluated files, 307 nuclides have an unresolved resonance range defined. Among those 307, 7 are isomeric states at first excited level of nuclides also provided at ground state; this is the case of ^{110}Ag, ^{115}Cd, ^{131}Te, ^{152}Eu, ^{166}Ho, ^{180}Ta, and ^{115}Am. Considering the content of other libraries, like the more recent JEFF library JEFF-3.3, ENDF/B-VII-1 and ENDF/B-VIII libraries, and the Japanese JENDL-4, one may find up to 477 distinct isotopes with an unresolved resonance range, among which 20 are actually isomeric states. The lightest nuclide for which an unresolved resonance range is defined is ^{21}Ne, and the heaviest ^{253}Es, both found in JEFF-3.2.

A crucial point in a compound nucleus reaction is the conservation of the total angular momentum J, and the conservation of l which is assumed implicitly by the ENDF format in the unresolved resonance range. As a consequence, cross sections are the sum of several components corresponding to each spingroup[6], which do not interfere, as displayed in the R-Matrix formulas in Equations (2.5)–(2.7). In other words, it is always possible to decompose the computations of cross sections in the unresolved resonance range for a particular isotope at a particular energy into several sub-calculations, corresponding to the different spingroups. The important part is then to remark that each of these cross section sub-calculations in the unresolved resonance range only depends on 17 *scalar* parameters[7], that can be classified as follows:

1. Five "nucleus-only" related quantities: the target mass and spin, the competitive threshold, and the true and scattering channel radii[8]. These parameters are usually fixed for a nuclide, and are the same for all spingroups at all energies in the unresolved resonance range[9]. A summary for this data can be provided for instance in Table 3.1. Let us point

---

[5]The reason is related to the random matrix theory and is explained in Section 4.1.3

[6]Plus a potential cross section for elastic scattering.

[7]The provided classification is valid for the models used in the unresolved resonance range, such as "theoretical" average calculations as in Section 2.2, and the ladder method. In the resolved range, the nature of the resonance parameters differs, and depends on the formalism used.

[8]Actually, the scattering channel radius may depend on the energy, but that is an almost unused feature, and the radius remains a slowly-varying function of energy.

[9]Even if for instance the channel radius might differ between the resolved and unresolved range.

JEFF-3.2	Mass (u.a.)	Spin	True radius $(10^{-12}$ cm$)$	Scattering radius $(10^{-12}$ cm$)$	Threshold (eV)
min	20.81	0.00	0.42	0.26	-3.29e+06
max	250.91	9.00	0.86	1.05	1.82e+05
mean	137.74	1.49	0.70	0.69	-3.43e+05
median	136.72	0.50	0.71	0.69	-1.23e+05
standard deviation	57.79	1.71	0.10	0.15	4.68e+05
Combined libraries	Mass (u.a.)	Spin	True radius $(10^{-12}$ cm$)$	Scattering radius $(10^{-12}$ cm$)$	Threshold (eV)
min	20.81	0.00	0.42	0.22	-3.83e+06
max	250.91	9.00	0.86	1.05	5.27e+05
mean	132.46	1.65	0.69	0.68	-3.49e+05
median	129.78	1.00	0.70	0.67	-1.23e+05
standard deviation	56.45	1.80	0.10	0.15	4.95e+05

Table 3.1: Characteristics of the distinct isotopes with an unresolved range contained in JEFF-3.2 (307 isotopes), and considering all libraries JEFF-3.2, JEFF-3.3, ENDF/B-VII-1, ENDF/B-VIII, JENDL-4, (477 isotopes). It should be remarked that the maximum value found for QX in the libraries is positive, which would correspond to a negative threshold energy for the competitive width. Actually, these positive values are found for isomers evaluated at the first excited state.

out that performing statistics for these quantities over all nuclides present in a library have a physical meaning.

2. One reference energy. During processing, the calculations are performed at the reference energies at which average resonance parameters are tabulated in the evaluation[10]. This is part of the methodology of calculations explained in Section 2.3, in order to provide probability tables representative of the cross sections at the reference energy[11].

3. Ten spingroup related quantities: the quantum numbers l and J, the resonance average spacing, the four average resonance reaction widths corresponding to neutron, capture, fission and competitive reactions, and their associated degrees of freedom. It should be emphasized that the degree of freedom for capture is always set to 0. Usually, the widths and spacings are energy-dependent, but are provided at the given reference energy.

4. One temperature, which is the only input parameter whose value is fixed by the user rather than found in libraries. This quantity plays no role in the resonance sampling, but intervenes at the cross section calculations step, when Doppler-broadening is taken into account.

From these considerations, a common pattern to process the libraries contents in the unresolved resonance range emerges. The goal is no more to process the data isotope by isotope, but as a collection of *elementary spingroups*, defined as the combination for a particular isotope of one of its reference energy, and the associated resonance parameters for each particular spingroup. Transforming an existing library into a collection of such elementary spingroups is an

[10]This point will be addressed more in detail in Section 6.1.2. In fact, calculations can be performed at intermediate energies across the energy range, relying on interpolations of the average resonance parameters.

[11]This is at least the method retained in this thesis. For instance, PURR module from NJOY rather defines an energy grid around the reference energy to compute cross section values.

easy task. JEFF-3.2 for instance can be turned into 41 486 elementary spingroups, presented on Table 3.2, which are as many sets of input parameters for the sub-calculations. Cross-sections calculations for such converted libraries are exactly the same ones than during the typical processing of a library isotope by isotope: a decomposition of computations into spingroups and energies has just been carried out.

	Library	Nu-clide	l	J	Reference energy	Mass	Spin	True radius	Scat. radius	QX
1	jeff32	NE21	0	1.0	3.07e+05	20.81	1.5	0.42	0.51	-3.51e+05
2	jeff32	NE21	0	1.0	3.47e+05	20.81	1.5	0.42	0.51	-3.51e+05
3	jeff32	NE21	0	2.0	3.07e+05	20.81	1.5	0.42	0.51	-3.51e+05
	. . .					. . .				
41485	jeff32	ES253	0	3.5	7.00e+03	250.91	3.5	0.86	0.88	0.00e+00
41486	jeff32	ES253	0	3.5	1.00e+04	250.91	3.5	0.86	0.88	0.00e+00

	Library	Nuclide	$\overline{D}$	$\overline{\Gamma_n^0}$	$\overline{\Gamma_\gamma}$	$\overline{\Gamma_f}$	$\overline{\Gamma_x}$	ν_n	ν_f	ν_x
1	jeff32	NE21	1921.84	14.93	0.89	0.0	0.0	1.0	0.0	0.0
2	jeff32	NE21	1905.58	14.72	0.90	0.0	0.0	1.0	0.0	0.0
3	jeff32	NE21	1635.34	12.71	0.32	0.0	0.0	1.0	0.0	0.0
	. . .					. . .				
41485	jeff32	ES253	3.73	1.371e-03	0.02	0.0	0.0	1.0	0.0	0.0
41486	jeff32	ES253	3.73	1.371e-03	0.02	0.0	0.0	1.0	0.0	0.0

Table 3.2: Elementary sets of input parameters of JEFF-3.2, sorted from the lightest to the heaviest.

Developing a methodology to compute cross sections in the unresolved resonance range is much easier from such converted libraries, as the input parameters are defined with a common formalism: there are just 16 scalar parameters[12]. More than just a matter of convenience, thinking in terms of elementary spingroups is useful when trying to quantitatively estimate the differences between several methods to process cross sections in the unresolved resonance range. In particular, such conversion may provide some relevant information about the sensitivity of a model output to each of the 16 input parameters, when the question of interest is related to the quality of cross section computations. When some aspects of the ladder method will be looked for later in this document, it will be possible to relate the outcome of the calculations to the value of the input parameters.

Note that according to the computed quantity and the model used, not all these 16 parameters are useful. For instance, scattering radius is only used in the elastic scattering cross section formula, and has no impact for fission and capture cross section calculations.

One may go further than converting libraries such as JEFF-3.2 into sets of input elementary spingroups with 16 parameters: several libraries can be converted, and merged together. In this work, all the elementary spingroups from the five libraries JEFF-3.2, JEFF-3.3, ENDF/B-VII.1, ENDF/B-VIII, JENDL-4 were extracted, and combined. Then, all duplicates were dropped.

---

[12]Reminding that although temperature is an input parameter, it is not found in the libraries.

Note that only the elementary spingroups for which all 16 parameters were identical were considered to be duplicates. Such a situation frequently occurred, since many evaluated files are reused from a library to another for example. Once dropped, there remained 151514 distinct elementary spingroups from the combined libraries. Such an ensemble of elementary spingroups exactly corresponds to the input data to be processed in the unresolved resonance range when the five libraries are considered.

The statistics of the elementary spingroups from the combined libraries is displayed on Table 3.3, to be compared with the statistics of the elementary spingroups from JEFF-3.2 on Table 3.4. It must be pointed out that these statistics do not have a real physical meaning. Indeed, each elementary spingroup is considered independently from its original nuclide, and all nuclides do not have the same number of spingroups nor reference energies defined in the unresolved range. As a consequence, all nuclides do not have the same "weight". For instance, adding a reference energy in a nuclide evaluation artificially changes the nucleus-related data[13]. On the other hand, they can be interpreted as statistics over the input parameters phase space for the upcoming calculations. This is even more interesting, as the objective of the present document is to study the models used in the unresolved resonance range, that are actually used with the elementary spingroups as input data.

	l	J	Energy	Mass	Spin	True radius	Scattering radius	QX
min	0	0	0.3	20.81	0	0.42	0.06	-3.83e+06
max	3	10.5	5.06e+06	250.91	9.00	0.86	1.05	5.27e+05
mean	1.04	2.34	8.68e+04	134.95	1.94	0.70	0.67	-2.72e+05
median	1.00	2.00	2.50e+04	133.75	1.50	0.71	0.66	-1.13e+05
standard deviation	0.73	1.8	1.99e+05	48.87	1.82	0.08	0.14	3.74e+05

	$\overline{D}$	$\overline{\Gamma_n^0}$	$\overline{\Gamma_\gamma}$	$\overline{\Gamma_f}$	$\overline{\Gamma_x}$	ν_n	ν_f	ν_x
min	0.325	1.0e-06	1.0e-09	0	0	1	0	0
max	3.99e+05	112.95	5.44	2.84	974.57	2	4	2
mean	1.29e+03	0.24	0.18	0.01	0.52	1.22	0.14	0.38
median	5.66e+01	7.2e-03	0.10	0.0	0.0	1.0	0.0	0.0
standard deviation	9.04e+03	2.12	0.32	0.11	13.46	0.41	0.57	0.69

Table 3.3: Statistics of the 151514 distinct elementary spingroups from the combined libraries JEFF-3.2, JEFF-3.3, JENDL-4, ENDF/B-VII.1, ENDF/B-VIII.

In this thesis, working with all 151514 elementary spingroups resulting from the combined five libraries was too demanding from both the calculation and computer memory management point of view. As a consequence, only the 41486 elementary spingroups from JEFF-3.2 were used as a base of test cases. Considering Table 3.3 and Table 3.4, it seemed that JEFF-3.2 was representative enough of the input elementary spingroups from the five libraries. In particular, the maximum and minimum values for all parameters were almost always found in JEFF-3.2. This is explained by the fact JEFF-3.2 is a slightly older library than the other ones. Many nuclides have a wide unresolved resonance range, making it a good candidate to be used to test the models in use in this domain.

Before concluding this subsection, let us present some joint histograms for three parameters that will prove to be of particular importance, namely the spacing, the reduced neutron width

---

[13]One can notice the slight difference between Table 3.1 and Table 3.3 for mass, spin, channel radii and threshold.

	l	J	Energy	Mass	Spin	True radius	Scattering radius	QX
min	0	0	1.0	20.81	0	0.42	0.26	-3.29e+06
max	3	10.5	5.06e+06	250.91	9	0.86	1.05	1.82e+05
mean	1.01	2.25	8.29e+04	145.59	1.88	0.72	0.7	-2.56e+05
median	1.0	2.0	2.00e+04	143.67	1.5	0.72	0.7	-9.10e+04
standard deviation	0.72	1.74	2.15e+05	54.81	1.72	0.09	0.16	3.63e+05

	$\overline{D}$	$\overline{\Gamma_n^0}$	$\overline{\Gamma_\gamma}$	$\overline{\Gamma_f}$	$\overline{\Gamma_x}$	ν_n	ν_f	ν_x
min	0.33	3e-5	1e-09	0h	0	1	0	0
max	364536.00	111.54	5.44e+00	2.84	856.26	2	4	2
mean	1519.03	0.31	1.70e-01	0.03	0.52	1.22	0.31	0.29
median	34.19	0.00	8.96e-02	0.0	0.0	1.0	0.0	0.0
standard deviation	11910.99	2.94	3.44e-01	0.15	18.56	0.41	0.86	0.63

Table 3.4: Statistics of the 41486 distinct elementary spingroups from JEFF-3.2.

and the reference energy. Such histograms complete the statistics of Table 3.4. Figure 3.3 displays these joint histograms for the elementary spingroups of JEFF-3.2, using a hexagonal binning. It appears clearly that the reference energies are especially present between 10^3 and 10^5 eV, and that a close positive correlation between the spacing and the reduced neutron width emerges.

The elementary spingroups of JEFF-3.2 will be used in the next subsections as a base of test cases to estimate the required size of the ladders, and the minimal number of Monte-Carlo iterations to be performed to obtain relevant cross sections samplings.

3.2.2 Methodology for the size of the ladders

One of the objectives of this chapter is to determine the required size of the ladders, defined as a sufficient number of pairs of resonances to sample around a reference energy E_{ref} at which resonance parameters are provided[14]. For such a study, calculations for the same inputs have been made with ladders from different sizes, and their outputs compared. Let us now define proper inputs, outputs, and the exact adopted procedure.

First of all, the required number of pairs can be expressed as a cross sections calculation problem. More precisely, as each added pair of resonances has a statistically weaker contribution than the previous one, our objective is to estimate the minimum number of resonances so that farther resonances contribution to the cross section is marginal. This decrease will thus depend on the resonance parameters provided, and will differ for each spingroup for a particular nuclide. In fact, one is faced to the situation described in previous subsection, and it is interesting to work out the question with elementary spingroups in place of nuclides. In this thesis, the required number of pairs of resonances to calculate accurate probability tables will be investigated as a function of the 17 scalar input parameters which determine each sub-calculation.

The output of the ladder method is an ensemble of $3n$ cross section values; n is the number of Monte-Carlo iterations, and for each iteration three partial cross sections are computed, for elastic scattering, capture and fission reactions. They form a sampling, from which probability tables can be derived. The construction of a probability table from a cross sections sampling is

---

[14]Relying on resonance parameters interpolation, this may be the case of any energy.
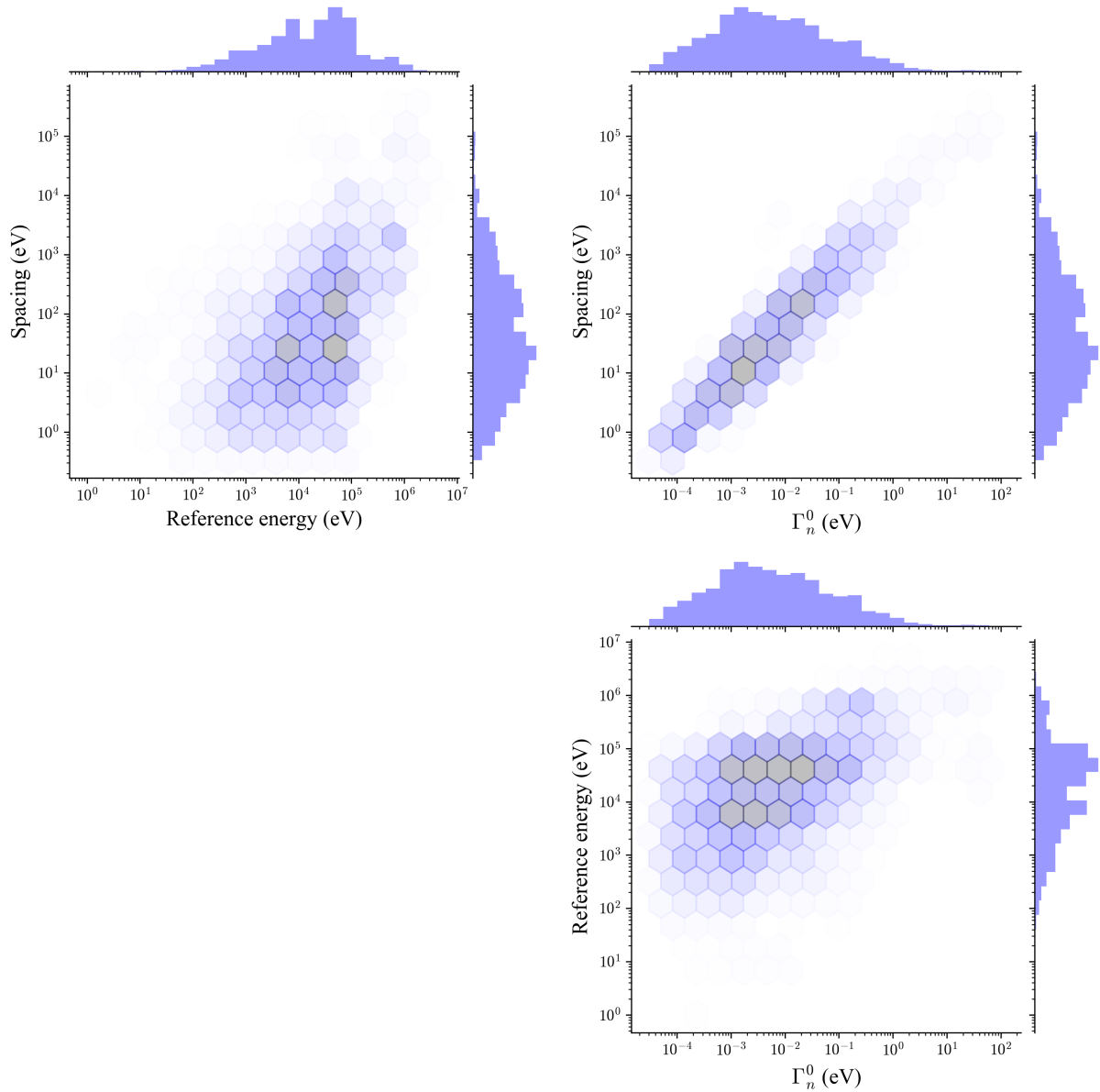
Figure 3.3: Histogrammed joint plots of reference energies, average resonance spacings $\overline{D}$ and average reduced neutron widths $\overline{\Gamma_n^0}$ for the 41486 elementary spingroups from JEFF-3.2. The central joint plots use a hexagonal binning to represent 2D histograms, where the color of the cells indicates the number of occurrences.

a secondary step, tackled in Chapter 5, during which information is lost to obtain a tractable representation of the probability distribution of the cross sections. For this reason, probability tables are not considered as the output of the ladder method for now. Instead, the samplings of computed cross section values are directly considered to be the real output of the method, as they contain more information. When it comes to comparing several samplings, some statistics might be used to describe them[15]:

- Moments of the distribution. The infinite series of the moments $\left(\frac{1}{n}\sum_{i=1}^{n}X_i^k\right)_{1\leq k\leq\infty}$ entirely defines the distribution. The four first moments are used as shape parameters of the distributions. They are namely the mean, variance, skewness, and kurtosis. These

---

[15]Alternatively, such statistics describe the empirical distribution they compose. As a reminder, the empirical cumulative distribution function (ecdf) is an estimator of the cumulative of the distribution function which has generated the sample. Probability tables are then a discretized form of this function.

quantities correspond to centered and reduced moments.

- Quantile quantities. They measure the value below which a given percentage of observations fall. One commonly uses the 25th and 75th *percentile*, also referred to as the first and third *quartile*, which indicate the values below which 25% (respectively 75%) of observations are found. In order to estimate the proper estimation of the weight of the tails, the 95th percentile is also used.

- Kolmogorov-Smirnov statistics. Here, this statistics is used to compare two samples. This statistics is defined as the maximum of the distance[16] between the empirical cumulative distributions of the samples. The more the samples look alike, the smaller the Kolmogorov-Smirnov statistics is. Compared to moments and quantiles, this quantity does not characterize a single sample, but its degree of similarity with another one.

In brief, next investigations will be based on comparisons between sampled sets of cross sections obtained with ladders of different sizes. Such comparisons will be carried out on the grounds of the presented statistics, and calculations will be performed for each elementary spingroup found in the libraries, rather than isotopes. In order to get rid of the randomness of diverse samplings, next methodology is adopted. First, a very large ladder is drawn. Basically, we chose to sample up to 500 pairs of resonances, to get ladders filled with 1000 resonances[17]. Then, partial cross sections are computed taking into account *truncations* of this large ladder, centered around the reference energy. More precisely, cross section values are computed taking into account the 5 first pairs of resonances around the reference energy, then 10 pairs, 15 pairs, and so on, until the 500 pairs of resonances are considered. As a consequence, differences between cross sections obtained for ladders of different sizes are only due to the additional resonances considered, and no longer depend on the fluctuations of the first common resonances[18]. In the following, computations performed with 500 pairs of resonances are considered as a reference calculation, to be compared with calculations made with fewer resonances. Consequently, the influence of the performed number of Monte-Carlo iterations does not interfere much anymore.

Besides, next strategy is adopted for the cross sections computations: cross sections for elastic scattering, capture and fission are always reconstructed at each elementary spingroup's reference energy, which is used as a base-point for the pairs sampling. For each Monte-Carlo iteration, cross sections are thus computed at the exact energy at which resonance parameters are furnished. As a consequence, each ladder only provides a single cross section value for each reaction: the size of the final cross sections sets equals the number of sampled ladders. Calculations make use of the SLBW formalism as described in Section 2.1.2, which is the only format permitted in the ENDF libraries, and the default formulas commonly used in the unresolved resonance range. In order to take into account the effect of temperature, calculations are performed at 0K and room temperature (T=293.6K), using the $\psi - \chi$ Doppler broadening, which is the state of the art in the unresolved resonance range. Finally, the potential cross section is added to the resonant elastic scattering cross section. The contribution of each spingroup to the potential scattering can be expressed as[19] $\sigma_p^{lJ} = \dfrac{\pi}{k_\alpha^2} g_J \sin^2(\phi_l)$.

We believe such calculations are representative of the usual processing practices in the unresolved resonance range. Figure 3.4 summarizes the adopted methodology.

Once all Monte-Carlo iterations and all computations have been carried out, we are left with sets of $3n$ sampled cross sections, for each particular elementary spingroup, temperature, and number of pairs of resonances considered. It is then possible to calculate for each set the moments and quantiles statistics mentioned previously. Then, the relative difference of these

---

[16]The distance is there expressed as an infinity norm.

[17]One may remark this is the maximum number of resonances allowed for each ladder in the NJOY code.

[18]Note that fluctuations still occur, but are due to the large ladder sampling only.

[19]To get back to the expression in Equation (2.7), one must notice that $\sum g_J = 2l + 1$.
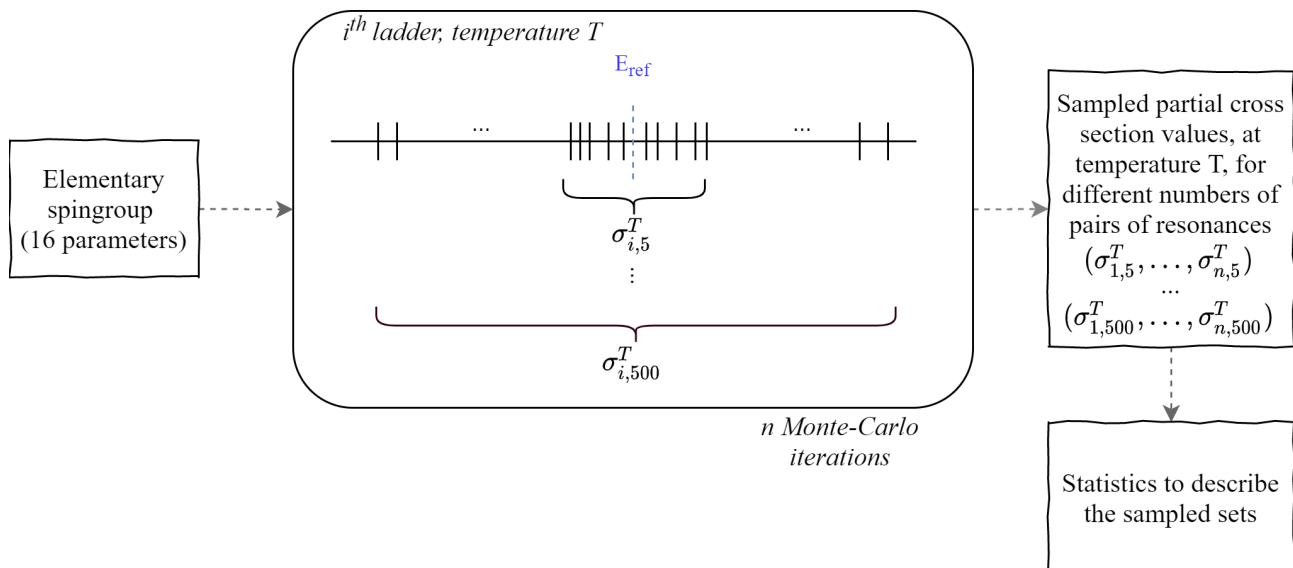
Figure 3.4: Computations methodology to estimate the required number of resonances to sample in the ladders.

statistics is computed for sets corresponding to the same reactions, elementary spingroup and temperature, but different number of resonances, taking the 500 pairs result as a reference. The Kolmogorov-Smirnov distance between the 500 pairs set and the sets for smaller ladders is also computed.

Before moving to the next subsection, it must be pointed out that nothing seems to guarantee that 500 pairs of resonances may be enough to yield "asymptotic" results, which may constitute reference calculations. This remains an inherent flaw of the presented methodology, *a priori*. However, the outcome of the calculations presented later in Section 3.3.1 seems to confirm that this number is reasonable, as the speed of convergence of the various statistics is relatively fast for a vast majority of cases.

3.2.3 Methodology for the number of Monte-Carlo iterations

The size of the ladders is susceptible to impact the cross sections and probability tables computations, but the number of Monte-Carlo iterations is too. There again, the more iterations are run, the more the calculations will be statistically precise. There, a theoretical result holds: the Dvoretzky–Kiefer–Wolfowitz inequality mentioned in Section 2.3, which indicates that the rate of convergence of the empirical distribution to the cumulative distribution is roughly in $\sqrt{1/n}$. Hence, it is possible to investigate the required number of Monte-Carlo iterations in the case of the ladder method.

As previously, the number of iterations will impact the properties of the sets of calculated cross sections. It is then expected that the behavior of the sets as a function of the number of iterations will differ according to the input parameters. As before, an investigation of the impact of the number of iterations seems more relevant when carried out for the elementary spingroups. Here, the model outputs are the sampled partial cross sections rather than the probability tables, for the same reasons as stated before.

In order to estimate the speed of convergence of the ladder method according to the input spingroups, several calculations with different numbers of Monte-Carlo iterations have been compared together. In order to get rid of the bias due to the ladder size, large ladders filled with 1000 resonances have been considered. The reconstruction methodology is the same as before. The method is summarized on Figure 3.5.

To be slightly more precise, four numbers of Monte-Carlo iterations were used. Taking into
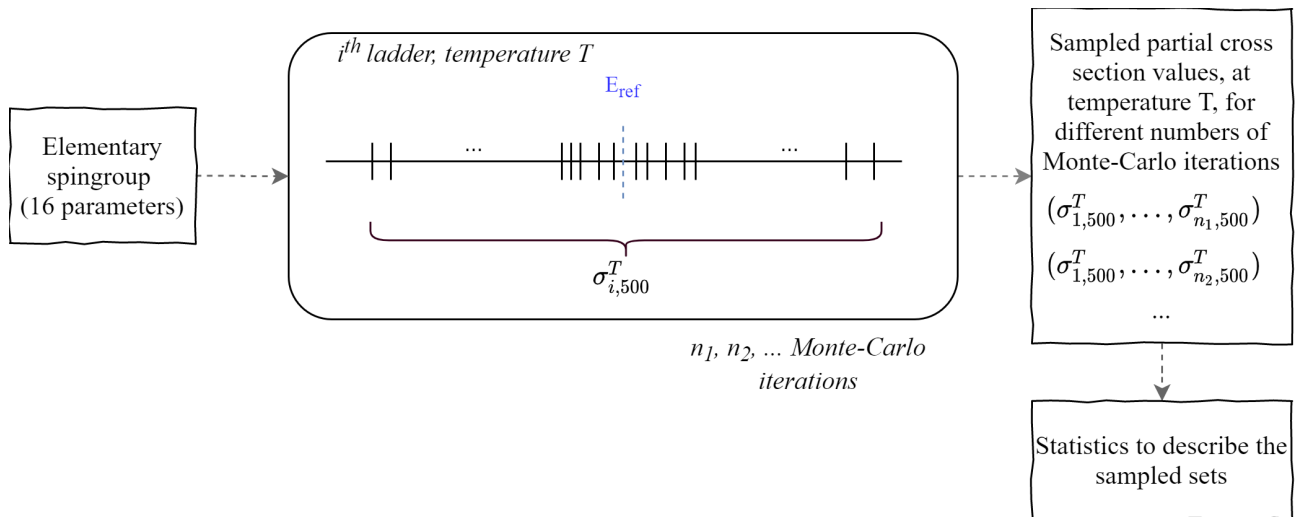
Figure 3.5: Computations methodology to estimate the number of Monte-Carlo iterations to be run in the ladder method.

account the DKW inequality, $n = 10000$ Monte-Carlo iterations seemed to be a good start point. Indeed, with such a large number, the empirical cumulative distribution function was supposed to be close up to 1% to the cumulative one statistically. In order to estimate the stability of calculations made at this order of magnitude, $n = 20000$ iterations was also considered. Then calculations have also been performed at the next order of magnitude, taking $n = 100000$ and $n = 200000$ Monte-Carlo iterations. All computations made use of different random seeds[20].

3.3   Results

3.3.1   Size of the ladders

The GAIA-2 code has been slightly modified to enable the implementation of the proposed methodology described in Section 3.2.2, to estimate the required number of pairs to sample for each elementary spingroup found in the JEFF-3.2 library. This represents 41 486 cases, which are representative of the diversity of the nuclides, and of the work to be achieved during a library processing. Looking at Table 3.1 and Table 3.3, it appears that the general statistics of resonance parameters over the JEFF-3.2 do not differ from the other libraries significantly, even if the detail of the resonance parameters may change. For this reason, we believe JEFF-3.2 is a good starting point, plus it is widely used in global-purposes nuclear safety studies.

In the following, the convergence of the cross sections statistics as a function of the number of pairs of resonances will be showed first. Then, the influence of all the input parameters over the rate of convergence will be described more in detail, using parallel plotting. Finally, a more precise relationship between the parameters and the number of resonances to be sampled in ladders will be investigated.

Convergence of the statistical properties of the sampled cross sections sets

For each reaction and each temperature, *convergence plots* of each statistics of interest have been produced. They are displayed for T=0K on Figures 3.6–3.8. Such plots were obtained taking for each elementary spingroup the relative difference between the moments and quantiles

---

[20]In that case, and unlike the case of the number of resonances to sample, none of the performed computations to be compared together were nested. The cross sections values for the case $n =20\,000$ were not obtained from the 10 000 first cross sections, plus 10 000 other ones; they are, in fact, entirely different. This is relevant because in this case, we aim at evaluating the real impact of the random fluctuations.

Figure 3.6: Convergence of various statistics of the sampled elastic cross sections toward the reference (500 pairs of resonances), at T=0K. (a) mean, (b) variance, (c) skewness, (d) kurtosis, (e) first quartile, (f) fourth quartile, (g) 95th percentile, (h) Kolmogorov-Smirnov distance
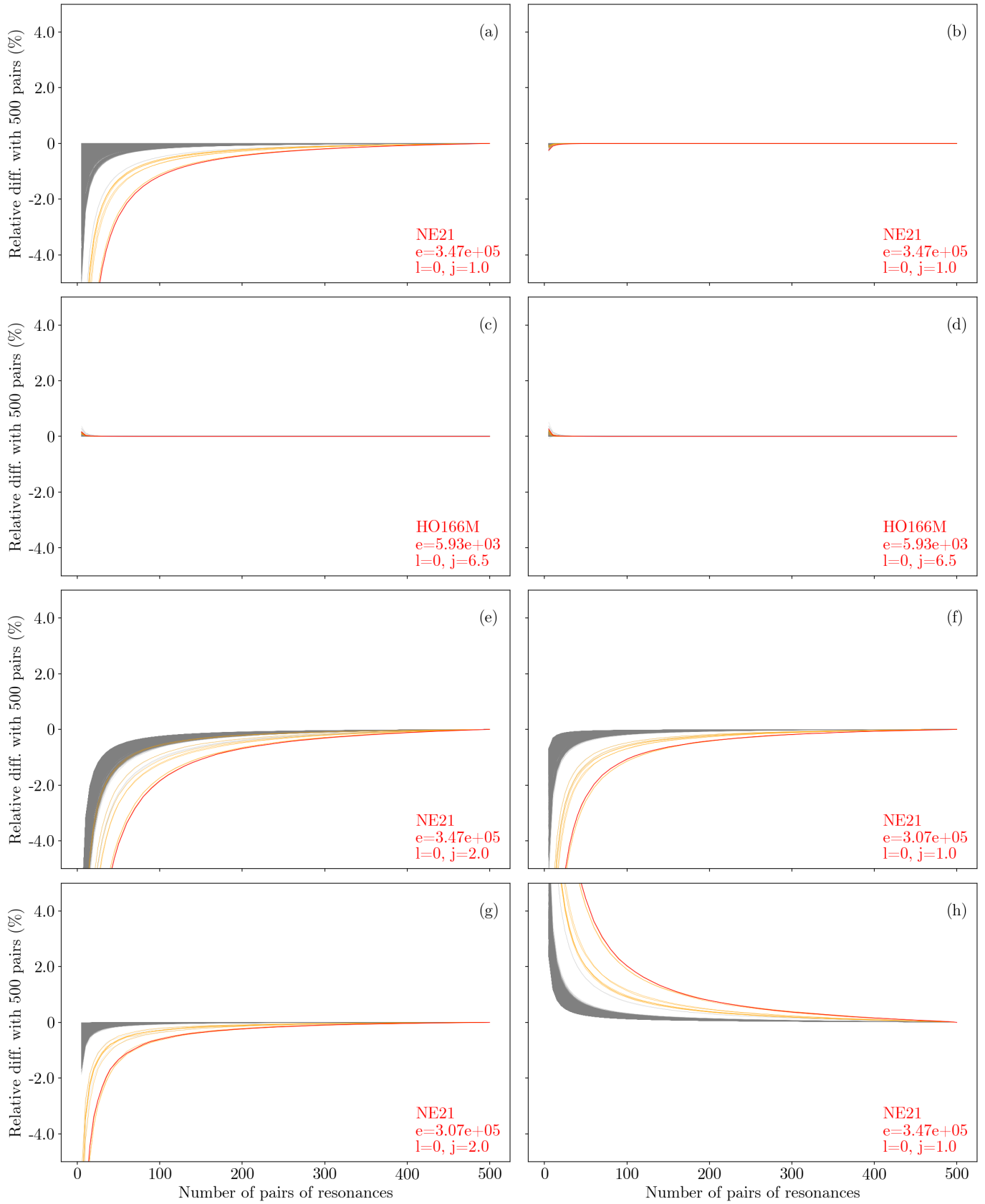
Figure 3.7: Convergence of various statistics of the sampled capture cross sections toward the reference (500 pairs of resonances), at T=0K. (a) mean, (b) variance, (c) skewness, (d) kurtosis, (e) first quartile, (f) fourth quartile, (g) 95th percentile, (h) Kolmogorov-Smirnov distance
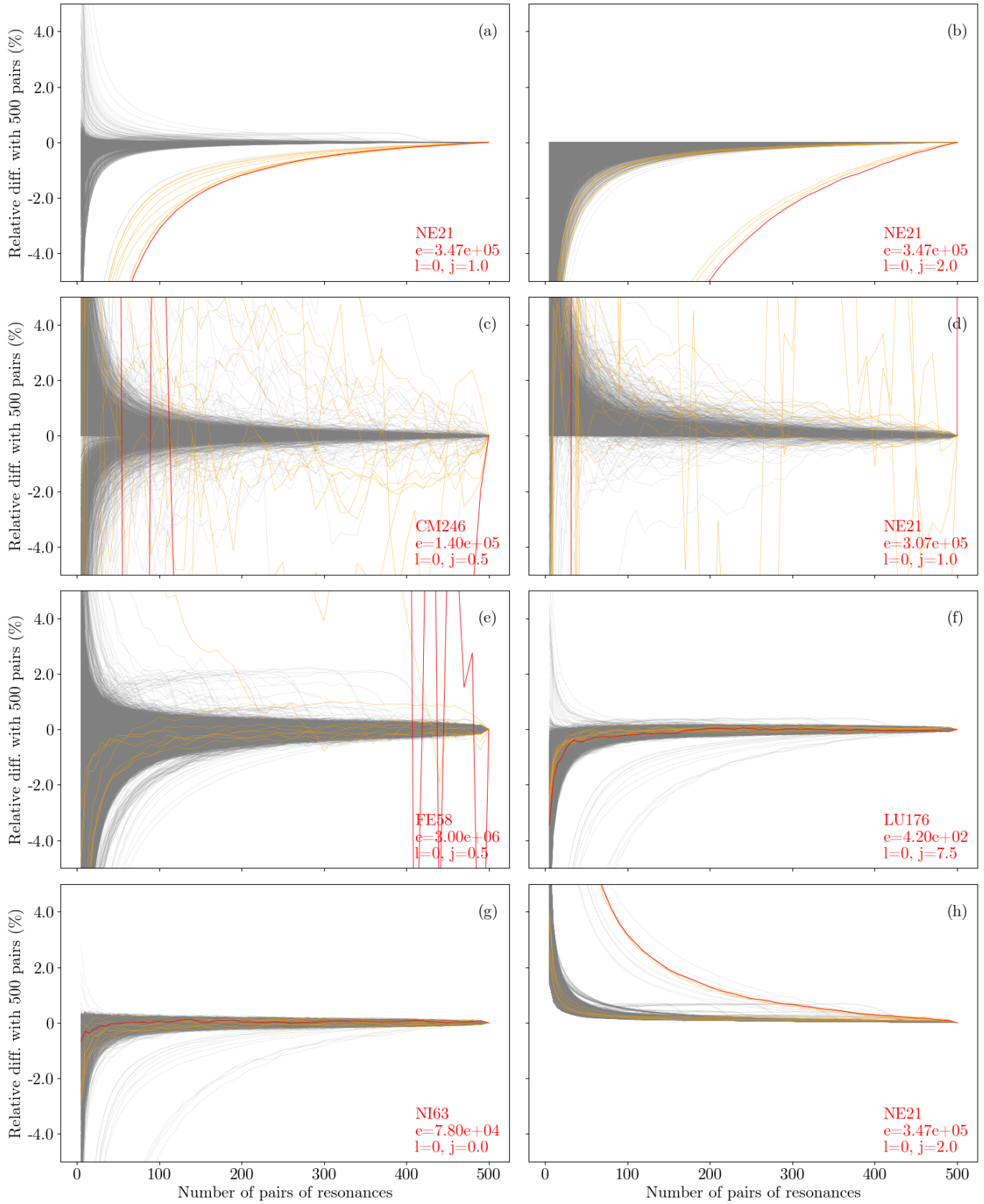
Figure 3.8: Convergence of various statistics of the sampled fission cross sections toward the reference (500 pairs of resonances), at T=0K.. (a) mean, (b) variance, (c) skewness, (d) kurtosis, (e) first quartile, (f) fourth quartile, (g) 95th percentile, (h) Kolmogorov-Smirnov distance
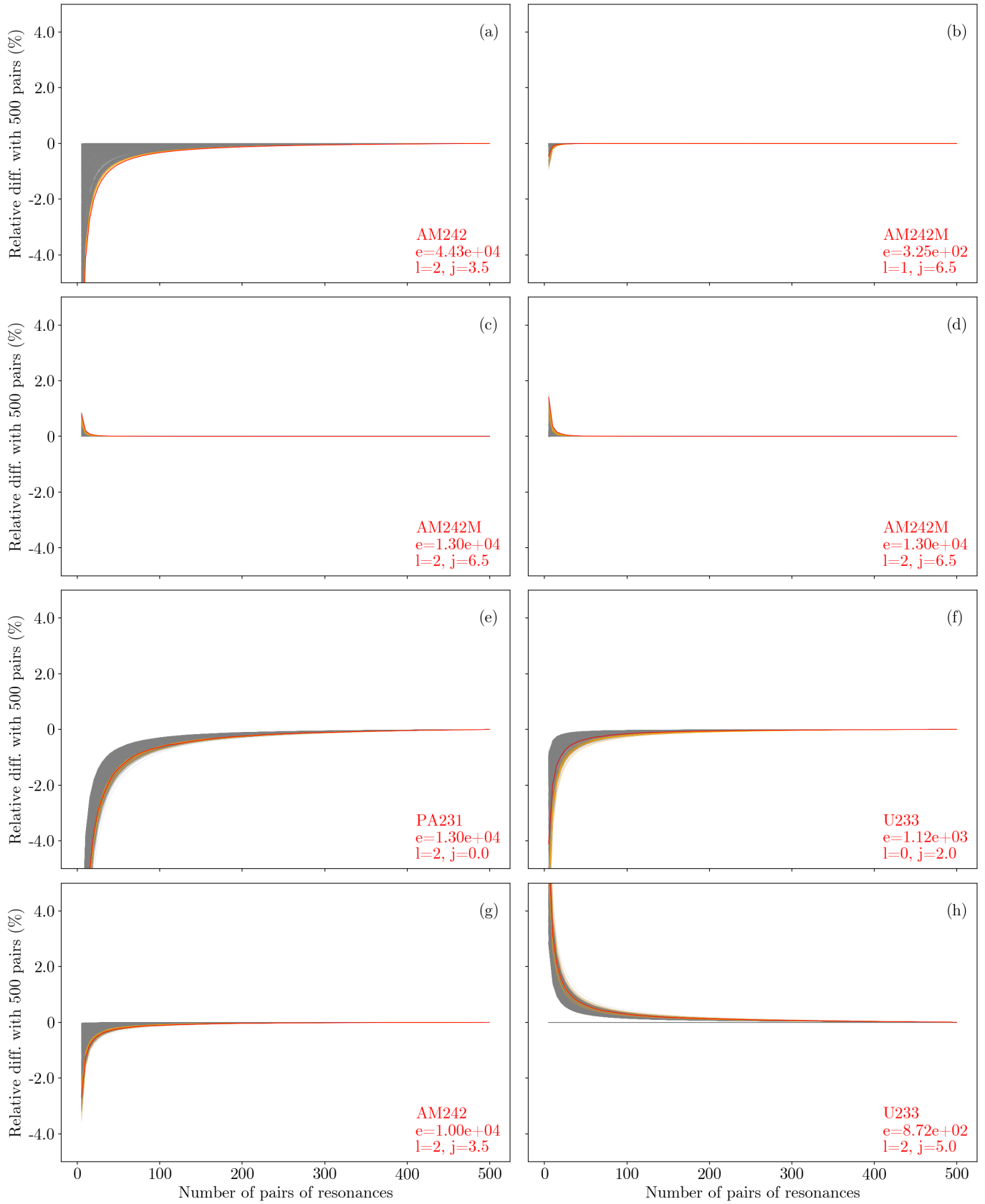
of the cross sections calculated with 500 pairs of resonances in the ladders, and the ones with fewer resonances. As such, the definition of the relative difference used for each statistics (and so the definition of the y-axis of the graphs) is the next one, calling "stat(n)" the value taken by a statistics (mean, variance, first quartile...) computed with n pairs of resonances, so that it expresses a percentage difference:

$$\mathrm{d}_r^{\mathrm{stat}}(n) = 100 \times \frac{\mathrm{stat}(n) - \mathrm{stat}(500)}{|\mathrm{stat}(500)|} \tag{3.1}$$

In the same spirit, the Kolmogorv-Smirnov distance has been computed for each elementary spingroup between the sets of cross sections obtained with 500 pairs and the ones calculated with fewer resonances. This quantity is the maximum absolute value between the two empirical distributions, that are scaled over $[0, 1]$. On the plots, it has been multiplied by 100 to be displayed on the same scale than the other statistics.

The x-axis of the graphs is the number of resonances which have been considered in the ladders to calculate the cross sections. On the plots, all elementary spingroups of JEFF-3.2 have been displayed; each line corresponds to a particular one. In order to make such graphs more readable, some cases have been highlighted in red or orange. The red line corresponds to the less converged case, ie. for which the statistics value obtained from ladders filled with 490 pairs of resonances differed most from the result at 500 pairs. On each graph, the corresponding nuclide of the elementary spingroup, as well as its energy and the (l, J) values were indicated. Orange lines correspond to the next 50 less converged cases. The less converged case corresponding nuclide, energy, and (l, J)-values have been detailed on the bottom right corner of each figure.

Computations have been performed using 100 000 Monte-Carlo iterations, which appeared as a sufficient large number for our needs (cf. Section 3.3.2). Again, let us remind that the randomness of the ladder method is attenuated in the study by the fact the truncations of the main ladder with 500 pairs are actually considered. Computing sets of 100 000 cross section values obtained for increasing numbers of pairs of resonances from 1 to 500 was a too heavy task from a computer memory management point of view. Instead, ladder sizes evenly spaced from 5 to 50 with a step of 5 resonances were considered, and with a step of 10 resonances from 50 to 500. Such a mesh was considered thin enough for a safe interpretation of the results.

Figures 3.6–3.8 call many comments. It is of interest first to summarize in a table the proportions of converged elementary spingroups for the diverse statistics, according to several levels of convergence considered, at different number of pairs of resonances, in order to get a more quantitative understanding of the figures. Indeed, on the figures, all fast-converging elementary spingroups form a cluster of thin overlapping gray lines, which makes them difficult to differentiate. This is achieved in Tables 3.5–3.7. In these tables, each entry corresponds to the percentage of elementary spingroups which converged for less than the indicated number of pairs of resonances, considering a given level of tolerance. The levels considered were 0.1% and 1%. In each case, these thresholds are compared to the percentage difference with the 500-pairs results, considered as a reference calculation. The number of pairs considered in the tables to estimate the proportions were 10, 50, 200, and 490. A result different from 100% for the 490 entry indicates that some elementary spingroups are not converged compared to the 500-pairs result with the selected level of tolerance.

From these considerations, a first very general but actually crucial remark should be made: except for a few cases, most of the elementary spingroups statistics seem to converge very quickly, with less than some dozen of resonances required for all reactions. That means that in most cases encountered in practice, only a few pairs of resonances contribute to the cross sections. As a consequence, taking a random test case is more than likely not to produce a relevant outcome. In particular, even the classical distinction between "light", "medium", or "heavy" nuclei does not seem very relevant. For instance, the lightest ^{21}Ne, the medium ^{55}Mn, and the heavy ^{242}Am are part of the hard-to-converge cases, whereas the second-lightest ^{22}Na converges for only a few resonances. One of the aims of this section will be to establish a more relevant criterion

Level $\epsilon = 0.1\%$	Mean	Var.	Skew.	Kurt.	Qt1	Qt4	95 Pct.	K.S.
≤ 10 pairs	72.87 %	74.91 %	74.07 %	72.47 %	0.11 %	0.32 %	26.76 %	0.0 %
≤ 50 pairs	95.76 %	84.91 %	83.72 %	81.66 %	3.85 %	10.67 %	57.13 %	0.0 %
≤ 200 pairs	99.90 %	97.18 %	96.23 %	94.58 %	32.49 %	76.90 %	88.26 %	5.30 %
≤ 490 pairs	100.0 %	100.0 %	99.92 %	99.95 %	98.68 %	100.0 %	100.0 %	100.0 %
Level $\epsilon = 1\%$	Mean	Var.	Skew.	Kurt.	Qt1	Qt4	95 Pct.	K.S.
≤ 10 pairs	98.49 %	90.15 %	89.10 %	86.80 %	25.09 %	40.96 %	98.08 %	17.01 %
≤ 50 pairs	99.97 %	99.12 %	98.64 %	98.00 %	79.66 %	99.98 %	99.97 %	99.97 %
≤ 200 pairs	99.99 %	99.99 %	99.90 %	99.89 %	99.94 %	99.99 %	99.99 %	99.98 %
≤ 490 pairs	100.0 %	100.0 %	99.99 %	99.99 %	99.98 %	100.0 %	100.0 %	100.0 %

Table 3.5: Proportion of cases for which the statistics values of the elastic cross section samplings converged for less resonances than indicated, for levels of convergence $\epsilon = 0.1\%$ and $\epsilon = 1\%$. The convergence is measured from the percentage difference to the 500-pairs result.

Level $\epsilon = 0.1\%$	Mean	Var.	Skew.	Kurt.	Qt1	Qt4	95 Pct.	K.S.
≤ 10 pairs	68.05 %	99.99 %	99.99 %	99.98 %	0.0 %	0.0 %	92.55 %	0.0 %
≤ 50 pairs	96.13 %	100.0 %	100.0 %	100.0 %	0.0 %	91.73 %	99.23 %	0.0 %
≤ 200 pairs	99.97 %	100.0 %	100.0 %	100.0 %	13.63 %	99.97 %	99.97 %	98.93 %
≤ 490 pairs	100.0 %	100.0 %	100.0 %	100.0 %	100.0 %	100.0 %	100.0 %	100.0 %
Level $\epsilon = 1\%$	Mean	Var.	Skew.	Kurt.	Qt1	Qt4	95 Pct.	K.S.
≤ 10 pairs	97.91 %	100.0 %	100.0 %	100.0 %	0.0 %	97.44 %	99.97 %	0.0 %
≤ 50 pairs	99.97 %	100.0 %	100.0 %	100.0 %	98.88 %	99.97 %	99.99 %	99.97 %
≤ 200 pairs	100.0 %	100.0 %	100.0 %	100.0 %	100.0 %	100.0 %	100.0 %	100.0 %
≤ 490 pairs	100.0 %	100.0 %	100.0 %	100.0 %	100.0 %	100.0 %	100.0 %	100.0 %

Table 3.6: Proportion of cases for which the statistics values of the capture cross section samplings converged for less resonances than indicated, for levels of convergence $\epsilon = 0.1\%$ and $\epsilon = 1\%$. The convergence is measured from the percentage difference to the 500-pairs result.

to distinguish the few cases that require more resonances. As an example to stress out the immense majority of fast-converged cases, after only 50 pairs of resonances, around 95.76% of the elementary spingroups of JEFF-3.2 reach an elastic mean value closer than 0.1% to the 500-pairs outcome, as listed in Table 3.5.

Besides, this fast convergence of most elementary spingroups to the 500-pairs result strengthens the method assumption that the 500-pairs results can be considered as a reference. Note that this claim still depends on the considered statistics and reactions as explained in the following.

Starting with a discussion about the reactions, it looks like more resonances are required to obtain accurate elastic cross sections values than for capture or fission, whatever the statistics of interest. This is easily explained. There is a compensating phenomenon observed for elastic scattering, between the positive and negative contributions of below and above resonances which might cancel each other. Among other things, it is possible to obtain negative cross sections:

Level $\epsilon = 0.1\%$	Mean	Var.	Skew.	Kurt.	Qt1	Qt4	95 Pct.	K.S.
$\leq$ 10 pairs	28.69 %	95.57 %	95.19 %	91.41 %	0.0 %	0.0 %	67.42 %	0.0 %
$\leq$ 50 pairs	70.92 %	100.0 %	100.0 %	100.0 %	0.0 %	22.95 %	88.06 %	0.0 %
$\leq$ 200 pairs	99.03 %	100.0 %	100.0 %	100.0 %	0.0 %	99.98%	100.0 %	64.03 %
$\leq$ 490 pairs	100.0 %	100.0 %	100.0 %	100.0 %	100.0 %	100.0 %	100.0 %	100.0 %
Level $\epsilon = 1\%$	**Mean**	**Var.**	**Skew.**	**Kurt.**	**Qt1**	**Qt4**	**95 Pct.**	**K.S.**
$\leq$ 10 pairs	78.13 %	100.0 %	100.0 %	100.0 %	0.0 %	77.70 %	93.466 %	0.0 %
$\leq$ 50 pairs	100.0 %	100.0 %	100.0 %	100.0 %	32.31 %	100.0 %	100.0 %	100.0 %
$\leq$ 200 pairs	100.0 %	100.0 %	100.0 %	100.0 %	100.0 %	100.0 %	100.0 %	100.0 %
$\leq$ 490 pairs	100.0 %	100.0 %	100.0 %	100.0 %	100.0 %	100.0 %	100.0 %	100.0 %

Table 3.7: Proportion of cases for which the statistics values of the fission cross section samplings converged for less resonances than indicated, for levels of convergence $\epsilon = 0.1\%$ and $\epsilon = 1\%$. The convergence is measured from the percentage difference to the 500-pairs result.

looking at the convergence figures for the mean cross sections Figure 3.6, the 500-pairs results can be reached from above in the case of elastic scattering, whereas it is necessarily reached from below for capture and fission. In fact, the contribution of each resonance cannot be negative for capture and fission, while it might be the case for the elastic scattering in the framework of the SLBW formalism. From a practical point of view, it looks like the elastic scattering is the reaction which must dimension the number of resonances to sample in the ladders.

Among all the statistics to be converged, some look more stable than other ones. Let us focus on the mean first. Basically, the more resonances are added, the more the mean values look like the 500-pairs cases. Soon after 200 pairs, the computed mean value is close to less than 1% from the 500-pairs results for all spingroups and reactions. Moreover, the convergence looks quite regular: the more the added resonances are close from the energy of calculation, the more their contribution seems important. This results in such exponential-like curves, which are a good sign of regularity.

Next comes the variance, which looks even more regular than the mean for all reactions, and converges very fast. Note that for all reactions, the convergence goes from below, which indicates the variance obtained from the 500-pairs ladder is greater than for smaller ladders. The main reason is that computations make use of nested ladders. The dispersion of cross sections is thus more important for larger ladders, which have additional resonances which bring out greater cross sections values. This behaviour is observed for all reactions. As in the case of the mean, elementary spingroups issued from ^{21}Ne seem to be the limiting cases. Note that when this nuclide – which is the lightest found in the library – is discarded, the variance appears as a very fast and regular converging quantity.

Skewness and kurtosis convergences should be discussed a little more in detail. As a reminder, skewness measures the asymmetry of the probability distribution, and kurtosis stands for the weight of the tails compared to the central part of the distribution[21]. They are important statistics to describe the empirical distribution from which the probability tables are to be derived, and cannot be left out. For capture and fission, the number of required resonances looks very small to obtain accurate precision. The situations looks like the variance case, except for the fact this time, it mainly converges from above: skewness and kurtosis tend to be smaller

---

[21]It has not been mentioned yet, but all cross sections distributions are unimodal, ie. they have a single highest value.

for large ladders, which can be explained considering the *stabilization effect* of large ladders.

For the skewness, the highest the value, the more the distribution is skewed on the right, ie. the more huge cross section values weight in the distribution. A smaller value for cross section sets issued from large ladders means their distribution is a little less skewed. For the kurtosis, a smaller value means the relative weight of the tails for the cross sections distribution[22] obtained with more resonances is less important than in the case of small ladders. In both cases, this signifies that with more resonances, the weight of the right tail in the distribution is smaller. There is actually a stabilization of the cross section values around the mean, which is justified by the huge number of small values brought by distant resonances: their huge number compensate randomness. As a consequence, cross sections obtained from larger ladders are more regular, ie. their values are closer from the mean (when corrected from dispersion, which is measured from the variance). This is a very important point that will be found again later: large ladders compensate randomness.

For the case of elastic scattering on the other hand, the situation is less clear. A small but non-negligible amount of cases do not seem to converge regularly for both skewness and kurtosis. Even up to more than 5% difference are observed for an elementary spingroup from ^{246}Cm (skewness) and ^{21}Ne (kurtosis), for ladders composed of 490 pairs. Moreover, the convergence seem pretty erratic for some hundreds of cases, where the addition of ten or twenty pairs of resonances looks enough to shamble the convergence dynamic.

For quantile-related statistics, the convergence is well-established for fission and capture. Once again, the convergence is from below, which is easily explained with the positiveness of each resonance contribution to the cross sections. Additional resonances for larger ladders lead to greater cross sections values, and thus increase the quantile and percentile results. This shift is clearly appreciated from the first quantile. Not a single elementary spingroup of JEFF-3.2 has a first quantile value which remains the same between the reference 500 pairs and the 50 pairs outcome for instance. If this underlines the weight of distant resonances better than the moment-related statistics did, this should be tempered though when one looks at the two other quantile statistics. As they do not change a lot, that means huge values of cross sections are not brought by distant resonance. The first quantile result is just more sensitive to the tiny contributions brought by the distant resonances than the other ones. For elastic scattering, the results are more difficult to apprehend, due to the compensation effect of below and above resonances. The convergence looks more regular than for skewness and kurtosis though.

Finally comes the last statistics of interest, namely the Kolmogorov-Smirnov distance between the empirical distribution of cross sections from whole ladders and its truncations. By definition, this distance is positive. It seems to decrease very regularly. This statistics is of huge interest, because it is an integral measure of the whole distribution from which probability tables are computed. For all reactions, this distance is below 1%[23] after 50 pairs for almost all elementary spingroups, which underlines the speed of convergence of the empirical distribution toward the reference 500-pairs cases, and thus, the relevance of the ladder method to produce probability tables.

Temperature effect

The exact same calculations have been performed at room temperature (T=293.6K). Overall, the results are the same as in the 0K case. The behavior of each statistics remains the same in average, and in order to keep the body of this document a little lighter, results have been moved to the Appendix B on Figures 13–15. Let us stress out that the resonance ladders used to draw these graphs are the exact same ones than at T=0K.

---

[22]Actually, the relative weight of the tails when compared to the central part of the distribution.

[23]Actually, the real value is 0.01 if we consider the $[0, 1]$ interval in which the real image of the empirical cumulative distribution lies.

The influence of temperature is explicit for the variance, for which more resonances seem necessary to converge toward the reference asymptotic 500-pairs outcome than at T=0K. This effect is also visible for the mean, skewness and kurtosis, although it seems less preponderant. In order to justify this behavior, one has to remember that the temperature effect broadens the cross sections around the resonances. Thus, when the temperature increases, farther resonances are expected to have an effect, which is indicated in the plots. Depending on the input elementary spingroups, the effect is more or less marked, but it looks significant enough to shift the required number of pairs of resonances from 100 to 200 to obtain an accurate elastic scattering variance for instance.

This underlines the complexity of the question we are faced to, but clearly exhibits the effect of temperature. Higher values of temperature require more resonances in the ladders. Let us remind that the temperature broadening has another effect though, it flattens the cross sections. As a consequence, cross sections are expected to be more regular, as peaky ones are smoothed by the broadening.

Let us now try to figure out the influence of the other input parameters in the convergence of the cross sections distribution.

Influence of the resonance parameters

The impact of the input parameters on the number of pairs of resonance to sample to obtain good cross sections calculations will be tackled in this paragraph. As a first step, a criterion is required to state whether enough resonances have been sampled. The most straightforward way would be to consider a tolerance threshold for the relative difference between the final 500-pairs case and smaller ladders, for the statistics of interest. In this paragraph, the exact value of that threshold is not very important[24]. It just needs to be carefully chosen to be selective enough to highlight the effect of the input parameters. For instance, it could be set to 0.1% for the Kolmogorov-Smirnov distance in the case of elastic scattering. Let us remind that such a criterion is for now arbitrary.

Once set, the idea is just to obtain the number of pairs for which the threshold is reached. It is just equivalent to plotting over Figures 3.6–3.8 a horizontal line, then considering for each elementary spingroup the corresponding number of pairs above which the threshold is not exceeded. To be slightly more precise, as not all numbers of pairs of resonances have been considered, it is the linearly interpolated numbers that are kept. Once a link has been established between each elementary spingroup and a required number of pairs to sample, it is easy to relate it to the 16 input parameters of the elementary spingroup.

As a first step in the way to identify the important input parameter, parallel plots have been drawn. On these plots, each line represents an elementary spingroup. The last column value is the number of required pairs for a particular statistics, and all previous columns stand out as input parameters values. As an example, the mean and Kolmogorov-Smirnov distance have been considered for elastic and fission at T=0K, on Figures 3.9–3.12. There, the obtained number of pairs on the farthest right column is the minimum number of pairs to sample to obtain a statistics value close to at least 0.1% to the 500-pairs result. The same convention for orange and red than previously has been used: red is the critical case, and the next 50 ones are in orange.

Such plots are useful, as they exhibit input parameters that seem to matter, and for which a relation can be searched for. In particular, from these plots, the importance of the average spacing value appears unquestionable. Small spacings seem to be often related to more resonance needed to obtain accurate resonance cross sections. For the mean, this looks just logical, when one reminds that the decrease is mainly due to the $(E - E_r)^2$ term in the denominator of the cross sections. If the spacing is small, more resonances are necessary to reach a given energy E

---

[24]One may note that for instance, in Tables 3.5–3.7, the number of converged elementary spingroups has been presented for the various statistics according to two threshold levels (1% and 0.1%).
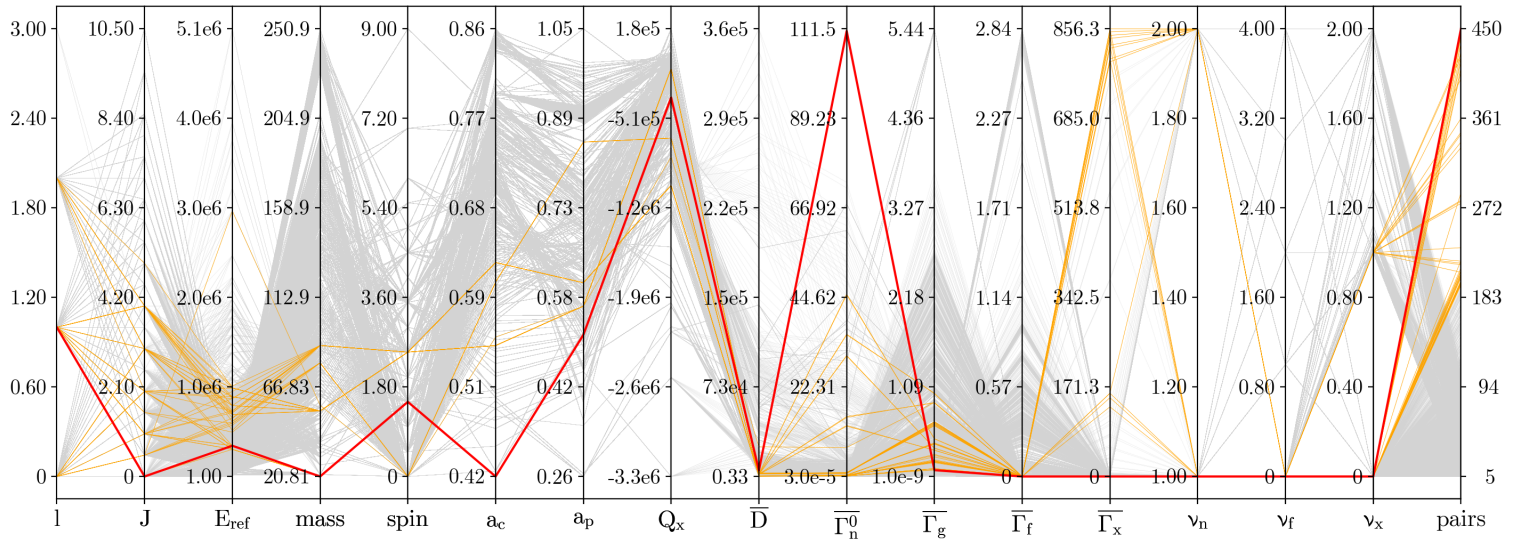
Figure 3.9: Parallel plot of input parameters of elementary spingroups of JEFF-3.2. Last column is the number of pairs of resonances required for the mean elastic cross section to be converged up to 0.1% at T=0K. In red, the critical case, in orange, the next 50 ones.

Figure 3.10: Parallel plot of input parameters of elementary spingroups of JEFF-3.2. Last column is the number of pairs of resonances required for the Kolmogorov-Smirnov distance for elastic scattering to be converged up to 0.1% at T=0K. In red, the critical case, in orange, the next 50 ones. Only the fissionable isotopes of JEFF-3.2 were retained (they are 5311).
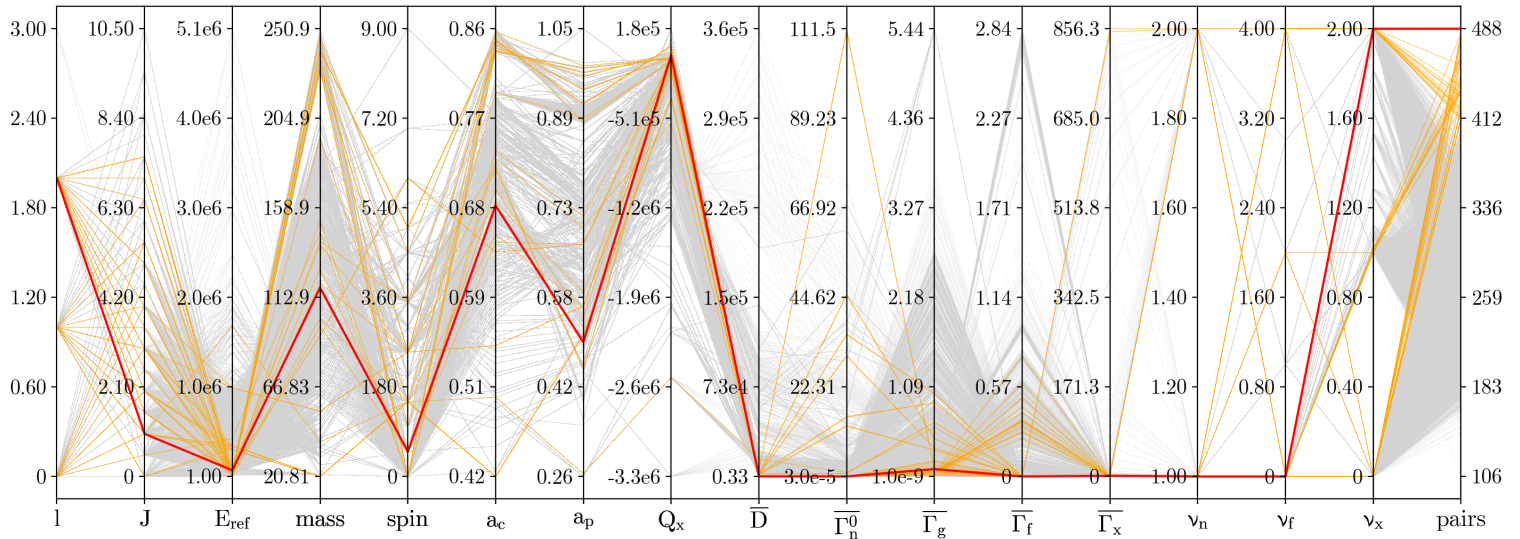
Figure 3.11: Parallel plot of input parameters of elementary spingroups of JEFF-3.2. Last column is the number of pairs of resonances required for the mean fission cross section to be converged up to 0.1% at T=0K. In red, the critical case, in orange, the next 50 ones. Only the fissionable isotopes of JEFF-3.2 were retained (they are 5311).
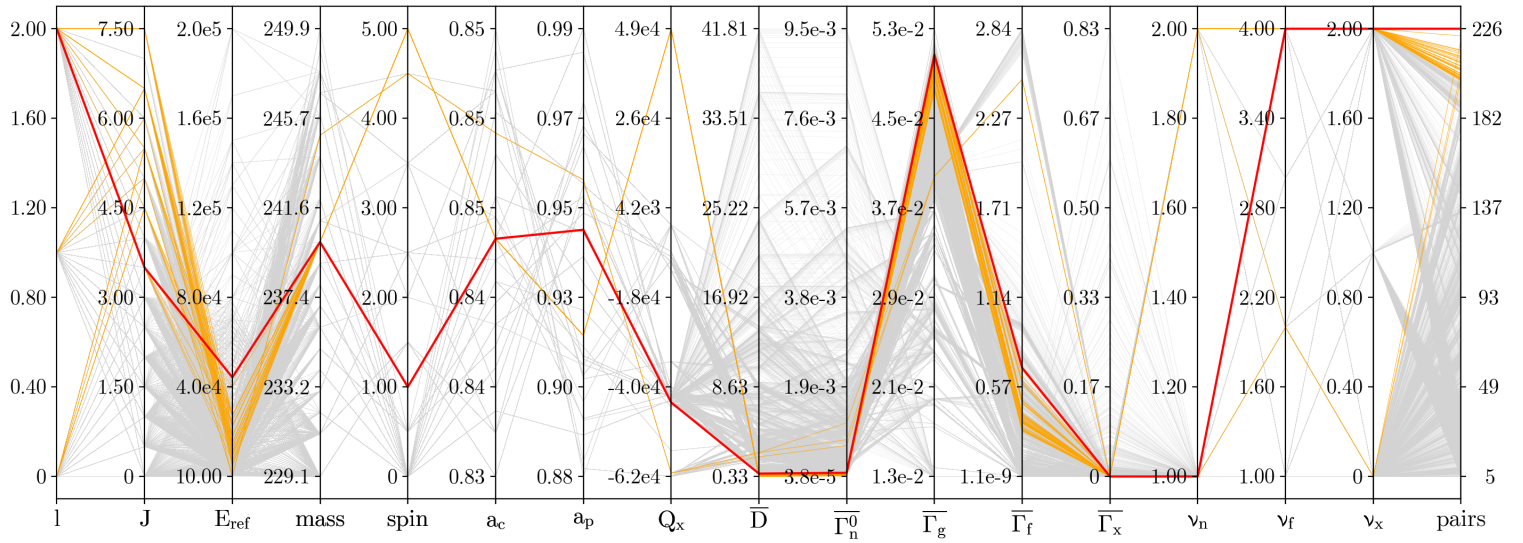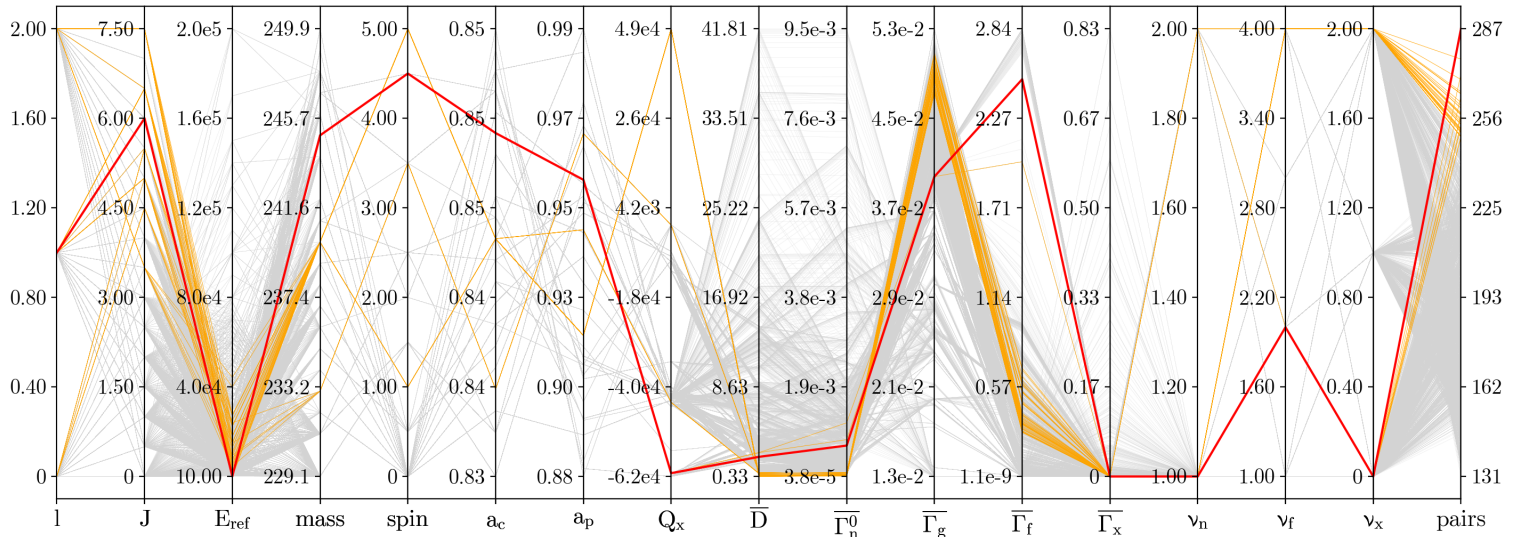

Figure 3.12: Parallel plot of input parameters of elementary spingroups of JEFF-3.2. Last column is the number of pairs of resonances required for the Kolmogorov-Smirnov distance for fission to be converged up to 0.1% at T=0K. In red, the critical case, in orange, the next 50 ones. Only the fissionable isotopes of JEFF-3.2 were retained (they are 5311).
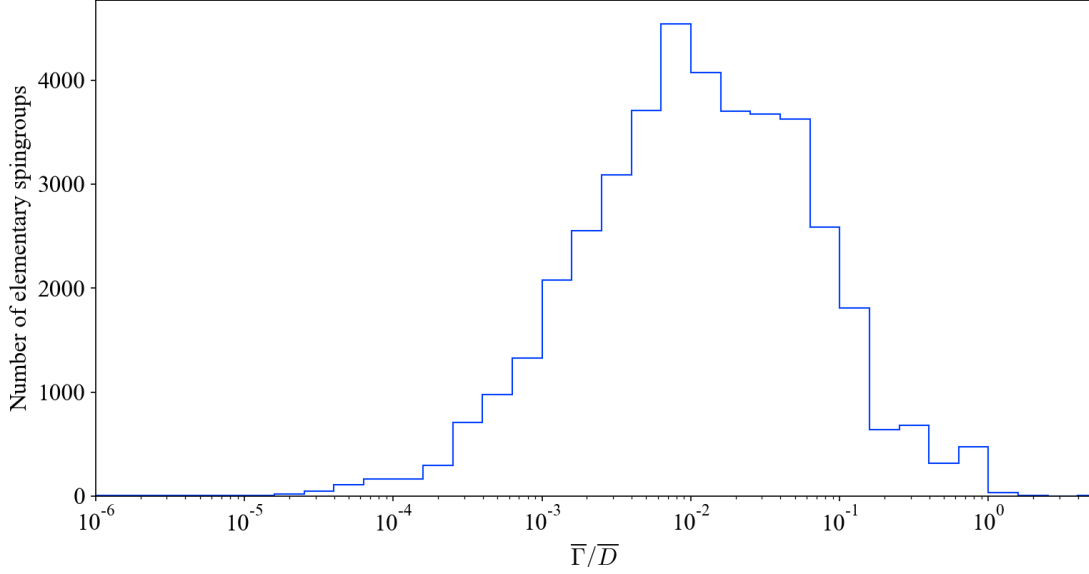
Figure 3.13: Histogram of all the $\overline{\Gamma}/\overline{D}$ values for all elementary spingroups of JEFF-3.2

when the sampling starts from E_{ref}. Actually, this dependence seems to have a influence on the Kolmogorov-Smirnov distance too, and so on the whole empirical distribution. This influence is visible for all the other statistics, even if this has not been presented in this document.

Trying to go further in the exploration of the link between the input parameters and the required number of pairs, it appeared that the spacing was not enough alone. After several attempts, the more interesting variable to introduce turned out to be the ratio $\overline{\Gamma}/\overline{D}$ of the total average width associated with the elementary spingroup and the average spacing. The average total width $\overline{\Gamma}(E)$ is there simply calculated at the reference energy of the elementary spingroup[25]:

$$\overline{\Gamma} = \overline{\Gamma_n}(E_{ref}) + \overline{\Gamma_\gamma} + \overline{\Gamma_f} + \overline{\Gamma_x} \tag{3.2}$$

Note that a proper definition of this quantity is thus only possible in the framework of the elementary spingroups calculations. The reason why this quantity seems more adapted to describe the necessary number of resonances to fill the ladders is again related to the denominator in the cross sections formulas, which exhibit a competition between the square of the total width and the average spacing. This quantity looks like a well-known value in the evaluator community, namely the *strength function*. However, the strength function S is usually defined as the ratio of the reduced neutron width, which does not depend on the energy, and the average resonance spacing, such that $S = \overline{\Gamma_n^0}/\overline{D}$. As an example, previous Figure 3.3 exhibited the strong relation that occurs between these values in average. There, the quantity put forward is slightly different. Figure 3.13 displays the histogram of all $\overline{\Gamma}/\overline{D}$ values found in the elementary spingroups of JEFF-3.2.

In most cases encountered in JEFF-3.2, $\overline{\Gamma}/\overline{D}$ is below 1, which means the average spacing between the resonances is usually greater than the average total width. This remains logical as in the unresolved resonance range, although resonances are indistinguishable, they do not fully overlap. The grater value obtained for $\overline{\Gamma}/\overline{D}$ in JEFF-3.2 equals 4.552, and is obtained for the upper limit of the unresolved resonance range of the first spingroup of the light nuclide ^{21}Ne, namely $E_{ref} = 0.347221$ MeV, $l = 0$, $J = 1$. The smallest value, which equals $2.842201.10^{-7}$, is found for the smallest reference energy of ^{197}Au, for $l = 2$, $J = 1$.

The required number of pairs of resonances estimated for each elementary spingroup to reach a relevant level of convergence compared to the asymptotic case have been plotted against cor-

---

[25]Actually, it is the neutron width which is calculated at the reference energy from the reduced neutron width.

responding $\overline{\Gamma}/\overline{D}$ values on Figure 3.14 for T=0K, and Figure 3.15 for T=293.6K. The threshold level has been set to 0.1% of the reference 500-pairs outcome.

From these figures, the ratio $\overline{\Gamma}/\overline{D}$ looks like a relevant quantity to consider to estimate the required number of resonances to sample. Even if the behavior slightly changes according to the reaction, temperature, and statistics, a positive correlation between $\overline{\Gamma}/\overline{D}$ and the number of resonances to sample in the ladder is undeniable. The more the spacing is big compared to the average total width, the less resonances need to be sampled. This makes sense compared to what has been said previously about the role of the spacing in the formulas, and even precise its weight compared to the average widths.

Let us be slightly more precise, starting with capture and fission reactions. Both reactions are computed from the same formulas, where $\overline{\Gamma_\gamma}$ and $\overline{\Gamma_f}$ play an interchangeable role. As such, they roughly adopt the same behaviour on Figures 3.14–3.15. For all statistics, the required number of resonances to sample seems to increase according to the $\overline{\Gamma}/\overline{D}$ value of the elementary spingroups. Although this remains a crude statement, this increase seems to follow an exponential trend, which really starts after $\overline{\Gamma}/\overline{D}$ exceeds a given value. For the mean, variance, skewness, kurtosis and 95th percentile in particular, the 5-pairs result corresponds to the 500-pairs result before such threshold, which depends on the statistics. For the mean, the number of required pairs exceeds 5 (the smallest ladder size considered) when[26] $\overline{\Gamma}/\overline{D} \geq 10^{-2}$. Of course, this latter value is purely arbitrary, as it depends on the previously fixed convergence criterion, here 0.1% of the reference 500-pairs outcome. It is also statistics-dependent. For instance, it seems that the required number of resonances to obtain an accurate variance, skewness, or kurtosis estimation starts to raise around $\overline{\Gamma}/\overline{D} = 0.5$ for both capture and fission at T=0K. For the 95th percentile, a quadratic increase occurs around $\overline{\Gamma}/\overline{D} = 0.1$. For the first and third quartile, as well as for the Kolmogorov-Smirnov distance, greater $\overline{\Gamma}/\overline{D}$ values seem to increase the number of required resonances too after the same 10^{-2} threshold. The main difference for these latter statistics is that even for very small values of $\overline{\Gamma}/\overline{D}$, the required number of resonances remains high; it lies around 200 for the first quartile at 0K for instance. For T=293.6K – and although the figures are more complex, especially for quantile-related quantities – the same trends appear.

As expected, the number of resonances to be considered for the elastic scattering is more difficult to apprehend, due to the cross sections more complex shape. Still, the required number of resonances for the ladders to be filled seems to follow the same trend than fission and capture. Namely, the number of resonances increase with $\overline{\Gamma}/\overline{D}$. Even more useful, it seems that this number starts to raise at the same level too. Having set a 0.1% tolerance threshold, the number of required resonances starts to increase for input sets which verify $\overline{\Gamma}/\overline{D} > 5.10^{-3}$ for the mean for instance. For elastic scattering, all moment-statistics seem to raise around this point. A main difference with capture and fission is there the possibility to require only a few number of pairs of resonances to be converged even at high $\overline{\Gamma}/\overline{D}$ values. Inversely though, an important required number of resonances seems to imply a high $\overline{\Gamma}/\overline{D}$ value. The quantile-related statistics are more difficult to interpret there, in particular because the convergence criterion is too strong: the 500 pairs-result is often reached. Instead, one may consider Figure 16 and Figure 17 in the appendix B, which are the same scatter plots than Figures 3.14–3.15, except the retained convergence criterion was only 1% of the 500-pairs result. Even if a direct relationship is still hard to decipher, it must be underlined that the hardest-to-converge spingroups are again the ones with a high $\overline{\Gamma}/\overline{D}$ value. The same behaviour is observed for the Kolmogorov-Smirnov distance.

It seems that the $\overline{\Gamma}/\overline{D}$ value is a relevant quantity to estimate, in order to determinate the size of the ladders to sample. Providing such criterion will be useful, but let us for now focus on the detail of the number of Monte-Carlo iterations to be run in the ladder method.

---

[26]Considering Figure 3.13, half of the elementary spingroups have a $\overline{\Gamma}/\overline{D}$ value greater than 10^{-2}.

Figure 3.14: Required number of resonances to reach close to 0.1% of the 500-pairs values for each spingroup, plotted against their $\overline{\Gamma}/\overline{D}$ value, at T=0K. Each figure corresponds to a statistics of interest: (a) mean, (b) variance, (c) skewness, (d) kurtosis, (e) first quartile, (f) fourth quartile, (g) 95th percentile, (h) Kolmogorov-Smirnov distance
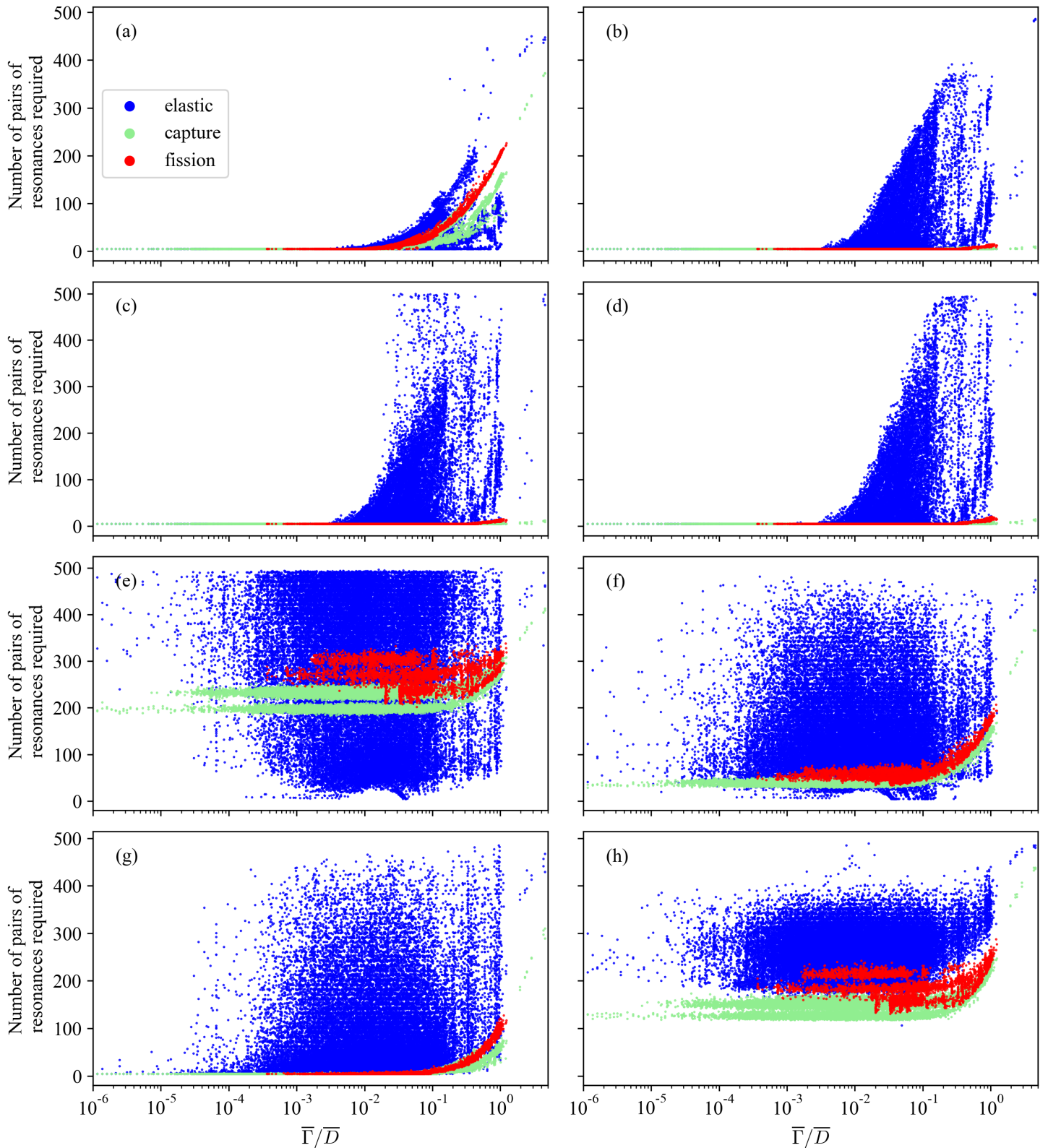
Figure 3.15: Required number of resonances to reach close to 0.1% of the 500-pairs values for each spingroup, plotted against their $\overline{\Gamma}/\overline{D}$ value, at T=293.6K. Each figure corresponds to a statistics of interest: (a) mean, (b) variance, (c) skewness, (d) kurtosis, (e) first quartile, (f) fourth quartile, (g) 95th percentile, (h) Kolmogorov-Smirnov distance
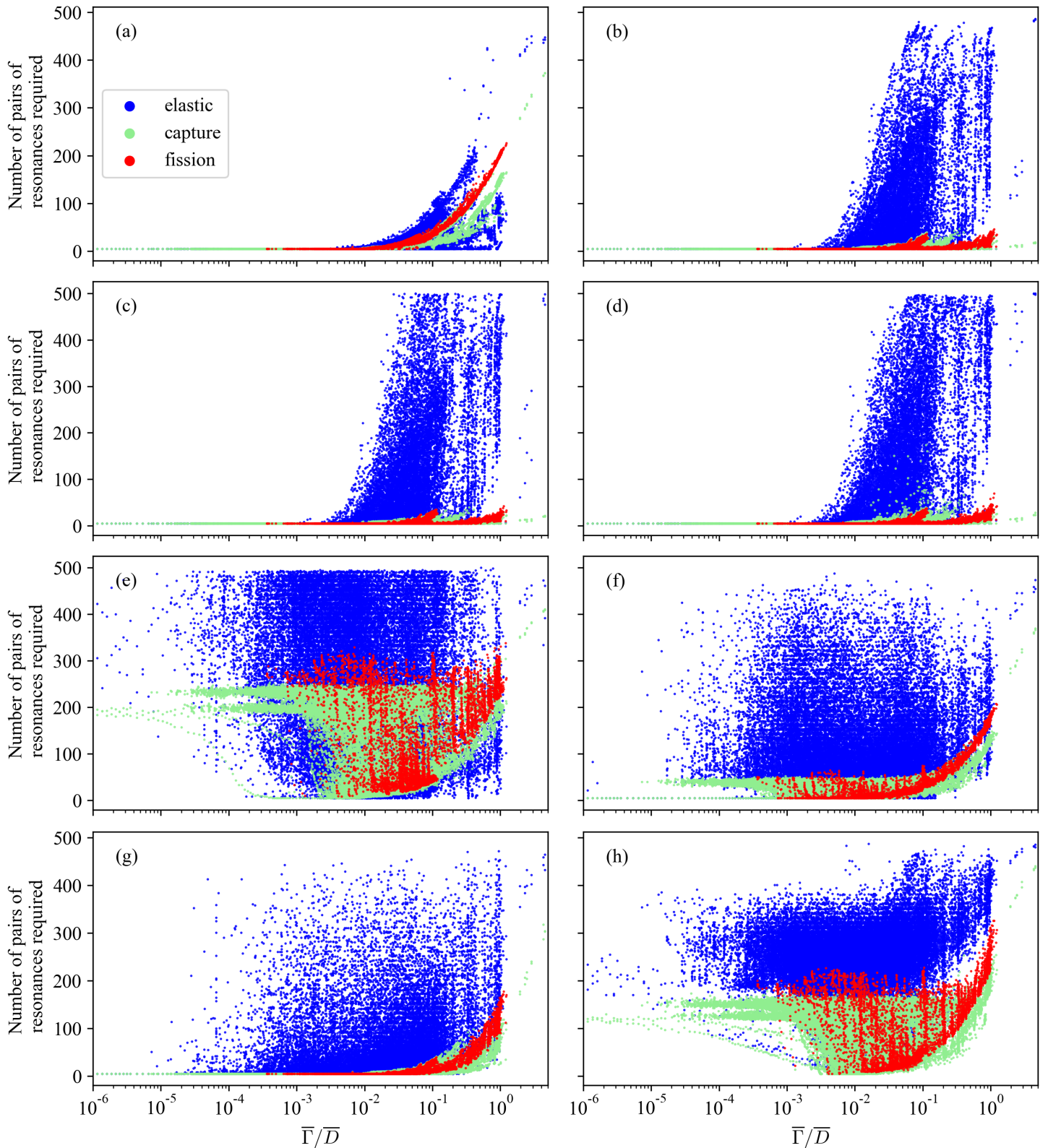
3.3.2   Number of Monte-Carlo iterations

The goal of this subsection is to observe the impact of additional Monte-Carlo iterations over the sampled cross sections sets for each elementary spingroups, as put forward in Section 3.2.3. Here, only large 500-pairs ladders are considered. An important goal is to observe the evolution of the cross sections sets when the number of Monte-Carlo iterations increases – keeping in mind that the more Monte-Carlo iterations are run, the more the results are precise. As such, the objective is twofold. First, roughly estimating a minimum number of repetitions for the ladder method in order to get acceptable results seems to be a minimum target. Secondly, it is of main interest to investigate the dependence of the convergence according to the input parameters sets, like what has been carried out in the previous subsection for the size of the ladders.

The most straightforward idea is to compare cross section distributions obtained with different numbers of Monte-Carlo iterations, in order to estimate the influence of additional runs. Thus, ladder method calculations have been performed using different random seeds, for 10000, 20000, 100000, and 200000 Monte-Carlo iterations, for each elementary spingroups of JEFF-3.2. Moment and quantile statistics have been computed, and their percentage difference computed. In particular, it is interesting to focus on the impact on the outcomes when the number of iterations is doubled, as it brings a comparable amount of iterations, which still remain in the same order of magnitude. As a result, the percentage of difference between 10000 and 20000 iterations was computed for all quantile and moment statistics, as well as between 100000 and 200000 iterations.

The results have been displayed for all elementary spingroups on Figure 3.16 for T=0K, and Figure 3.17 for T=293.6K. Each figure corresponds to a particular statistics – four moment ones, and three quantile ones. The left column displays the percentage difference for each elementary spingroup between 10000 iterations and 20000 iterations. On the right column stands the percentage difference between 100000 and 200000 runs. On these figures, the x-axis displays the indexed 41 486 elementary spingroups of JEFF-3.2. Instead of displaying them in an arbitrary order[27], a more clever option is to sort all spingroups according to their $\overline{\Gamma}/\overline{D}$ value, which has been proven to be relevant in the number of resonances study. On Figures 3.16–3.17, spingroups have been sorted in ascending order by $\overline{\Gamma}/\overline{D}$ values, so that the more the points are on the left, the more their ratio $\overline{\Gamma}/\overline{D}$ is small[28].

As in previous subsection, these figures call out many comments. First of all, the percentage difference observed between the 10 000 and 20 000 cases is much bigger than between 100 000 and 200 000, for both temperatures and reactions. At T=0K, 100% difference is even reached regularly, for moment-related statistics of the elastic scattering[29]. Even if the immense majority of the cases reaches acceptable levels of convergence, this pushes forward the idea that 10 000 iterations do not constitute a sufficient order of magnitude.

The most interesting feature is the apparent correlation between the low $\overline{\Gamma}/\overline{D}$ values and huge percentage differences, especially for moment-related quantities such as average. Even if less marked, quantile-related statistics seem to follow the same trend. Accordingly, the density of highly-fluctuating outcomes is more important in the left part of the plots than on the right, ie. for elementary spingroups whose average total width is lower than average spacing. Such density seems to decrease regularly when moving toward higher $\overline{\Gamma}/\overline{D}$ values[30]. As a reminder,

---

[27]For instance, on Table 3.2, elementary spingroups are sorted in ascending mass units, then l-value, J-value, and finally reference energy. This corresponds on a straightforward way of parsing libraries.

[28]Note that the x-axis has not been chosen as the $\overline{\Gamma}/\overline{D}$ quantity directly, even if such a choice would have been possible. However, it turned out that choosing an x-axis on which all points are arbitrarily fixed and equally distant was just more efficient to exhibit the calculations sensibility to fluctuations. To be more precise, setting the $\overline{\Gamma}/\overline{D}$ as the x-axis would have resulted in many points in the middle of the graphs, making it less readable. As a consequence, sorted-indexed x-axis were preferred in this part.

[29]Let us notice that this reaction is once more the limiting case, as it fluctuates much.

[30]Again, there is no such thing as a regression in this affirmation, as the x-axis is not $\overline{\Gamma}/\overline{D}$, but sorted indexes. At best, this defines a rank correlation.

Figure 3.16: Percentage of difference for several statistics ((a) mean, (b) variance, (c) skewness, (d) kurtosis, (e) first quartile, (f) fourth quartile, (g) 95th percentile) of the cross section sets corresponding to the elementary spingroups of JEFF-3.2 sorted in ascending $\overline{\Gamma}/\overline{D}$, at T=0K. On the left, the comparison is between 10 000 and 20 000 iterations, on the right for between 100 000 and 200 000 iterations.
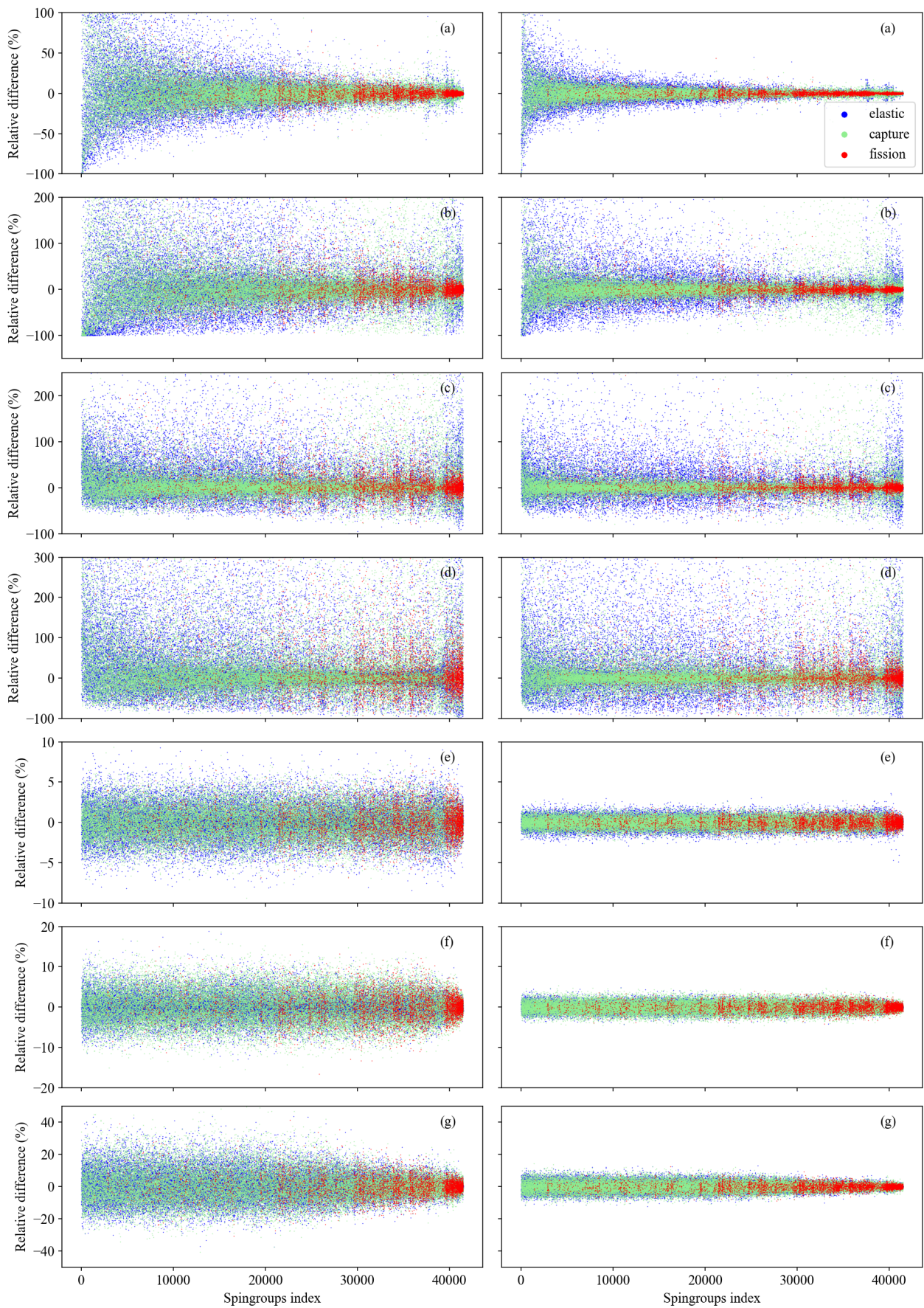
Figure 3.17: Percentage of difference for several statistics ((a) mean, (b) variance, (c) skewness, (d) kurtosis, (e) first quartile, (f) fourth quartile, (g) 95th percentile) of the cross section sets corresponding to the elementary spingroups of JEFF-3.2 sorted in ascending $\overline{\Gamma}/\overline{D}$, at T=293.6K. On the left, the comparison is between 10 000 and 20 000 iterations, on the right for between 100 000 and 200 000 iterations
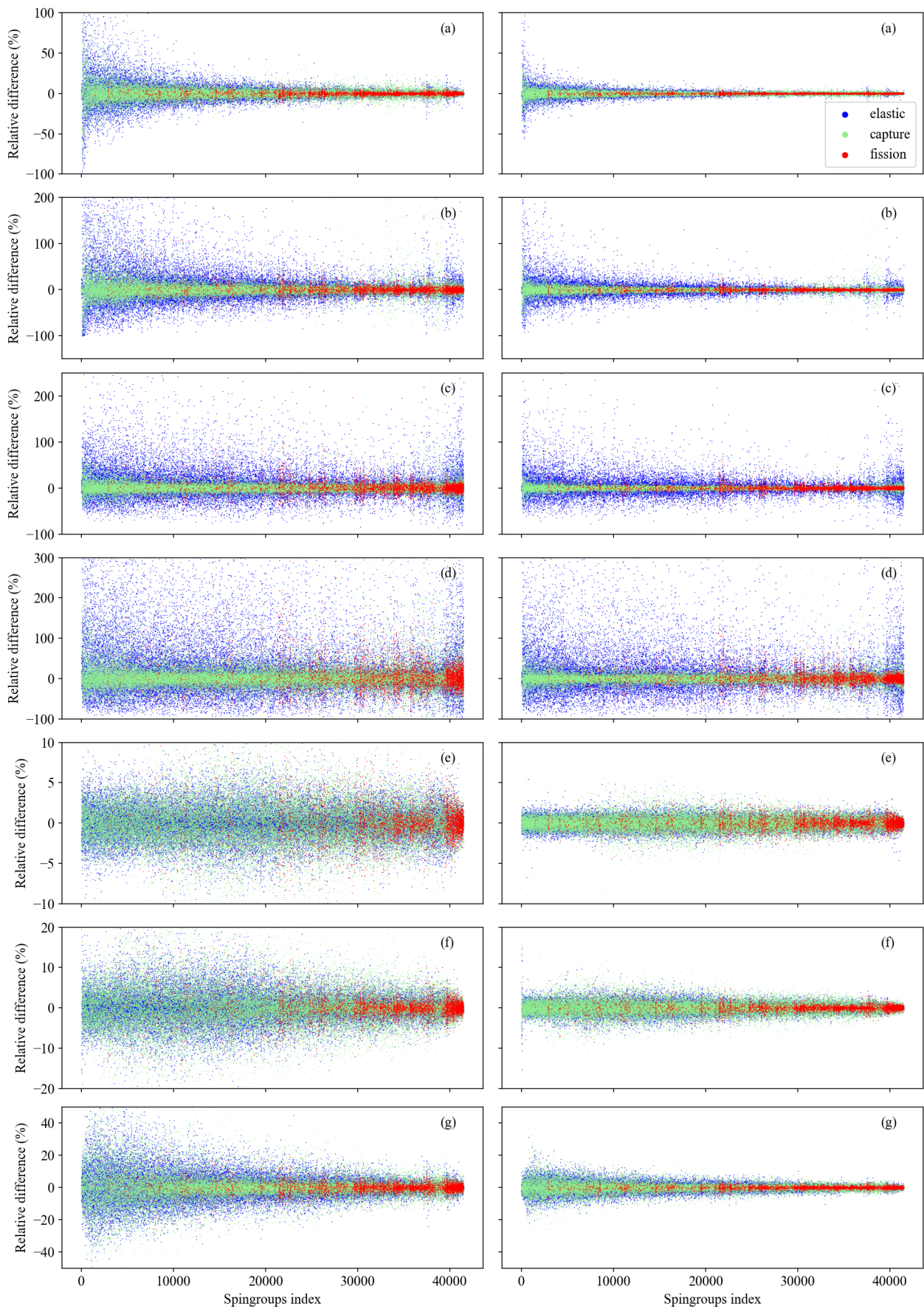
the median of the set is around $\overline{\Gamma}/\overline{D} = 10^{-2}$. This is important from a practical point of view, as this supposes that more iterations could be required for elementary spingroups whose average spacing is much greater than average total width.

This behavior is actually related to the apparent size of the ladders at the energy of calculations. As seen in the previous subsection, low $\overline{\Gamma}/\overline{D}$ lead to only a few resonances contributing to the cross sections at E_{ref}. However in this case, this also means their randomness is less susceptible to be compensated by other resonances from the ladder. In other words, when $\overline{\Gamma}/\overline{D}$ is huge, many resonances from the 500-pairs ladders effectively contribute to the cross sections, so that from the basic point of view of random numbers generation, more generated numbers are taken into account. As a consequence the Monte-Carlo technique that underpin the ladder method is more efficient. This interpretation is supported by another fact: when temperature increases, the percentage difference between the several numbers of iterations decreases. This is due to the flattening effect of the Doppler-broadening, which implies that more resonances contribute to the cross sections, and thus stabilize the Monte-Carlo fluctuations.

From a very practical point of view, a trade-off seems to emerge: huge $\overline{\Gamma}/\overline{D}$ values means the ladders have to be filled with many resonances, and on the other hand, small $\overline{\Gamma}/\overline{D}$ implies more Monte-Carlo iterations. Let us underline that a structural difference remains between the number of resonances to consider and the number of Monte-Carlo iterations to be run. The latter one behaves more like a numerical artifact than it relies on a strong physical meaning. Cross section distributions obtained with a few Monte-Carlo iterations could lead to precise results even for elementary spingroups with a low $\overline{\Gamma}/\overline{D}$, if the random numbers are "luckily drawn". On the contrary, taking small ladders for huge $\overline{\Gamma}/\overline{D}$ is more than likely to lead to false results: the physical reason is that ignored resonances would actually have contributed to the cross sections. Considering too small ladders in such case actually adds a systemic error to the statistical one, whereas running too little Monte-Carlo iterations only brings up statistical uncertainty.

The case of the average cross section values is particular for several reasons. First of all, it remains the most important statistics to obtain in the unresolved resonance range. Average cross sections are sometimes used directly in the unresolved range in neutronics codes, and even if probability tables are preferred, the crucial reaction rates quantities still depend on them. Secondly, average cross sections are useful in the context of the ladder method because they also can be computed from the resonance parameters directly.

In the present work, mean values derived from the ladder method cross sections sets have been compared with the average values computed from the resonance parameters. These latter ones were gotten from the Moldauer method of calculation of the widths fluctuation factor, as in Section 2.2. Average comparisons have been carried out with the values corresponding to several numbers of Monte-Carlo runs. The percentage differences have been summarized on Figure 3.18 for T=0K and T=293.6K. On this figure, the x-axis is the same one than previously: it is just the indexed elementary spingroups, sorted according to their $\overline{\Gamma}/\overline{D}$ ratio.

Very briefly, the more Monte-Carlo iterations are run, the closer the averages draw up the Moldauer calculations. The less converged cases are obviously the low $\overline{\Gamma}/\overline{D}$ values regardless of the number of Monte-Carlo runs, but it has been proven they were the more fluctuating cases. Moreover, adding Monte-Carlo runs seems to bring the average values closer to the Moldauer calculations for any $\overline{\Gamma}/\overline{D}$ value. It is also of interest to remark that the calculations at T=293.6K need less iterations than at T=0K to reach the same level of convergence. It is believed the reason is here again related to the more important number of contributing resonances in the ladder, which reduces the fluctuations.

This brings up two important consequences: the proposed implementation of the ladder method provides average values in agreement with the theory developed in Section 2.2. Secondly, and even if the immense majority of spingroups seems to converge, the number of iterations definitely needs to be raised for elementary spingroups with low $\overline{\Gamma}/\overline{D}$ values for practical applications, especially at low temperatures. The proposed 100 000 iterations reference was fine enough for the studies conducted in this chapter, which were quite computationally intensive,
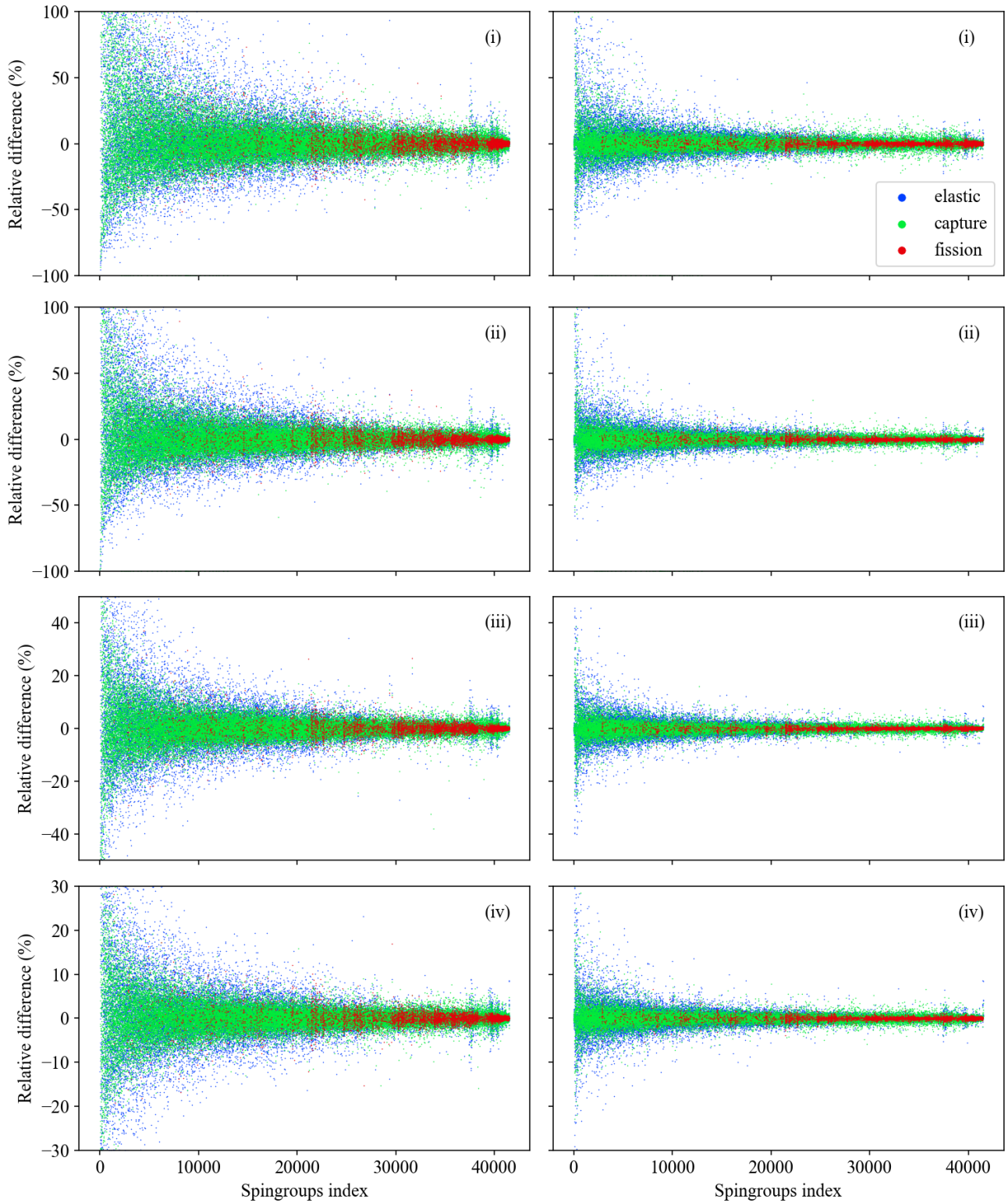
Figure 3.18: Percentage of difference between cross sections mean values from the ladder method, and average calculations using the Moldauer method to compute widths fluctuation factors. Elementary spingroups of JEFF-3.2 sorted in ascending $\overline{\Gamma}/\overline{D}$ are indexed on the x-axis. On the left, calculations are made at T=0K, on the right at T=293.6K. Each line deals with cross section sets of different sizes: (i) 10 000, (ii) 20 000, (iii) 100 000, (iv) 200 000 iterations.

but we believe an additional order of magnitude could be required for low (below 10^{-2}) $\overline{\Gamma}/\overline{D}$ spingroups in practical applications. Let us finally note that in some cases, an additional possibility exists: when the LSSF flag is set to 1 in the ENDF evaluation, the calculations only serve to produce probability tables which are normalized on a mean value provided in the evaluation. As a conclusion, the present study recommends the evaluators to consider this option in the case of low $\overline{\Gamma}/\overline{D}$ values.

Conclusion of the chapter

The work carried out in this chapter consisted to develop a resonance sampling methodology for the ladder method, in the perspective to compute probability tables in the unresolved resonance range. The sampling aims at building sets of resolved resonances around a reference energy in the unresolved resonance range – referred as ladders – from the tabulated average parameters provided in the evaluations. The most straightforward way is to sample successive resonances, using the classical Wigner law for the resonance spacings, and χ^2 distributions for the resonance widths.

The choice of the first resonance to place must be handled carefully. Two methods, implemented in the NJOY and AMPX codes respectively, have been investigated. The first one defines two energies as the limits of the ladder, and fills the interval with resonances. The second method starts with setting the two resonances which surround the reference energy, and then successively adds the next lower and upper resonances, which defines a *paired* sampling. In both methods, it has been shown in this chapter that the central spacing which contains the reference energy must follow a distribution slightly different than the Wigner surmise $W(x)$. Indeed, the situation is a natural application of the well-known *bus waiting time paradox*, which states that the law of the central spacing must rather be $xW(x)$, in case of an infinite number of resonances. In the second method of sampling, this asymptotic law can be obtained by construction. For the NJOY energy-based method of sampling, a numerical simulation proved that a few resonances were enough to ensure this result.

The next crucial question tackled in this chapter is related to the size of the ladders. Indeed, all resonances in the sampled ladders contribute to the cross sections calculation at the reference energy, but their influence decreases when they are distant. As a consequence, resonances have to be sampled until their contribution to the final cross sections becomes marginal. In this thesis, a methodology has been developed to estimate the required number of pairs of resonances to sample around a reference energy, according to the value of the input resonance parameters. To do so, the calculations in the unresolved resonance range for each nuclide have been divided into cross sections sub-calculations for independent spingroups at each reference energy. These sub-calculations make use of 16 scalar input parameters (plus the temperature), referred to in this document as *elementary spingroups*. The number of required resonances in the ladder sampling is actually easier to investigate for such elementary spingroups than for nuclides directly, especially because the role of each resonance parameters can be highlighted. In order to obtain a base of test cases, the unresolved resonance ranges of the entire nuclear data library JEFF-3.2 have been converted into 41 486 elementary spingroups. Working with an entire library presents the interest to explore most of the practical situations. The choice has been made to focus on JEFF-3.2, which is well-used in the industry and criticality safety studies, and contains more "extreme cases" than some other more recent libraries. The decomposition of libraries into elementary spingroups is a major component of the work carried out in this thesis. In particular, it turned out to be very practical to investigate several questions about the in-use methodologies in the unresolved resonance range, starting with the size of the ladders to be sampled.

Relying on the proper definition of the elementary spingroups, a methodology to estimate a sufficient number of pairs of resonances to sample has been established. The idea is to consider the output distribution of cross sections sampled from large ladders composed of 500 pairs of resonances as a reference result. Then, cross sections distributions calculated from truncations of

these ladders were considered, and compared to the reference result. The resulting distributions were tested against each other relying on diverse statistics, such as several moments, quantiles, and the Kolmogorov-Smirnov distance between the empirical distributions. This operation has been performed for all the elementary spingroups of JEFF-3.2, to identify the input sets of average resonance parameters which require more pairs of resonance to converge toward the reference 500-pairs result. It has been shown that the convergence is more difficult for the elastic scattering reaction systematically, for all the considered statistics. Actually, a compensating phenomenon between the upper and lower resonances exists for the elastic scattering, which explains the more difficult convergence. This makes elastic scattering the reaction to consider when choosing a number of resonances to fill the ladders. In the same way, it has been observed in this chapter that higher temperatures calculations require wider resonance ladders, as the Doppler-broadening effect extends the resonances influence.

Looking for a relation between the input resonance parameters and the required size of the ladders, a clear positive correlation has been highlighted between the number of resonances to sample and the ratio between the total average width and the average resonance spacing of each considered elementary spingroup, $\overline{\Gamma}/\overline{D}$. It is believed this constitutes one of the more important result of this chapter. An exact value of the number of resonances to sample depends on the level of precision required for the cross section distributions. Such a criterion of convergence is uneasy to define, and may probably be chosen differently for the diverse statistics considered in this chapter. If a value were to be given – it is believed it is the role of this document –, we would recommend to estimate if the ratio $\overline{\Gamma}/\overline{D}$ exceeds 10^{-2}. Below this threshold, it seems that 100 pairs of resonances enable tractable calculations with a minor loss of information. In particular, the mean cross sections thus sampled are close to 0.1% of the reference 500-pairs result. On the other hand, if $\overline{\Gamma}/\overline{D}$ exceeds this threshold value, the number of resonances to consider should be increased to maintain an acceptable precision.

A close exercise was carried out for the number of Monte-Carlo iterations to be performed, or in other words, for the number of resonance ladders to sample. There, large ladders were considered, and cross sections distributions computed for each elementary spingroup with 10000, 20000, 100000, and 200000 Monte-Carlo iterations. The same statistics than previously were used to compare the distributions. There again, the ratio $\overline{\Gamma}/\overline{D}$ of each elementary spingroup looked like a relevant quantity to consider. Unlike for the number of resonances, cases with low $\overline{\Gamma}/\overline{D}$ ratio required more Monte-Carlo iterations to get accurate results. This latter fact was easily explained by a "stabilization effect" for large ladders. When many resonances contribute to the cross sections, which corresponds to cases with high $\overline{\Gamma}/\overline{D}$ ratio, the effect of the sampling randomness is attenuated as more resonances intervene in the cross sections computations for each Monte-Carlo iteration. Thus, elementary spingroups with low $\overline{\Gamma}/\overline{D}$ values necessitate to sample more ladders to converge statistically. In order to give an idea of the number of Monte-Carlo iterations to perform, it seems that 100000 iterations is a relevant order of magnitude, even if low $\overline{\Gamma}/\overline{D}$ values (below 10^{-4}) should be probably handled with more iterations. In particular, the mean values derived from the ladder method appear in fairly good agreement with the the average cross sections computed from the resonance parameters directly, using the Hauser-Feschbach formulas presented in Chapter 2 with the Moldauer approximation for the width fluctuation correction factor.

In a nutshell, the work carried out in this chapter fixed a methodology for the resonance sampling in the framework of the ladder method. The use of elementary spingroups highlighted the competition between the average total resonance width and the average spacing. Cases with small ratios $\overline{\Gamma}/\overline{D}$ require only a few resonances but many Monte-Carlo iterations, whereas more resonances and less Monte-Carlo iterations are required for elementary spingroups with high $\overline{\Gamma}/\overline{D}$ values. Subsequently, this will be useful to tackle a more tricky issue, that is the replacement of the Wigner law for the resonance spacing by the more general use of random matrix theory. This theory reflects more accurately the observed physics of the nuclear energy levels, which appear to be all correlated in the same manner than eigenvalues of random matrix

of high dimension. Such developments are the core of the upcoming chapter, dedicated to the use of the random matrix theory in the unresolved resonance range.

Resonances correlations and random matrix theory

In the previous chapter, some settings of the ladder method algorithm have been investigated, such as the required number of Monte-Carlo iterations or resonances to sample in the ladders. These analyses rely on the assumption that the resonance spacings and widths distributions are well-known, and follow the Wigner and Porter-Thomas distributions respectively. In this approach, resonances are almost independent; actually, each one is only related to its immediate neighbors only, which enables to sample them one by one.

However, considering resonances with such a level of independence is an over-simplification of the physical reality. Energy levels of nuclei – and thus resonances – are highly correlated as they are all related to the same – unknown – Hamiltonian. It turns out that both Wigner and Porter-Thomas distributions can be recovered as limit cases of a more elaborated framework, known as the *random matrix theory*. This powerful mathematics tool is particularly adapted to estimate the spectral fluctuations properties of the nuclear systems dealt with in this work. In this chapter, the objective is to take into account the existing correlations between resonances during the ladders construction[1], and to investigate the impact on the cross section calculations in the unresolved resonance range.

4.1   Random matrix theory and its application in the unresolved resonance range

This section aims at presenting some basics of the random matrix theory workable in nuclear physics. After a brief digression about the origin of the Wigner law for the resonances spacing, the introduction of an useful ensemble of matrices, the so called Gaussian Orthogonal Ensemble, will be performed. The consequences for the resonance ladders shape will be then addressed. Notably, the so-called spectral statistics of the ladders are impacted by the use of the random matrix theory.

4.1.1   Origin of the Wigner law

The Wigner surmise for the resonance spacings used until now was originally obtained by E.P. Wigner in 1957. Wigner actually derived the expression Equation (2.1) from a Poisson

---

[1]In this work, only the correlations between the resonance *spacings* will be dealt with. That means the Wigner law of the spacings will no longer be used as such, but the Porter-Thomas law will be kept as a default for the resonance widths sampling.

distribution, and proved it to agree quite well with experimental observations. It is of interest to provide an insight of the intuition that led to such a result.

The problem is well described in [42], and can be set as follows: nucleus energy levels $\{E_n\}$ belonging to a single spingroup are randomly distributed over an energy interval ΔE of the real line, with a mean spacing $\overline{D} = \langle S_n \rangle = \langle E_{n+1} - E_n \rangle$. We are looking for the probability distribution of normalized resonance spacings $s = S/\overline{D}$.
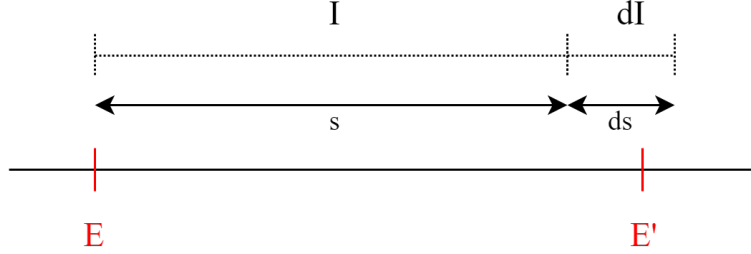

Figure 4.1

A resonance is located at an energy E. For the next resonance E' to be distant of s from E, this means that no level is found in $I = [E, E + s]$, meanwhile one is present in $dI = [E + s, E + s + ds]$. This situation is depicted over Figure 4.1. Thus, the problematic is about finding the probability of these events to occur concomitantly. This can be formulated as the next probabilistic equation:

$$p(s)ds = p(\text{level in } dI \mid \text{no level in } I).p(\text{no level in } I) \tag{4.1}$$

The probability that no resonance lies in I is the complementary of the probability that a resonance is found in I. A resonance is in I if the sampled spacing between E and E' is lower than s. As a consequence[2],

$$p(\text{no level in } I) = 1 - \int_0^s p(s')ds' = \int_s^\infty p(s')ds' \tag{4.2}$$

Introducing the variable $\mu(s)ds = p(\text{level in } dI \mid \text{no level in } I)$, Equation (4.1) may be rewritten $p(s)ds = \mu(s)\int_s^\infty p(s')ds'$, which is an integral equation whose solution may be expressed in terms of μ and a constant C:

$$p(s) = C\mu(s)e^{-\int_s^\infty \mu(s')ds'} \tag{4.3}$$

If the energy levels are uncorrelated and randomly distributed over the interval (which means according to a Poisson process), the probability for a level to fall between E and $E + dE$ is independent from E, and is simply $\frac{1}{\overline{D}}dE$. In terms of normalized spacings, it simplifies to dE. In that case, the function $\mu(s)$ is simply a constant, $\mu(s) = \mu$, and the expression of the spacing between resonances can be expressed in the case of a Poisson process as $p(s) = C\mu e^{-\mu s}$. Setting the double condition that p must be a distribution, and that the average of the spacings must be[3] 1:

$$\int_0^\infty p(s)ds = \int_0^\infty sp(s)ds = 1 \tag{4.4}$$

This leads to $\mu = 1$, $C = 1/\mu$, and $p(s) = e^{-s}$. As a conclusion, in the case of a random distribution of uncorrelated energy levels, the probability distribution of the normalized resonance spacings $p(s)$ is an exponential law of parameter $\lambda = 1$. This is a classical result.

---

[2]Sampled spacings cannot be negative.
[3]As the dimensionless variable $s = S/\overline{D}$ is considered.

It turned out a Poisson process did not match the experimental observations of nuclear levels. In particular, Wigner noticed that the probability to find two levels from the same spingroup very close to each other seemed very small, a phenomenon called *level repulsion*, which is in huge disagreement with the exponential distribution of spacings obtained from the Poisson process, which gives a maximal probability at 0.

In fact, such demonstration performed for a Poisson process can be easily adapted to mimic the level repulsion. This was achieved by Wigner in 1957. Assuming that the probability of finding a level in dI should be proportional to s instead of being energy-independent, $\mu(s) = a.s$ (a being a constant) so that the probability that two levels are very close tends to zero. One obtains $p(s) = Case^{a.s^2/2}$. The same conditions as before for $p(s)$ to be a distribution, and for the normalized average spacing to equal 1, result in $a = -\pi/2$ and $C = -1$, so that the final expression of the spacing distribution is the Wigner surmise, $p(s) = \frac{\pi}{2} s e^{-\frac{\pi}{4} s^2}$.

As a consequence, the Wigner surmise simply emerges from the supposition that the probability to find a level at s is proportional to s. This idea originally came out to simulate a level repulsion for small s, and was assumed to hold for larger values. Almost surprisingly, this result matched very well the experimental data.

4.1.2 Introducing the Gaussian ensembles of random matrices

After these almost empirical arguments were put forward and successful, Wigner looked forward a better description of nucleus energy levels along with F. Dyson. Bohr had proposed the compound nucleus model, motivated by the idea that the observed narrow resonances were mainly due to strong nucleon-nucleon interactions. Such considerations inspired Wigner and Dyson to renounce obtaining a description of the nuclear interactions at high energies where resonances were numerous. Instead, they worked to develop a statistical theory of levels. Their goal was no more to work out the properties of a particular system, but to investigate the properties of very complex systems in order to describe their general appearance. The mathematical framework they introduced to support this idea is the random matrix theory.

A quantum system is described with the eigenvalues problem

$$H\psi_n = E_n \psi_n \tag{4.5}$$

that has already been set in Section 1.3.2 to derive the R-Matrix theory of neutron-nucleus interactions. In this equation, H is the Hamiltonian, a linear operator that describes the system. ψ_n are eigenfunctions associated to the eigenvalues E_n, which are the energy levels of the system. The simple idea of Wigner was to replace this unknown Hamiltonian with a random operator, simply expressed by a matrix H whose entries $(h_{ij})_{1 \le i,j \le N}$ are random variables. Studying the statistics of the eigenfunctions and eigenvalues of such systems corresponds to studying the statistics of nucleus levels. In order to compensate for the fact that a matrix has a finite size N while the operator H evolves in an infinite-dimensional space, statistical properties of the system spectrum are studied in their asymptotic form, when $N \to \infty$.

This simple approach defines the random matrix theory, which has then be applied in many contexts in physics, economics, biology, mathematics, etc. For instance, it found applications in the study of quantum and classical chaos. An emblematic example is found when a particle evolves freely in a billiard [43]. Its motion is chaotic for certain forms of the billiard (stadium for instance) and integrable for others (rectangular). It turns out that the statistics of diverse operators for chaotic billiards are related to random matrix theory expressions. In mathematics, random matrices have been used in number theory. For instance, the zeroes of the Riemann ζ function[4] seem to have the same statistical distributions than the eigenvalues of a particular subset of random matrices, the GUE [44]. Random matrices are also widely used in graph

---

[4]The interest comes from the fact a well-known conjecture links the zeroes of the Riemann function to prime numbers.

theory and telecommunications where adjacency matrices are very common, or in finance where correlation matrices of portfolios often intervene [45].

In the context of quantum physics, the choice of the random matrix H to replace the nuclear Hamiltonian is restricted by the symmetries of the system. In most cases, the Hamiltonian must be Hermitian as all eigenvalues must be real and diagonalizable in an orthonormal basis. As a consequence, the random matrices used to replace it must be Hermitian too. Actually, a crucial component of the success of the random matrix theory is its *universality*: some key statistics, such as the eigenvalues correlation functions for example, depend solely on these symmetry properties[5]. This implies that the choice of the random variables h_{ij} is not a key-point in most situations[6]. Universality for random matrices has been first pioneered for Gaussian variables, and then propagated to many classes of matrices [46][7].

Let us focus for now on the case of square matrices with real eigenvalues, keeping in mind they may have symmetries. Two subgroups of these matrices are quite useful [48]:

- Matrices with independent variables h_{ij}. Such matrices are called Wigner matrices. In this case, the joint probability of the matrix entries is

$$\rho[H] = \rho(H_{11}, H_{12}, ..., H_{NN}) = \prod_{i=1}^{N} \rho(H_{ii}) \prod_{1 \leq i < j \leq N} \rho(H_{ij})\rho(H_{ji}) \qquad (4.6)$$

- Matrices with rotational invariance. This property states that for two random matrices which are related with a change of base $H' = UHU^{-1}$, entries have the same joint probability density function, $\rho[H] = \rho(H_{11}, H_{12}, ...H_{NN}) = \rho[UHU^{-1}]$[8]. This imposes a constraint on the entries of the matrix, which must be a function of the trace of the first N powers of H:

$$\rho[H] = f(\text{Tr}(H), ..., \text{Tr}(H^N)) \qquad (4.7)$$

These conditions were imposed by Wigner to replace the quantum mechanics Hamiltonian. The second one is essential; all orthogonal bases must be equivalent in quantum mechanics. The first one was introduced in order to obtain tractable calculations. It is thus more contestable, as the underlying physics of the two-body interaction does not imply any kind of independence. However, some arguments from information theory proved that this condition was equivalent to a maximum entropy principle, whose application is relevant in the case of minimal information on the Hamiltonian [30].

Gaussian matrices

If both conditions Equations (4.6)–(4.7) are fulfilled at the same time, the joint probability distribution of the entries takes the form $\rho[H] = C \exp(-a \text{Tr}(H^2) + b \text{Tr}(H) + cN)$ [49], and the only matrices which fulfill such conditions are the so-called *Gaussian matrices*, whose entries are Gaussian independent variables. Taking into account the symmetry properties of the Hamiltonian so that eigenvalues are real, three ensembles of the Gaussian matrices were introduced by Wigner and Dyson, indexed by the so-called Dyson index $\beta = 1, 2, 4$.[9]:

---

[5]A simple example of "universality" in statistics is the Central Limit Theorem, which ensures that for a random sequence of n independent identically distributed variables $(X_1, ..., X_n)$ that follow a distribution T with expected value μ and finite variance σ^2, the rescaled variable $\frac{(\overline{X_n} - \mu)}{\sigma/\sqrt{(n)}}$ converges in distribution to $\mathcal{N}(0, 1)$. Universality holds as this result is true whatever the distribution T is.

[6]Even if like in the case of the Central Limit Theorem, some characteristics of the random variables such as mean or variance must be taken into account as rescaling parameters.

[7]Reference [47] provides a progressive approach to the conditions under which universality holds for the so-called random Wigner matrices for instance.

[8]In fact, the rotational invariance property even requires that $\rho[H]dH_{11}dH_{12}...dH_{NN} = \rho[UHU^{-1}]dH'_{11}dH'_{12}...dH'_{NN}$, but the Lebesgue's measure is invariant by conjugation with U.

[9]This index corresponds to the number of real parameters needed to define a matrix entry: 1 (real), 2 (complex), 4 (quaternions).

- **The Gaussian Orthogonal Ensemble (GOE)**, $\beta = 1$:

  This ensemble is composed of *real* and symmetric matrices, which are thus diagonalizable with orthogonal matrices, hence the name. This ensemble corresponds to systems invariant under time reversal[10]

  In the following, the most widely applied choice in literature for the matrix entries is taken[11]:

  - Diagonal elements h_{ii} are independent Gaussian variables with mean 0 and variance 1.
  - Off-diagonal elements h_{ij} are independent Gaussian variables with mean 0 and variance $1/2$.

  These conditions are met if one generates a matrix M composed of N^2 Gaussian variables with mean 0 and variance 1, and symmetrize it from $H = (M + M^T)/2$.

- **The Gaussian Unitary Ensemble (GUE)**, $\beta = 2$:

  This ensemble is composed of complex and Hermitian matrices, which are thus diagonalizable with unitary matrices. This ensemble corresponds to systems which do not present time reversal independence.

- **The Gaussian Symplectic Ensemble (GSE)**, $\beta = 4$:

  This ensemble is composed of quaternion matrices, which are $2N \times 2N$ matrices built from two complex matrices X and Y of size N, such that $H = (M + M^T)/2$ with $M = \begin{pmatrix} X & Y \\ -Y^* & X^* \end{pmatrix}$. These matrices are used to represent systems which are time-invariant but not invariant under rotations, and have a half-odd integer total angular momentum.

Eigenvalues

The eigenvalues of these matrices are of main interest since they correspond to the nucleus energy levels. Just like the matrices entries, the eigenvalues are random variables. For the Gaussian ensembles the joint probability distribution of the eigenvalues is known theoretically, and for $N \times N$ matrices ($\beta = 1, 2, 4$) it takes the form:

$$\rho(x_1, ..., x_n) = \frac{1}{\mathcal{Z}_{N,\beta}} e^{-\frac{1}{2}\sum_{i=1}^{N} x_i^2} \prod_{1 \leq j < k \leq N} |x_j - x_k|^\beta \tag{4.8}$$

There, $\mathcal{Z}_{N,\beta} = (2\pi)^{N/2} \prod_{j=1}^{N} \frac{\Gamma(1 + j\beta/2)}{\Gamma(1 + \beta/2)}$ is a normalization constant. This joint probability distribution cannot be factorized and all eigenvalues remain strongly correlated. In this expression there is a competition between the factor $e^{-\frac{1}{2}\sum x_i^2}$ which tends to attract the eigenvalues around the origin, and a repulsive term $\prod |x_j - x_k|^\beta$ which forces the eigenvalues not to be too close from each other. Let us underline that the repulsion intensity depends on the choice of the Gaussian ensemble ($\beta = 1, 2, 4$). The linear repulsion used in Section 4.1.1 to retrieve the Wigner surmise can be found considering the GOE ensemble ($\beta = 1$)[12].

In fact, the Wigner surmise can be deduced from Equation (4.8) in the case of a GOE matrix of size 2. Indeed, the distribution of the resonance spacings in that case can be obtained (modulo the average spacing normalization condition) from:

---

[10]The time-reversal operator $\mathcal{T}$ is an anti-unitary operator: $\mathcal{T} = \mathcal{U}\mathcal{K}$ where $\mathcal{U}$ is unitary and $\mathcal{K}$ is complex conjugation. Without loss of generality one can set $U = I_d$, and if the system has time-reversal symmetry, $\mathcal{K}H\psi = H\mathcal{K}\psi$, so that $H^*\psi^* = H\psi^*$, which means that time-reversal symmetry implies the Hamiltonian is real symmetric.

[11]Universality here applies, as the choice of the entries could be different, but lead to same results.

[12]Assuming a quadratic repulsion $\mu(s) = a.s^2$ would have yield a spacing distribution related to the GUE. More precisely, it would have yield the distribution followed by the spacing between the eigenvalues of a 2×2 GUE matrix: $p(s) = \frac{32}{\pi^2} s^2 e^{-\frac{4}{\pi} s^2}$.

$$p(s) = \int_{-\infty}^{\infty} \int_{-\infty}^{\infty} dx_1 dx_2 \rho(x_1, x_2) \delta(s - |x1 - x2|) \tag{4.9}$$

Thus, the Wigner surmise used until now for the spacing between resonances corresponds to the case of a 2×2 GOE matrix. This underlines its weakness, as it is clear from Equation (4.8) that actually all eigenvalues are correlated and have a strong influence on each other.

In practical applications the joint probability distribution of eigenvalues is less useful than the marginal distribution $\rho(x) = \int \int ... \int dx_2 ... dx_N \rho(x_2, ..., x_N)$, called the spectral density, which *is* the probability density function of each eigenvalue[13]. For finite N, this function is quite complex. Its expression for the Gaussian ensembles has been established theoretically though [50] [48], and makes use of Hermite polynomials. It is is presented later in this document in Equation (4.28), where it will be used to *unfold* the eigenvalues.

On the other hand, the expression of the level density in the asymptotic limit $N \to \infty$ is very simple and quite famous. The spectral density for rescaled eigenvalues $x_i \leftarrow x_i/\sqrt{\beta N}$, converges toward the so-called *Wigner semi-circle law*[14] ρ_{SC}:

$$\rho_{SC}(x) = \begin{cases} \frac{1}{\pi}\sqrt{2 - x^2} & \text{if } |x| \leq \sqrt{2} \\ 0 & \text{otherwise} \end{cases} \tag{4.10}$$

This expression is the asymptotic expression of the probability density for the eigenvalues of Gaussian matrices when $N \to \infty$. In this expression, the eigenvalues have been rescaled so that they span the interval $[-\sqrt{2}, \sqrt{2}]$ and their density looks like a semi-circle. Without considering this rescaling, the radius of the semi-circle grows as $\sqrt{N}$. Let us also mention that the expression Equation (4.10) is valid when the off-diagonal entries of the random Gaussian matrices have been sampled with a variance $\sigma^2 = 1/2$. A more general expression for the Wigner semi-circle law in case the off-diagonal elements variance is a free parameter σ^2 can be established too [51]. It can be proven that the semi-circle radius $a_{N,\sigma,\beta}$ is:

$$a_{N,\sigma,\beta} = 2\sigma\sqrt{\beta N} \tag{4.11}$$

and the corresponding semi-circle law is in the most general case:

$$\rho_{SC}^{\beta,\sigma,N}(x) = \frac{2}{\pi a_{N,\sigma,\beta}^2}\sqrt{a_{N,\sigma,\beta}^2 - x^2} \tag{4.12}$$

Note that in this equation, the rescaling of eigenvalues over $[-\sqrt{2}, \sqrt{2}]$ has not been performed, contrary to Equation (4.10). Instead, the radius of the semi-circle extends as $\sqrt{N}$, and so does the expression of the semi-circle law[15]. In the following, the off-diagonal elements variance is always set to $\sigma^2 = 1/2$ so that $a_{N,\beta} = \sqrt{2\beta N}$, and the rescaling of eigenvalues is not performed.

In a nutshell, the probability density of the random matrices eigenvalues is known theoretically for the Gaussian ensembles, but its complex expression is often approximated by its asymptotic limit, the so-called Wigner semi-circle law. In order to give a better overview of the situation, Figure 4.2 displays some histograms of the eigenvalues of random matrices from the GOE and GUE at finite N, along with the exact level density expression[16], and the asymptotic Wigner semi-circle law. When N increases, the exact density gets closer to the asymptotic density. It is explicit from these figures that the semi-circle radius only marks a "loose border" at finite N, as it is always possible to obtain some eigenvalues out of the limits of the semi-circle. This issue will be of importance in the following when dealing with the so-called *unfolding* of eigenvalues.

---

[13]This can be proved from the fact that $\rho(x_1, ..., x_N)$ does not change when $x_i \to x_j$, cf [48].

[14]This law defines in fact an ellipse. It must not be mistaken with the Wigner law for the resonance spacing. Here, the semi-circle is the probability distribution of the random matrix eigenvalues, that are the resonance energies (levels).

[15]Choosing $\sigma^2 = 1/2$ and rescaling eigenvalues retrieve the expression Equation (4.10).

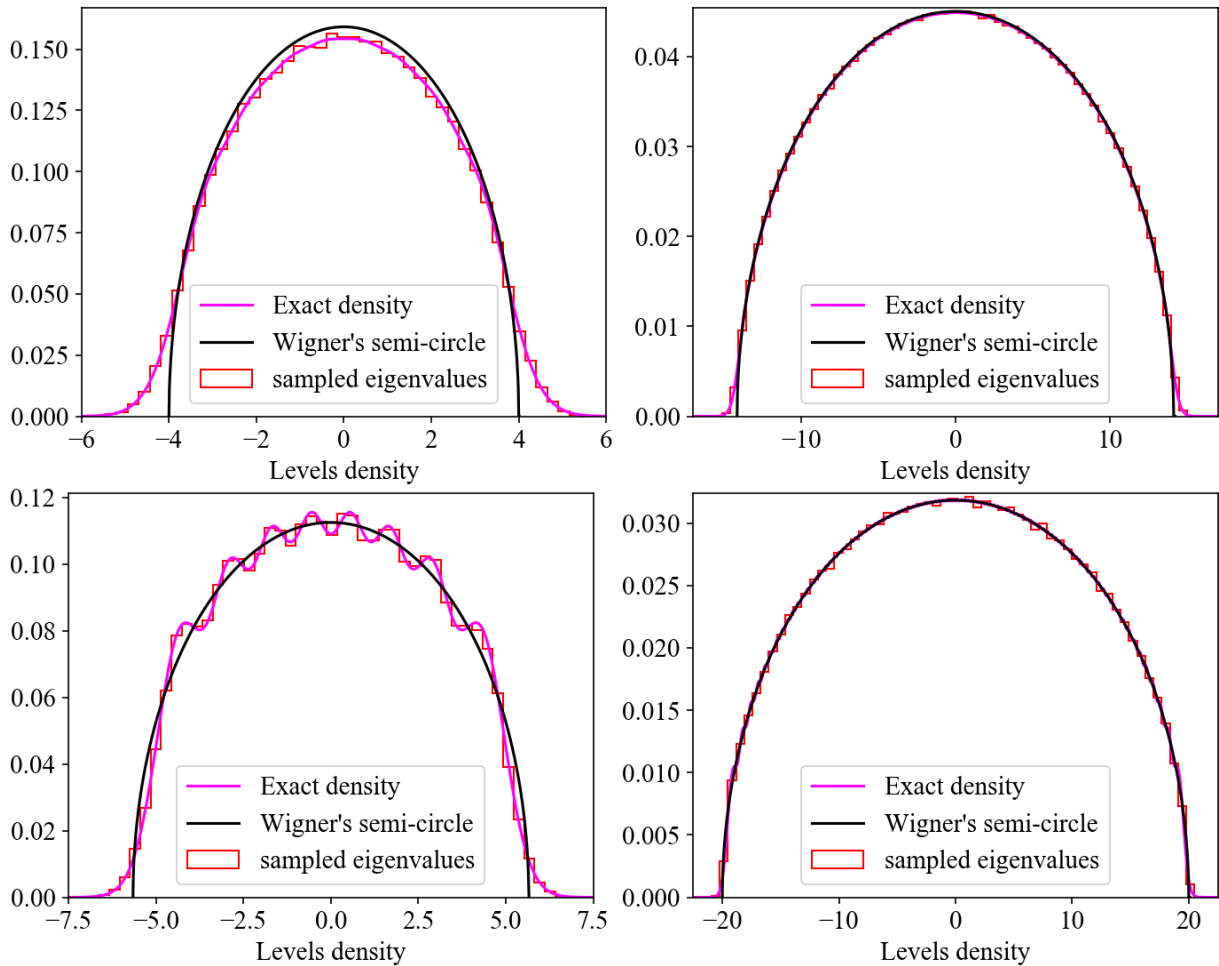[16]For the GOE, the exact density is presented in Equation (4.28).

Figure 4.2: Spectral density for the GOE ($\beta = 1$) ensemble on top and GUE ($\beta = 2$) ensemble on bottom. Histograms of eigenvalues of matrices of size $N = 8$ (left) and $N = 100$ (right) are presented, along with the exact spectral density ρ (pink) and Wigner's semi-circle law $\rho_{SC}^{\beta,N}$ (black), for the corresponding N values. When $N \to \infty$, the exact density converges toward the Wigner semi-circle law. In both cases, eigenvalues are found out of the semi-circle, which grows in $\sqrt{\beta N}$.

Eigenvectors

Eigenvalues of the Gaussian random matrices spectrum have been presented, but eigenvectors play an important role too. In the R-Matrix theory, they are related to the reduced reaction widths, as presented in Section 1.3.2. Relating random matrices eigenvectors to resonance widths in the R-Matrix theory has not been carried out in this work though. Let us only mention that theoretically, the eigenvectors of Gaussian matrices are asymptotically Gaussian [50], which justifies the use of χ^2 (Porter-Thomas) distributions for the resonance widths.

As a final remark, using the Gaussian ensembles as a reference framework may seem quite arbitrary at first sight. However, the study of quantum systems whose classical counterpart is chaotic proved that their spectral fluctuations matched with the ones from the Gaussian ensembles. This is the so-called Bohigas-Giannoni-Schmit conjecture formulated in 1984 [52], which describes the statistical property of chaotic spectra, and established a strong link between the random matrix theory and chaos. This conjecture has been largely accepted since then. In the broadest sense, it implies that Gaussian ensembles statistics would apply to *all* quantum systems whose classical analog is chaotic, making spectral fluctuations of such systems a signature of

chaos. Note that only *spectral fluctuations* are concerned by such properties of universality[17]. In particular, random matrix theory cannot capture the *average* properties of the system. Thus, the correspondence between the nuclear spectral statistics and the Gaussian ensembles would be a further evidence of the universal features of chaotic microscopic quantum systems. Once more, it is the universality of the fluctuations properties of the random matrices spectra which makes the Gaussian Ensembles so valuable compared to other matrix ensembles. They present the same spectral distributions, and they enable tractable calculations.

It turns out that among the Gaussian ensembles, the GOE, which corresponds to systems invariant under time reversal, agreed best with the theory of nuclear reactions. It is the one which will be used in the rest of this thesis. This was supported with experimental evidences over the aforementioned spectral statistics of the nuclear energy levels, which will be described more in detail in the next subsection.

4.1.3 Spectral statistics of interest

In this part, some important statistics used to characterize the energy shape of the ladders are addressed. Resonances ladders obtained with eigenvalues of GOE random matrices will be compared with ladders obtained with the one by one resonance sampling already used. The detail of the implementation of the random matrix theory in the ladder method is presented later in Section 4.2.1, even if a very important point should be underlined now: before comparing these spectra[18], random matrices eigenvalues must be *unfolded*. Unfolding may be understood as removing the average part of the spectrum, in order to compare the actual fluctuations properties independently from the eigenvalues density. More pragmatically, this operation is carried out by normalizing the spectra over the cumulative number of levels. Several methods of unfolding will be selected in Section 4.2.1, where their impact is studied over the same set of statistics that are about to be presented. Let us for now just keep in mind that unfolded eigenvalues are used in next presentation.

Finally, let us underline once more that all statistics presented here only concern the resonance *energies*. No work about the resonance widths based on the random matrix theory has been carried out in this thesis.

Next nearest spacing distribution (NNDS)

One of the most important statistics to describe resonance ladders is the resonance spacings distribution. In the context of random matrices, this distribution is called the next nearest spacing distribution, and corresponds to the distribution of the spacings between sorted eigenvalues. This is the main tool used until now to build resonance ladders. In the case of 2×2 matrices from the GOE, this spacing corresponds exactly to the Wigner surmise. In the case of many correlated resonances from the GOE, an expression has been obtained by Gaudin in the asymptotic case $N \to \infty$ [53]. Surprisingly, it looks very close to the Wigner surmise (up to 2%), which may explain the fairly good agreement between experimental results and the early attempts from Wigner. This expression involves a fast-converging infinite product, whose tabulated expression is provided in the reference.

In order to estimate the speed of convergence towards this distribution, numerical simulations have been conducted with several values of N. For each case ($N = 8$, 100), ladders of corresponding sizes have been sampled using the Wigner-like approach and the GOE method[19]. For both of them normalized spacings have been stored. The operation has been repeated over

---

[17]Spectral fluctuations must be understood as the dynamic of the eigenvalues (and eigenvectors). For eigenvalues, this implies their statistical distributions and related properties, such as spacings correlations.

[18]"Spectrum" designates the set of resonance energies, as they are the eigenvalues of the system Hamiltonian.

[19]In the Wigner one by one resonance sampling, the pair-sampling approach is used. As a consequence, the number of sampled *pairs* is N/2.

many ladders to obtain acceptable statistics. Figure 4.3 displays the obtained patterns, super-posed to both Wigner surmise and Gaudin's asymptotic law, using the tabulated expression provided in [53] for the resonance spacings. The difference between both laws has also been represented.
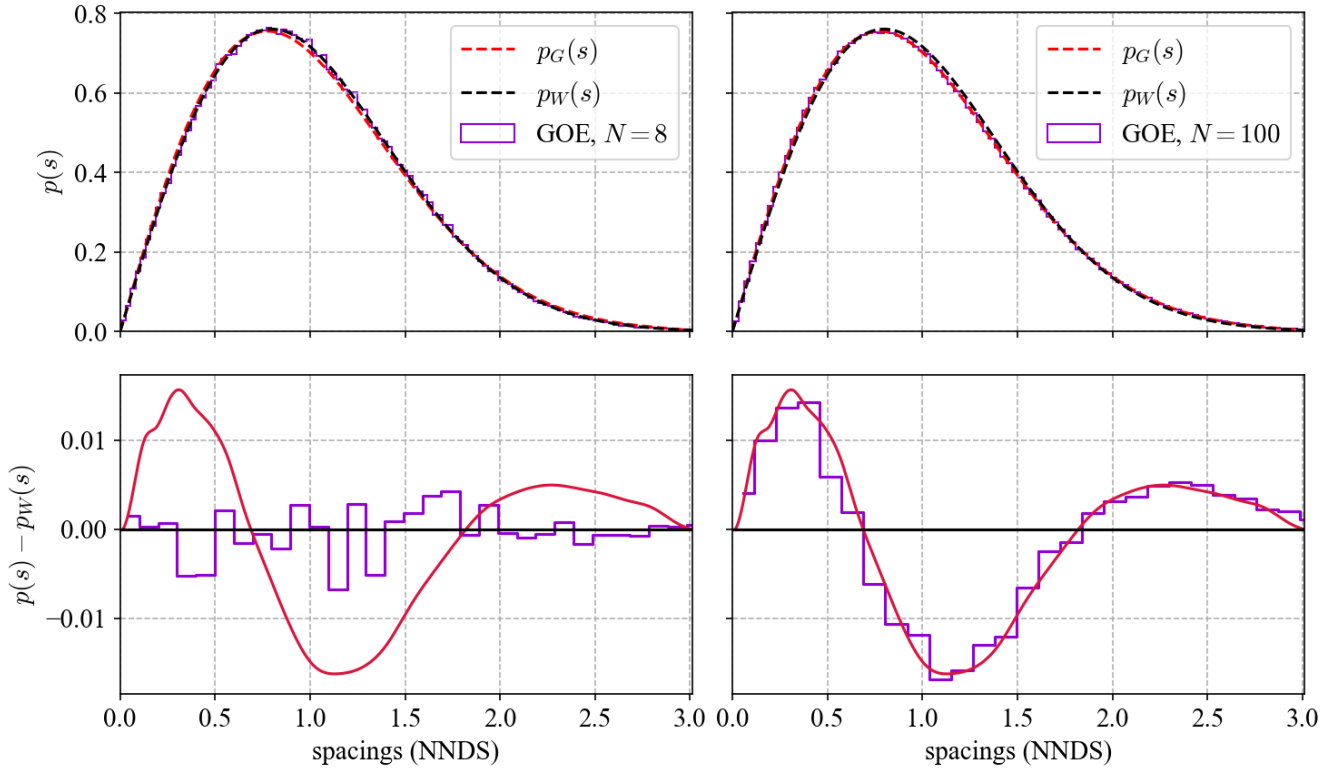

Figure 4.3: On top, next-nearest spacing distribution for resonances obtained from matrices of the GOE of size $N = 8$ (left), and $N = 100$ (right). Both Wigner distribution p_W and the asymptotic distribution derived by Gaudin p_G are also displayed. On the bottom, the difference compared to the Wigner distribution is shown.

From the figure, it appears clear that the Wigner surmise is a good approximation of the Gaudin asymptotic law. The maximal difference between both curves is obtained just after the mode, where the Wigner law slightly dominates the asymptotic expression, and remains below 2%. After that the trend reverses, and the asymptotic expression dominates the Wigner law in the tail. The asymptotic result seems to be reached quickly for GOE-like resonances, as a matrix of size $N = 100$ suffices to retrieve the asymptotic trend.

Spacing autocorrelation

When relying on random matrices, the most emblematic change in the shape of the ladder is achieved when one calculates the resonance spacings *autocorrelation*. Calling the λth spacing D_λ, this statistics is defined as:

$$R_1 = \frac{\mathrm{Cov}(D_\lambda, D_{\lambda+1})}{\mathrm{Var}(D)} = \frac{1}{N-1} \sum_{\lambda=1}^{N-2} \frac{(D_{\lambda+1} - \overline{D})(D_\lambda - \overline{D})}{\mathrm{Var}(D)} \qquad (4.13)$$

R_1 captures the correlation between consecutive level spacings[20]. In the previous chapter, all spacings were sampled independently from each other, and thus were not correlated: $R_1 = 0$.

---

[20]Equivalently, R_k could be defined as the correlation between each spacing of the set and the kth next one.

In the case of eigenvalues from the GOE this is not true anymore. The spacing autocorrelation value is known theoretically, and equals -0.27 [50]. As foreseen, the several spacings are not independent anymore. This has a huge consequence: a negative autocorrelation value indicates that a large spacing will be more likely followed by a small one, and vice-versa. As a result, resonance ladders issued from random matrices are expected to be more stable than ladders obtained from previous one by one sampling method. In particular, such series of resonances will be more susceptible to bracket the true spacing mean, which is good news in practice.

As previously, some numerical simulations have been performed. Figure 4.4 presents histograms of calculated autocorrelation based on Equation (4.13) over many ladders (of size $N = 8$ and $N = 100$), from Wigner or GOE samplings. Such histograms display a quasi-normal distribution. The mean in both case has been represented by a dotted line, and both values 0 and -0.27 with a dashed gray line.
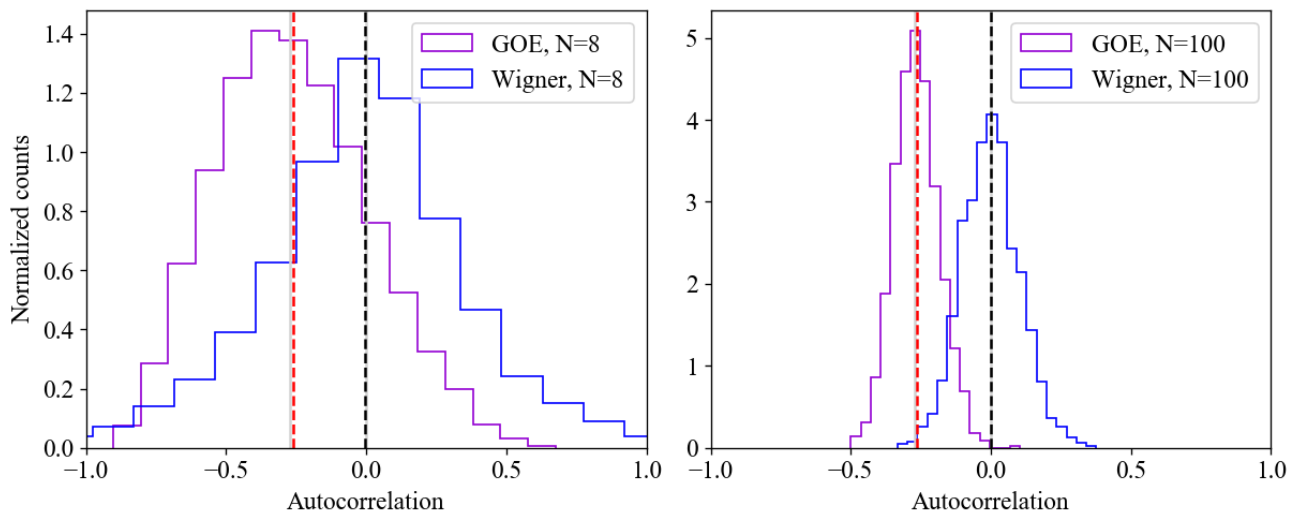

Figure 4.4: Histograms of the spacing autocorrelation for $n = 10000$ Wigner-like and GOE-like resonance ladders of size $N = 8$ (left) and $N = 100$ (right). The counts in the histograms are normalized to approach a probability density.

Negative autocorrelations directly arise even for small sizes of the random matrices, which underlines the interconnection between all the eigenvalues. However, the bigger the matrix the better the estimation of the autocorrelation, and the closer it brackets the -0.27 value for GOE-like ladders, and 0 for Wigner-like ladders. In particular, the variance in the autocorrelation estimation is very reduced in the case $N = 100$ compared to $N = 8$. This is justified, as the autocorrelation actually depends on all the ladder's spacings. Moreover, the spacings mean $\overline{D}$ and variance $\text{Var}(D)$ in Equation (4.13) have been replaced with their estimators on the set; the longer the set, the more these estimators are precise.

Δ_3 statistics

The measure of the spacing autocorrelation proves that the GOE-based and Wigner-based methods do not create ladders of same shape. This is even more obvious considering some long-range statistics, as the Δ_3-statistics. Such quantity has been first introduced by F. Dyson and M. Mehta in [54] as a least-square statistics. In a nutshell, the cumulative number of levels over an energy interval $N(E)$ can be plotted as a staircase function (exactly like a kind of non-normalized empirical distribution function). It is possible to fit such a staircase with a straight line, and to compute a least square statistics to estimate the deviation from the straight line, as shown in Figure 4.5. This is the purpose of the Δ_3, whose expression is:

$$\Delta_3(L) = \min_{a,b} \frac{1}{L} \int_{\Delta L} [N(E) - (aE + b)]^2 \, dE \qquad (4.14)$$

In this relation, the least square calculation is performed over an energy interval ΔL of length L; a and b are the slope and interception of the best linear fit over this interval.
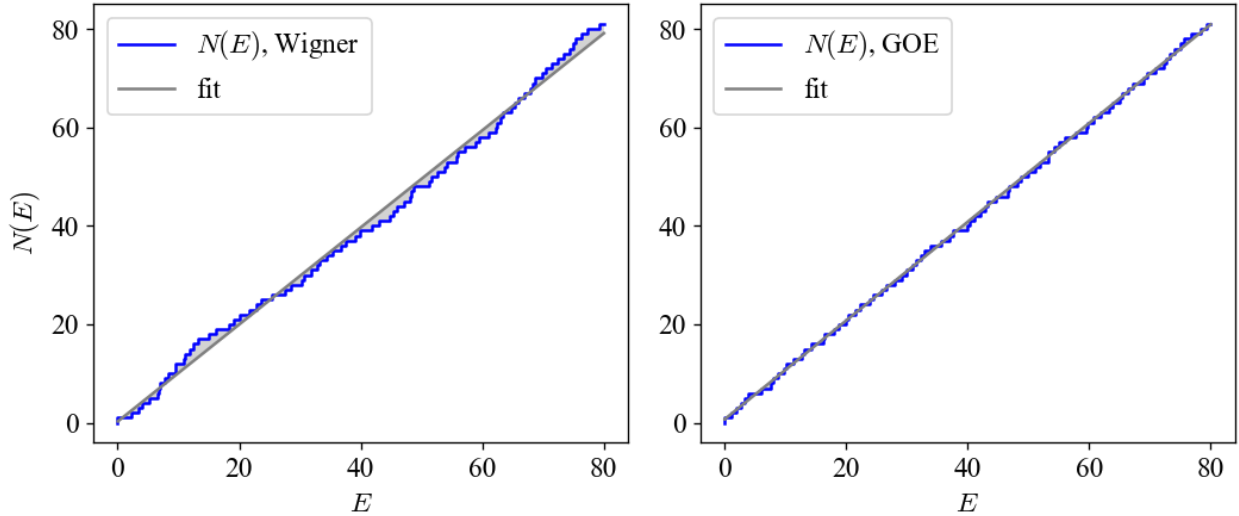

Figure 4.5: Cumulative number of levels for ladders with $N = 80$ resonances and an average level spacings $\overline{D} = 1$ eV. On the left, a ladder built from one by one resonance sampling. On the right, a ladder built from a matrix from the GOE. The cumulative number of resonances in that case sticks to the straight line.

As seen in Figure 4.5, the cumulative number of levels in the case of GOE-sampled ladders is well-fitted with a straight line, at least much better than the Wigner-sampled ladders. In the case of GOE, the spectrum is very regular, even rigid. This is in agreement with the negative autocorrelation of GOE-like ladders, stating that small spacings are more likely to be followed with a big one and so on. The Δ_3 statistics provides a measure of an integral correlation result over the whole ladder, and consists of a *long-range* measurement of the correlation between resonance energies.

Unlike the autocorrelation, this statistics is a functional quantity whose value can be calculated for each energy interval of length L. It is also possible to get advantage of the bijection between $N(E)$ and E to reinterpret this statistics as an integration over a number of resonances instead than over a strict energy window. In that case, least square calculations are actually performed over a certain number of resonances L considered in the spectrum. Basically, this has no impact on the statistics's behavior, but simplifies the calculations.

The Δ_3 statistics is highly ergodic. For a given L, the average statistics performed over many ladders is the same than the average over all the sequences of size L of a single – infinitely long – set[21]: $\Delta_3(L) = \langle \Delta_3^i(L) \rangle_i$, where the least square calculation is performed between E_i and E_{i+L}. This interesting feature can be used in practice to obtain a better accuracy of the calculation of the $\Delta_3(L)$ statistics, which can be computed for each non-overlapping sequences of size L of a ladder, before averaging them.

Finally, next considerations which are well presented in [55] and [56], are taken into account to avoid an actual numerical fit. Between levels E_j and E_{j+1}, $\mathcal{N}(E) = j$, so that for arbitrary a and b:

---

[21]This is of course valid because the average spacing does not change.

$$\Delta_3^i(L) = \frac{1}{L} \int_{E_i}^{E_{i+L}} [N(E) - (aE + b)]^2 \, dE$$

$$= \frac{1}{L} \sum_{j=i}^{i+L-1} \int_{E_j}^{E_{j+1}} [j - (aE + b)]^2 \, dE \qquad (4.15)$$

$$= \frac{1}{L} \left[C + Va^2 + Wa + Xab + Yb + Zb^2 \right]$$

C, V, W, X, Y, Z are constants given as:

$$C = \sum_{j=i}^{i+L-1} j^2 (E_{j+1} - E_j)$$

$$V = \frac{1}{3}(E_{i+L}^3 - E_i^3)$$

$$W = - \sum_{j=i}^{i+L-1} j(E_{j+1}^2 - E_j^2) \qquad (4.16)$$

$$X = (E_{i+L}^2 - E_i^2)$$

$$Y = -2 \sum_{j=i}^{i+L-1} j(E_{j+1} - E_j)$$

$$Z = E_{i+L} - E_i$$

This provides a simple algebraic expression of the least square between the cumulative number of levels and a linear fit. The coefficients a and b must minimize $\Delta_3^i(L)$, thus $\frac{\partial \Delta_3^i(L)}{\partial a} = 0$ and $\frac{\partial \Delta_3^i(L)}{\partial b} = 0$. Next expression for a and b follows:

$$a = \frac{XY - 2WZ}{4VZ - X^2} \quad b = \frac{WX - 2VY}{4VZ - X^2} \qquad (4.17)$$

Substituting all these variables in Equation (4.15) provides an efficient way to compute the long-range Δ_3 statistics.

In the case of GOE random matrices, the Δ_3 statistics is known theoretically [50], and can be computed using the next expression, where $\gamma \approx 0,5772$ is the Euler constant:

$$\Delta_3(L) = \frac{1}{\pi^2} \left[\ln(2\pi L) + \gamma - \frac{\pi^2}{8} - \frac{5}{4} \right] = \frac{1}{\pi^2} \left[\ln(L) - 0.0687 \right] \qquad (4.18)$$

This expression can be compared to the one obtained if the successive spacings are Poissonian: $\Delta_3(L) = L/15$, or even to the case of evenly-spaced resonances (picket fence): $\Delta_3(L) = 0$. The GOE case lies between both, but its logarithmic form makes it differ from the Wigner-like case where the statistics quickly adopt a linear trend, as displayed on the simulations results in Figure 4.6. Once again, it appears clear that GOE ladders are much more rigid than the Wigner-like ones.

The random matrix theory takes into account the correlations between all resonances of a ladder, interpreting resonance energies as correlated eigenvalues of $N \times N$ random matrices. This has a deeper physical meaning than considering successive eigenvalues of 2×2 matrices as achieved in the ladder method implemented in previous chapter. Ladders obtained from the GOE ensemble of random matrix theory are somehow different than in the previous chapter;
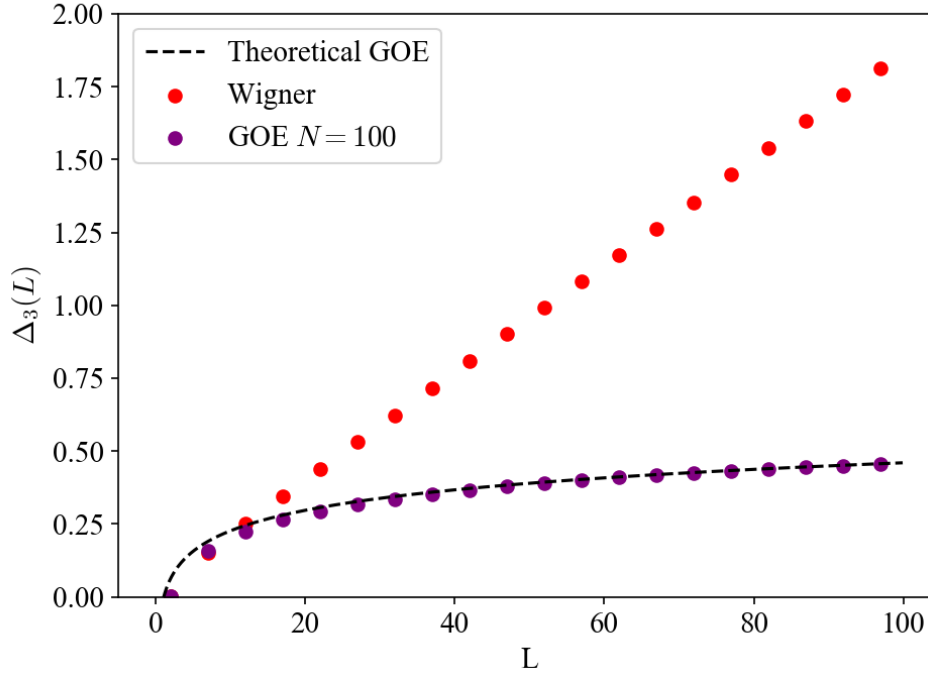
Figure 4.6: $\Delta_3(L)$ statistics computed for 10 000 ladders of size $N = 100$, obtained from GOE ensembles or using Wigner spacings. The computations of the $\Delta_3(L)$ statistics has been made for all non-overlapping possible sequences of L resonances in the ladders.

the difference can be appreciated from the use of various statistics performed over the resonance energies. In the next section, the impact of the correlation of resonance spacings will be investigated in the context of the ladder method[22].

4.2 Correlated resonance spacings in the ladder method

4.2.1 Implementation in GAIA-2

In GAIA-2, a methodology to sample resonance ladders based on the random matrix theory has been implemented. The used method aims at producing ladders with correlated resonance energies. Such resonance energies correspond to the energy levels of the compound nucleus, that are supposed to be the eigenvalues of the Hamiltonian, now replaced by GOE random matrices of sufficient size.

The spectral statistics of such matrices have been presented in previous chapter. The behavior of the statistics of interest seemed to be significantly different from the Wigner sampling for $N = 100$ resonances and above. Consequently, ladders of greater or equal sizes are considered. A straightforward implementation of the random matrix theory in the framework of the ladder method could consist in sampling matrices whose size equals the number of resonances required to fill the ladders. To be consistent with all the work carried out until now, cross sections are again only computed at the reference energy of interest, and each ladder yields a single cross section value. As a consequence, the method still requires to perform a huge number of Monte-Carlo iterations[23].

Generating a GOE-compliant ladder composed of N resonances from the same spingroup is

---

[22]Both terminologies "correlated spacings" and "correlated energies" denominate ladders whose resonance energies were yielded from the GOE.

[23]As a reminder, a single Monte-Carlo iteration equates to a resonance ladder sampling.

simply achieved following the next steps. First, a GOE-like random matrix of size N is sampled, and diagonalized. Note that the probability of obtaining degenerated eigenvalues is null, so that all eigenvalues are clearly distinct. There, eigenvalues need to be unfolded. Several unfolding methods are possible and are described a little further. Once unfolded, these eigenvalues are sorted[24] and their spacings are kept; they form a set of $N-1$ correlated resonance spacings. They only need to be rescaled over the average spacing $\overline{D}$ found in the ENDF evaluation, and dispatched around the reference energy of calculation E_{ref}. This latter step calls for a little attention. A mistake would be to set as many resonances on both sides of the reference energy. However, this would bring back the waiting time paradox of Section 3.1.3, leading to erroneous results. The best way of proceeding is to mimic the energy-based sampling of Section 3.1.1 instead. The left edge of the ladder is chosen as $E_1 = E_{ref} - \left(\dfrac{N}{2} + \xi\right)\overline{D}$, with ξ a random shift. Then, the rescaled spacings are used successively to obtain the resonance energies. If enough resonances are sampled, it has been proven in Section 3.1.3 that this method seemed to provide a correct central resonance spacing after a dozen resonances only. In the context of the GOE-like sampling, if matrices of size $N = 100$ at least are sampled, this is not a problem.

Two key-points of the method remain. First of all the method is very time-consuming. Each iteration requires to solve a large matrix eigenproblem. Secondly, an efficient unfolding method has to be adopted.

Tridiagonal matrices substitution

In order to speed up the sampling of GOE-like random matrices, a method presented in [57] has been implemented. This method is based on a substitution of the square symmetric GOE matrices with well-chosen tridiagonal matrices.

In the journey toward the computation of a symmetric matrix's eigenvalues, an usual method consists in performing successive Householder transformations in order to tridiagonalize the matrix. Such an operation results in a matrix whose only diagonal and immediate upper an lower diagonals are non-empty, from which eigenvalues are much easier to compute. The so-called Householder transformation is defined as a reflection about a hyperplane of the $\mathbb{R}^n$ space. Defining a vector v orthogonal to the hyperplane the reflection is simply the linear application f_v so that for $u \in \mathbb{R}^n$,

$$f_v(u) = u - \frac{2\langle u, v\rangle}{\|v\|^2}v \tag{4.19}$$

where $\langle.,.\rangle$ defines the Cartesian scalar product. Its associated matrix – the Housholder matrix – is simply defined as $H_v = I_n - \dfrac{2vv^T}{\|v\|^2}$. The main idea is to perform successive Householder reflections to tridiagonalize a GOE symmetric matrix. If this $N \times N$ matrix A is chosen as defined in Section 4.1.2, it can be written as

$$A = \begin{bmatrix} a_N & x_2 & \dots & x_N \\ x_2 & & & \\ \vdots & & B & \\ x_N & & & \end{bmatrix} \tag{4.20}$$

where a_N follows a standard Gaussian, $x = [x_2, \dots, x_N]^T$ is a vector of $N-1$ independent variables that follow $\mathcal{N}(0, 1/2)$, and B is a $(N-1) \times (N-1)$ GOE matrix, independent from a_N and x. It is of interest to introduce the Householder matrix H of size $N-1$ associated to the vector $v = x - \|x\|_2 e_2$, where e_2 is the base vector corresponding to the coordinate x_2, and

---

[24]This is simply equivalent to reindexing the base vectors.

$\|.\|_2$ is the Euclidean norm[25]. As a consequence, applying H over x makes all its coordinates but one disappear: $Hx = [\|x\|_2, 0, \ldots, 0]^T = \|x\|_2 \, e_2$, so that:

$$
\begin{bmatrix} 1 & 0 \\ 0 & H \end{bmatrix} A \begin{bmatrix} 1 & 0 \\ 0 & H \end{bmatrix}^T = \begin{bmatrix} a_N & \|x\|_2 & 0 & \ldots & 0 \\ \|x\|_2 & & & & \\ 0 & & & & \\ \vdots & & & HBH^T & \\ 0 & & & & \end{bmatrix}
\tag{4.21}
$$

The procedure can be repeated for the $(N-1) \times (N-1)$ GOE-like matrix HBH^T. This implements an iterative procedure to tridiagonalize the matrix. The main consideration here is the fact that H is orthogonal, so that all performed transformations do not change the matrix spectrum. Here, the diagonal elements remain unchanged, and still follow a normal law with mean 0 and variance 1. On the other hand, the upper and lower diagonal elements distribution change. Here, $\|x\|_2$ is the square root of the sum of the square of $N-1$ independent normal laws with variance $1/2$. As a consequence, the distribution it follows is $\frac{1}{\sqrt{2}}\chi_{N-1}$, where χ_{N-1} is a χ distribution with $N-1$ degrees of freedom. Finally, the tridiagonal matrix whose eigenvalues statistics is equivalent to the GOE is:

$$
T = \begin{bmatrix} \mathcal{N}(0,1) & \chi_{N-1}/\sqrt{2} & & & & \\ \chi_{N-1}/\sqrt{2} & \mathcal{N}(0,1) & \chi_{N-2}/\sqrt{2} & & & \\ & \chi_{N-2}/\sqrt{2} & \mathcal{N}(0,1) & & & \\ & & & \ddots & \ddots & \chi_1/\sqrt{2} \\ & & & & \chi_1/\sqrt{2} & \mathcal{N}(0,1) \end{bmatrix}
\tag{4.22}
$$

In the previous expression, all diagonal elements must be obtained from independent Gaussian laws with mean 0 and variance 1, whereas the upper and lower diagonal elements are obtained from rescaled independent χ laws with i degrees of freedom[26].

The advantages of using the matrix T in place of symmetric matrices from the GOE is mainly numerical[27]. From a computer memory management point of view first, this replacement provides a net gain. Instead of filling the entire $N \times N$ symmetric matrices, only $2N-1$ entries are required which correspond to the diagonal and the upper diagonal. The spatial complexity in this case is reduced to $\mathcal{O}(N)$, rather than $\mathcal{O}(N^2)$. This is very useful when large matrices $(N = 10^4, 10^5)$ are to be sampled using a double precision. From a time-complexity point of view, the advantages are even more worth the trouble. The classical algorithms used to obtain the eigenvalues in the case of tridiagonal symmetric matrices require a computing time proportional[28] to N^2 while the ones for symmetric real matrices are usually proportional to N^3. Considering large matrices, this makes the computations feasible. As an example, the several processing times for a single spingroup have been displayed in Table 4.1[29].

---

[25] For $y = [y_1, \ldots, y_n]^T \in \mathbb{R}^n$, $\|y\| = \sqrt{\sum_{i=1}^n y_i^2}$.

[26] The upper and lower diagonal elements must be the same, as the resulting matrix remains symmetric.

[27] This method also has been used to define a wide class of matrices *from the β ensembles* in [58]. This theoretically enlarges the definition of the Gaussian ensembles, providing intermediate matrices between the cases $\beta = 1, 2, 4$.

[28] In fact, an algorithm with a $\mathcal{O}(N \log N)$ complexity has even been designed to compute eigenvalues of tridiagonal symmetric matrices [59]. Its implementation, based on a complex divide-and-conquer algorithm, has never been implemented in the classical linear algebra's packages – such as LAPACK – though, mainly because its field of applicability is quite narrow. Indeed, starting from a given matrix, the Householder transformation required to obtain the tridiagonal symmetric form is a $\mathcal{O}(N^3)$ procedure. In the present case however, starting directly from the tridiagonal symmetric form is relevant because the considered matrices are random.

[29] The times indicated correspond to the sampling of both resonance spacings and widths. The spingroup used in the table had three resonance widths, with a single degree of freedom for the neutron and fission width. Note that the time required to sample the resonance widths become negligible compared to the time required for correlated spacings.

N	Wigner-like sampling	GOE-like sampling (symmetric)	GOE-like sampling (tridiagonal)
10	0.007 s.	0.020 s.	0.016 s.
100	0.05 s.	1.05 s.	0.44 s.
200	0.10 s.	5.45 s.	1.54 s.
500	0.25 s.	64.2 s.	8.44 s.
1000	0.98 s.	462.3 s.	31.75 s.

Table 4.1: Required time to sample 1000 ladders of different sizes, with or without correlated spacings (from symmetric or tridiagonal matrices).

As a comparison, the time required to compute a single cross section value using the SLBW formalism at E_{ref} is of the same order as the time required for the Wigner-like sampling[30]. As such, it appears clear that the time required by the sampling of correlated spacings becomes the key factor for the method's speed, and that it is definitely reduced by the tridiagonal matrix substitution.

Eigenvalues of those tridiagonal matrices are exactly the same as GOE-like matrices. The sampling of the entries is just performed a step ahead in the process of the matrix diagonalization. Accordingly, the distributions and correlations of the eigenvalues are the same as that for the GOE ensemble. However, the same cannot be said for eigenvectors in this method. In the diagonalization process, eigenvectors are computed from the Hermitian matrices in an iterative process. Here, the idea is to start with tridiagonal matrices directly, making use of the statistical distribution of the entries obtained from the successive Householder transformations. The statistics of the original eigenvectors is not conserved when the tridiagonal form is considered in lieu of the GOE matrices. In other words, eigenvectors corresponding to the tridiagonal matrices do not have a physical meaning, and cannot be used to work with resonance widths. In this thesis, only the influence of eigenvalues has been considered, which means only the resonance spacings have been correlated. Keeping this in mind, the presented tridiagonal substitution is the fastest route to sample GOE-like resonances energies.

Unfolding the eigenvalues

Once N eigenvalues have been computed from a GOE-like $N \times N$ matrix or from its tridiagonal counterpart, they can be sorted which is just equivalent to reindexing the base vectors. The spacings between sorted eigenvalues follow the statistical properties described in Section 4.1.3, such as the Gaudin distribution, negative autocorrelation, and Δ_3 rigidity, which makes the ladders structure more physical than traditional resonance ladders. As mentioned previously, a very important step must be performed once eigenvalues have been computed and before retrieving the spacings, that is known as the eigenvalues *unfolding*.

The distribution followed by the eigenvalues has been tackled in Section 4.1.2; the level density approaches the Wigner semi-circle law when $N \to \infty$. The cases $N = 8$ and $N = 100$ have been displayed on Figure 4.2. It must be realized that the level density is not uniform. As a consequence the spacings between eigenvalues depend on the part of the spectrum considered. Working with spacings directly is thus impossible, because the average "macroscopic" energy density dependency mixes with the local fluctuations. As such, one has to remove the average

---

[30]From a time complexity point of view, it is a $\mathcal{O}(N)$ computation, as each added resonance only contributes once in the formula. Note that this time would be much greater using the MLBW formalism for instance, as each resonance would also contribute in an extra cross-term, making it a $\mathcal{O}(N^2)$ calculation.

level density first in order to keep the fluctuations only. This is the aim of the unfolding, which consists in rescaling the eigenvalues so that the mean level density is unity over the spectrum.

In practice, this is simply carried out using the spectral cumulative density function $I(E)$. Given a spectrum, this quantity can be separated into two components, an average $I_{av}(E)$ and a local fluctuating part $I_{fl}(E)$. In order to remove from the given set of eigenvalues $\{\lambda_i\}_{1 \leq i \leq N}$ the average part, it is enough to simply apply the next rescaling:

$$\epsilon_i = I_{av}(\lambda_i) \tag{4.23}$$

and define the spacings from the dimensionless $\{\epsilon_i\}_{1 \leq i \leq N}$.

In most of the situations encountered in literature, two cases prevail. First of all is the situation in which the local fluctuations of a set of levels are investigated, without any assumption about the underlying level density. This happens when real-life spectra are looked for, like in [43]. In this case, the average part of the levels cumulative has to be estimated from the spectrum itself to perform the unfolding. Two methods are mainly used, whose efficiency in the framework of the random matrix theory has been tested in [51] and [60]:

- Polynomial unfolding: in that case, the empirical cumulative of levels is simply fitted with a polynomial of degree three or five.

- Gaussian unfolding: in that case, the mean level density ρ_G is defined using a Gaussian convolution:

$$\rho_G(E) = \frac{1}{\sigma\sqrt{2\pi}} \sum_{i=1}^{N} \exp\left[-\frac{(E-\lambda_i)^2}{2\sigma^2}\right] \tag{4.24}$$

There, the free parameter σ is to be chosen in order to choose a window over the spectrum large enough to capture enough information over the spectrum, and small enough to keep the local fluctuations. The average cumulative density is simply defined as the primitive of this function: $I_{av}(E) = \int_{-\infty}^{E} \rho_G(E')dE'$.

The second situation occurs when the underlying distribution from which a spectrum has been yielded is known. In this case, the spectral density $\rho(E)$ is known. There, I_{av} is simply the cumulative distribution corresponding to the level density: $\int_{-\infty}^{E} \rho(E')dE'$. In the ladder method, the random matrix theory is used to generate resonance energies. The level density is thus well-known and so is the cumulative distribution. Several details must be precised though. Usually, the Wigner semi-circle law 4.12 is used as the level density. In the most general case of a free choice of the GOE matrices off-diagonal elements variance like in Equation (4.12), the corresponding cumulative levels distribution I_{av}^{SC} usually found in literature is [51]:

$$I_{av}^{SC}(E) = \begin{cases} \frac{1}{2} + \frac{E}{\pi a_N^2}\sqrt{a_N^2 - E^2} + \frac{1}{\pi}\arctan\left(\frac{E}{\sqrt{a_N^2 - E^2}}\right) & \text{if } |E| \leq a \\ 0 & \text{if } E \leq -a_N \\ 1 & \text{if } E \geq a_N \end{cases} \tag{4.25}$$

where a_N is the Wigner semi-circle radius, previously defined in Equation (4.11). This expression is obtained by directly integrating Equation (4.12). An elegant rescaling may provide another expression, which makes the unfolded eigenvalues close to the Wigner semi-circle law. Such an expression of the cumulative level density $\tilde{I}_{av}^{SC}$ is only used for drawing purposes, and does not improve the unfolding. The transformation only consists in a translation and a homothety, and is simply:

$$\tilde{I}_{av}^{SC}(E) = \pi\sqrt{N}\left[I_{av}^{SC}(E) - 0.5\right] = \sqrt{N}\left[\frac{E}{a_N^2}\sqrt{a_N^2 - E^2} + \arcsin\left(\frac{E}{a_N}\right)\right] \tag{4.26}$$

This transformation is for instance used in CALENDF, and is very useful to compare the different unfolding methods on the same scale. Note that finally, the mathematical relation

$\arctan(\frac{y}{\sqrt{1-y^2}}) = \arcsin(y)$ has bee used to simplify the previous equation even more. This formula is easily tractable and is an easy-to-go unfolding expression.

A main issue appears at finite N though, when eigenvalues are sampled out of the semi-circle boundaries. For instance, if two eigenvalues λ_1 and λ_2 are smaller than the lower bound of the radius (which may happen when $N < \infty$), their unfolded counterparts ϵ_1 and ϵ_2 both equal 0. As a consequence, the spacing between these resonances is null, which has no physical meaning. This is due to the use of the Wigner semi-circle law, which only matches the exact density asymptotically, when $N \to \infty$. Thus, the only way to stick on Equation (4.26) for the unfolding is to discard the eigenvalues that fall outside the semi-circle bounds. However, doing so, the number of resonances in the sampled ladders after the unfolding step is smaller than N. In order to correct this issue, an empirical method based on experience can be used, in which random matrices of the GOE to be sampled are chosen bigger than N. For instance, choosing matrices of size M 5% bigger than N might be enough to obtain more than N unfolded eigenvalues. Once this is done, the extra unfolded eigenvalues can be discarded on the edges. This method provides N unfolded eigenvalues from the GOE, and is referred in the following as the *asymptotic unfolding*. Let us underline that the use of the cumulative of the Wigner semi-circle to unfold the levels is the typical method employed in the literature for which random matrices are used [51] [61].

The exact tabulated unfolding method

At small N however, the asymptotic unfolding is more than likely to produce some bias. In this work we introduce another method, which has turned out to be quite efficient for the intermediate matrix sizes considered in the ladder method ($N \approx 10^2 - 10^3$), which are not so much used in the framework of the random matrix studies[31]. The idea is simply to use the exact GOE level density at finite N instead of the Wigner semi-circle law, whose expression can for instance be found in [48] or [50]. Difficulties arise from the non-algebraic form of the level density, which implies numerical computations of an integral over Hermite polynomials. These polynomials are defined as[32]

$$H_k(x) = (-1)^k e^{x^2} \frac{d^k}{dx^k} e^{-x^2} \tag{4.27}$$

The exact form of the level density for the GOE ensemble at finite N is:

$$\rho(x) = \frac{1}{2N} \sum_{k=0}^{N/2-1} e^{-\frac{x^2}{2}} \left[R_{2k}(x)\Phi_{2k+1}(x) - R_{2k+1}(x)\Phi_{2k}(x) \right] \tag{4.28}$$

where the next intermediate functions have been defined:

$$\Phi_k(x) = \int_{-\infty}^{\infty} e^{-\frac{y^2}{2}} R_k(y)\mathrm{sign}(x-y)dy \tag{4.29}$$

$$R_{2k}(x) = \frac{\sqrt{2}}{\pi^{1/4}2^k(2k)!!} H_{2k}(x)$$
$$R_{2k+1}(x) = \frac{\sqrt{2}}{\pi^{1/4}2^{k+2}(2k-1)!!} \left[4kH_{2k-1}(x) - H_{2k+1}(x) \right] \tag{4.30}$$

This expression corresponds to the pink curve in Figure 4.2. It cannot be algebraically integrated in a single point, unlike the Wigner semi-circle density of Equation (4.12) used in

---

[31]The field of study of random matrices usually focuses on the behavior of random matrices of very large size, before focusing on the bulk or on the edges of the spectrum.

[32]The definition of the Hermite polynomials in use corresponds to the classical "physicists" Hermite polynomials, in opposition to the "probabilist's" form.

the asymptotic method. However, a numerical integration over an energy interval is possible, defining a thin grid around the energy of calculations. In the present situation, the size of the matrix N is chosen by the user and is defined all along the algorithm, as it corresponds to the size of the resonance ladders to be sampled. It makes sense to actually tabulate several level densities for many N values prior to their use in the ladder method. This has been performed and incorporated into the GAIA-2 program. For values of N ranking from 8 to 1000[33], energy meshes have been generated between the values $-1.2a_N$ and $1.2a_N$ (because the level densities extends slightly further than the semi-circle radius), using a step of 0.01. The exact level densities and their corresponding cumulatives I_{av}^{ex} have been computed over this grid. The N GOE-yielded eigenvalues can be unfolded using a linear interpolation of I_{av}^{ex}. This method is referred in the following as the *exact tabulated unfolding*. The only difference with the asymptotic method is the use of the cumulative of the exact level density for the GOE eigenvalues in lieu of the corresponding Wigner semi-circle law at N.

In order to estimate the impact of the several unfolding methods presented until now, a small simulation has been run for matrices of sizes $N = 8$, $N = 100$, and $N = 500$. Obtained spectra have been unfolded with the asymptotic method, the exact tabulated one, and a polynomial fitting in order to compare the result of a method which does not assume the form of the levels distribution. For all cases, the shift from Equation (4.26) has been performed to improve readability[34]. Results are presented on Figure 4.7, which displays folded and unfolded histogrammed eigenvalues, along with the theoretical semi-circle law Equation (4.12) and the exact level density Equation (4.28), for the corresponding size of the ladders N. The number of runs used to obtain such histogrammed eigenvalues has been adapted to provide sets of same sizes according to the matrices sizes; this number has been set to 500 000 eigenvalues, distributed into 30 bins.

An efficient unfolding is supposed to average the level density to make the consideration of the local fluctuations possible. As a result, the mean level density is supposed to be constant all along the spectrum. On Figure 4.7, histogrammed eigenvalues should approach an uniform distribution. This is quite the case for the "exact tabulated" method, for all sizes of random matrices. The polynomial unfolding on the other hand completely fails at low N, especially when $N = 8$ on Figure 4.7. This is logical, as it becomes very hard to obtain a meaningful fit of the empirical levels cumulative when N is small. When N increases, the polynomial unfolding works better.

Finally, some words may be said about the use of the Wigner semi-circle law for the unfolding, in the asymptotic method. It turns out that the density of the corresponding unfolded eigenvalues decreases at the edges. This phenomenon is less marked when N increases, which makes sense as the real underlying level density Equation (4.28) approaches the Wigner semi-circle when N increases. In the implemented asymptotic method, one should recall that the eigenvalues are actually sampled from matrices 5% larger than the required N. Then, extra eigenvalues are dropped at the edges. As the middle of the spectrum looks to be pretty well unfolded, it looks practicable to sample even bigger matrices before dropping the edge eigenvalues. However, the proper size is difficult to estimate, and necessarily depends on N. It seems than even for large matrices of size 1000, choosing matrices 5% larger does not ensure a perfect unfolding. At low N, this phenomenon is even worse; for instance for $N = 8$, not only the edges are less dense than the middle of the spectrum, but their vicinity is higher than the middle. This complex behavior is due to the poor approximation of the real density (pink curve) by the Wigner semi-circle (black curve). For $N = 100$, the situation looks better except for the edges. In any case, the exact tabulated unfolding provides a more regular level density.

As a consequence, the exact tabulated looks a more efficient method for the unfolding. From a numerical point of view, the computing time is very comparable to the asymptotic unfolding, due to the use of the tabulated expression of the density. This method is thus the default used

---

[33]Which corresponds to ladders of 500 pairs of resonances.

[34]Despite Equation (4.26) has been presented for the cumulative of the semi-circle law I_{av}^{SC}, the shift and homothety are still applicable for I_{ex}^{SC}
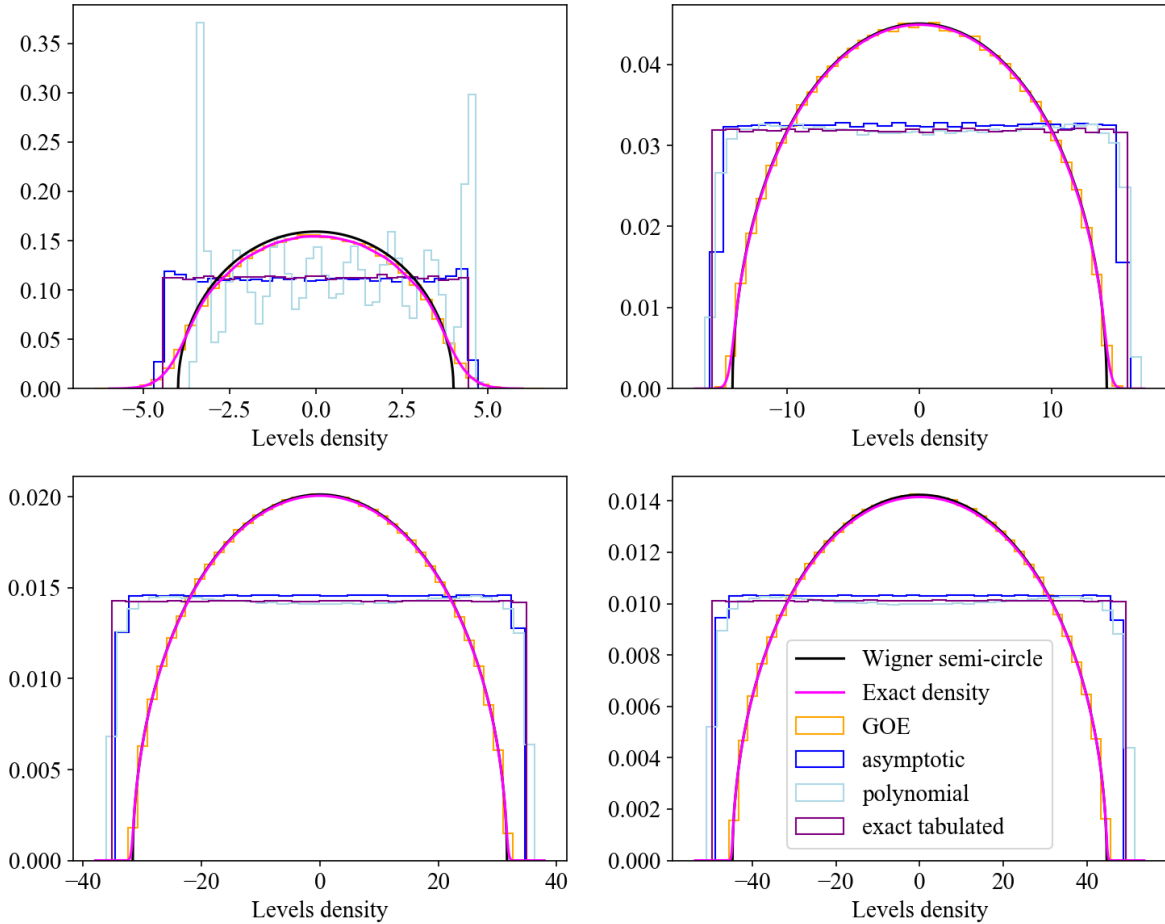
Figure 4.7: Effect of several unfolding methods for GOE histogrammed eigenvalues for matrices of several sizes $N = 8$ (top left), 100 (top right), 500 (bottom left) and 1000 (bottom right). Folded eigenvalues of the GOE have been represented too, along with the exact level density at finite N and the corresponding asymptotic Wigner semi-circle.

in GAIA-2. All statistics presented in Section 4.1.3 have been obtained with this unfolding method.

4.2.2 Impact of the correlated spacings on the cross sections statistics

A simple question arises: what is the impact of correlating resonance spacings in the context of the ladder method ? In order to answer this question, several points have been dealt with. First of all, the same analyses as those in previous chapter about the required number of pairs have been performed. Ladders of 1000 resonances have been generated with correlated spacings for all 41486 elementary spingroups of JEFF-3.2, and truncated to compute cross sections values for various ladder sizes. As a reminder, each elementary spingroup is defined as the set of scalar parameters corresponding to the data related to a single isotope in the unresolved resonance range, for a single pair of quantum numbers (l, J), at a single reference energy. These sets of input parameters correspond to the actual sub-calculations made in the unresolved resonance range during the processing of the whole library. Such sets have been widely used in the previous chapter, to tune the implementation of the ladder method.

In a second time, statistics and statistical two-sample tests have been computed to compare cross sections sets derived from ladders with correlated or uncorrelated spacings. These tests constitute the most straightforward way to explore a potential impact of the change in the Monte-Carlo sampling over the results. The interpretation of the outcomes of such tests must

be tempered though, as it will be detailed later.

One of the main issue of correlating the resonance spacings is numerical. The time required by the sampling is way more important for the GOE-like sampling, even when relying on tridiagonal matrices, as pointed out in Table 4.1. Finally, had all cross sections for all elementary spingroups of JEFF-3.2 be kept for the sake of comparisons, this would be an issue from the storage point of view. As a consequence, only 20 000 Monte-Carlo iterations were run with correlated spacings, for all elementary spingroups of JEFF-3.2, and two temperatures (T=0K and T= 293.6K). Considering all cross section values for various numbers of resonances, two temperatures, three reactions and all elementary spingroups already require a storage capacity up to 5To.

Convergence graphs equivalent to Figures 3.6–3.8 have been drawn in Figures 4.8–4.10. These graphs display the convergence of the various statistics already used in previous chapter as a function of the number of "pairs" of resonances considered in the sets. Note that contrary to the classical Wigner sampling, resonances are not drawn as pairs in the correlated spacings approach, in order to avoid the inspection paradox. In that case, the choice is made to select the closest resonances around the reference energy, except for the case of 500 pairs, where all resonances are selected.

The results look a lot like the Wigner case. The dynamic for all statistics is more or less the same, and the same nuclides are found to be the ones with the more resonances needed. The more wobbly aspect of the curves is mainly due to the smaller number of iterations performed. As such, we believe that all considerations made in previous chapter about the number of required resonances to fill the ladder still hold.

The scalar statistics used in previous chapter have been computed for the GOE-like full 1000-resonances ladders, and compared to the Wigner-like ladders. Because of the relatively small amount of Monte-Carlo iterations, differences due to the method implementation are hard to separate from the random sampling fluctuations. Such statistics are still displayed in the Appendix C.

In order to investigate more in detail the possible differences, two integral statistics have been computed between the sets directly. The first is the two-sample Kolmogorov-Smirnov statistics (KS), which has already been presented. The second is the so-called two-sample Anderson-Darling statistics (AD), which is also based on the distance between both empirical distributions of the sets. The main difference lies in the choice of the distance in question. The Kolmogorov-Smirnov distance between the empirical distributions is chosen to be the infinite norm. In the case of the Anderson-Darling statistics, a quadratic distance is introduced. In the case of two samples of same size n with associated empirical distributions F_n and G_n, the two-sample Anderson-Darling statistics is defined as

$$A_n^2 = \frac{n}{2} \int_{-\infty}^{\infty} \frac{[F_n(x) - G_n(x)]^2}{H_n(x)[1 - H_n(x)]} dH_n(x) \tag{4.31}$$

where $H_n = \dfrac{F_n(x) + G_n(x)}{2}$. Compared to the two-sample Kolmogorov-Smirnov statistics, the Anderson-Darling captures the change in the tails more accurately, and offers an interesting alternative to estimate the change brought by the correlating of spacings in the ladder method.

The computed distances for all spingroups between the cross sections sets of 20 000 elements are displayed in Figure 4.11 for the Kolmogorov-Smirnov statistics, and in Figure 4.12 for the Anderson-Darling. They are displayed for each reaction and elementary spingroup of JEFF-3.2, for cross sections computed at T=0K or T=293.6K, and for ladders composed of 100 or 500 pairs of resonances.

Let us describe these figures more in detail. First of all, the results between the ladders with only 100 pairs of resonances, and the ones with 500 pairs are surprisingly similar. This underlines the importance of the closest resonances in general. Beyond this observation, both Kolmogorov-Smirnov and Anderson-Darling statistics seem to behave accordingly. At high $\overline{\Gamma}/\overline{D}$

Figure 4.8: Convergence of various statistics of the sampled elastic cross sections toward the reference (1000 resonances) according to various number of central resonances considered. Calculations are performed with correlated spacings at T=0K. (a) mean, (b) variance, (c) skewness, (d) kurtosis, (e) first quartile, (f) fourth quartile, (g) 95th percentile, (h) Kolmogorov-Smirnov distance
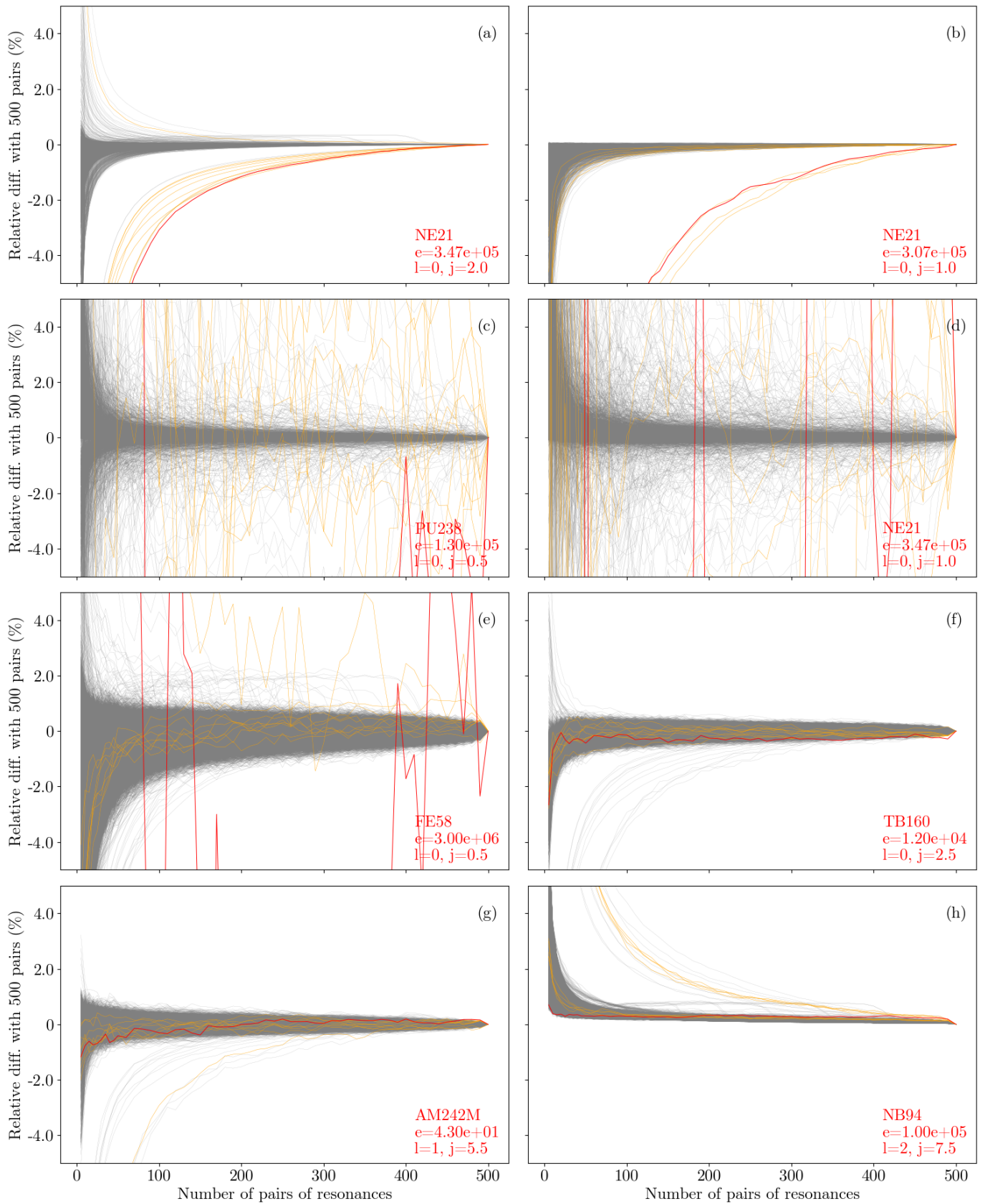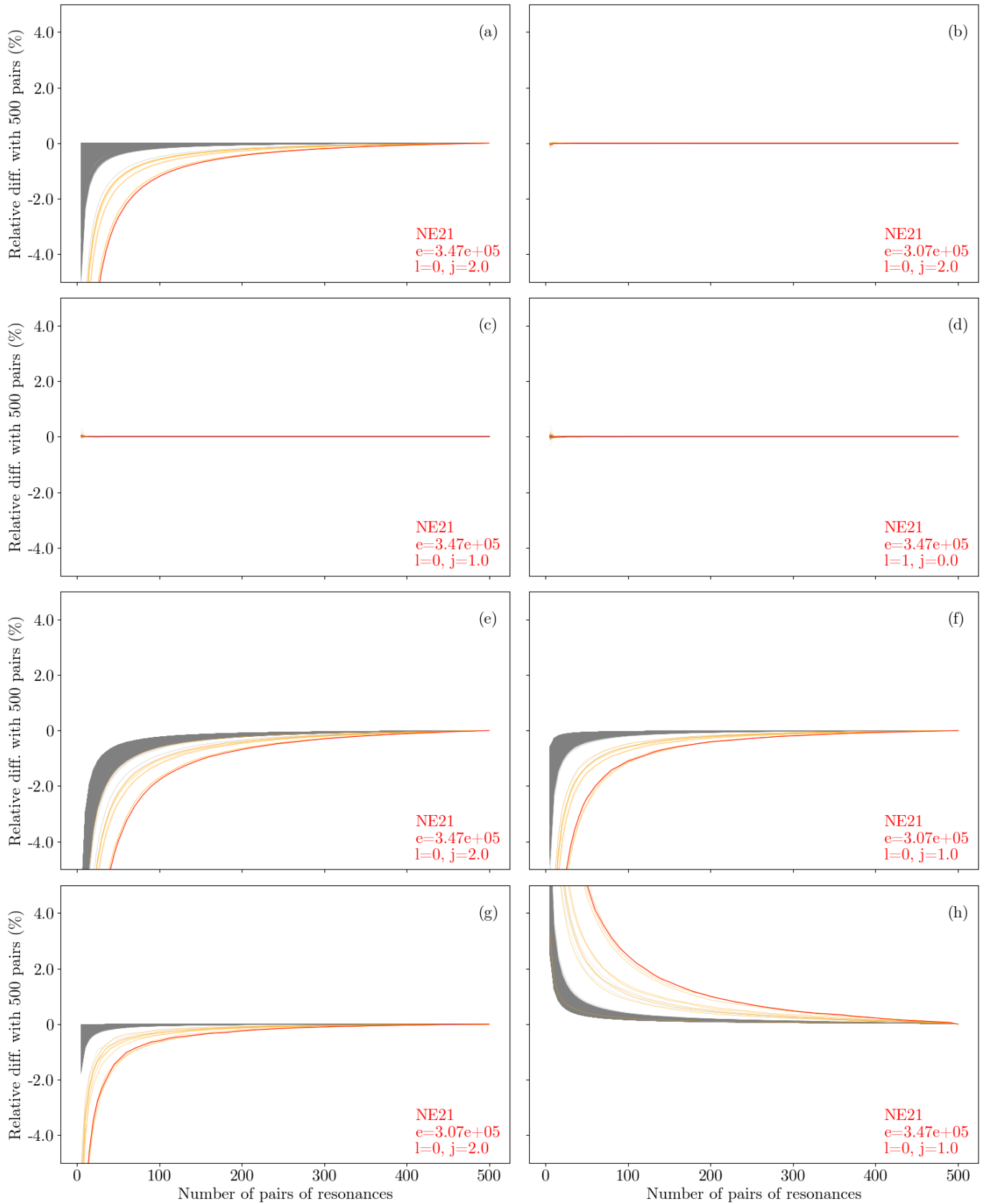
Figure 4.9: Convergence of various statistics of the sampled capture cross sections toward the reference (1000 resonances) according to various number of central resonances considered. Calculations are performed with correlated spacings at T=0K. (a) mean, (b) variance, (c) skewness, (d) kurtosis, (e) first quartile, (f) fourth quartile, (g) 95th percentile, (h) Kolmogorov-Smirnov distance

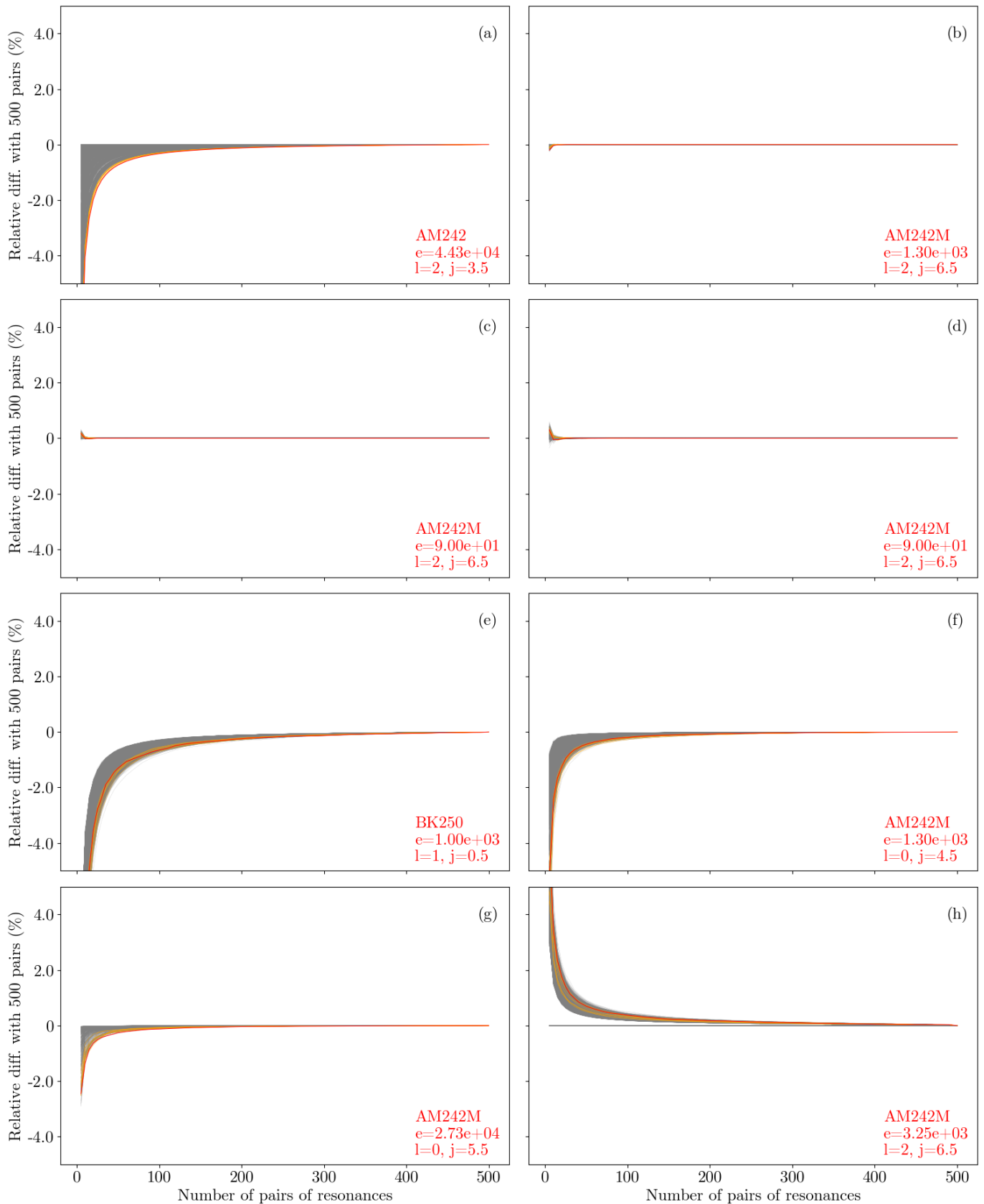Figure 4.10: Convergence of various statistics of the sampled fission cross sections toward the reference (1000 resonances) according to various number of central resonances considered. Calculations are performed with correlated spacings at T=0K. (a) mean, (b) variance, (c) skewness, (d) kurtosis, (e) first quartile, (f) fourth quartile, (g) 95th percentile, (h) Kolmogorov-Smirnov distance
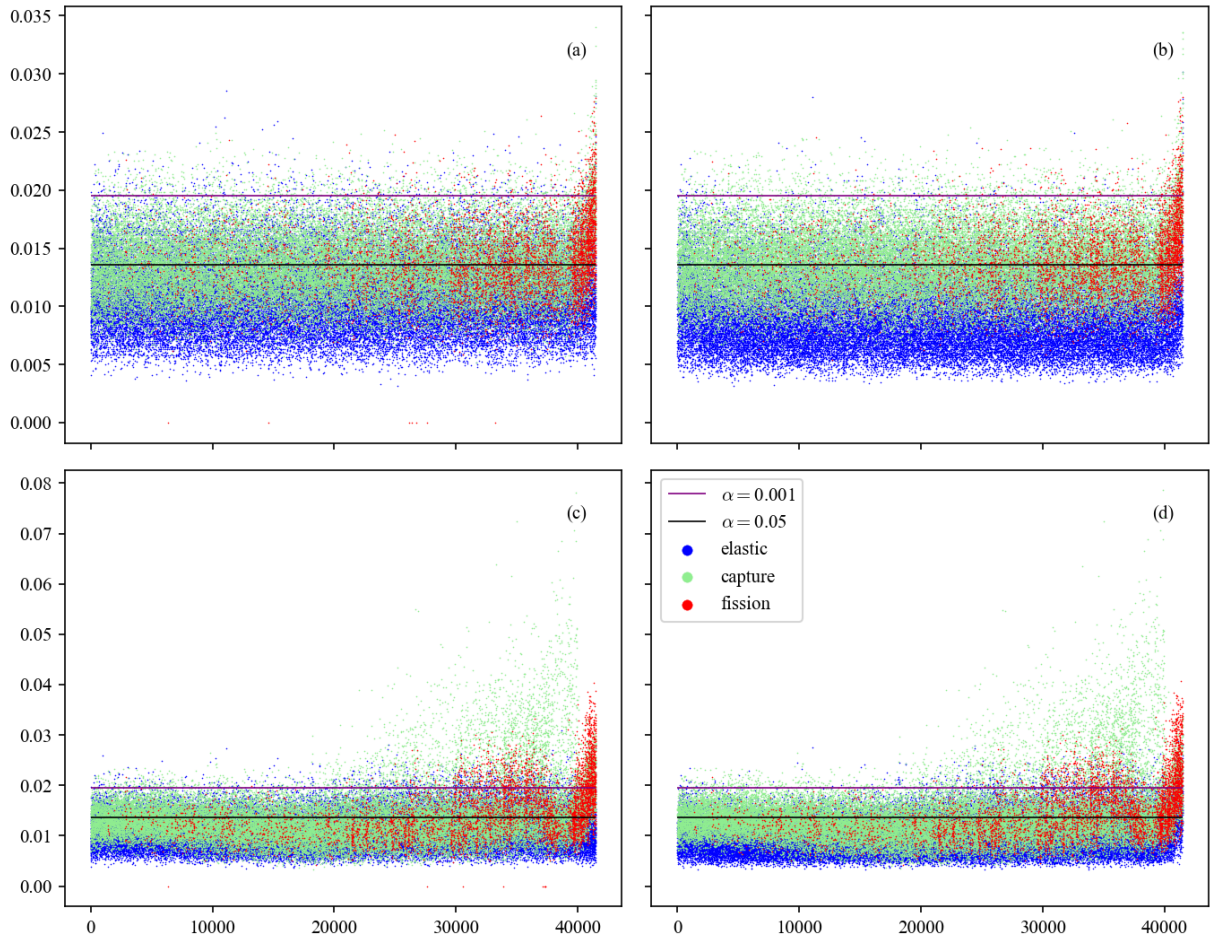
136

Figure 4.11: Two-sample Kolmogorov-Smirnov statistics between cross sections sets for all elementary spingroups of JEFF-3.2 (sorted in increasing $\overline{\Gamma}/\overline{D}$) obtained with correlated or uncorrelated spacings. On the left, the sets derived from ladders with 100 pairs of resonances have been considered. On the right, 500 pairs. On top are the results for T=0K. On bottom, results for T=293.6K. Both critical values for significance levels $\alpha = 0.05$ and $\alpha = 0.001$ have been plotted.

values, the statistics seem to increase, in particular for fission and capture. This means that the differences in the global shape of the empirical distributions – as measured by both distances – is greater in this region of the input phase space. As a reminder, this region requires resonances in the ladders to obtain correct results. This has a physical meaning. The more resonances contribute to the cross sections in a ladder, the more the spacing correlations introduced by the random matrix theory may have an impact.

The question of the magnitude of this impact is more difficult to tackle. A first attempt can be made casting the AD- and KS-statistics into corresponding well-defined hypothesis tests. Indeed, the Kolmogorov-Smirnov and Anderson-Darling statistics serve as a base distance for classic adequation tests. In both cases, the null hypothesis claims that "both sets are drawn from the same underlying distribution". If the statistics values exceed a critical value with significance levels α, the null hypothesis is rejected. The significance levels correspond to the threshold probability to reject the null hypothesis while it is true, only because of the sampling randomness. Critical values for both tests can be computed from theoretical formulas[35], and have been plotted as horizontal lines on Figures 4.11–4.12 for significance levels $\alpha = 0.1\%$ and $\alpha = 5\%$. If the KS or AD statistics exceed the critical values, the null hypothesis is rejected,

---

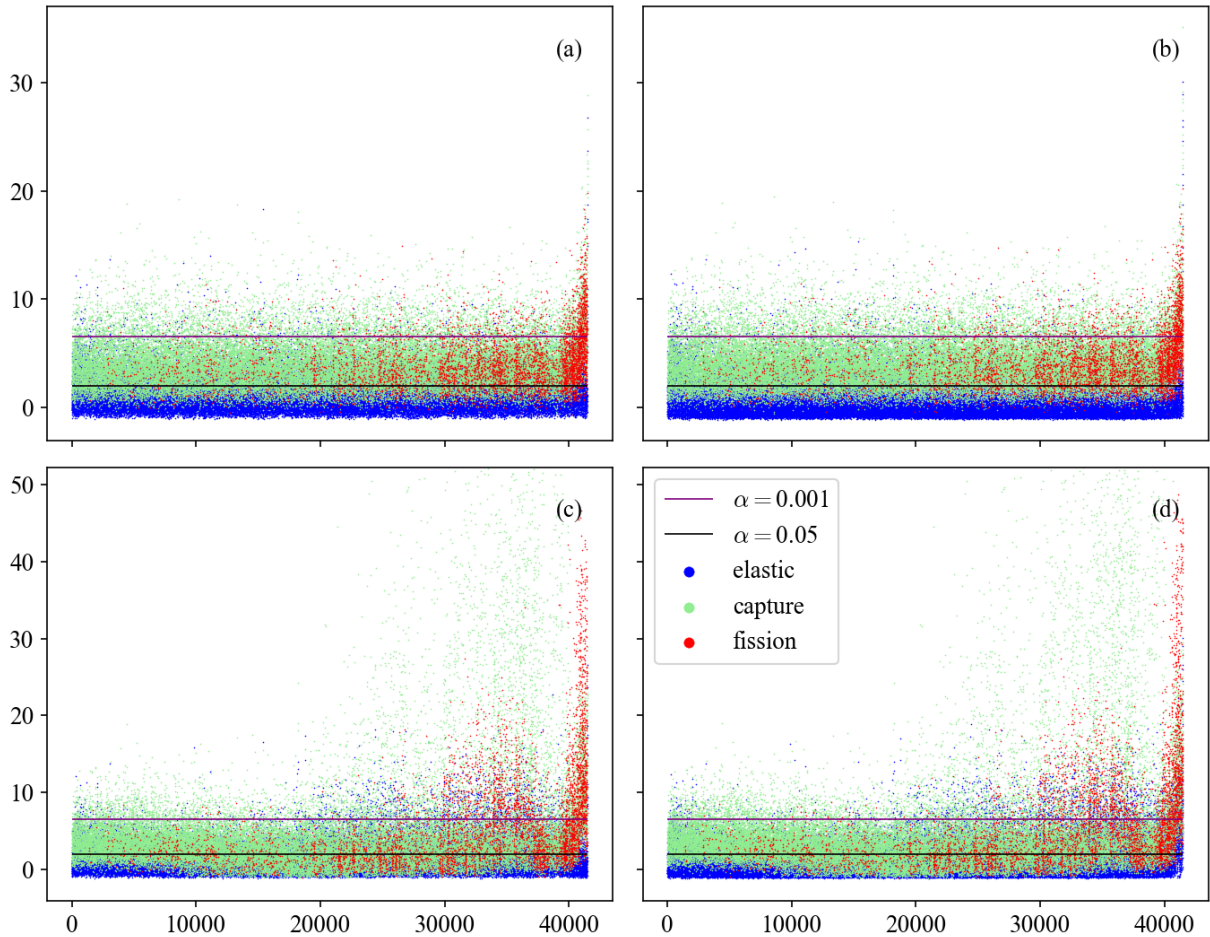[35]Critical values for the two-sample Anderson-Darling statistics have been explored by A. Pettitt in [62] for instance.

Figure 4.12: Two-sample Anderson-Darling statistics between cross sections sets for all elementary spingroups of JEFF-3.2 (sorted in increasing $\overline{\Gamma}/\overline{D}$) obtained with correlated or uncorrelated spacings. On the left, the sets derived from ladders with 100 pairs of resonances have been considered. On the right, 500 pairs. On top are the results for T=0K. On bottom, results for T=293.6K. Both critical values for significance levels $\alpha = 0.05$ and $\alpha = 0.001$ have been plotted.

which means that cross sections distributions are found to differ significantly. As output cross section distributions are obtained with two versions of the ladder method, with or without correlated spacings, rejecting the null hypothesis would mean that correlating the spacings has a significant impact. Often, p-values are calculated as an alternative to using statistics and critical values, with the exact same results. P-values are thus directly compared to the significance levels α to accept or reject the null hypothesis.

A blunt affirmation would be to claim that all cases whose critical values are exceeded by the statistics is a manifestation of a "significant" difference. This cannot be said however, as there are many chances of "false positive": cases in which the critical value is exceeded due to sampling's randomness only. Moreover, the choice of the significance levels is arbitrary and depends on the expectations of the user. There, a smarter approach may take advantage of the fact that many tests are performed, comparing the percentage of tests whose KS- or AD-statistics exceed the critical values to the significance levels. These percentages are summarized in Table 4.2 for each reaction and temperature.

For now, this crude approach does treat all the input test cases on an equal footing. The idea is to compare the percentage of significant outcomes for both tests to the α level. For instance, in the case of elastic cross sections at T=0K, the distributions between correlated and uncorrelated spacings cases are found to be significant at the $\alpha = 5\%$ level in 8% of the 41486 input cases. If the null hypothesis were true, this statistics would be expected to lie around 5%.

T=0K		Kolmogorov-Smirnov	Anderson-Darling
$\alpha = 0.05$	elastic	8.05%	12.47 %
	capture	47.42 %	85.56 %
	fission	53.95%	83.80 %
$\alpha = 0.001$	elastic	0.27%	0.67%
	capture	2.56%	12.42%
	fission	5.50%	17.71%
T=293.6K		Kolmogorov-Smirnov	Anderson-Darling
$\alpha = 0.05$	elastic	14.04%	20.37%
	capture	40.56%	70.06%
	fission	57.87%	76.61%
$\alpha = 0.001$	elastic	1.34%	3.37%
	capture	8.74%	16.37%
	fission	22.33%	36.94%

Table 4.2: Percentage of input cases of JEFF-3.2 whose statistics exceeds the critical value, or equivalently, for which the calculated p-value is smaller than the chosen significance level α.

The same goes with the $\alpha = 0.1\%$ level. The results at T=293.6K are even more marked; the same goes for fission and capture. In that latter case, the percentage of cases for which the null hypothesis can be rejected is much higher than the α level.

As a consequence, the most conservative choice in most cases (without considering the detail of the input parameters) would be to reject the null hypothesis that correlated and uncorrelated spacings produce the same distributions. This affirmation however needs to be tempered, as it does not constitute a strong result.

Actually in this kind of analysis, the more iterations are run, the stronger the tests get. This means that they are able to detect even tiny variations between the distributions, which convert to small p-values. Here, each set contains 20 000 iterations, which is actually a lot. As a consequence, both Anderson-Darling and Kolmogorov-Smirnov tests are powerful to detect variations between the distributions obtained with correlated and uncorrelated spacings. However, such hypothesis testing does not quantitatively determine the level of discrepancy between the distributions, but only a level of confidence to reject the null hypothesis. Here, it is almost a starting point to claim that obtained distributions with or without correlated spacings are not the same, as they are issued from different ladder methods. This is thus only confirmed by the tests outcome, but without any additional information about the impact of the difference in distributions. In support of this statement, the most discriminant case found for fission at T=0K can be investigated. For both Kolmogorov-Smirnov and Anderson-Darling tests, it is the spingroup of ^{242}Am with quantum numbers $l = 2$ and $J = 3.5$ at $E_{ref} = 25$ keV which provides the smallest p-value, around 10^{-7}. This case also provides the 11th smaller p-value found among all elementary spingroups for the capture. Such low p-values indicate that it is extremely unlikely that the compared sets have been obtained from the same distribution. However, the maximum difference – in the sense of the Kolmogorov-Smirnov distance between the empirical distributions – is at max of 3% only, as may be noticed on Figure 4.11. To be more precise the probability density functions of capture and fission are displayed in Figure 4.13. On this figure,

the distributions seem to slightly differ, but not so much. Moreover, their global shape remains the same. All that supports the idea that the performed tests are mainly strong enough[36] to detect small differences between the distributions, considering the high number of Monte-Carlo iterations performed.
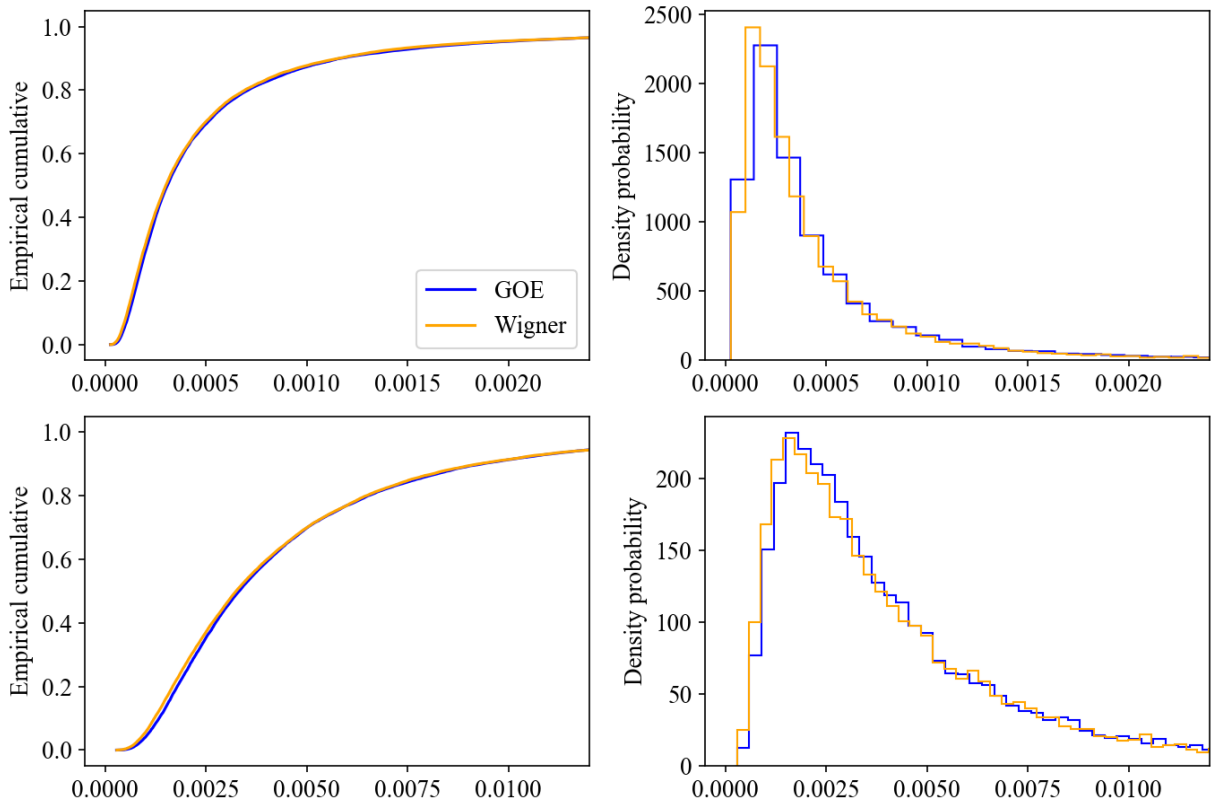

Figure 4.13: Empirical cumulative distributions (left) and probability densities (right) for capture (top) and fission (bottom) cross sections sets of ^{242}Am (T=0K, $E_{ref} = 25$ keV, $l = 2$, $J = 3.5$), obtained from the ladder method in its classical or GOE-like implementation. The figures have been zoomed to exhibit the most disagreeing part of the cumulative for both distributions.

In fact, the most remarkable fact of Table 4.2 is no longer the rejection of the null hypothesis, as it turns out it is the case even for small deviations between the sets, but the difference between the reactions. In particular, the elastic scattering reaction appears to be less impacted than the capture and the fission by the correlating of resonance spacings. This is clearly visible on Figures 4.11–4.12 and Table 4.2, but can be even put forward with a histogram of the p-values for the Kolmogorov-Smirnov test for example. In such a histogram, presented in Figure 4.14, the distribution of p-values for the elastic reaction almost draws an uniform distribution on $[0, 1]$. Such a distribution would be obtained if the null hypothesis were true, ie. if the underlying cross sections distributions yielded by both methods were the same. It is not exactly the case, as the extreme left bin seems slightly higher, but it is clear that the impact of correlating the spacings on the elastic cross section is very weak – at least weaker than for fission and capture.

To conclude, the comparison between cross sections sets obtained from GOE-like ladders and ladders with uncorrelated spacings has been carried out using some statistics such as the Kolmogorov-Smirnov and the Anderson-Darling distances. A classic hypothesis testing based on these two statistics is feasible, although the result is of poor relevance. Indeed, such tests provides a binary answer about a potential significant difference between the distributions, which is very likely to be always positive for large samples. On the other hand, information based on

---
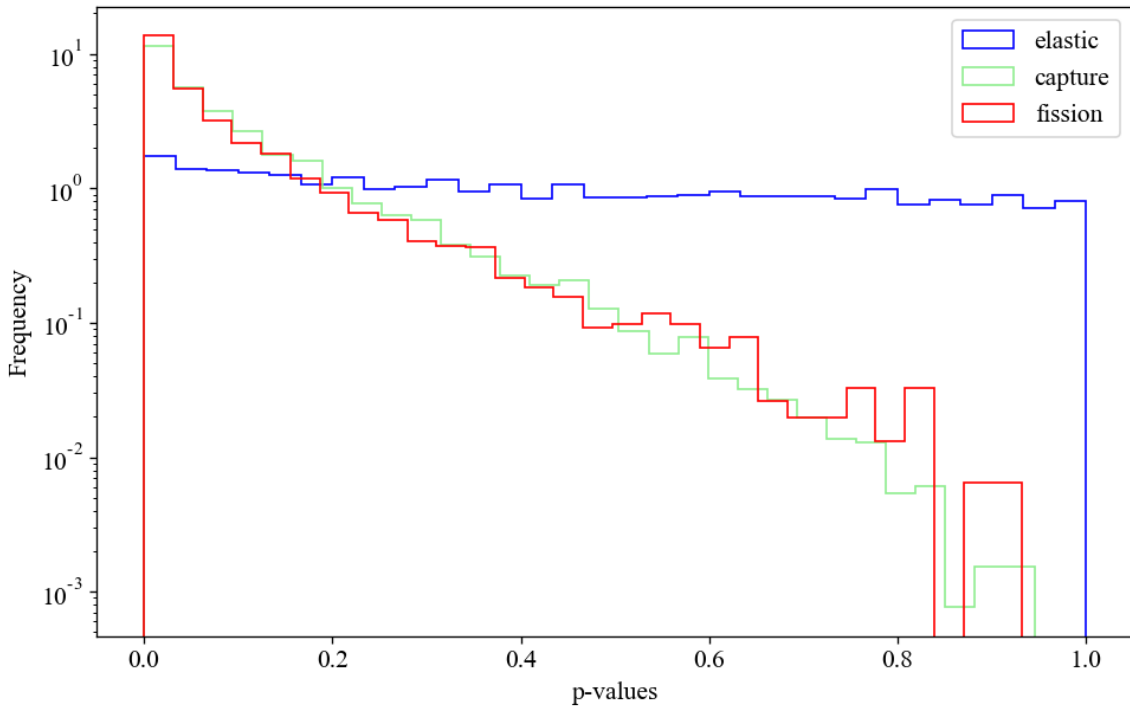
[36]And so, maybe even too strong.

Figure 4.14: Histogram of the p-values of the Kolmogorov-Smirnov tests performed between cross sections obtained from ladders with or without correlated spacings at T=0K, for all elementary spingroups of JEFF-3.2.

these statistics seemed to hold still: the higher the ratio $\overline{\Gamma}/\overline{D}$ of the input parameters is, the more the output distributions differs. The same applies for temperature. Accordingly, this seemed to be explained as the ladders are composed of more contributing resonances in these cases, in agreement with Chapter 3. Moreover, the elastic cross sections seem to be way less impacted than the two other reactions. In all cases, the output cross section distributions obtained from the two different implementations of the ladder method have been found to be quite similar in their shape. Before closing the topic of the correlated spacings, it is of much interest to focus a little more on the mean cross sections, which is the most important statistics in applications.

4.3 Average calculations

4.3.1 Some additions on the Hauser-Feschbach approach

Before anything else, let us recall some details discussed in the second chapter in which a theory of average cross sections calculations has been presented. There, the Moldauer method to compute the width fluctuation correction factor in the Hauser-Feschbach problem 2.37 was addressed. The main hypotheses of this approach consider that the resonance widths follow a χ^2 law with certain degrees of freedom, and that resonance spacings do not fluctuate too much. It has been also mentioned that the average over the product of elements $\overline{U_{ab}U_{cd}^*}$ was pretty difficult to carry out, but was needed for an exact expression of the average cross sections.

In 1985 however, Verbaarschot, Weidenmüller and Zirnbauer [63] were able to derive the exact expression of the average product calculations within the framework of the Gaussian Orthogonal Ensemble. The demonstration is very technical and is not displayed here. The authors were able to perform an ensemble average over the resonance parameters distributions induced by the GOE.

After the very complex analytical calculations detailed in [63], an expression of the width fluctuation correction which exactly takes into account the GOE fluctuations was established as

a function of the transmission ratios T_c as a triple integral:

$$W_{cc'} = \frac{\sum_d T_d}{8} \int_0^\infty d\lambda_1 \int_0^\infty d\lambda_2 \int_0^1 d\lambda \frac{\lambda(1-\lambda)|\lambda_1 - \lambda_2|}{\sqrt{\lambda_1(1+\lambda_1)}\sqrt{\lambda_2(1+\lambda_2)}(\lambda+\lambda_1)^2(\lambda+\lambda_2)^2}$$

$$\times \prod_\beta \left(\frac{1-T_d\lambda}{\sqrt{1+T_d\lambda_1}\sqrt{1+T_d\lambda_2}} \right) \times \left[\delta_{cc'}(1-T_c) \left(\frac{\lambda_1}{1+T_c\lambda_1} \frac{\lambda_2}{1+T_c\lambda_2} \frac{2\lambda}{1-T_c\lambda} \right)^2 \right. \tag{4.32}$$

$$\left. + (1+\delta_{cc'}) \left(\frac{\lambda_1(1+\lambda_1)}{(1+T_c\lambda_1)(1+T_{c'}\lambda_1)} + \frac{\lambda_2(1+\lambda_2)}{(1+T_c\lambda_1)(1+T_{c'}\lambda_2)} + \frac{2\lambda(1-\lambda)}{(1-T_c\lambda)(1-T_{c'}\lambda)} \right) \right]$$

to be used together with the Hauser-Feschbach Equation 2.37. The details of the implementation of such integrals have been explained in papers by Verbaarschot [64] and Hartney [65], and well summarized in [38]. In order to remove the singularities in the integral expression, the change of variable $p = 2\lambda + \lambda_1 + \lambda_2$ is performed. Then, both cases $p > 2$ and $p < 2$ are distinguished, and the integral is splitted in two parts: $\mathcal{I} = \mathcal{I}_{02} + \mathcal{I}_{2\infty}$[37].

For $p < 2$, changes of variable $s = \sqrt{\dfrac{\lambda_1 + \lambda_2}{2\lambda + \lambda_1 + \lambda_2}}$ and $t = \sqrt{\dfrac{\lambda_1}{\lambda_1 + \lambda}}$ are achieved. For $p > 2$, the simpler $s = \sqrt{\lambda + \lambda_1}$ and $t = \sqrt{\dfrac{\lambda_1}{\lambda_1 + \lambda}}$ suffice. For both integrals, one has:

$$\mathcal{I}_{02} = \int_0^2 dp \int_0^{\sqrt{2}/2} ds \int_0^1 dt \frac{T_c T_{c'}(1-ps^2+ps^2t^2)(1-2s^2)(1-t^2)}{p(1-s^2)^2\sqrt{(1+s^2t^2-2s^2)(1+ps^2t^2)(1+p+ps^2t^2-2ps^2)}}$$

$$\times \prod_d \left(\frac{1-T_d\lambda}{\sqrt{1+T_d\lambda_1}\sqrt{1+T_d\lambda_2}} \right) \times \left[\delta_{cc'}(1-T_c) \left(\frac{\lambda_1}{1+T_c\lambda_1} \frac{\lambda_2}{1+T_c\lambda_2} \frac{2\lambda}{1-T_c\lambda} \right)^2 \right. \tag{4.33}$$

$$\left. + (1+\delta_{cc'}) \left(\frac{\lambda_1(1+\lambda_1)}{(1+T_c\lambda_1)(1+T_{c'}\lambda_1)} + \frac{\lambda_2(1+\lambda_2)}{(1+T_c\lambda_1)(1+T_{c'}\lambda_2)} + \frac{2\lambda(1-\lambda)}{(1-T_c\lambda)(1-T_{c'}\lambda)} \right) \right]$$

and

$$\mathcal{I}_{2\infty} = \int_2^\infty dp \int_0^{\sqrt{p/2}} ds \int_{f(s)}^1 dt \frac{T_c T_{c'}\left[1-s^2(1-t^2)\right](p-2s^2)(1-t^2)}{(p-s^2)^2\sqrt{(1+s^2t^2-2s^2)(1+ps^2t^2)(1+p+ps^2t^2-2ps^2)}}$$

$$\times \prod_d \left(\frac{1-T_d\lambda}{\sqrt{1+T_d\lambda_1}\sqrt{1+T_d\lambda_2}} \right) \times \left[\delta_{cc'}(1-T_c) \left(\frac{\lambda_1}{1+T_c\lambda_1} \frac{\lambda_2}{1+T_c\lambda_2} \frac{2\lambda}{1-T_c\lambda} \right)^2 \right. \tag{4.34}$$

$$\left. + (1+\delta_{cc'}) \left(\frac{\lambda_1(1+\lambda_1)}{(1+T_c\lambda_1)(1+T_{c'}\lambda_1)} + \frac{\lambda_2(1+\lambda_2)}{(1+T_c\lambda_1)(1+T_{c'}\lambda_2)} + \frac{2\lambda(1-\lambda)}{(1-T_c\lambda)(1-T_{c'}\lambda)} \right) \right]$$

The function f is defined as $f(s) = \Theta(s-1)\sqrt{1-s^{-2}}$, where Θ is the Heaviside function. The limits for the p-variable integration in the second integral can be set to $]0,1[$ using a classic change of variables. For instance, it suffices to introduce the variable change $p = 2 + \frac{y}{1-y}$ to ensure such a change.

Like in Section 2.2, radiative capture is a special case, as there are many open channels. As a consequence the product over all the channels in the previous equations can be simplified. Defining $T_\gamma = \sum_{d\in\gamma} T_d$,

$$\prod_{d\in\gamma} \frac{1-T_d}{\sqrt{(1+T_d\lambda_1)(1+T_d\lambda_2)}} \approx \exp\left[-T_\gamma \left(\lambda + \frac{\lambda_1}{2} + \frac{\lambda_2}{2} \right) \right] \tag{4.35}$$

and intgerals $\mathcal{I}_{02}$ and $\mathcal{I}_{2\infty}$ become

---

[37]$\mathcal{I}$ is defined so that $W_{cc'} = \dfrac{\sum_d T_d}{8}\mathcal{I}$.

$$\mathcal{I}_{02} = \int_0^2 dp \int_0^{\sqrt{2}/2} ds \int_0^1 dt \frac{T_c T_\gamma (1 - ps^2 + ps^2 t^2)(1 - 2s^2)(1 - t^2)}{p(1 - s^2)^2 \sqrt{(1 + s^2 t^2 - 2s^2)(1 + ps^2 t^2)(1 + p + ps^2 t^2 - 2ps^2)}}$$

$$\times \prod_{d \notin \gamma} \left(\frac{1 - T_d \lambda}{\sqrt{1 + T_d \lambda_1} \sqrt{1 + T_d \lambda_2}} \right) \times \exp \left[-T_\gamma \left(\lambda + \frac{\lambda_1}{2} + \frac{\lambda_2}{2} \right) \right] \qquad (4.36)$$

$$\times \left(\frac{\lambda_1 (1 + \lambda_1)}{(1 + T_c \lambda_1)} + \frac{\lambda_2 (1 + \lambda_2)}{(1 + T_c \lambda_1)} + \frac{2\lambda(1 - \lambda)}{(1 - T_c \lambda)} \right)$$

and

$$\mathcal{I}_{2\infty} = \int_2^\infty dp \int_0^{\sqrt{p/2}} ds \int_{f(s)}^1 dt \frac{T_c T_\gamma \left[1 - s^2 (1 - t^2) \right] (p - 2s^2)(1 - t^2)}{(p - s^2)^2 \sqrt{(1 + s^2 t^2 - 2s^2)(1 + ps^2 t^2)(1 + p + ps^2 t^2 - 2ps^2)}}$$

$$\times \prod_{d \notin \gamma} \left(\frac{1 - T_d \lambda}{\sqrt{1 + T_d \lambda_1} \sqrt{1 + T_d \lambda_2}} \right) \times \exp \left[-T_\gamma \left(\lambda + \frac{\lambda_1}{2} + \frac{\lambda_2}{2} \right) \right] \qquad (4.37)$$

$$\times \left(\frac{\lambda_1 (1 + \lambda_1)}{(1 + T_c \lambda_1)} + \frac{\lambda_2 (1 + \lambda_2)}{(1 + T_c \lambda_1)} + \frac{2\lambda(1 - \lambda)}{(1 - T_c \lambda)} \right)$$

All triple integrals can be evaluated numerically with an adaptive Gaussian-Legendre quadrature without any difficulty. To be more precise, the used numerical integration starts by performing a Gauss-Legendre quadrature on 16 points over the integration interval, and a Gauss-Kronrod quadrature over 33 points. The difference between these two calculations gives an estimation of the numerical error. If an objective error threshold is provided, a dichotomous algorithm can be implemented to reach the required level: the integration interval is divided in two, and the quadratures are applied to both intervals. Until the numerical error is acceptable, the process is repeated on the most erroneous interval. Such a procedure is developed in [66]. The required numerical precision for each of the integral is 10^{-5}.

An important question remains about the possibility to use these expressions with the average resonance parameters provided in the format of the ENDF evaluations. The ENDF format is compliant with the GOE computations of the width fluctuation correction factor (WFCF) in the Hauser-Feschbach problem if the next two hypotheses are made:

- Transmission ratios are related to the average reaction widths using the same narrow resonance approximation than in the Moldauer method: $T_c = 2\pi \dfrac{\overline{\Gamma_c}}{\overline{D}}$;

- If the degree of freedom ν_c associated to a reaction width is greater than 1, the reaction is assumed to happen through ν_c distinct channels, each one with a new reaction width Γ_c / ν_c (the reaction width is equally splitted). Average cross sections are then computed adding the contributions of all $\sigma_{cc'}$ for all combinations of entrance and exit channels c and c' which contribute to the reaction.

Using these hypotheses, the average Hauser-Feschbach cross sections using the GOE calculations of the WFCF may now be computed over the whole set of 41486 input parameters that correspond to the decomposed library JEFF-3.2 as in Section 3.2.1. For each calculation, the transmission ratio conservation (Equation (2.42)) has been used as a tool to verify the quality of the performed numerical calculations.

The percentage difference between average Hauser-Feschbach calculations with Moldauer or GOE WFCF are displayed on Figure 4.15. In this figure, the x-axis is an index along which elementary spingroups have been ranged. As previously, they have been sorted in ascending values of the $\overline{\Gamma}/\overline{D}$ ratio, which proved to be a relevant quantity. From this figure, the differences between the two methods of average calculation indeed depend on the average input resonance
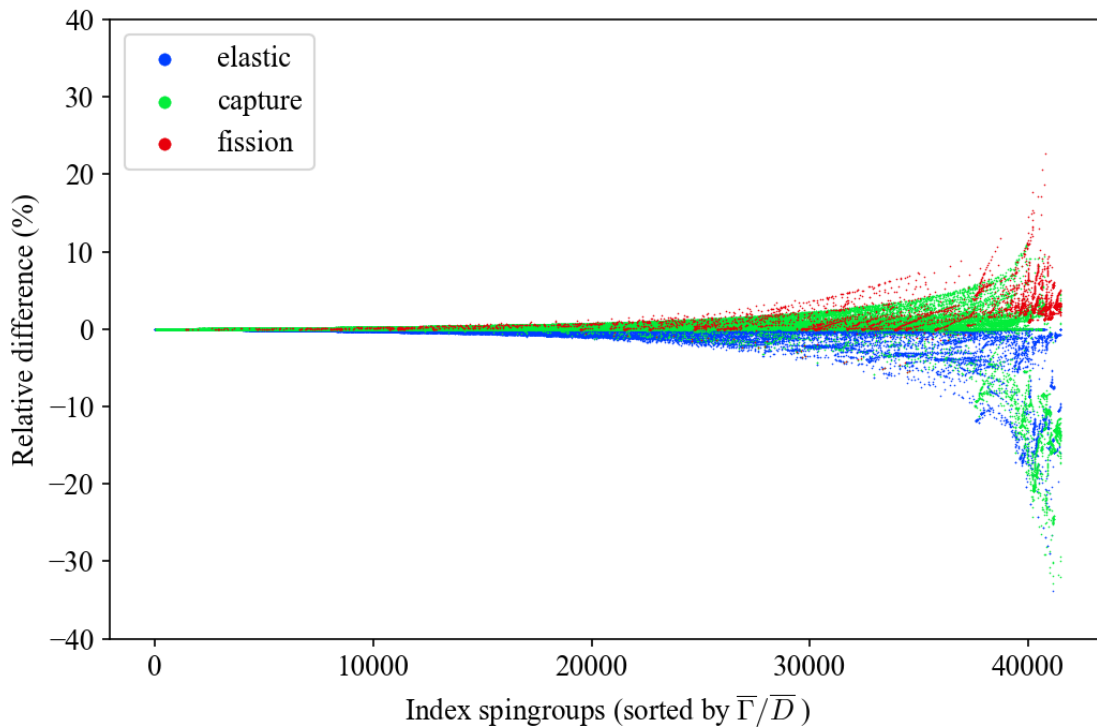
Figure 4.15: Comparison between average Hauser-Feschbach cross sections computed over all elementary spingroups of JEFF-3.2, with Moldauer or GOE width fluctuations correction factor.

parameters. The higher the ratio $\overline{\Gamma}/\overline{D}$ is, the more the disagreement between the calculations seems to arise. The percentage difference is as high as more than 30% for a few spingroups in this region of the input phase space, even if the vast majority of cases closely match. The comparisons with numerical studies will enable to give more details about these differences.

4.3.2 Comparison with numerical studies

In the previous chapter, the average cross sections calculated from the average resonance parameters with Moldauer method was compared to the mean cross sections from the usual ladder method with uncorrelated resonances. The results seemed to match closely for all elementary spingroups of JEFF-3.2 if enough Monte-Carlo runs were performed. In particular, the convergence seemed slower at low temperature and low $\overline{\Gamma}/\overline{D}$, due to a fewer number of contributing resonances. In this chapter, the random matrix theory has been used to produce ladders with correlated resonance energies, whose statistics agrees with the GOE. It is thus of interest to compare the mean cross sections values obtained from the ladder method with correlated spacings to the average calculations from resonance parameters, especially with the GOE-like computations of the width fluctuations factor (method of Verbaarschot and al.). Figure 4.16 displays the results. The relative difference between the mean cross sections from the ladder method with correlated spacings has been compared with the Hauser-Feschbach average cross sections using Moldauer or GOE WFCF, for all elementary spingroups of JEFF-3.2 sorted in ascending $\overline{\Gamma}/\overline{D}$. In order to reduce the impact of massive percentage difference yielded by very low cross sections values, relative differences for cross sections smaller than 10^{-5} barn were not calculated, and not presented.

Figure 4.16 can be explained having in mind the work carried out until now. The huge fluctuations obtained on the left part of the figure can be attributed to the Monte-Carlo variations. As seen, spingroups with low $\overline{\Gamma}/\overline{D}$ ratios require less resonances to converge and are more sub-
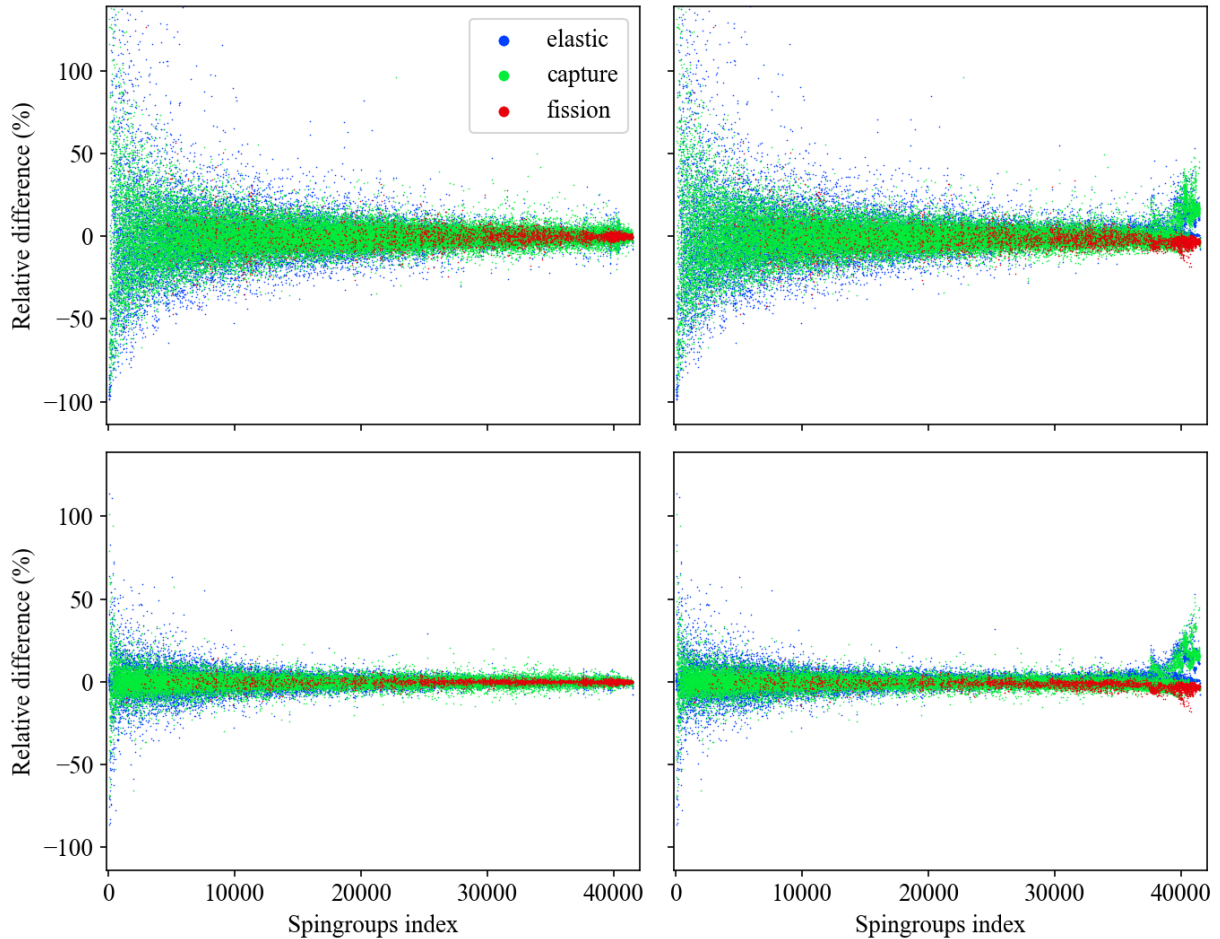
Figure 4.16: Percentage difference for all elementary spingroups of JEFF-3.2 between the mean cross sections obtained from the ladder method with correlated spacings at T=0K (top) and T=293.6K (bottom), with the Hauser-Feschbach average values using Moldauer (left) or GOE (right) formulas for the WFCF.

ject to Monte-Carlo fluctuations. This affirmation is also supported by the symmetric shape of the variations around 0, and the fact the same pattern is observed for both GOE and Moldauer comparisons, while the average calculations closely match for these elementary spingroups on Figure 4.15. The case of elementary spingroups with a large $\overline{\Gamma}/\overline{D}$ is more interesting. Less Monte-Carlo iterations are required for these ones and differences between the outcomes of the Hauser-Feschbach methods are much more pronounced. There, it seems that the ladder method with correlated spacings provides mean cross sections that agree best with the Moldauer method of calculation. This result is not so unexpected when one reminds the hypotheses performed in the Moldauer calculation of the Hauser-Feschbach problem, namely that resonance widths followed χ^2 law, and that resonance spacings did not fluctuate much. There, the absence of impact of the spacings correlation on the cross sections mean values looks like an argument to be pushed in favor of Moldauer's latter assumptions.

The global disagreement between average Haueser-Feschbach with GOE WFCF still calls for two open-problems that we judge worth being mentioned here.

First of all, the implemented ladder method only takes into account correlations between resonance spacings, and not between resonances widths. In the usual ladder method, resonance widths were sampled from χ^2 distributions with a certain degree of freedom. In the global framework of random matrix theory, both eigenvalues and eigenvectors are correlated, so that one should generate the whole matrix ensemble to obtain a proper representation of the GOE-

like fluctuations in the ladder method[38]. However, the relation between eigenvectors of GOE matrices and resonance widths in the R-Matrix is not an easy task, and has not been achieved yet to our knowledge. Currently, the definition of the resonance widths from reduced resonance widths follows the experimental definition $\Gamma_\lambda(E) = P_l(E)\sqrt{E}\Gamma_\lambda^0$ which is still a hurdle to the integration of the random matrix theory into the R-Matrix theory. Last but not least, the presented substitution of GOE matrices with tridiagonal ones does not allow to keep suitable eigenvectors from the GOE. As a consequence, solving the complete eigenproblem would become much more time-consuming than what has been performed in this work.

Secondly, trying to conciliate the GOE WFCF calculations with the ENDF formalism, a strong hypothesis has been made with the narrow resonance approximation $T_c = \dfrac{2\overline{\Gamma_c}}{\overline{D}}$ to relate transmission ratios to average resonance parameters. It seems that the disagreement between the average Hauser-Feschbach cross sections is maximal when the average resonance widths become large compared to the average spacing. As a consequence, it is possible that the huge obtained differences are a consequence of the lack of physical meaning of this hypothesis. In that case, performing the more precise average Hauser-Feschbach with GOE WFCF calculations at the processing step would require providing accurate transmission ratios instead than average parameters, or at least the relation between them.

Conclusion of the chapter

In this chapter, the random matrix theory has been used to sample more physically acceptable resonances in the framework of the ladder method. The core idea of this theory is due to E. Wigner, who introduced in the late 50s the idea to replace the unknown Hamiltonian of the system with a matrix with random entries, and observe the statistical distribution of the eigenvalues when the matrix becomes infinitely large. These eigenvalues correspond to the energy levels of the system, which are the resonance energies. The most impressive fact, and the key-point of the success of the random matrix theory, is the invariance of the eigenvalues fluctuations as long as some matrix symmetries are respected. The fluctuations correspond here to the statistical property of the eigenvalues, such as the resonance spacings distribution and autocorrelation, without taking into account average properties like the average spacing. Confronting theoretical considerations with measurements performed in the resolved resonance range, matrices from so-called Gaussian Orthogonal Ensemble (GOE) had been identified in the 80s as the relevant objects to mimic the Hamiltonian of nuclear system in the compound nucleus model.

In this work, a method to sample eigenvalues from the GOE has been implemented, in order to produce resonance energies during the sampling of the ladder method. There, all resonance energies are obtained at once as eigenvalues of GOE matrices, so that they are actually correlated. This sampling replaces the Wigner surmise for the resonance spacings used in previous chapter, which corresponds to the case of a GOE matrix of size 2×2 only. As a consequence, the use of $N \times N$ GOE random matrices better reflects the correlations between the resonances energies, so that generated ladders are more physical. As a matter of fact, the resulting resonance energies spectra proved to be slightly different from the ones obtained with uncorrelated spacings. The next-nearest spacing law has been found to be different from the Wigner surmise up to 2%. More emblematic, the resonance spacing autocorrelation for resonances from the GOE is negative, which is typical of quite rigid resonance ladders. Such correlations can be precisely measured in terms of the long-range Δ_3 statistics, which measures the deviation from the straight line of the cumulative number of levels. In this work, some simulations have been performed to estimate a minimal size of the random matrices so that the eigenvalues fluctuations approach the asymptotic behavior. On the basis of the three aforementioned statistics, it has been shown that matrices of size 100 already yield very correct outcomes.

---

[38]As a reminder, eigenvectors elements of GOE-like matrices are asymptotically Gaussian.

In practice, the proposed implementation of the GOE-based resonance sampling in GAIA-2 makes use of two important elements. First of all, the real GOE matrices have been replaced by tridiagonal symmetric matrices with the same eigenvalues, following a result of the literature. These tridiagonal matrices correspond to the typical matrices obtained after successive Householder reflections of the GOE matrices. This replacement speeds up the calculations significantly, and makes possible the use of the random matrix theory in the Monte-Carlo sampling of the ladder method. The second important point concerns the eigenvalues unfolding, a mandatory step to be performed once eigenvalues have been computed to retrieve their fluctuations. The idea is to normalize the eigenvalues using the cumulative of the underlying level density, in order to correct for the unequal distribution of eigenvalues. In this chapter, several methods of eigenvalues unfolding have been studied to be carried on random matrices of intermediate size (between 10^2 and 10^3). In particular, a new method has been proposed, which simply relies on a tabulated version of the cumulative of the exact form of the level density of the GOE eigenvalues. This method is an alternative to the common use of the cumulative of the well-known Wigner semi-circle law, which is only an asymptotic result. This new method has been proved to be slightly more precise, and evacuates the need to discard eigenvalues on the edges of the spectrum.

Cross section distributions derived from the ladder method with correlated or uncorrelated spacings have been compared, for all the elementary spingroups of JEFF-3.2. First, the same analysis than in Chapter 3 has been carried out to estimate the influence of the input parameters of the elementary spingroups on the required number of resonances to fill the ladders. It turned out the cases which required the more resonances were the same ones than in previous chapter, with no major impact of the spacings correlation. In a second time, the differences between the sampled cross section distributions have been measured with the Kolmogorov-Smirnov and Anderson-Darling statistics. The influence of the correlation has been shown to be quite weak. In order to fix ideas, the most differing case was found for a spingroup of ^{242}Am for the fission reaction, which exhibited a maximal difference of 3% for the Kolmogorov-Smirnov statistics. Two important facts have been highlighted however. First, the influence of the spacings correlation increases with the ratio $\overline{\Gamma}/\overline{D}$. In other words, if many resonances contribute to the cross sections, the spacings correlations is more likely to play a role. Secondly, it seems the elastic cross sections is only slightly affected by the correlation, and at least much less than the capture and fission reaction.

Finally, in this chapter, the Hauser-Feschbach average cross sections have been recalculated, using another method of calculation of the widths fluctuations correction factor (WFCF) than the classical Moldauer method presented in Chapter 2. This implementation followed a reference which derived the average cross sections directly from the hypothesis of GOE-like fluctuations of the Hamiltonian. The resulting expression of the WFCF is a complex triple integral involving transmission ratios in lieu of the usual resonance parameters. Two hypotheses have been made to make this expression compliant with the ENDF formalism. First, a narrow resonance approximation has been used to relate the transmission ratios to the average resonance widths $T_c = \dfrac{2\overline{\Gamma_c}}{\overline{D}}$. Secondly, the number of degrees of freedom given in the ENDF evaluations has been used to define the number of open channels for the reactions. Then, each channel width has been attributed the average width from the evaluation divided by the number of degrees of freedom. Once these hypotheses were made, the Hauser-Feschbach average cross sections have been computed for all the elementary spingroups of JEFF-3.2., using the Moldauer or GOE approximations of the WFCF. The obtained values match well for elementary spingroups with small $\overline{\Gamma}/\overline{D}$ ratios. However, the observed disagreement keeps increasing with $\overline{\Gamma}/\overline{D}$, and finally reaches around 30% difference at maximum. The reason is supposedly linked to the relation between the transmission ratio and the resonance parameters. Further tests are required to ensure this fact though. Moreover, additional comparisons between the average values computed from the Hauser-Feschbach formalisms and the mean cross sections derived from the ladder methods exhibited a good agreement when WFCF was calculated with the Moldauer method,

even if spacings were correlated in the ladder sampling. This supports the assumption that the resonance spacings fluctuations play a minor role for the calculation of the average cross sections. However, it may be very interesting to take into account GOE-like correlations between the resonance widths in the ladder method, in order to estimate the impact on the average calculations.

Part III

Integration of probability tables calculations in a nuclear data processing pipeline

Construction of probability tables

In the unresolved resonance range the common practice consists of providing average resonance parameters due to the lack of resolution of experimental measurements. The issues are related to the fact that in this energy regime the experimental resolution is degraded and only clusters of resonances are seen. There exist approaches to treat the cross sections in the unresolved resonance range, among which the most valuable is the ladder method – highly investigated in the previous chapters – which captures the cross sections fluctuations at particular reference energies. This Monte-Carlo-based method serves to obtain relatively large samplings which approach the underlying probability distributions of the cross sections at the reference energies. Those distributions are the most informative quantities reachable for describing the energy-dependent cross sections. In particular, they are much more valuable than the simpler average cross section values, which cannot serve to handle important features, such as the self-shielding effect in the unresolved resonance range.

Quite obviously though, these cross section samplings cannot be used directly in Monte-Carlo neutronics codes for criticality and nuclear safety applications. They need to undergo an additional step to be converted into *probability tables*, which are in this context a *quantization* of the probability distributions. The aim of this chapter is to describe the methods used to turn the sampled cross section sets of the ladder method into suitable probability tables for Monte-Carlo neutronics codes.

First, the requirements of the Monte-Carlo codes as well as some of the existing practical methods in use will be presented. Then, two innovative ways of computing probability tables, based on a k-clustering algorithm, will be described in detail.

5.1   General description and state of the art

Let us start with a slight digression about the nature of the probability tables. In this thesis, the concept of probability tables was first introduced in Section 1.1.6, as a way to represent the cross sections with a set of couples (p_i, σ_i), with the condition $\sum_i p_i = 1$, so that p_i can be interpreted as the probability for the cross section to equal σ_i. In fact, probability tables can be simply reinterpreted as a discrete version of the probability density function (pdf) of the cross sections, which is the *probability mass function* (pmf). The probability mass function is the exact equivalent of the probability density in the framework of discrete probabilities.

Probability tables were seen earlier in this document as an alternative to describe cross sections over an *energy interval*, less informative than the exact energy-functional quantity, but more valuable than the rough average values used in deterministic multigroup neutronics application codes. Let us insist that one may convert energy-functional cross sections defined over an energy interval into a probability table, that is only a discrete version of the probability

distributions of the cross sections over the interval. Several methods exist to perform this operation, among which one of the most efficient is probably the *moments method* described more in detail in Section 5.1.2. As an example, probability tables have been used in the CEA deterministic neutronics codes APOLLO-2 [67] and APOLLO-3 [68] to efficiently handle self-shielding. The usefulness of such probability tables actually comes from the Lebesgue theory of integration. In particular, probability tables computed from the moments method can be used as powerful quadrature formulas which enable the computation of any integral over the cross section depending of the energy, such as reaction ratios.

Later in this thesis, the ladder method has been introduced to handle the average nature of the resonance parameters in the unresolved resonance range. There, the probability distributions of cross sections were approached by a Monte-Carlo sampling of cross section values at a reference energy. A discrete version of these distributions also defines probability tables. These probability tables capture the distribution of the cross section values at a single reference energy.

In practice this implies a subtle distinction. In a first case, probability tables are computed from the exact energy-functional cross sections over an energy interval, using the moments method described in Section 5.1.2 for instance. In the second case, probability tables are derived from a sampling which directly approaches the cross section probability distribution at a single energy. In practice thus, the methods used in both cases do not have the same constraints. Moreover, the probability tables in the second case represent the cross sections distributions at single reference energies, and are said to be *punctual*. Finally, due to statistical nature of the sampling, the probability tables in the second case are not an exact equivalent of the real energy-functional cross sections. In this work, the probability tables which are manipulated belong to the second category. Let us recall that in the unresolved resonance range, the exact cross sections are simply out of reach.

After making use of the ladder method in the unresolved resonance range, the issue here is thus related to the derivation of probability tables from the sampled cross sections. Let us also precise that the work carried out here is restrained to the use of probability tables in Monte-Carlo neutronics codes. As a consequence, the requirements of these codes will be tackled first, to get a proper insight of the path to be followed.

5.1.1 Probability tables in Monte-Carlo codes

Monte-Carlo codes such as MCNP or MORET use probability tables in the unresolved resonance range, mainly to capture the self-shielding effects due to the resonant fluctuations of the cross sections. A probability table at a reference energy is composed of k bins. Each bin is composed of a probability value p_i $(1 \leq i \leq k)$, associated to several reaction cross section values $\{\sigma_{\alpha i}\}$ $(1 \leq i \leq k)$, one for each partial reaction α. In the unresolved range formalism developed until now, only the scattering elastic, radiative capture and fission reactions are defined. The probability values are referred as the *weights* of the table, and the cross section values as the *base-points*. As already mentioned, the weights are defined so that $\sum_{i=1}^{k} p_i = 1$ so that the cross sections can take only k distinct values, each of them with a probability p_i $(1 \leq i \leq k)$. This defines a probability mass function. The whole point of the present chapter actually consists of turning a density function into a mass function. Let us underline that no general method exists to solve that problem.

In practice, Monte-Carlo codes use cumulative probability tables. These tables have the same base-points than regular probability tables, and weights c_i simply defined as the sum of all the previous bin weights: for $1 \leq i \leq k$, $c_i = \sum_{1 \leq j \leq i} p_j$. In neutronics calculations, when a cross section value is needed in the unresolved range during a Monte-Carlo history, a random number is sampled from an uniform distribution between 0 and 1. This number is compared to the cumulative probability table bin weights c_i. The bin with a cumulative probability value directly upper the sampled value is selected [69]. Once a bin is selected, reaction cross section values are all taken from the bin, and they are added to retrieve the total cross section value. The contribution of other reactions to the total cross section may be considered at this stage,

such as the inelastic scattering or various absorption reactions, which are usually provided as average tabulated values in the processed nuclear data file. These cross section values are then kept along the particle flight path, to be used from collision to collision. Note that once sampled, cross section values must be kept for a nuclide in order to retain correlations[1].

In that context, a little more attention shall be dedicated to the reaction cross sections. According to the compound nucleus theory, the total cross section corresponds to the probability for a reaction to occur. Accordingly, the sum of the partials must always equal the total, and all reaction cross sections cannot be sampled independently. This explains why a single probability is provided for all partial reactions in the table's bins. Accordingly, the provided partial reaction cross sections $\sigma_{\alpha i}$ must be provided as the *conditional probabilities* for the reaction α to occur, knowing that the total cross section is σ_{ti}. Thus, from a mathematical point of view, converting the reaction cross sections probability densities into a probability table is equivalent to defining $k+1$ "bin limits"[2] $\widetilde{\sigma}_i$, so that the weights and base-points are defined for $1 \leq i \leq k$ [70]:

$$p_i = \int_{\widetilde{\sigma}_i}^{\widetilde{\sigma}_{i+1}} p_t(\sigma')d\sigma' \tag{5.1}$$

$$\sigma_{ti} = \frac{1}{p_i} \int_{\widetilde{\sigma}_i}^{\widetilde{\sigma}_{i+1}} \sigma p_t(\sigma)\, \mathrm{d}\sigma \tag{5.2}$$

$$\sigma_{\alpha i} = \frac{1}{p_i} \int_{\widetilde{\sigma}_i}^{\widetilde{\sigma}_{i+1}} \mathrm{d}\sigma p(\sigma) \int_0^{\sigma} \mathrm{d}\sigma_\alpha \sigma q_\alpha(\sigma_\alpha|\sigma) \tag{5.3}$$

where $p_t(\sigma)$ is the probability density of the total cross section, and $q_\alpha(\sigma_\alpha|\sigma)$ is the conditional probability of the reaction α cross section knowing that the total cross section is σ. First two equations mark the transformation of the probability density function into a probability mass function, and the last one defines the conditional reaction cross section binned values. It must be remarked that the choice of the bin limits $\widetilde{\sigma}_i$ is not unique, which is in line with the absence of general solutions to convert a density function to a mass function. Actually, most methods of construction of the probability tables are related to the choice of these bin limits.

The previous discussion about correlations between the partial reactions can be extended when more than one temperature intervenes in a Monte-Carlo calculation, as described in [70]. During a Monte-Carlo history, if the particle exit energy after a collision lies in the unresolved range, a bin of the probability table is sampled as described before. Let us imagine that the mean free path then moves the particle in a region composed of the same material at a different temperature. There, the cross section to be used for the material must be correlated to the one already sampled. However, the cross section probability density is different as it depends on the temperature, and so does the table. In order to keep the correlations, the probability tables for a single material at a particular energy but for different temperatures must have the same weights. In order to ensure this fact, a master temperature T_0 is used to define the probability table weights. Usually, probability tables are computed at room temperature, and it seems logical to choose this temperature as the reference. This feature has been integrated into GAIA-2.

Several additional constraints are related to the use of probability tables in Monte-Carlo codes. The number of bins to choose is an emblematic example, and of particular importance in the journey to select a method to build the tables. If too many bins are taken, the Monte-Carlo calculations are slowed down, because each sampling needs a binary search whose time complexity is $\mathcal{O}(k)$. Monte-Carlo computations are already very expensive, and the goal of processing is to facilitate the neutronics calculations. As a consequence, the number of bins must not be taken too big. On the other hand, if not enough bins are considered the cross

---

[1]To be more precise, it is the sampled random number which is banked.

[2]The upper and lower limits may extend to infinity. Sometimes, the word "bands" is also used.

section fluctuations may not be accounted for accurately enough. The most pathological case is $k = 1$, which is a single (average) value. In that case, the self-shielding is not taken into account. Finally a last practical constraint intervenes: for a single nuclide, probability tables for all the reference energies in the unresolved resonance range must have the same number of bins. This is a requirement of the ACE format, which is used as an input by both Monte-Carlo codes MCNP and MORET. As a consequence, the number of bins is usually set up by the user once for all, prior to the calculations. Often, the value $k = 20$ is put forward as a default value to be used in practice.

Let us now present some of the existing methods of construction of the probability tables found in the literature and current in-use software.

5.1.2 Existing methods of probability tables construction

In this subsection, several of the currently used methods of probability tables construction will be exposed. In order to get a clear view of their advantages and drawbacks, two examples will be used all along the presentation for each method, which are the uranium isotopes ^{235}U at 2.5 keV and ^{238}U at 40 keV. Probability tables in both cases are derived from a sampling performed in GAIA-2 with 100 000 iterations for all spingroups at T=293.6K, using 500 pairs of uncorrelated resonances in each sampled ladder. These examples have been chosen because both isotopes are used very often in nuclear applications, and because they are quite representative of the average shape of the cross section probability distributions.

Quantization-based methods

Starting from a set of sampled cross sections, the most straightforward way to compute the probability tables makes use of Equations (5.1)–(5.3) directly. The empirical probability distribution is assimilated to the cumulative density $\int p(\sigma) \, d\sigma$, and limit bins $\widetilde{\sigma}_i$ are chosen from the sampling, as explained later. Then, all cross sections values (total and partials) are attributed to a particular bin. Namely, for each sampled *total* cross section that falls between $\widetilde{\sigma}_i$ and $\widetilde{\sigma}_{i+1}$, the bin probability counter is increased by one, and the total and partial reaction cross section values are stored. When all elements of the sampling have been attributed to a bin, the weight in each bin is simply obtained dividing the counter by the total number of Monte-Carlo iterations. Cross section values in each bin are obtained averaging all the values in the bin. They are thus replaced by their *centroid*, which is the within-bin mean value. It must be underlined again that the cross sections are attributed to a bin using the total cross section only, so that partial cross sections in the tables are conditional to the total, and do not serve directly to build the tables. Moreover, the mean cross sections from the probability tables and from the original sampling are the same. Indeed, calling n the number of iterations in the sampling, k the number of bins in the table, n_i, the number of iterations attributed to bin i, $\bar{\sigma}_i$ the mean cross section in bin i and σ_j the sampled cross section value at iteration j:

$$\langle \sigma \rangle = \sum_{i=1}^{k} \bar{\sigma}_i p_i = \sum_{i=1}^{k} \frac{1}{n_i} \sum_{j=1}^{n_i} \sigma_j \frac{n_i}{n} = \frac{1}{n} \sum_{j=1}^{n} \sigma_j \tag{5.4}$$

Relying on bin limits is similar to what is done when drawing a histogram of the data. The only difference is that the centroid is chosen rather than the middle of the bin as the bin base-point[3]. This makes the situation completely different. That actually defines a *quantization* problem, which can be reformulated as choosing the bin limits $\widetilde{\sigma}_i$ to accurately separate the elements of the sampling into bins.

Several methods to define the bin limits have been found in the literature to create probability tables. In the following, these methods are presented, using the next notation: the sampling

---

[3]Let us note that a real histogram is a better approximation of the density though, as tackled in Section 5.1.3.

is composed of n total cross section values, $\sigma_1 < \sigma_2 \cdots < \sigma_n$. The upper limit of the table is always set as the max value of the sample, $\tilde{\sigma}_{k+1} = \sigma_n$ and the table lower limit is the minimum sampled value, $\tilde{\sigma}_1 = \sigma_1$.

- **Linear probability tables**.

    These tables are obtained by choosing bin intervals $\tilde{\sigma}_{i+1} - \tilde{\sigma}_i$ of same size. Taking k bins between $\tilde{\sigma}_1 = \sigma_1$ and $\tilde{\sigma}_{k+1} = \sigma_n$, the bin limits are fixed with next formula:

$$\tilde{\sigma}_i = \sigma_1 + i \frac{\sigma_n - \sigma_1}{k} \tag{5.5}$$

    A linear binning is the most basic method conceivable. Figure 5.1 displays the cumulative linear tables for ^{235}U at E = 2.25 keV and ^{238}U at E = 40 keV, at room temperature.
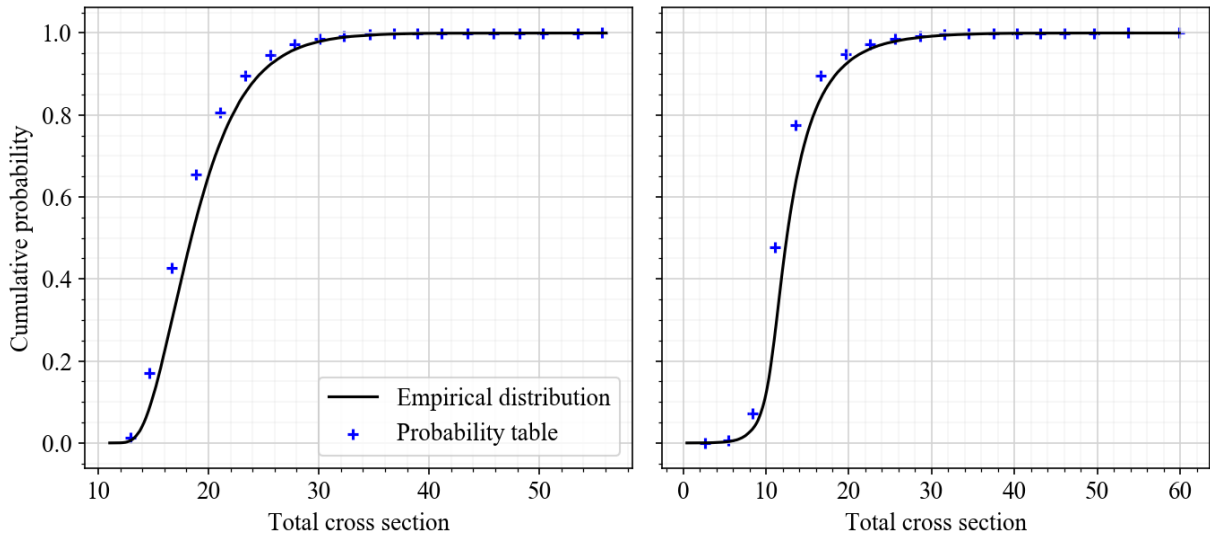

Figure 5.1: Cumulative probability tables with a linear binning and empirical distribution of the total cross section for ^{235}U at E = 2.25 keV and T=293.6K (left) and ^{238}U at E = 40 keV and T=293.6K (right)

    The main drawback of the linear binning appears on this simple example: it is very sensible to the maximum and minimum values of the dataset. If the distribution is skewed, which is often the case for cross section fluctuations, a thin mesh will be provided in the tails, and the main part of the distribution may be missed. Even more, it is possible that some bins are empty at the end of the cross sections banking, which is a loss of information.

- **Logarithmic probability tables**.

    Usually, the cross sections probability distributions are skewed on the right, which is an issue for linear binning. In order to circumvent that fact, a simple idea consists into using a logarithmic binning, where bin intervals are chosen to be equally large on a logarithmic scale. Bin limits are defined with the next formula:

$$\tilde{\sigma}_i = \sigma_1 \exp\left[\frac{i}{k} \ln\left(\frac{\sigma_n}{\sigma_1}\right)\right] \tag{5.6}$$

    Figure 5.2 displays the logarithmic tables for ^{235}U at E = 2.25 keV and ^{238}U at E = 40 keV, at room temperature.

    It seems on these examples that the rescaling implied by the logarithmic transformation is not that appropriate for the shape of the cross section distributions. It works very well for ^{235}U, it completely fails for ^{238}U. Too many points are set in the lower and higher
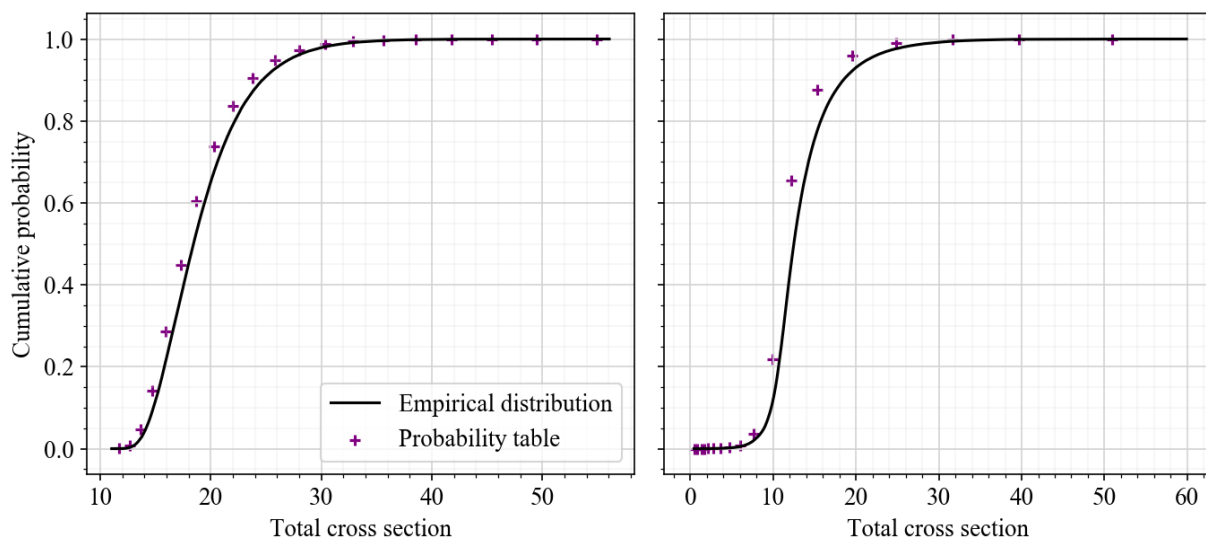
Figure 5.2: Cumulative probability tables with a logarithmic binning and empirical distribution of the total cross section for ^{235}U at E = 2.25 keV and T=293.6K (left) and ^{238}U at E = 40 keV and T=293.6K (right)

parts of the curve, and the central part is almost empty. A relevant method has to work in most situations. In practice there are many nuclides and many reference energies, and one cannot simply check all the tables manually. A robust method is thus required, and the logarithmic binning does not seem to fit.

- **Equiprobable tables**.

  In this method, the objective is to define bins with the exact same weight p_i, so that they have an equiprobable chance to be sampled in Monte-Carlo codes. Building such tables from a sampling is straightforward, but the number of elements in the sampling must be divisible by the number of required bins. If it is the case, the definition of the bin limits is simply:

  $$\widetilde{\sigma}_i = \sigma_{(i-1)\frac{n}{k}+1} \tag{5.7}$$

  Equiprobable binning is an attractive way to turn the sampling into a probability table. Its main interest comes from a potential implementation in Monte-Carlo codes. With equiprobable bins indeed, there is no need anymore to implement a comparison routine between the sampled random number over $[0, 1]$ and the bin limits. The selected bin can be immediately deduced from the value of the sampled random number, which might speed up the calculations. On the other hand, an equiprobable binning presents some similar drawbacks of the linear binning[4]. In particular, it requires a very thin mesh to capture the tails of the distributions when the fluctuations are skewed. As an example, Figure 5.3 displays the equiprobable tables for ^{235}U at E = 2.25 keV and ^{238}U at E = 40 keV, at room temperature.

  The first and last points in particular poorly represent all the bins cross section values. This is seen on Figure 5.3. There is a clear deviation from the empirical distribution in the tails, which is a sign of a huge variance.

The NJOY method

The probability tables construction implementation in the PURR module of NJOY tries to avoid the pitfalls of the previous methods. Its scheme is based on quantization as well, as bin

---

[4]Note that an equiprobable binning is simply a linear binning along the y-axis.
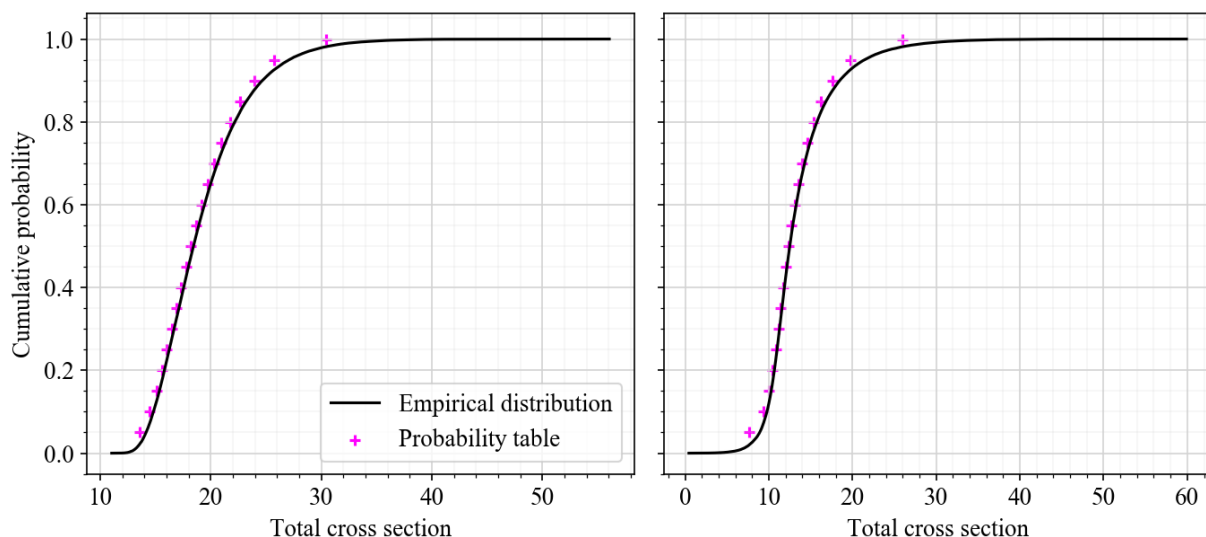
Figure 5.3: Cumulative probability tables with an equiprobable binning and empirical distribution of the total cross section for ^{235}U at E = 2.25 keV and T=293.6K (left) and ^{238}U at E = 40 keV and T=293.6K (right)

limits are first defined, and cross sections are banked in the table before being averaged. The choice of the bin limits however is highly empirical, and determined in the course of the sampling itself. Presenting the algorithm requires to reexplain some of the aspects of the ladder method implemented in NJOY. Once a ladder has been sampled in the vicinity of a reference energy in the unresolved resonance range, NJOY not only computes cross sections at the reference energy, but on a thin grid around it. To be more precise, the retained energy mesh is composed of 10 000 *randomly selected* points between two energy values, e_{min} and e_{max}. These values are chosen to lie inside the resonance ladder's limits defined in Section 3.1.1, called then E_1 and E_2. NJOY introduces the quantity dbarin $= \sum_{l,J} \frac{1}{\overline{D}^{lJ}}$, the sum of the inverses of all average spacings values found in the evaluation for the different spin sequences (l, J). This parameter serves as a scale factor to be applied to an approximate number of resonances to avoid, set to 300 in NJOY[5]. The next piece of pseudo-code sets the energy grid of calculations in NJOY:

```
navoid = 300                #approximate number of resonances to avoid
emin = E1 + navoid/dbarin   #minimal possible energy of calculation
emax = E2 - navoid/dbarin   #maximal possible energy of calculation
espan = emax - emin

nsamp = 10000               #number of points in the energy grid
egrid = []                  #final energy grid
for i from 0 to nsamp:
    egrid[i] = emin + espan * random(0, 1)
```

Listing 5.1: NJOY's definition of an energy grid of calculations

Once a ladder has been sampled, NJOY performs the cross section reconstruction for all energies in this mesh. In order to speed up the calculations, NJOY does not rely on the exact SLBW formulas, but rather on some quadrature approximations of the SLBW shape. As a result, each sampled ladder raises up to 10 000 cross section values which serve to constitute the sampling. NJOY probability tables are thus representative of the region around the reference energy. This approach seems at first as legitimate as the method retained in this thesis, which

---

[5]As a reminder from Section 3.1.1, NJOY defines the ladder energy limits from a (rescaled) number of resonances to be sampled, fixed around 1000.

only reconstructs cross sections at the reference energy. Let us mention that it brings additional sources of uncertainty though, as the sampled cross section values greatly depend on the chosen energy grid. This latter must be chosen very thin, and/or randomly, which seems to be achieved by the hard-coded set-up of NJOY. The main advantage is a clear numerical gain, since less resonance ladders are required to reach a statistical significance. Usually, only 64 ladders are used in NJOY[6].

Probability tables limits $\widetilde{\sigma}_i$ are defined from the 10 000 cross sections computed from the first ladder, using a method which is about to be presented. Once the bin limits are set up, cross sections yielded by the other ladders are directly banked in the corresponding bins[7]. At the end of the process, each bin's probability and cross sections are averaged as usual to retrieve the actual probability tables. The procedure relies on the principle that the cross sections obtained from the first ladder will be already representative of the cross section fluctuations in the region, so that they can be used as a start point to determine relevant bin limits that match the distribution shape. The bin limits are defined using the *sorted* set of computed total cross sections, **cross_sections**. The choice of $\widetilde{\sigma}_i$ introduces a scale parameter **nebin**, and a progressive width of the bins to match the distribution shape. The next piece of pseudo-code details the method:

```
nebin = nsamp / (nbin − 10 + 1.76)   #scale parameter
                                      #nsamp = 10 000, and usually nbin = 20
ibin = nebin / 200                    #index of the bin limit in cross_sections.
bin_limits = []                       #store bin limits

#loop on the bin limits
for i from 0 to nbin − 1:

    #the bin limits are obtained from the sorted cross section values
    bin_limits[i] = cross_section[ibin]

     #artificial reset if the bin limits are too close
    if i > 0 and bin_limits[i] <= bin_limits[i−1]:
        bin_limits[i] = bin_limits[i−1] * (1.05)
    endif

    #set ibin to a farther point in cross_sections
    if (i == 0): ibin = ibin + nebin/40
    if (i == 1): ibin = ibin + nebin/10
    if (i == 2): ibin = ibin + nebin/4
    if (i == 3): ibin = ibin + nebin/2
    if (i > 3 && i < nbin − 6): ibin = ibin + nebin
    if (i == nbin − 6): ibin = ibin + nebin/2
    if (i == nbin − 5): ibin = ibin + nebin/4
    if (i == nbin − 4): ibin = ibin + nebin/10
    if (i == nbin − 3): ibin = ibin + nebin/40
    if (i == nbin − 2): ibin = ibin + nebin/200

enddo
```

Listing 5.2: NJOY's definition of bin limits

Then, the bin limits are extended to infinity. The NJOY method is a sort of on-the-fly quantization-based method. One may note that the cross section shape is expected to be partially symmetric with more values in the central part of the distribution. Indeed, the number of cross section values to pass before selecting the bin limits increases, then remains constant[8], and

---

[6]This number may be set up by the user in the NJOY input dataset. However, most examples available in the literature make use of that amount, and NJOY input datasets are rarely modified by the users.

[7]The upper and lower limits of the table extend to infinity.

[8]Except for the three first and six last bins, the NJOY-like bins are equiprobable.

then decreases. This assumption on the cross section shape is quite supported by numerical computations.

The NJOY method has been adapted in GAIA-2 to provide NJOY-like probability tables. In GAIA-2, ladders only yield cross section values at a single reference energy, and the first ladder cannot be used alone to determine the bin limits. In order to fix them, the choice has been made to use 10% of the cross sections from the complete sampling. In the case of 100 000 Monte-Carlo iterations thus, this represents 10 000 cross section values which are used to build the probability table limits. Figure 5.4 displays the NJOY-like probability tables computed by GAIA-2 for ^{235}U at E = 2.25 keV and ^{238}U at E = 40 keV, at room temperature.
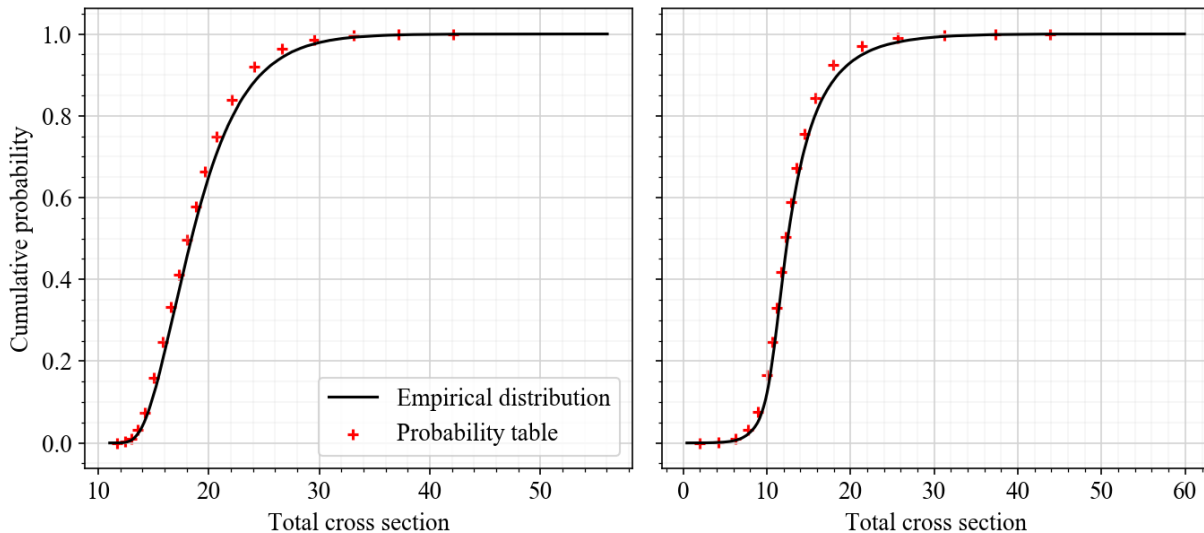

Figure 5.4: Cumulative probability tables with a NJOY-like binning and empirical distribution of the total cross section for ^{235}U at E = 2.25 keV and T=293.6K (left) and ^{238}U at E = 40 keV and T=293.6K (right)

In principle, this method provides high quality probability tables. Both the tails and the central parts seem to be well represented on the selected examples. The main critics which can be made is related to the more inflected part of the empirical curve (around 12-15 barn for ^{235}U), where the deviation of the tables from the empirical distribution seems more marked. This method is however highly empirical, and nothing seems to guarantee it works in every case, and especially for the more pathological.

The moments method used in GALILEE

The CEA code GALILEE relies on a method already developed in its predecessor CALENDF, known as the moments method to build the probability tables. The idea was first introduced by P. Ribon in [71], and aims at taking advantage of the relation between a probability distribution and its moments $M_i = \int x^i p(x) \, dx$. Indeed, a probability distribution is uniquely determined by the infinite collection of all its moments, from 0 to ∞. The goal of the moments method is to compute a probability table which preserves moments $M_i = \sum_{j=1}^{k} p_j \sigma_j^i$. These moments can be computed from the sampling in the unresolved resonance range[9]. The principle differs deeply from the other presented methods of probability tables construction, as the table weights and base-points are not determined through the banking of sampled cross sections in bins[10]. Instead, only the moments of the cross sections sampling are kept. Of course, not all moments can be

---

[9]When used in the resolved resonance range, this method computes the moments from direct integrals of the cross section over the energy range, and using the equivalence between the Riemann and Lebesgue integral defined in Equation (1.17).

[10]It is the only one of this nature which will be mentioned in this thesis.

kept between the empirical distribution and the probability table. Actually, for a table of order k, only $2k$ moments can be conserved. More precisely, as k base-points and k weights have to be determined, a system of $2k$ equations arises when the base-points and weights are matched to the moments. Even if the choice of the moments is partially free, it is advised to consider the sequence of increasing moments from $L_{min} = 1 - k$ to $L_{max} = k$. The introduction of negative moments enables to take into account the cross section depressions more accurately.

The algorithm used to compute the probability tables makes use of a Padé approximant technique, and the resolution of successive linear systems to compute the weights and base-points of the probability table. The algorithm is well presented in [71] and [72]. Long story short, the so-called Stieltjes generating function of the moment $F(z)$ can be developed in the vicinity of 0:

$$F(z) = \int \frac{p(\sigma)(z\sigma)^{1-k}}{1-z\sigma} \, \mathrm{d}\sigma = \sum_{i=1-k}^{k} z^i M_i + \mathcal{O}(z^{k+1}) \tag{5.8}$$

Using a Padé approximant to approach $F(z)$ with a rational function,

$$z^{k-1} F(z) = \frac{\sum_{i=0}^{k-1} a_i z^i}{\sum_{i=0}^{k-1} b_i z^i + z^k} \tag{5.9}$$

Combining Equation (5.8) and Equation (5.9) and forcing the condition that $\mathcal{O}(z^{k+1})$ is negligible,

$$\left(\sum_{i=0}^{k-1} b_i z^i + z^k\right) \left(\sum_{i=0}^{2k-1} z^i M_{i-k+1}\right) = \sum_{i=0}^{k-1} a_i z^i \tag{5.10}$$

Identifying the coefficients of the polynomials between k and $2k - 1$ to get rid of coefficients a_i for now, the previous equation yields the next linear system to be solved for (b_i),

$$\begin{bmatrix} M_k & M_{k-1} & \ldots & M_1 \\ M_{k-1} & M_{k-2} & \ldots & M_0 \\ \vdots & \vdots & & \vdots \\ M_1 & M_0 & \ldots & M_{2-k} \end{bmatrix} \begin{bmatrix} b_0 \\ b_1 \\ \vdots \\ b_{k-1} \end{bmatrix} = - \begin{bmatrix} M_0 \\ M_{-1} \\ \vdots \\ M_{1-k} \end{bmatrix} \tag{5.11}$$

The coefficients b_i are directly related to the probability table base-points σ_i. The base-points are simply the roots of the polynomial $\sum_{i=0}^{k-1} b_i z^i + z^k$. Once the base-points have been determined, the weights (p_i) of the table can be found solving the linear system that arises from the moment matching condition $M_i = \sum_{j=1}^{k} p_j \sigma_j^i$ directly.

Note that handling the partial cross sections is another issue not detailed here, which can be solved computing additional moments of the conditional distributions, as in [71].

This method is extremely powerful when integrals of functions of the cross sections intervene, such as reaction rates. In particular, such probability tables are used as quadrature formulas in the CEA deterministic transport codes APOLLO-2 and APOLLO-3 in the resolved and unresolved resonance ranges.

On the other hand, the main drawback of this method arises in the context of interest of this PhD, where probability tables are not computed from a resolved cross section, but from a statistical cross section sampling. Indeed, the moments method relies on the accuracy of the computed moments. However, the higher moments of a sampling are inherently unstable. In other words, a robust estimation of the higher moments requires a very large sampling. This intrinsic instability of the sampling's moments itself is even doubled with a numerical difficulty to compute high-order moments. Considering for instance tables with 20 bins requires to retain 40 moments of the sampling, which is a lot. In fact, the number of moments that may be kept in practice is usually less than that, and the number of bins in the tables is lower than 20.

Figure 5.5 displays the moments probability tables computed by GALILEE[11] for ^{235}U at E = 2.25 keV and ^{238}U at E = 40 keV, at room temperature. These tables have been computed with only 10 bins.
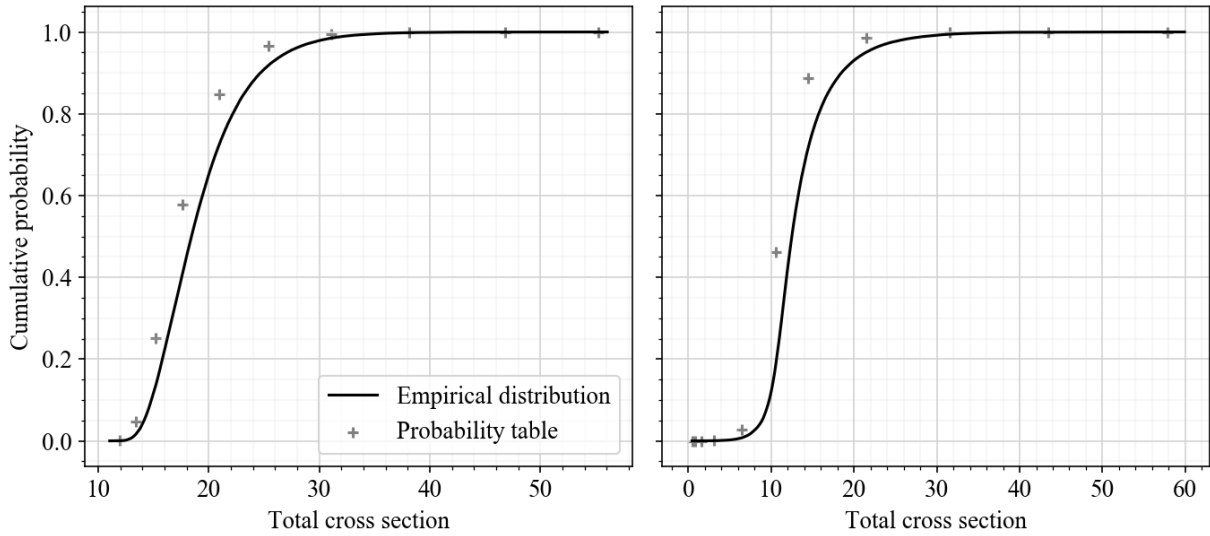

Figure 5.5: Cumulative probability tables with a binning from the moments method and empirical distribution of the total cross section for ^{235}U at E = 2.25 keV and T=293.6K (left) and ^{238}U at E = 40 keV auyfnd T=293.6K (right)

5.1.3 Alternatives to the probability tables method

The main drawback of the probability table method is related to the finite number of possible cross section values that can be sampled by the neutronics Monte-Carlo codes. This has a poor physical meaning, as a continuous quantity is treated as discrete. In order to avoid this flaw, Monte-Carlo codes could be adapted to handle real probability distributions of the cross section values, instead of relying on probability tables. For instance, one could use a direct parametric or non-parametric estimation of the cross section probability density, using common methods. The aim of this subsection is to detail some ideas that have been investigated, and explain why they have not been implemented.

At first sight, two non-parametric methods would be practicable, namely a histogram or a Kernel Density Estimation (KDE). These methods are useful as they do not make any assumption about the shape of the cross section distributions. Starting from the cross sections sampling, building a histogram requires to define bin limits $\tilde{\sigma}_i$ like in most probability table methods, but instead of computing base-points as the centroids, the middles of the bins are used. Such a histogram approaches the underlying density, and the error due to the discretization can be easily estimated. This is achieved for example in [73], which provides an optimal estimation of the density from regularly binned histograms. Alternatively, the kernel density estimation is a generalization of the histogram, in which the density is smoothly approached in all points of the support by a function $\widehat{f}_h$ so that

$$\widehat{f}_h(x) = \frac{1}{nh} \sum_{i=1}^{n} K\left(\frac{x - x_i}{h}\right) \tag{5.12}$$

where K is a kernel function – for instance a Gaussian function –, and $h > 0$ a scalar parameter called bandwidth. Intuitively, the kernel density estimation works by placing a kernel on each

---

[11]The moments method has not been implemented in GAIA-2.

of the sampled cross section value along the x-axis. Then, each point of the density is obtained by averaging over the kernels.

These methods are powerful as they do not assume the form of the underlying density, and are still able to provide a good approximation of its shape. One may imagine to perform a kernel density estimation of the cross section density, and provide for instance a linearly tabulated version of the obtained density function, or the corresponding cumulative function. Monte-Carlo codes could handle such function easily. Once a random number is sampled between $]0, 1[$, they would simply need to perform a linear interpolation to retrieve a cross section value. Such a work would turn the current discrete spectrum of the possible cross section values into a continuous one, although tabulated.

Relying on a tabulated version of the probability density may have some drawbacks though, that make their use in Monte-Carlo codes probably less tractable than the simpler probability tables approach. First, let us mention that the mean cross section value is likely not to be conserved from the ladder method's sampling to the density tabulated estimation. This would not consist in a major flaw if the average cross section value did not have an immoderate importance for neutronics codes, mainly because it relates to the reaction rates. As the sampling mean value is the best estimator of the cross section expected value, keeping its value may make sense. Secondly, the size of the sampling obtained from the ladder method may be quite huge. It has been underlined in Section 3.3.2 that situations occur where 10^5 elements at least should be sampled to obtain accurate results. With as many elements, a KDE-based density is numerically unreachable in an acceptable time[12]. Finally, the main drawback is related to a possible significant performance hit in the Monte-Carlo codes calculations. Instead of sampling and selecting a single value in a table, Monte-Carlo codes would have to implement an additional interpolation routine, that is likely to be time-consuming. In summary, a simple probability table with many bins might become competitive enough confronted to a tabulated density, from both points of view of calculation time and ability to account for the cross section fluctuations.

An other option would be to use a parametric estimation of the density. In this approach, the shape of the cross section would be fitted with a well-known distribution, depending on some parameters estimated from the outcome of the ladder method sampling. The Monte-Carlo codes should just be provided with the information of the chosen distribution, and the value of the parameters. Cross section fluctuations share common characteristics that support the idea that a common base-distribution may be searched for. In particular, they are unimodal, usually fat-tailed, and should be defined on a semi-finite interval as negative cross sections are nonphysical. The main drawback of this approach is to find a distribution that could fit the cross sections distributions accurately and automatically, as this fit would occur during the cross sections processing, along with many other operations. Moreover, efficient fit can be performed for distributions with a few parameters only, often 2 or 3, that might not be able to represent the cross section fluctuations. More generalized distributions could serve though, like the hypo-exponential distribution[13] which matches the presented constraints of uni-modality and semi-infinite support, and has an arbitrary number of parameters. This idea has not been explored deeper in this work.

In any case, replacing the probability tables by a more continuous approach requires to change the Monte-Carlo codes behavior, as well as the input ACE format used by MCNP and MORET. This requires a huge amount of work, which could not be carried out during this thesis. Instead, the probability tables method was kept as a default path. However, two methods based on an "optimal" choice of the bins $\widetilde{\sigma}_i$ have been investigated, which are based on *k-clustering* algorithms.

---

[12]Histograms are still possible though.

[13]Sometimes referred to as the generalized Erlang law.

5.2 K-clustering probability tables

5.2.1 K-means probability tables and dynamic programming

The quantization-based methods which have been presented attempt to define the probability tables bin limits $\widetilde{\sigma}_i$ from the sampled total cross section values, before banking them all into the bins. This way of proceeding produces coherent probability tables which conserve the mean value, and whose construction is stable. Thus, all the difficulty resides in the choice of the bin limits to obtain relevant probability tables. The objective is to condensate in a fixed number of bins k the maximum of information contained in the continuous probability distribution. As an example, linear or equiprobable tables do not always represent the underlying probability distribution efficiently. In particular, the right tail has to be well represented, because it should be possible for neutronics Monte-Carlo codes to sample large – even scarce – cross sections values, especially for shielding problems.

The situation actually looks like a *clustering* problem. Clustering a dataset aims to sort and classify the elements into relevant subgroups called clusters, which share common properties. This situation often occurs in data analysis or machine learning for instance. A clustering problem may be solved by various algorithms according to the constraints and the objectives: clustering problems do not have a closed-form solution in general. A very common way of clustering the dataset consists into minimizing in each group the distance between the group's elements and a representative value. A very natural choice is to choose the Euclidean distance (the L2-norm) and the mean of the subgroup. Such a partitioning is named *k-means* clustering. Applied to our situation, the objective is to find $k+1$ bins limits $\widetilde{\sigma}_i$ so that the sum for all bins of the Euclidean distance of the cross sections values to the within-bin mean is minimized. This can be formulated into the next optimization problem, where $\widetilde{\sigma} = (\widetilde{\sigma}_0, \ldots, \widetilde{\sigma}_k)$ are the bin limits that define the bin regions $S_i = [\widetilde{\sigma}_{i-1}, \widetilde{\sigma}_i]$ and μ_i is the total[14] cross section mean in bin i:

$$\arg\min_{\widetilde{\sigma}} \sum_{i=1}^{k} \sum_{\sigma_{tj} \in S_i} |\sigma_{tj} - \mu_i|^2 \tag{5.13}$$

Probability tables with such bin limits minimize the within-bin variance and maximize the variance between bins, which sounds extremely appealing in our situation of interest, as the mean bin values are to be used in neutronics Monte-Carlo codes.

The k-means algorithm is a NP-hard[15] problem when the dimension exceeds 2. This means the solution of Equation (5.13) always exists, but cannot be solved in polynomial time. When the sampling is large (which is our case referring to Chapter 3, since at least 10^5 elements may be required), solving the k-means problem becomes impossible using brute force. It is there usually solved by efficient heuristic methods, that do not necessarily enforce the optimality of Equation (5.13). In the present situation however, the sampled total cross sections form a one-dimensional set. It turns out that a very efficient algorithm based on *dynamic programming* exists to find the optimal bin limits for the k-means problem.

Before presenting the algorithm to compute k-means tables, two points may be mentioned. First, the particular k-means method for one-dimensional data is also referred to in literature as the *Jenks natural breaks classification method*, who first introduced this idea to produce statistical maps for diverse problems [74]. Secondly, a crucial drawback of the k-means compared to other clustering methods is the fact the number of clusters k is an input parameter fixed by the user prior to the calculations. In traditional clustering problems, this is often a strong assumption about the underlying data. In our case however, this number corresponds to the

---

[14]As a recall, all the reaction cross section values in the probability tables are contingent to the total reaction cross section values.

[15]NP stands for non-deterministic polynomial-time. That means the solution cannot be solved in a polynomial time from a deterministic manner. At best, a solution can be proposed by non-deterministic techniques, and verified in polynomial time. In the worst case, the exact solution has to found using brute force.

order of the table which has to be set by the user anyhow, because Monte-Carlo codes require all the probability tables for a particular nuclide to have the same number of bins. Setting the parameter k does not constitute a real issue here, because it is a requirement of the codes that use the probability tables. As a consequence, the k-means algorithm looks like the perfect clustering method for our needs.

The algorithm which is about to be presented has been developed in the statistics-oriented software R package **Ckmeans.1d.dp** by H. Wang and M. Song in 2011, and is presented in reference [75]. The algorithm has then be improved by the same authors in [76]. It is based on dynamic programming, which is a mathematical optimization method[16] that can be used to solve large problems by breaking them into equivalent subproblems when they can be solved recursively. The main difference with usual "divide and conquer" algorithms is that the sub-problems have to repeat themselves, and thus can be solved only once and their results *stored*, which is called *memoization*. The whole point here is to solve Equation (5.13) with an increasing number of bins and an increasing number of sampled cross section values from the sorted set, as a recursive relation can be found between the solutions of Equation (5.13) with different numbers of cross sections and different numbers of clusters.

Following the reference [75], let us call $D[i, m]$ the sum of the within-bin distances to the mean for the solution of Equation (5.13) with only m bins and a subsample of size i ($\sigma_1, \ldots, \sigma_i$) of the original *sorted* sampling of total cross sections. As such, calling n the actual number of Monte-Carlo iterations, $D[n, k]$ is the sum of the within-bin distances of the optimal clustering, ie. the minimal reachable value for this quantity. Let us call j the index of the smallest cross section value in bin m in the optimal solution of $D[i, m]$. The fact is, considering $m - 1$ clusters and the first $j - 1$ elements only, $D[j - 1, m - 1]$ has to be the minimal within-bin distance reachable for the problem with $m - 1$ clusters and $j - 1$ cross sections, else $D[i, m]$ would not be the solution for m clusters and i cross sections. This defines the next recurrence relationship, where $d(\sigma_j, \ldots, \sigma_m)$ is the sum of Euclidean distance of all the elements $(\sigma_j, \ldots, \sigma_m)$ to the mean of the cluster m:

$$\begin{cases} D[i, m] & = \min_{m \leq j \leq i} \{D[j - 1, m - 1] + d(\sigma_j, \ldots, \sigma_i)\} \\ D[0, m] & = 0 \\ D[i, 0] & = 0 \end{cases} \tag{5.14}$$

Relying on this equation, the matrix $D[i, m]$ can be computed recursively, until $D[n, k]$ is obtained, which is the minimal sum of within-bin distances reachable by the clustering. The first column is filled first:

$$D[i, 1] = \sum_{j=1}^{i} (\sigma_j - \overline{\sigma}_i)^2 \tag{5.15}$$

where $\overline{\sigma}_i$ is the mean cross section taking into account the i first cross sections. Then, each next column is built based on Equation (5.14), which leads to the construction of a triangular matrix. In the meantime, another matrix $B[i, m]$ of same dimensions is constructed to keep track of the indexes of the smallest cross section values in cluster m.

$$\begin{cases} B[i, m] & = \arg \min_{m \leq j \leq i} \{D[j - 1, m - 1] + d(\sigma_j, \ldots, \sigma_i)\} \\ B[0, m] & = 0 \\ B[i, 0] & = 0 \end{cases} \tag{5.16}$$

Once both matrices are built, the bin limits corresponding to the minimal sum of the within-bin distances to the means $D[n, k]$ have to be retrieved. Both matrices D and B are then backtracked. Starting from the final result, the path that leads to the minimal $D[n, k]$ is retrieved, and the corresponding indexes from B are obtained. These indexes correspond to the

---

[16]Despite the name, which was chosen in the 50s by the inventor of the method, R. Bellman, to sound appealing.

bin limits that lead to the minimal sum of the within-bins distances to the means, and form the optimal k-means clustering.

The global complexity of the algorithm presented is $\mathcal{O}(n^3k)$, which is a great enhancement compared to the initial NP-hard problem. However, this complexity makes computations impossible for the usual size of the sampled total cross section sets. It can be greatly improved though. First of all, $d(\sigma_j, \ldots, \sigma_i)$ does not need to be recomputed everytime. Instead, it is possible to take advantage of a recurrence relation:

$$\begin{cases} d(\sigma_1, \ldots \sigma_i) & = d(\sigma_1, \ldots \sigma_{i-1}) + \frac{i-1}{i}(x_i - \mu_{i-1})^2 \\ \mu_i & = \frac{\sigma_i + (i-1)\mu_{i-1}}{i} \end{cases} \tag{5.17}$$

to greatly improve the algorithm complexity, which becomes $\mathcal{O}(n^2k)$. This is much better, even if still problematic for our needs. The complexity may actually be again improved using a divide and conquer algorithm to compute the matrices columns, as described in [76]. This reduces the algorithm complexity to $\mathcal{O}(n \log(n)k)$. Such a complexity is way enough for our needs: a k-means probability table from a sampling with 10^5 Monte-Carlo iterations is only computed in a few seconds.

5.2.2 Descriptive of tables

Figure 5.6 displays the probability tables obtained with the k-means algorithm described previously, for ^{235}U at 2.5 keV and ^{238}U at 40 keV and room temperature, like in previous figures 5.1-5.4.
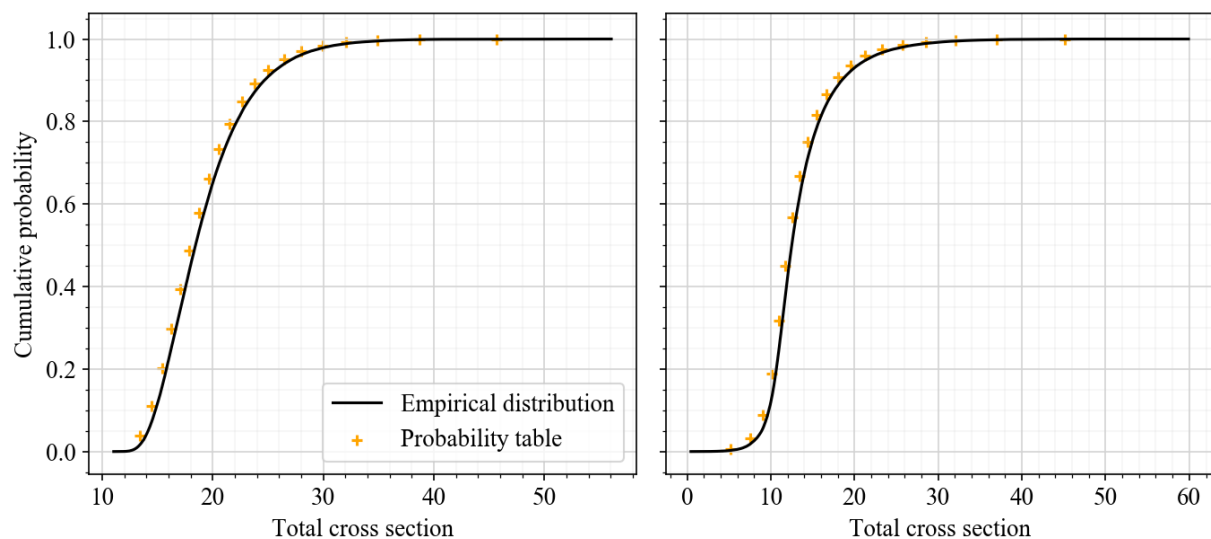

Figure 5.6: Cumulative probability tables with a k-means binning and empirical distribution of the total cross section for ^{235}U at E = 2.25 keV and T=293.6K (left) and ^{238}U at E = 40 keV and T=293.6K (right)

The tables seem to match quite well both the central part and the tails of the distributions. Even more, it seems that the depressions and inflected parts of the cumulative probability distribution are especially well represented. Many points are present in the inflections of the curves, for instance in the interval between 12 barn and 15 barn for ^{235}U. Compared with the tables obtained with other methods, the points better match the real empirical curve in this region, which is a direct consequence of the low variance in each bin. K-means tables indeed aim at finding the partition of the probability distribution which minimizes the global within-bins variance. As such, k-means tables mays behave very well in Monte-Carlo codes.

It is of interest to present some more examples though. An interesting one is to consider ^{235}U at 2.5 keV and ^{238}U at 40 keV again, but processed at T=0K. In practice, nuclear data are

never processed at this temperature, which is of no use in practical applications. However, it is a good test, as empirical distributions are more difficult to fit. At null temperature indeed, resonances are not broadened nor flattened so that the ladder method may yield some very large cross sections values, when a peaked resonance is sampled close to the reference energy. Cross sections distributions are thus more skewed, which makes the probability tables construction more challenging. Figure 5.7 displays the k-means tables built for ^{235}U at 2.5 keV and ^{238}U at 40 keV at null temperature along with the empirical distribution of the cross section values, to be compared with the ones obtained with the NJOY method on Figure 5.8. At T=0k, the cross section distributions appear less smooth than at room temperature, but there again, k-means probability tables seem to describe the probability distributions well enough. In particular, the tables enable the sampling of large cross sections values, and present a thinner mesh in the inflected parts of the empirical distribution, which are the higher-variance zones.

Figure 5.7: Cumulative probability tables with a k-means binning for ^{235}U at E = 2.25 keV and T=0K (left) and ^{238}U at E = 40 keV and T=0K (right)
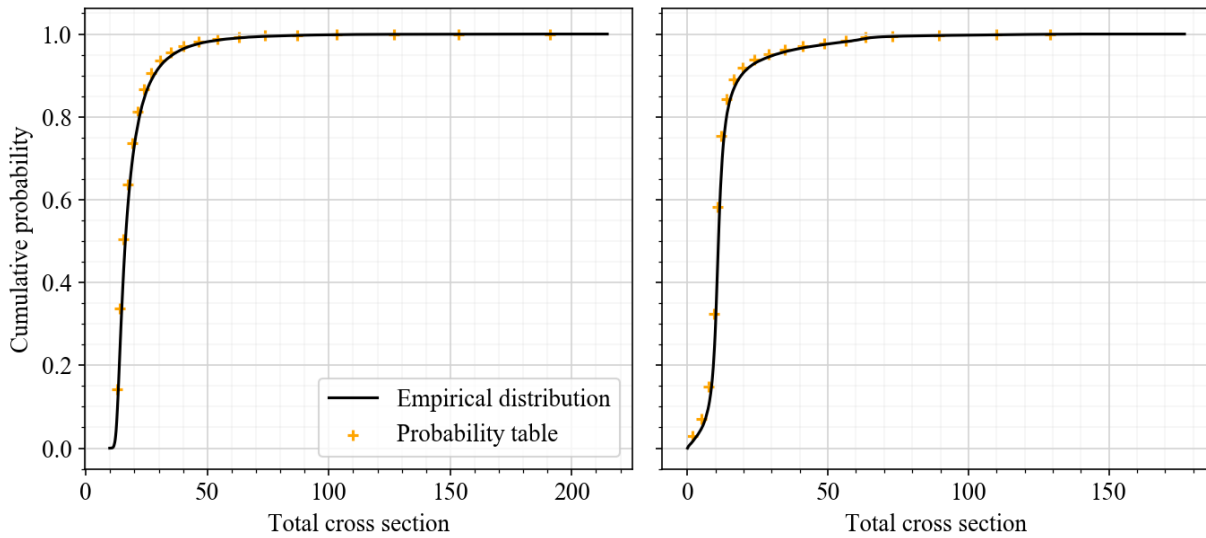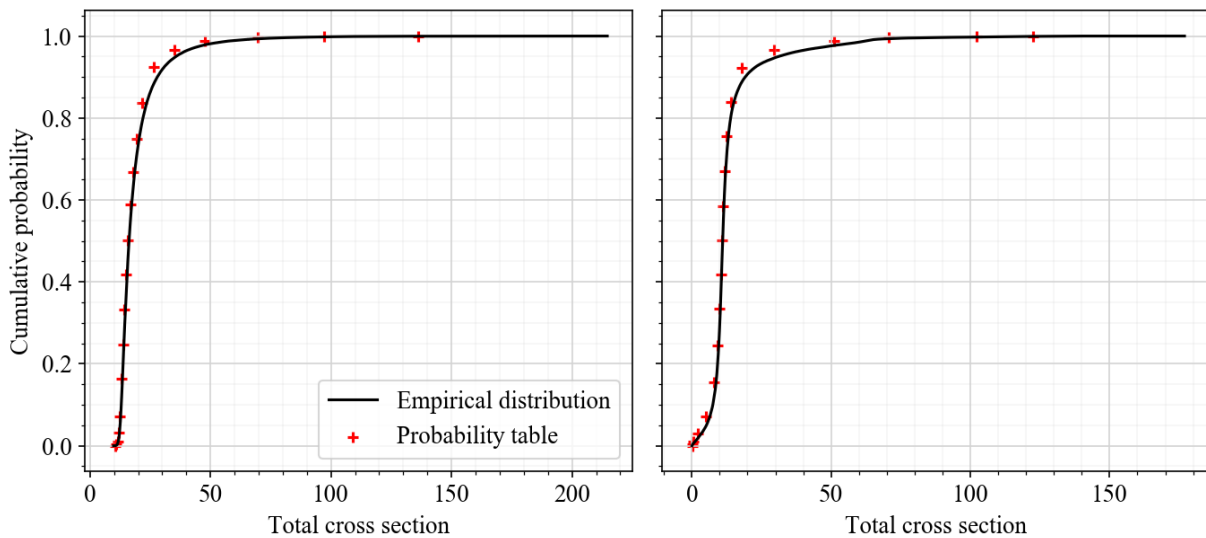

Figure 5.8: Cumulative probability tables with a NJOY-like binning for ^{235}U at E = 2.25 keV and T=0K (left) and ^{238}U at E = 40 keV and T=0K (right)

In order to test the strength of the k-means method more deeply, other nuclides than ^{235}U and ^{238}U can be considered. At this stage, a relevant approach is to find the "worst" possible case for

the k-means tables, and verify the validity of the method. To do so, the *elementary spingroups* of JEFF-3.2 defined in Section 3.2.1 have been used once more. As a reminder, each elementary spingroup is defined by a set of 16 input parameters that correspond to the combination of a single spingroup of a single nuclide of JEFF-3.2 at a particular reference energy found in the evaluation. Considering all the JEFF-3.2 library yields 41 486 elementary spingroups. For all of them, the ladder method has been used at room temperature with 20 000 Monte-Carlo iterations in Chapter 4. From these cross sections samplings, 20-bins probability tables have been computed from the total cross sections using the various reconstruction methods. Then, the statistics of Equation (5.13) has been calculated for all tables, which is simply the sum of the within-bin squared of distance to the mean. This statistics can be reinterpreted as a sum of squared errors (SSE), which is notably often used in regression analysis to measure the discrepancy between the data and a fitting model. From the probability tables modeling point of view, it seemed at first interesting to reduce this quantity, in order to get bin base-points close to the empirical distribution. A good candidate to test the probability tables is an isotope for which this SSE-statistics is high[17], since that means the table base-points are distant from the actual probability distribution, which testifies of a pathological distribution shape. From the k-means table results – which minimize this statistics – the most critical case is the first spingroup ($l = 0$, $J = 0.5$) from ^{156}Eu, at E = 1 eV. Before investigating the shape of the tables for this nuclide, it is interesting to have a quick look at the results of the SSE-statistics for all probability tables of JEFF-3.2. This is summarized on Figure 5.9 on which the statistics for all spingroups has been displayed for all probability tables construction methods, except the moments method. The spingroups have been indexed and first sorted by *l*-value, which yields three very distinct groups. In fact, the *l*-value has a strong influence on the SSE-statistics, as small *l* values raise more important cross sections, which produces greater within-bin distances to the mean. As such, there is no point comparing this statistics between spingroups with different *l*-values. Once sorted according to *l*, spingroups have been sorted by ascending reference energy values, and then masses. It turns out that a relation slightly emerges between the reference energy and the probability tables within-bin distances, which justifies this choice of sorting. Note that this relation seems negative at $l = 0$ and positive for $l = 2$, while it remains unclear for $l = 1$[18]. When combining the different spingroups to retrieve real nuclides calculations, ($l = 0$)-spingroups contribution to the cross section is bigger. As a consequence, Figure 5.9 implicitly suggests that probability tables are more difficult to build at small energies. This is reinforced by the fact the SSE-statistics follows the same trend for all the methods of probability tables construction, which implies the statistics closely depends on the cross section distributions shapes.

Let us focus now on ^{156}Eu at 1 eV, which is the leftmost case of Figure 5.9[19]. To be consistent with the previous examples performed with ^{235}U and ^{238}U, a complete sampling has been performed, with 100 000 Monte-Carlo iterations at room temperature, making use of ladders composed of 1000 uncorrelated resonances for all spingroups. The corresponding 20-bins k-means and NJOY-like tables have been calculated, and displayed on Figure 5.10.

First of all, the empirical probability distribution for this isotope is extremely skewed. Some very high cross section values have been sampled, up to several dozens of thousands of barns. In the same time, such values are still very scarce, as 80% of the cross section values lie between 0 and 100 barn only. For the k-means method, the consequence is quite clear, as it mainly provides bin limits in the higher part of the spectrum. In fact, it is much more useful to group the data in the higher part of the spectrum to reduce the global variance. As a consequence, the smallest weight in the table is around 0.95, which means a single cross section value will be sampled 19 times over 20 in average in neutronics Monte-Carlo codes that will use k-means tables. This is a real issue, as fluctuations may not be taken into account enough. In the meantime, NJOY

---

[17]Note that this statistics directly increases with the number of iterations, but can be used to compare tables derived from samplings of same size.

[18]The case $l = 3$, which only corresponds to four cases of ^{58}Fe, has not been represented.

[19]The unresolved resonance range starts at 1 eV for this isotope, which is an exceptionally low energy.
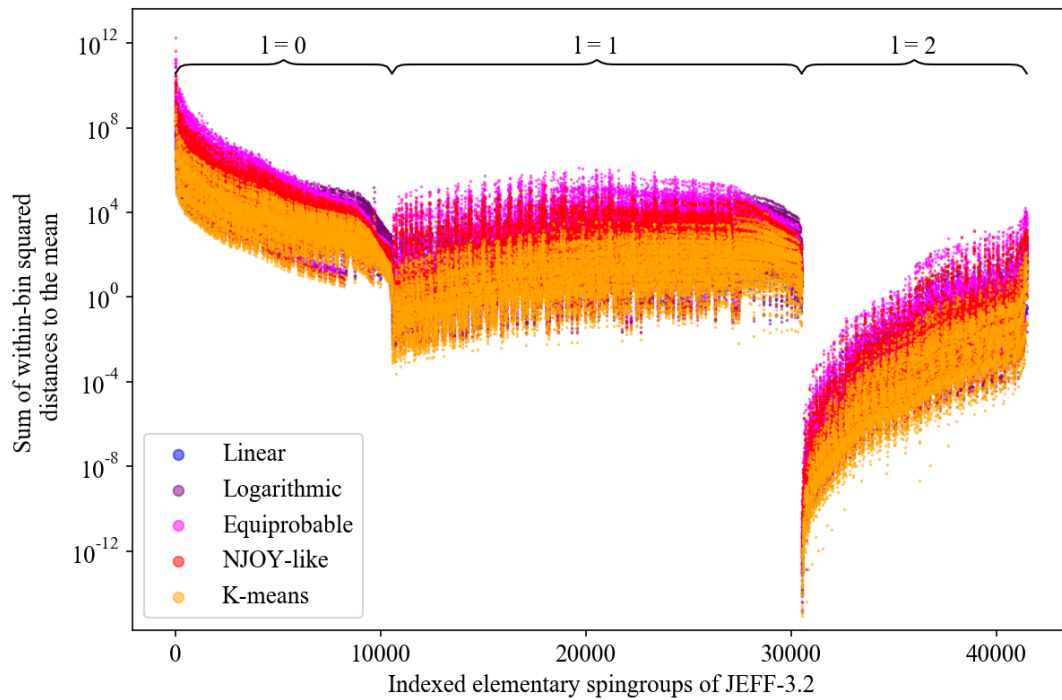
Figure 5.9: Sum of squared within-bin distances to the means for probability tables issued of all elementary spingroups of JEFF-3.2, composed of samplings of size 20 000. The elementary spingroups have been sorted in increasing l-values first, then in increasing reference energy values, then masses. The statistics for five table types built from the same samplings have been computed and displayed on the figure.
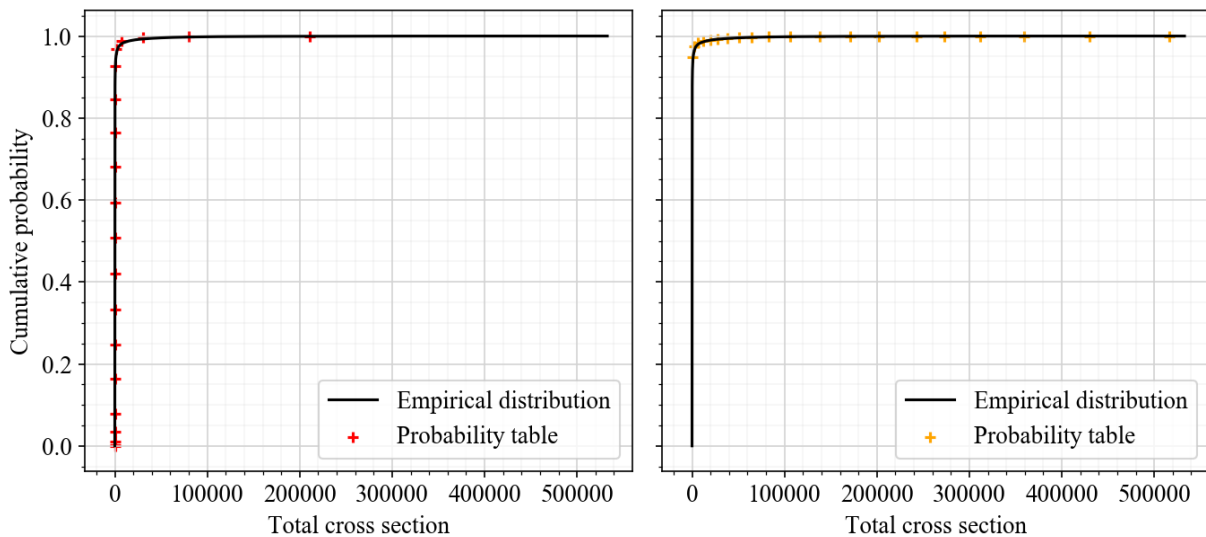
Figure 5.10: Cumulative probability tables for ^{156}Eu at E=1eV and T=293.6K, built with the NJOY-like method (left), and k-means method (right).

empirical method seems to provide a more regular binning at first sight. In order to get a better insight of the situation, Figure 5.11 provides a zoom on the upper part of the spectrum, for both tables. There, the disadvantage of the NJOY table is flagrant too. The distribution is so skewed that some of the probability table base-points are supposed to cover ranges up to ten

thousand barns. That means Monte-Carlo codes may sample a random number, and select a cross section value distant of several thousands of barns from the value that would have been sampled relying on continuous distributions instead of probability tables.

Figure 5.11: Cumulative probability tables for ^{156}Eu at E=1eV and T=293.6K, built with the NJOY-like method (left), and k-means method (right), zoomed over the maximum of variance part of the distribution.
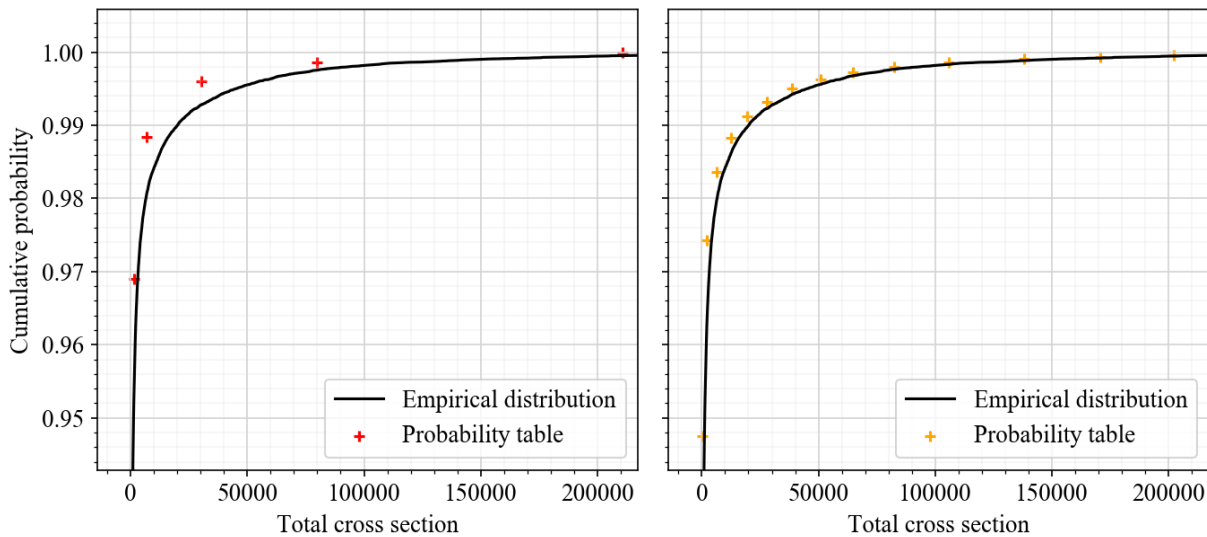
It seems to be pretty difficult to handle the case of ^{156}Eu at 1eV. In fact, all methods have difficulties to build probability tables for such an overly-skewed case, whether it be with the k-means method or NJOY-like empirical technique. Such samplings have to be handled though, and a compromise must be looked for.

5.2.3 K-medians tables

K-means tables seemed to work very well with ^{235}U and ^{238}U and fail with ^{156}Eu, due to the very skewed shape of the probability distribution. If the higher part of the spectrum was fairly well represented, the smallest values were not at all considered by the method. The main issue is the high dependence of the mean to the outliers. In order to get rid of that, a simple idea is to switch from the mean to the median in the k-clustering algorithm. Indeed, the median is more robust than the mean when dealing with skewed data. A well-known alternative to the k-means method is thus the *k-medians* clustering method, which aims to minimize the sum of the L1 distances[20] of the elements to the bin medians. The use of the L1-norm instead of the L2-norm[21] is justified here, as the mean is a least squares estimator of location, whereas the median is an absolute deviation estimator of location. The problem to be optimized can be reformulated as:

$$\arg\min_{\widetilde{\sigma}} \sum_{i=1}^{k} \sum_{\sigma_{tj} \in S_i} |\sigma_{tj} - M_i| \tag{5.18}$$

where $\widetilde{\sigma} = (\widetilde{\sigma}_0, \ldots, \widetilde{\sigma}_k)$ are the bin limits than define bin regions $S_i = [\widetilde{\sigma}_{i-1}, \widetilde{\sigma}_i]$ and M_i is the total cross section median in bin i.

This problem is very close to Equation (5.13), and can be solved with the exact same dynamic programming algorithm, making use of the median instead of the mean, and L1-norm instead of L2-norm. The bin limits then obtained provide a clustering of the distribution which can

---

[20]Also known as the taxicab or Manhattan distance.
[21]Which is the Euclidean distance.

serve to compute probability tables. Note that the k-medians algorithm only serves to find relevant bin limits. In particular, the probability table base-points are still the mean total cross section values in the bins, and not the median. Even if this is opposed to the philosophy of the k-medians algorithm which proposes to take the median as the representative value of the bin, the mean is logically the best value to be used by Monte-Carlo codes afterwards; that is even required to conserve the sampling total cross section mean value. The k-medians clustering is here only used as a tool to obtain relevant bin limits.

In next figures Figures 5.12–5.14, the k-medians tables have been represented for the examples used in previous subsection, ^{235}U at E=2.5keV and ^{238}U at E=40keV for T=293.6K and T=0K, and ^{156}Eu at 1eV and room temperature.

Figure 5.12: Cumulative probability tables with a k-medians binning and empirical distribution of the total cross section for ^{235}U at E = 2.25 keV and T=293.6K (left) and ^{238}U at E = 40 keV and T=293.6K (right)

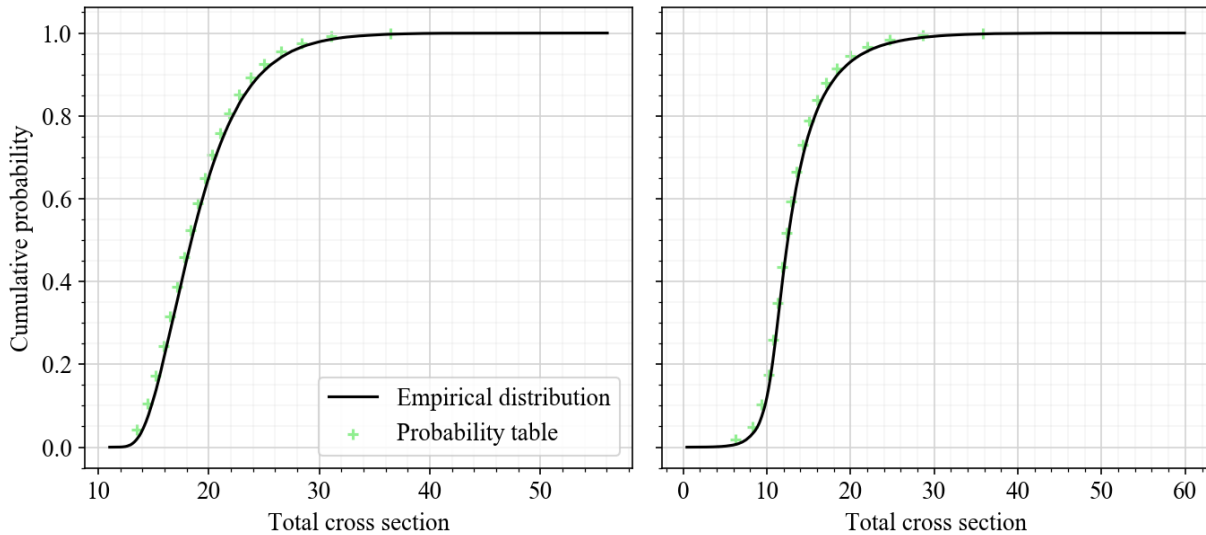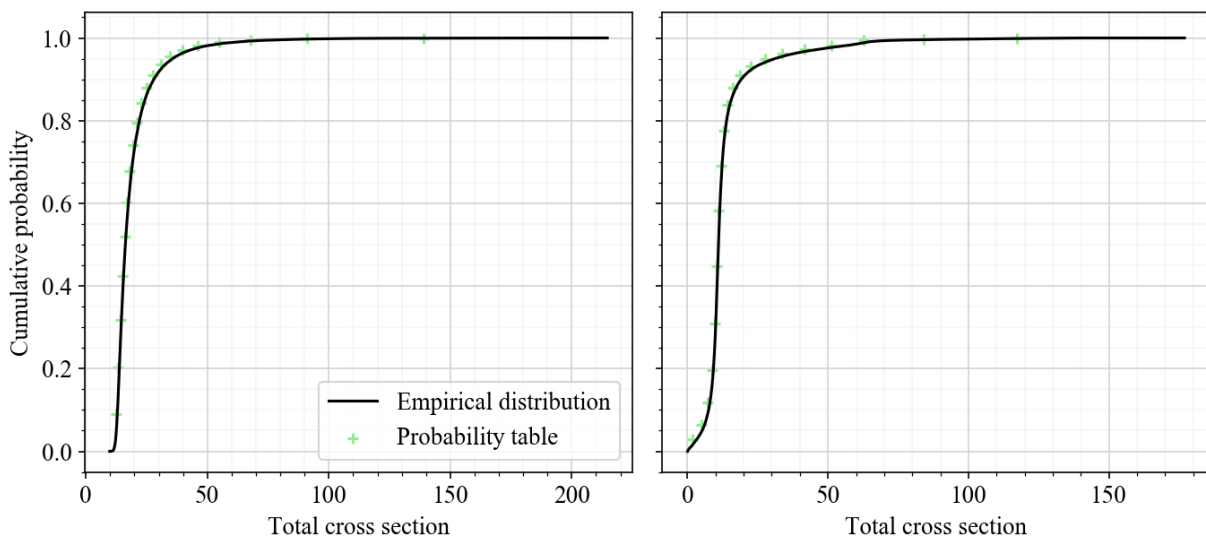Figure 5.13: Cumulative probability tables with a k-medians binning and empirical distribution of the total cross section for ^{235}U at E = 2.25 keV and T=0K (left) and ^{238}U at E = 40 keV and T=0K (right)

From these figures, the obtained k-medians tables approximately behave like the k-means tables. They are able to mesh the tails of the distributions efficiently, as well as the inflections.
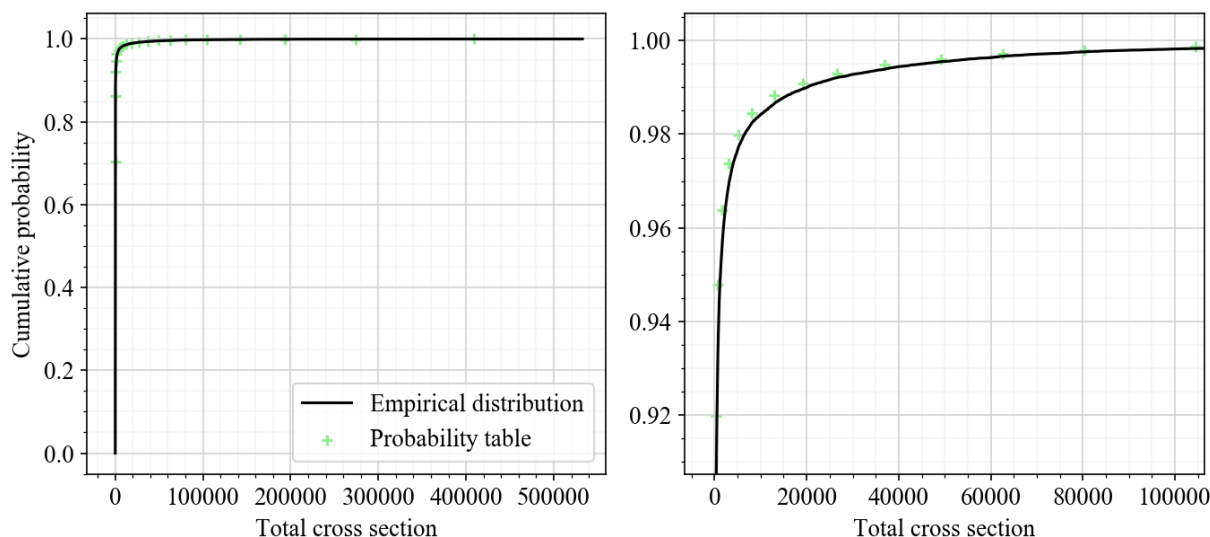
Figure 5.14: Cumulative probability tables for ^{156}Eu at E = 1eV and T=293.6K, built with the k-medians method. The right part is zoomed over the maximum of variance part of the distribution.

Like the k-means tables, a very interesting feature is their ability to adapt to the probability distribution even if its shape is irregular, like for ^{238}U at T=0K. On the other hand, faced to very skewed distributions like ^{156}Eu, they less intensively mesh the right tail. Looking at Figure 5.14, the first bin value is around 0.7, to be compared with 0.95 for the k-means tables. In the meantime, the inflected part seems to be well represented. This is a major improvement compared to the k-means tables, which might be tempered though: 0.7 is still a very high value for a first bin weight. However, in that situation, meshing the inflected part of the distribution seems mandatory. Moreover, a last resort is still available to get around this complex situation: increasing the number of bins.

5.2.4 About the number of bins

In the case of highly-skewed distributions, it may seem relevant to increase the number of bins in the tables to provide a better representation of the probability distributions. This work has been conducted for ^{156}Eu at 1 eV, which is among the worst case scenario found in JEFF-3.2. Figure 5.15 displays the probability tables with 100 bins for equiprobable, NJOY-like, k-means, and k-medians methods. Accordingly, Figure 5.16 displays the same probability tables, zoomed on the inflected part of the empirical distribution.

The number of bins does not seem to change the overall behavior of the tables. The diverse methods seem to have the same advantages and drawbacks than with 20 bins. The equiprobable and NJOY-like binning both have difficulties to mesh the tail and the inflected part of the probability distribution. In the meantime, the k-means table's first bin weight is around 0.75, which is a still a very high value. The most significant improvement comes for the k-medians tables, for which the first bin's weight is around 0.2, which is definitely acceptable. In the same time, the inflected part and tail are as well represented as in the k-means tables. This is a great support for the use of k-medians tables in Monte-Carlo applications. In order to appreciate the gain however, one should perform criticality benchmarks calculations with Monte-Carlo codes, which will be shown in the next chapter.

Before concluding this chapter, it is of interest to detail a little more the question of the number of bins. As mentioned, too many bins are likely to reduce the speed of the Monte-Carlo codes. On the other hand, not enough bins do not provide a good representation of the probability distributions. In practice, 20 bins are used as a reference number.

Figure 5.15: Probability tables for ^{156}Eu at E=1eV and T=293.6K, built with an equiprobable binning (top left), the NJOY-like method (top-right), the k-means method (bottom left), and the k-medians binning (bottom right), making use of 100 bins.

In order to get an insight about the choice of this value as an usual reference, the statistics Equation (5.13) has been used, defined in the k-means problem as the sum of the squared distances of the elements to the bin mean values. As mentioned, this statistics can be reinterpreted as a sum of squared errors (SSE) statistics. High SSE values are a marker of bin values very far from the empirical distribution. The k-means method aimed at optimally reducing that quantity, although it has been shown its use might lead to underestimate the lower part of the probability distribution in case it is very skewed. It is still interesting to observe the evolution of the SSE-statistics according to the number of bins in the tables. This is for instance used in cluster analysis to determine relevant number of clusters, where it is called the *elbow method*, or distortion analysis [77]. The idea is that adding bins in the table is likely to reduce the SSE-statistics[22], providing a decreasing curve. At some points however, the decrease might slow down, which means that adding extra bins does not greatly improve the fitting. This cut-off is graphically located in the "elbow" of the curve, hence the name.

This method has been applied to all probability tables of all elementary spingroups of JEFF-3.2 computed with 20 000 iterations. In particular, the first spingroup $(l = 0)$[23] of ^{235}U at E = 2.5 keV, ^{238}U at E = 40 keV, ^{156}Eu at E = 1 eV, and ^{21}Ne at E = 306.59 keV[24] have been investigated at room temperature. All the SSE-statistics have been computed for tables with increasing numbers of bins from 2 to 100, and represented on Figure 5.17.

---

[22]This is exactly the case for k-means tables.

[23]Which is the main contributor to the cross sections for any isotope.
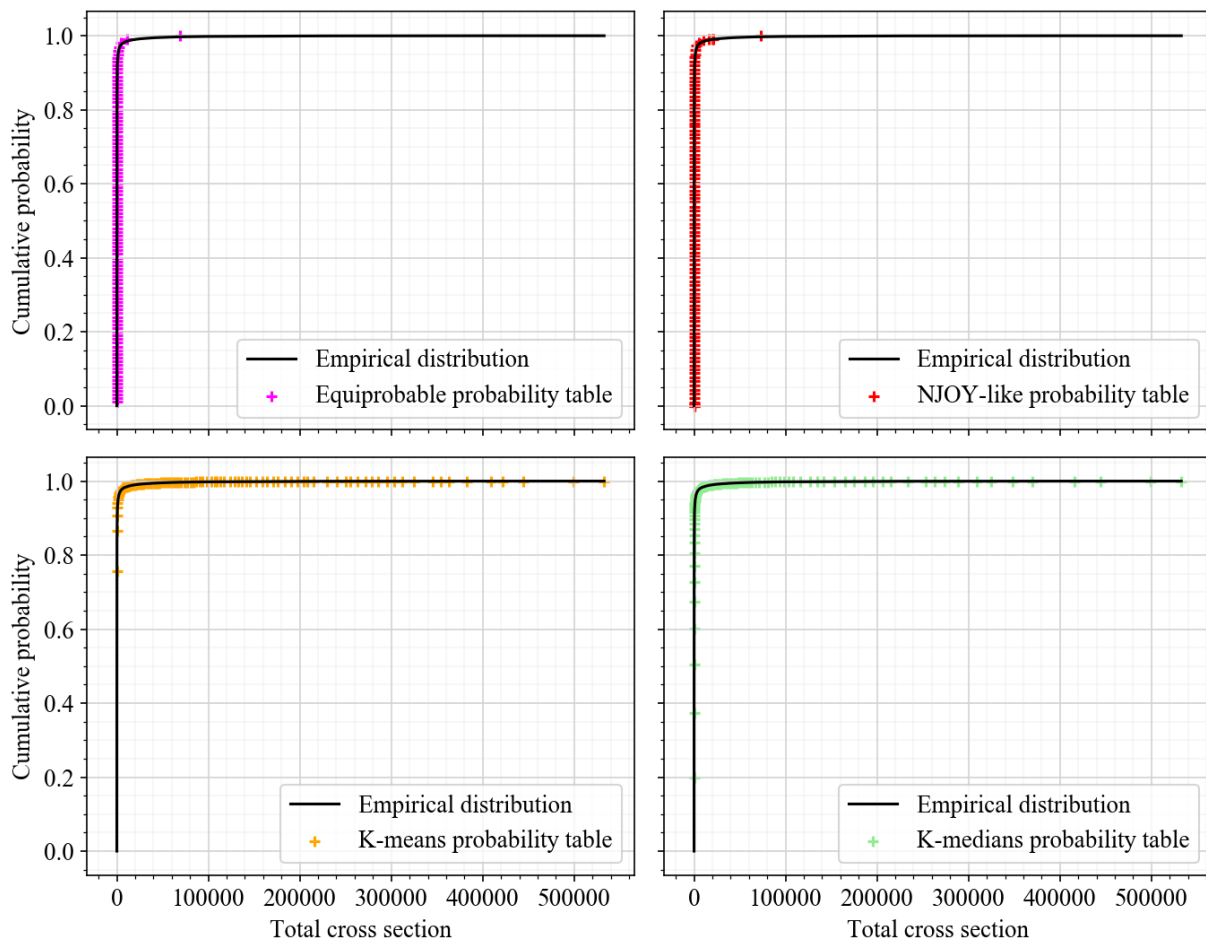
[24]In order to provide an extra example.
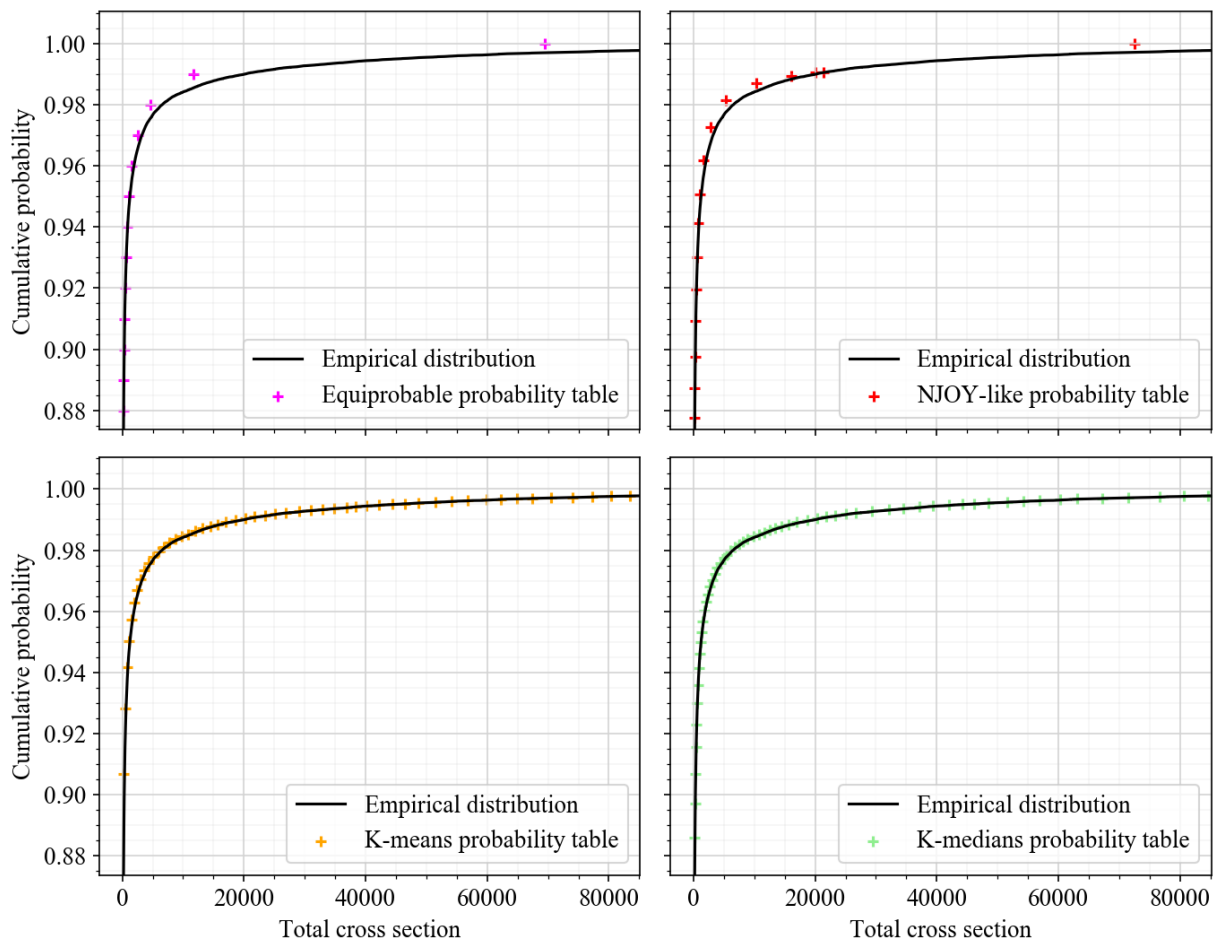
Figure 5.16: Probability tables for ^{156}Eu at E=1eV and T=293.6K, built with an equiprobable binning (top left), the NJOY-like method (top-right), the k-means method (bottom left), and the k-medians binning (bottom right), making use of 100 bins. The figure is zoomed on the higher-variance part of the distribution.

For the four cases considered, the "elbow" is located between 10 and 20 bins for all tables. Hence, this simple approach justifies the use of 20-bins tables. Furthermore, probability tables have a similar behavior, at least for the three typical cases ^{235}U, ^{238}U, ^{21}Ne. The k-means tables have the smallest sum of within-bin squared distances, but it must be noted that the k-medians method provides very close results. Certainly, it has been mentioned that the SSE-statistics is not the only statistics to consider, because our interest is not only to cluster data: the retained bin mean values must be sampled by Monte-Carlo codes afterwards. In that prospect, it has been seen that k-means tables seem to perform less well than k-medians when the distributions are skewed, because the first bin weight might be too high. And even in that case, k-medians tables may also require more bins than just 20 to obtain a good representation of the low cross section values. On the other hand, this analysis highly suggests that using tables with less than 15 bins may lead to an significant loss of information[25].

Lastly, the case of NJOY-like tables must be discussed especially for ^{156}Eu: while all the other methods exhibit a clear and regular decrease of the SSE according to the number of bins, high-order NJOY-like tables do not show this behavior. In fact, looking at the pseudo-code 5.2, NJOY-like tables are in fact equiprobable tables except for the first three and last six bins, that are designed to handle the inflected parts of the distributions. Actually, increasing the number of bins disrupts the NJOY calibration; the last six bins do not necessarily fall around the curve inflection, which may explain the sudden raise in SSE-statistics for the NJOY-like tables. As

---

[25]Besides, let us mention that 15 bins is the minimal table order which can be required by the users in NJOY.
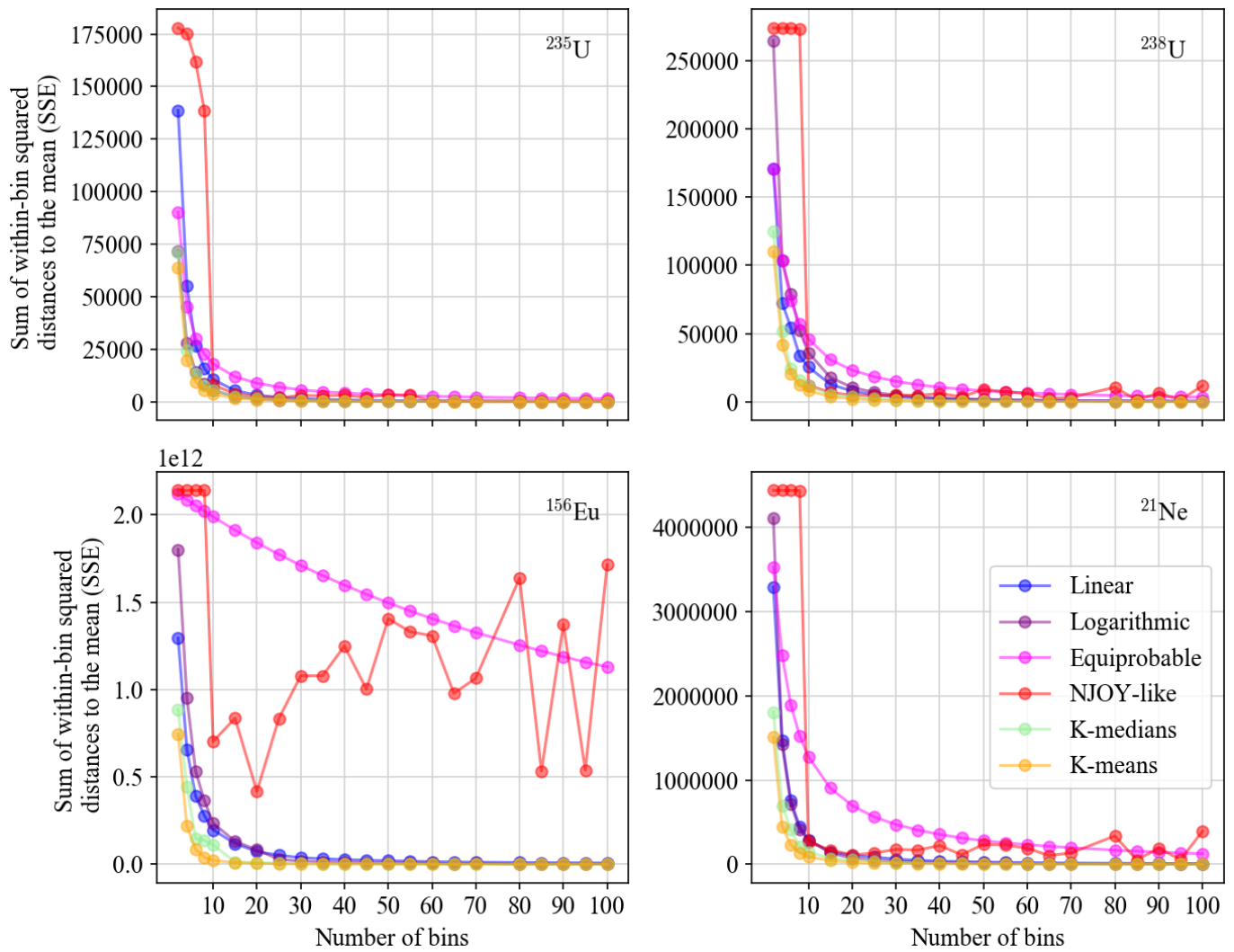
Figure 5.17: SSE-statistics for the first spingroups of ^{235}U at E = 2.5 keV, ^{238}U at E = 40 keV, ^{156}Eu at E = 1 eV, and ^{21}Ne at E = 306.59 keV, for several probability tables built with different methods at room temperature, according to the number of bins considered in the table.

such, Figure 5.17 underlines a particularly important point in practice: NJOY-like tables are tuned to be used with 20 bins exactly. No doubt this reinforces the current generalized use of 20-bins probability tables in nuclear applications.

Conclusion of the chapter

In the present chapter, the construction of the probability tables as the final step of the ladder method has been presented. The objective was to turn a set of sampled cross section values – which define a continuous probability distribution – into a discrete set, which constitutes a probability table. These probability tables are then used in Monte-Carlo neutronics codes for applications. A probability table is defined with several bins. Each bin is attributed a probability value (or weight), associated to a total cross section value (base-point), and several partial reaction cross section values. The partial reaction cross sections are conditional to the total cross section value, which means their sum equals the bin total cross section value. The sum of the bin probabilities equals one. In other words, a probability table is just a probability mass function (pmf) of the cross section values, the discrete counterpart of the probability density function (pdf) used for continuous random variables. Relying on a discrete set of probabilities to describe a continuous probability is here an approximation, introduced by the Monte-Carlo codes. In

this chapter, several alternatives to the probability tables method have been considered. Among them, the use of a parametric estimation of the cumulative density seems the most promising path. However, the implementation of this method in practice requires to change the Monte-Carlo codes, which was beyond the scope of this work.

There is not a single way to turn a probability density into a probability mass function, and as a consequence, there is not a single way to define the probability tables from the cross sections sampling. The best way of doing actually depends on their use in Monte-Carlo codes. Here, the accurate description of the cumulative seems to be the most important fact to guarantee. In particular, the tail of the cumulative distribution has to be well represented in order to enable the Monte-Carlo codes to sample high cross section values. This is especially important as the cross section distributions are usually right-skewed. Another important point relates to the number of bins in the tables, which must not be too high, not to slow down the Monte-Carlo codes. In practice, this number is set by the user to be the same for all probability tables because of the limitations of the ENDF and ACE formats; 20 bins are used typically.

Except for the so-called moments method, all the techniques tackled in this document start by defining bin limits over the sorted total cross sections set. Then, total and partial cross sections are banked in the corresponding defined bins, and their mean values are provided as the bin cross section values. Each bin probability is then simply obtained as the number of cross section values in the bins divided by the total number of elements sampled. In fact, the proposed procedure is equivalent to a histogram construction, except that the mean bin value is taken as representative of the bin, rather than its midpoint. This simple method provides partial cross sections given as conditional values to the total cross section value. Moreover, the probability table mean cross sections remain the same than the sampling ones, which is important in applications since mean cross sections are related to the reaction rates.

The main question thus relates to an efficient definition of the bin limits to obtain high-quality probability tables. Some existing binning techniques have been exposed in this chapter, among which linear, logarithmic and equiprobable binning. It has been shown that these binning methods do not seem to provide acceptable probability tables in various situations. Alternatively, the NJOY method of binning has been slightly adapted to be compliant with the GAIA-2 sampling, and seemed to perform much better. This method relies on empirical considerations though, and is not based on a strong theoretical basis.

One of the main points of interest of the work carried out in this chapter is the introduction of two innovative binning methods in the context of the probability tables generation, based on an existing k-clustering algorithm. Both methods aim at minimizing the global within-bin distances of each bin elements to a representative value of the bin. The first method is based on a k-means clustering algorithm, which defines the bin limits to minimize the global Euclidean distances of the elements to the mean of each bin. The second one is a k-medians algorithm, which minimizes the L1 distances between each bin elements and the bin median. Such k-clustering techniques can be solved in polynomial time for one-dimensional data, following a literature reference based on dynamic programming, which reaches a $\mathcal{O}(n \log n)$ time complexity. In practice, a probability table is built in less than a second. The k-means method seemed to be the most promising at first, as it minimizes the global within-bin variances. K-means probability tables looked very efficient when tested on two essential nuclides of the nuclear industry, namely ^{235}U and ^{238}U. It provided a binning that well took into account the tails of the distribution, and accurately meshed the inflections of the cumulative distribution, which are among the highest variance zones. The k-medians results looked very similar to the k-means ones.

Searching for more extreme scenarios to test the tables, the elementary spingroups from JEFF-3.2 defined in previous chapters have been used once more. K-means probability tables have been built for all cases relying on the cross sections samplings derived in Chapter 3, and their corresponding global within-bins distance computed. Then, the elementary spingroups have been sorted in order to exhibit a relation between the global within-bin distances and the input resonance parameters. For elementary spingroups defined with $l = 0$ (which have

175

the biggest contribution to the cross sections), the smallest reference energies seemed to yield the biggest within-bin distances. We believe this constitutes an important result, even if the physical reason to justify this fact remains unclear. Most critical cases seem to be very skewed distributions, and the most pathological case found in JEFF-3.2 is ^{156}Eu at 1 eV.

It turned out constructing a relevant probability table of order 20 is rather difficult for ^{156}Eu at 1 eV. The k-means tables meshed the high cross section values of the distribution with a too thin grid, whereas the NJOY binning did provide a poor representation of the tails. On the other hand, the k-medians clustering seemed to keep most of the advantages of the k-means method, without being too sensitive to the highest cross section values. It is thus considered in this work as a reference method. The idea is to drop the nice physical interpretation of minimizing the within-bin variance which characterizes the k-means method, in order to gain a more robust technique able to mesh the lower parts of the distribution in any case. The k-medians seemed to fulfill both requirements: it was not only able to avoid an over-fitting of the tail over the small cross sections values, but the sum of within-bin distances to the mean – that may be reinterpreted as a sum of squared errors (SSE) statistics – remained very close to the k-means results. For the critical case of ^{156}Eu, it seemed that the number of bins still required to be slightly increased to obtain an accurate representation of the lower parts of the spectrum; there again, the k-medians tables seemed to provide the more balanced representation of the cross section distributions .

In order to investigate the impact of the probability tables construction in practical applications, the tables have to be tested in integral benchmarks calculations. This is the topic of the upcoming chapter, in which all the work carried in this thesis will be tested in benchmarks calculations.

Validation of developed methods in integral calculations

Once the probability tables have been computed in the unresolved resonance range, they need to be passed to the neutronics Monte-Carlo codes. In this work, the well-known Los Alamos code MCNP-6.2 [78], and the IRSN code MORET-5.D [79] have been considered. Both codes use identical format of processed nuclear data which is based on the ACE (A Compact ENDF) file format [80]. The unresolved resonance range processing methods presented until now are based on the calculation of cross sections probability tables. As a consequence, these tables must be part of the ACE files used by the Monte-Carlo codes, and in this chapter, the last processing steps toward their integration in the ACE format will be presented.

Once ACE files containing the probability tables have been obtained, they can be used in benchmark calculations to estimate the quality of the processed data. Benchmarks are simple integral criticality experiments which can be easily modeled in Monte-Carlo codes and for which several quantities of interest can be computed. Among them, the most expressive is the effective neutron multiplication factor k_{eff} which measures the dynamic of the chain reaction. Another important quantity is the neutron flux, which is directly related to the power, and which can be computed in the various materials during a Monte-Carlo simulation. Integral experiment results are valuable assets that serve to test evaluated data and computer code algorithms. The process provides a way to draw conclusions about the quality of the nuclear data.

In this chapter, the results of several benchmark calculations on the basis of nuclear data files processed differently will be presented. First, the GAIA-2 processing using the most basic methods will be compared to NJOY, in order to get a reference starting point. Then, the impact of questions developed in this thesis such as the probability tables construction or the resonance correlations will be estimated taking into account the reference results in order to conclude about their relevance.

6.1 Processing probability tables over the whole energy range

6.1.1 Generating the ACE file

Once probability tables have been produced in the unresolved resonance range, they must be given to the Monte-Carlo codes. For MCNP and MORET, they need to be integrated in the ACE-formatted files. The ACE format contains all the relevant information found in processed nuclear data files for Monte-Carlo codes to run. In particular, they must contain the linearized broadened cross sections in the resolved resonance range, and the probability tables in the unresolved resonance range.

As a recall, linearized cross sections are simply tables of reaction cross section values versus energy, so that the cross sections can be computed at any energy using a linear interpolation. Such a linearized grid can be obtained when one relies on the calculation of the exact cross section values[1]. Starting from a given grid[2], a simple linearization recursive algorithm checks at intermediate energy points whether the absolute difference between the linearly interpolated value and the exact calculated value is below a certain threshold (usually, 0.1%). If not, the algorithm adds the energy until the convergence criteria indicated by the user are met. At the end of the procedure, unnecessary points are removed. In the resolved resonance range, the reconstruction of reaction cross sections, their Doppler-broadening, and the calculation of a linearized grid are performed by the GAIA-2 module DOP. The DOP module – which abbreviates *Doppler* – performs equivalent tasks as the NJOY modules RECONR and BROADR.

Regarding the probability tables, all the developments achieved in the unresolved resonance range and presented in this thesis have been integrated in GAIA-2 in a module named TOP, which abbreviates *Tables Of Probabilities*. The TOP module takes as an input the initial ENDF file which contains the unresolved resonance parameters, and computes probability tables for all reference energies and required temperatures. Note that in order to keep the temperature correlations, TOP computes the temperature-dependent probability tables from the same sets of sampled resonance ladders. The calculation of the probability tables is not reliant on the resolved resonance range computations, and DOP and TOP modules can be used independently. Only their outputs have to be merged in the ACE files.

The ACE files are not easily human-readable, and no parser has been developed during this PhD to handle that specific format. In order to produce ACE files, the choice has been made to rely on the ACER module of NJOY which is able to cast the produced PENDF files – usually used by NJOY to transmit the processed data between its modules – into ACE files. The PENDF format is a simple extension of the ENDF format already handled by GAIA-2 to read the evaluations content. GAIA-2 thus produces NJOY-like PENDF files rather than ACE files directly. In the present work, the PENDF files have been used like in NJOY to store the processed data between the modules. More precisely, the DOP module first produces a PENDF file which contains the linearized cross sections. The TOP module then completes this file with the computed probability tables in the unresolved resonance range. Then, the ACER module is called to turn the PENDF file in an ACE-formatted one to be used in applications. Probability tables are stored in the section MF2 MT153 of the PENDF files, which is not an ENDF-6 standard but can be handled by ACER. The MF2 MT153 section is simply defined with the next ENDF-like formatting [10]:

```
[MAT,2,153/ ZA,    AWR, 0,    0,      0,   NBIN/]
[MAT,2,153/ TEMP, 0,    LSSF, ICOMP, NW, NUNR/
          ER(1),
          PROB(1,1), ..., PROB(1,NBIN),
          TOT(1,1), ...,  TOT(1,NBIN),
          ELAS(1,1), ..., ELAS(1,NBIN),
          FISS(1,1), ...,  FISS(1,NBIN),
          CAPT(1,1), ..., CAPT(1,NBIN),
          HEAT(1,1), ..., HEAT(1,NBIN),
          ER(2), ...
          <continue for all reference energies ER>]
```

Listing 6.1: Definition of the section MF2 MT153 in the PENDF files, used to store the probability tables in the unresolved resonance range [10]

---

[1]In the resolved resonance range, exact cross section values at any energy can be computed using the R-Matrix formalism and evaluated resolved resonance parameters.

[2]The grid must be carefully chosen, and actually already thin enough. For more details, check [1].

On the previous listing, the adopted notations are typical from then ENDF format: **ZA** is the ZAMID number of the processed nuclide, **AWR** its mass (in neutron mass unit), **NBIN** the number of bins in the probability tables, **TEMP** the temperature of the processed probability tables, **NW** the number of entries in the section, and **NUNR** the number of reference energies at which the probability tables are computed. Then, for each energy **ER**, the weights and base-points of the probability tables are given. In other words, the probability of each bin **PROB** is provided, along with the corresponding total cross section value **TOT** and the conditional partial cross sections for the elastic (**ELAS**), fission (**FISS**), and capture (**CAPT**) reactions. If the HEATR module of NJOY has been used before, the probability tables are also given for the heating (**HEAT**) cross sections which are used to compute the displacement per atom (DPA) cross sections, used in fluence calculations notably. These sections have not been considered in this work and the HEAT entry always equals 0. Finally, the **LSSF** flag indicates the use of the probability tables in Monte-Carlo codes[3], and the **ICOMP** flag indicates the reactions which have been considered as the competitive[4] in the processing.

The chaining of the modules is automatized in GAIA-2, which is able to handle the whole generation of ACE files for many nuclides and required temperatures. The code also handles the generation of auxiliary files required by the Monte-Carlo codes, called the ".xsdir" file for MCNP, and ".xml" for MORET. These auxiliary files are dictionaries summarizing the content of the ACE files[5]. GAIA-2 relies on a simple input file in YAML format[6] [81]. When used autonomously, both DOP and TOP modules make use of YAML-formatted files too.

Relying on such a modular structure based on the transmission of PENDF files not only enables the coupling with ACER, but with any NJOY module. In particular, this is extremely useful to cross-check the produced probability tables in the unresolved resonance range with the NJOY's ones, without taking into account the influence of the resolved resonance range processing. The idea is simply to issue the GAIA-2 probability tables computed by TOP in the PENDF file produced by the modules RECONR and BROADR of NJOY. The resulting PENDF file will contain the linearized Doppler-broadened cross sections from NJOY (RECONR + BROADR) and the probability tables from GAIA-2 (TOP). The different processing paths are presented on Figure 6.1. These paths correspond to different ways of arranging the modules of NJOY and GAIA-2.

On Figure 6.1, the module UNRESR of NJOY is mentioned. This module serves to compute the average Bondarenko self-shielded cross sections (sometimes referred as diluted cross sections) used in deterministic neutronics codes. For the objectives of this work, such a module is thus not important. In particular, its results are not transported to the ACE files. However, the calculations of UNRESR are very easily performed when ones rely on probability tables as described in Equations (1.22)–(1.24) of Section 1.1.6. The calculation of the Bondarenko self-shielded average cross sections has thus been implemented in the TOP module. The calculations can be performed for any dilution value σ_0 provided by the user. This approach is in line with the UNRESR module input card. Self-shielded average cross sections are issued in the specially dedicated PENDF section MF2 MT152. The average self-shielded cross sections provided in section MF2 MT152 are thus coherent with the probability tables furnished in section MF2 MT153.

As already mentioned in Section 1.2.3, the use of PENDF files introduces some weaknesses due to the ENDF format restrictions. For instance in the listing 6.1, only three partial reactions

---

[3]The use of this flag has been precised in Section 2.1.2. It indicates if the furnished tables represent the actual cross sections or factors to be applied to the average cross sections given in the PENDF file MF3 to handle the self-shielding.

[4]In fact MT=51 in this work, even if there may be other reactions which combine with MT51, for instance a second inelastic level.

[5]They essentially store the nature of the processed nuclide, the temperature, the length of the file, and the presence of probability tables.

[6]The YAML format is a *human-readable data serialization* language commonly used to write input or configuration files. It plays the same role as the more famous XML or JSON format, but is more user-friendly.
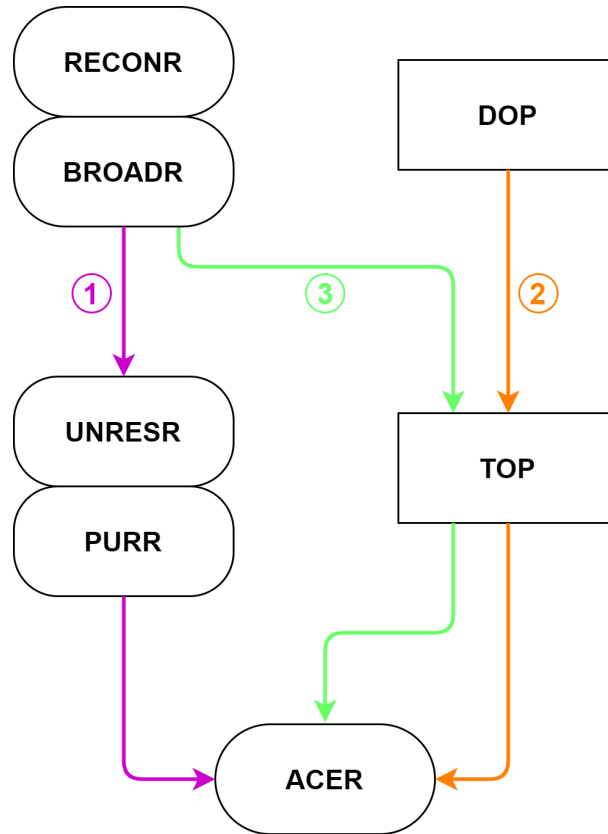
Figure 6.1: Several possible couplings between the modules from NJOY and GAIA-2 responsible for the linearization and Doppler-broadening of cross sections in the resolved resonance range (RECONR+BROADR / DOP), and for the computation of probability tables and diluted cross sections in the unresolved resonance range (UNRESR + PURR / TOP). These couplings correspond to the successive chainings of the modules used in this work to cross-check the quality of the probability tables generation in GAIA-2 and NJOY.

can be considered. In order to get rid of these limitations the transmission of the processed nuclear data between the modules of GAIA-2 is currently under work at IRSN to replace the PENDF files with a *Nuclear Data Handler*. This latter is a set of serialized C++ classes able to store the processed nuclear data between the execution of the successive modules in a format developed to be more in phase with the underlying physics. The development of this object echoes the current rise of the General Nuclear Data Structure (GNDS) format meant to replace the ENDF files in the future [19]. In this thesis the PENDF have been kept as only the coupling with NJOY has been considered, and only ENDF-formatted evaluations have been used.

6.1.2 Choice of the reference energy mesh

Until now the discussed problematic aimed at obtaining a probability table at a single reference energy. In the processed files to be passed to the Monte-Carlo codes however, probability tables must be provided at several reference energies that span the unresolved resonance range. In practice when a cross section value is required at a certain energy in the unresolved resonance range, Monte-Carlo codes use the two adjacent tables defined at the surrounding reference energies, and interpolate the tables. The considered codes MORET and MCNP adopt a slightly different procedure for the interpolation though. In MCNP the same sampled random number[7] is used in the two tables to retrieve the three partial cross sections from the chosen bins [69]. Then,

---

[7]It is the random number obtained from an uniform distribution between $]0, 1[$ that is compared to the cumulative probabilities of the table to select the bin.

an interpolation is performed to get the cross section value. In MORET, the same bin *index* is used in the two tables, and the interpolation is performed between the retrieved cross section values [82]. It must be remarked that both methods are strictly equivalent if the probability tables have the same bin weights. In particular, this is the case if the tables are equiprobable.

Let us underline that both these interpolation strategies have flaws, if the tables do not have the same bin weights. In the MCNP approach the bin indexes might not be the same, which might create a bias: if the selected bin in the second table has a high variance[8] for instance, partial cross section values quite distant from the actual sampled value may be retrieved, which provides a false interpolation. In MORET, keeping the same bin also creates a flaw as the chosen bin in the second table might not correspond to the sampled random number. In fact both methods rely on the same two assumptions. The first one is that probability tables have been built according to the same method, which is usually the case. The second one is much stronger. It supposes that the cross section distributions are smoothly-varying quantities of the energy across the unresolved resonance range, so that bin weights and cross sections in all tables are close, which legitimates an interpolation.

Under these conditions, the choice of the reference energy mesh seems actually quite important. The most natural solution at first sight would be to compute probability tables on the reference energy mesh provided in the ENDF evaluation[9]. In practice however, probability tables can be computed at any energy in the unresolved resonance range using linearly interpolated resonance parameters between two of these provided reference energies. Thus, it is possible to expand the energy mesh on which probability tables are given to the Monte-Carlo codes. In particular this is what the NJOY code does. How it does will be exposed in this subsection.

From that point of view the problematic looks like another one briefly tackled in Chapter 1, in which it was mentioned that any interpolation should rather be performed on resonance parameters than on cross sections. There, providing or not a thinner mesh for the probability tables is exactly the same problem. As a consequence, it seems interesting to estimate the impact of the choice of the reference energy mesh at which probability tables are computed.

In fact, three possibilities for the choice of the reference energy mesh seem practicable:

- Using the reference energies from the ENDF evaluation. This is the most straightforward choice.

- The NJOY solution. NJOY actually starts with the reference energy grid from the evaluation, but adds some pre-defined energies if some criterion is met on the width between the reference energies. This is described in the next algorithm:

```
#set of default energies to be potentially added in the unresolved range
default = [1.0e1,   1.25e1, 1.5e1,   1.7e1,   2.0e1, 2.5e1,   3.0e1,   3.5e1,
           4.0e1,   5.0e1,  6.0e1,   7.2e1,   8.5e1, 1.0e2,   1.25e2, 1.5e2,
           1.7e2,   2.0e2,  2.5e2,   3.0e2,   3.5e2, 4.0e2,   5.0e2,  6.0e2,
           7.2e2,   8.5e2,  1.0e3,   1.25e3, 1.5e3, 1.7e3,   2.0e3,  2.5e3,
           3.0e3,   3.5e3,  4.0e3,   5.0e3,   6.0e3, 7.2e3,   8.5e3,  1.0e4,
           1.25e4, 1.5e4,  1.7e4,   2.0e4,   2.5e4, 3.0e4,   3.5e4,  4.0e4,
           5.0e4,   6.0e4,  7.2e4,   8.5e4,   1.0e5, 1.25e5, 1.5e5,  1.7e5,
           2.0e5,   2.5e5,  3.0e5,   3.5e5,   4.0e5, 5.0e5,   6.0e5,  7.2e5,
           8.5e5,   1.0e6,  1.25e6, 1.5e6,   1.7e6, 2.0e6,   2.5e6,  3.0e6,
           3.5e6,   4.0e6,  5.0e6,   6.0e6,   7.2e6, 8.5e6]

#start with the reference energies from the evaluation
reference = reference_energies_endf()

#starting point
```

---

[8]Which occurs in the inflected part of the distribution cumulative, as seen in previous chapter.
[9]At which resonance parameters are defined.

```
        e_prev = reference[0]
        e_next = reference[1]

        #loop on the reference energies
        while e_next < min(5e6, max(reference)):

          #condition on the spacing between reference energies
          if (e_next > 1.26 * e_prev):

            #if possible, insert an energy from the
            #default list between e_prev and e_next

            #skip to the next reference energies
```

Listing 6.2: NJOY definition of the reference energy grid

This algorithm is designed to fill the unresolved resonance range with additional artificial reference energies when they are too spaced. The average resonance parameters are interpolated at the extra energies, and probability tables are computed making use of these interpolated average parameters.

- Using an *averaged-linearized* reference energy grid in the unresolved resonance range. A linearization procedure in the resolved resonance range is usually the first step of any processing. Notably, it is achieved by the modules RECONR from NJOY and DOP in GAIA-2. As explained before, a linearized grid is designed to be thin enough so that the tabulated cross sections can be linearly interpolated, which means the percentage error between the interpolated value and the exact calculation at any energy is below a certain threshold, for instance 0.1%. This linearization procedure is typical of the resolved range, in which cross sections are reconstructed from the resolved parameters and R-Matrix formulas. However, the idea can be transposed to the unresolved resonance range using the average resonance cross section values computed from the Hauser-Feschbach formalism of Equation (2.37) which makes use of the resonance parameters directly. A linearized grid in the unresolved resonance range is thus defined to enable a linear interpolation of the *average* cross section values. The computations of such an averaged-linearized energy grid is simple and very fast. The methods used in DOP and described in [1] have been adapted to provide a thin mesh on which probability tables can be computed. Such a mesh is actually more coherent with the usual representation of the tabulated cross sections in the unresolved resonance range in the PENDF file MF3. The calculation of the probability tables at the new energies makes use of interpolated average resonance parameters, like in the NJOY approach[10].

Let us precise that using a thinner mesh for the calculation of probability tables is actually recommended by the ENDF manual [2], which encourages the processing codes to take care of providing an accurate mesh. As such, a ten-per-decades spacings is recommended[11]. In the meantime, the evaluators are urged to provide a mesh dense enough so that the difference between cross sections and resonance parameters is less than 1%.

The NJOY method is once again highly empirical, but provides a reference energy mesh very close from the ENDF one. On the other hand an averaged-linearized mesh in the unresolved resonance range is likely to produce a mesh thinner than the ENDF and NJOY ones, especially if the tolerance criterion is fixed equal to 0.1% like it is often the case in the resolved resonance

---

[10]The Hauser-Feschbach successive average cross sections calculations during the linearization procedure also use interpolated average resonance parameters.

[11]This is mentioned in the section 2.4.2 of [2]. Note that in Appendix F.2 of the same manual the interpolation on cross sections is recommended, which is self-contradictory. It is believed the indication of Appendix F.2 can be discarded.

range[12]. As an example, Figure 6.2 displays the three reference energy meshes for several nuclides of JEFF-3.2 in the unresolved resonance range, namely ^{238}U, ^{96}Mo, ^{235}U, and ^{239}Pu, along with the corresponding average total cross section values obtained from Hauser-Feschbach calculations. On this figure the NJOY reference energy mesh looks a lot like the ENDF evaluation mesh. It is exactly the same for ^{238}U and ^{239}Pu, and simply adds a few energies for ^{96}Mo and ^{235}U. The linearized mesh, computed here with a linearization threshold of 0.1%, introduces many more points.
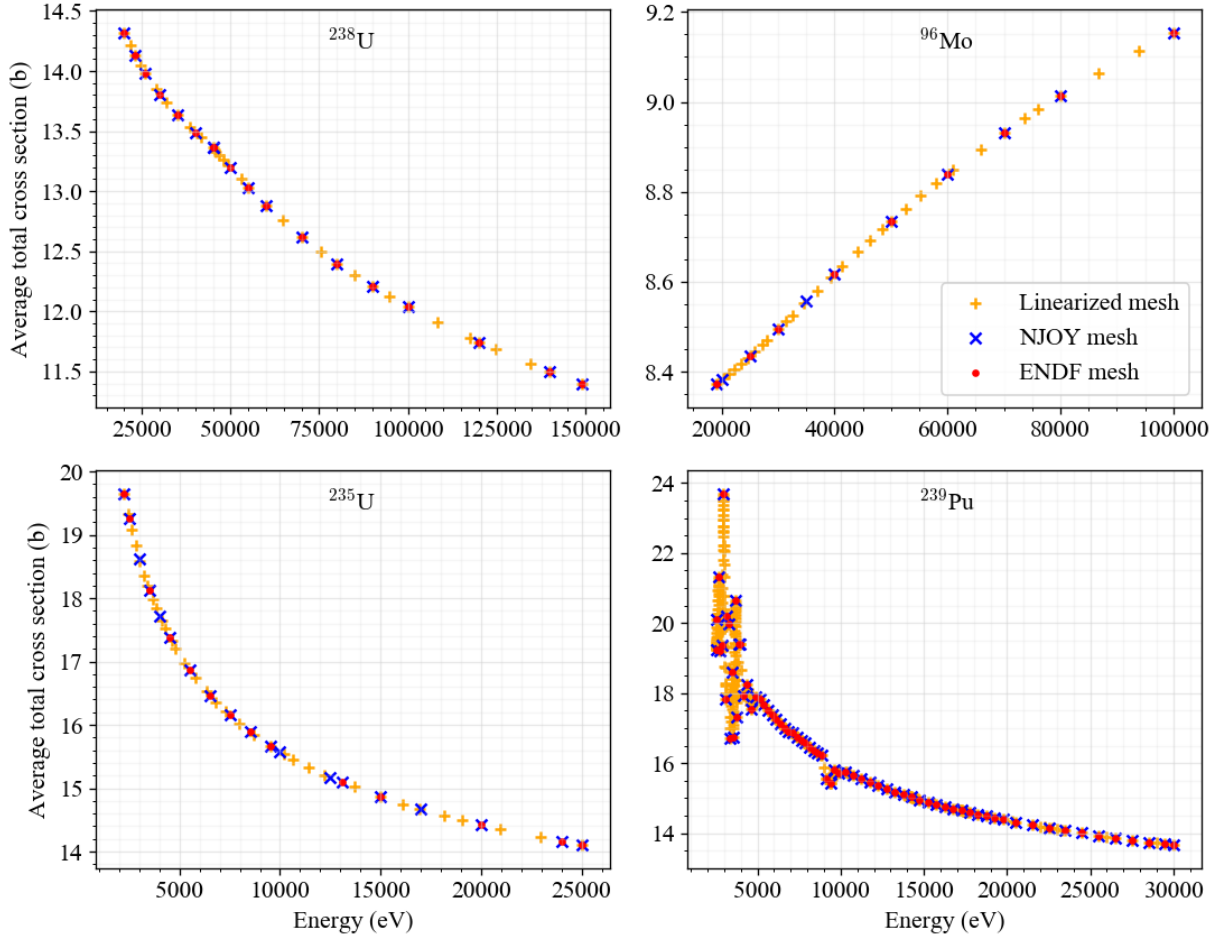
Figure 6.2: The three possible reference energy meshes in the unresolved resonance range for several nuclides of JEFF-3.2: ^{238}U (top left), ^{96}Mo (top right), ^{235}U (bottom left), and ^{239}Pu (bottom right). Total average cross section values have been computed using the Hauser-Feschbach formalism of Equation (2.37). The averaged-linearized meshes (obtained with a linearization threshold of 0.1%) exhibit many more reference energies than the NJOY and ENDF meshes respectively. The NJOY code only adds some predefined values, for example E = 35 keV for ^{96}Mo.

The impact of the choice of the reference energy mesh will be investigated in the benchmark integral calculations in Section 6.3. For now, a reference cross-checking between NJOY and the developments in GAIA-2 in the unresolved resonance range is about to be presented.

6.2 Elements of validation

The objective of this section is to present some elements of validation of the methodology established in this work for the probability tables computation implemented in the TOP module

---

[12]This is for instance the default value of the tolerance threshold used by DOP.

of GAIA-2. By "validation" one means the verification that the probability tables calculated with the methods developed in this thesis are accurate, and can be used in the context of criticality applications. In a first step this validation will be performed by comparing the GAIA-2 results with the NJOY code. In this cross-checking operation the GAIA-2 methods will be chosen to mimic as much as possible the NJOY behavior. In particular, all the "new" methods developed, such as k-clustering tables or correlated spacings, will be left aside. The accuracy of these developments will be tackled further in Section 6.3. For now, the presentation will thus stick to a basic implementation of the ladder method. The sampled ladders are large (300 pairs of resonances) and make use of uncorrelated resonances. The number of Monte-Carlo iterations is high (100 000). The probability tables are computed with the NJOY method, and the reference energy grid is the same as NJOY.

6.2.1 Presentation of several benchmarks

Probability tables must be tested on benchmarks sensitive in the unresolved resonance range. Such benchmarks are not so common because the epithermal range – in which lies the unresolved resonance range for most nuclides – is not the most influential for traditional reactor physics applications[13], and especially for PWR[14]. Moreover, it has been seen in the diverse parts of this document that the most critical nuclides are composed of spingroups with large or low $\overline{\Gamma}/\overline{D}$ ratios[15]. However, the nuclides commonly used in the nuclear applications (^{235}U, ^{238}U, ^{239}Pu...) present $\overline{\Gamma}/\overline{D}$ ratios "in the bulk". The most critical cases of previous chapters (^{21}Ne, ^{156}Eu, etc.) are actually quite exotic for the nuclear industry and no available benchmarks exist to validate them. Finally, many important nuclides simply do not have an unresolved resonance range defined. This is for instance the case of all isotopes of aluminum and all isotopes of iron except ^{58}Fe in JEFF-3.2.

There are benchmarks for which the effects of the tables are visible though, and which are thus relevant to test them. Three families of benchmarks have been used in this work to test three particular nuclides, ^{238}U, ^{239}Pu, and ^{96}Mo.

IEU-MET-FAST for ^{238}U

Three benchmarks of the series IEU-MET-FAST (like *Intermediate Enrichment Uranium and Metal* benchmarks, designed for fast spectra applications) have been found to be sensitive to the probability tables of ^{238}U. These benchmarks are described in the International Handbook of Evaluated Criticality Safety Benchmark Experiments [83], and are thus very popular. The project in charge of the emission of this handbook each year is better known as the ICSBEP[16] and is the international reference for criticality benchmarks.

The first benchmark, referred to as IEU-MET-FAST-003 in the ICSBEP handbook, is a Russian experiment composed of a bare spherical assembly of uranium, with a ^{235}U enrichment of 36%. The rest of the uranium sphere is composed of ^{238}U.

The second one, IEU-MET-FAST-007 [84] is very famous as it is a simplified version of the well-known Big Ten experiment. This criticality setup is composed of a large cylindrical assembly composed of a core of uranium, with a ^{235}U enrichment of 10%, and a large and thick reflector of ^{238}U mainly. Big Ten experiments have been designed in the early 1970s at Los Alamos National Laboratory, and reproduced several times in the following years.

The last one, IEU-MET-FAST-016 [85], is also a cylindrical design composed of a fissile core of uranium and a layer of depleted uranium mainly composed of ^{238}U around it. In the late

---

[13]The epithermal range plays a very important role in criticality safety on the other hand.

[14]As an example, benchmarks in the intermediate spectrum represent around 2% of the cases in the well-known ICSBEP benchmark database.

[15]As a recall, $\overline{\Gamma}$ is the average total reaction width and $\overline{D}$ is the average spacing (both quantities are usually energy-dependent). These notations have been used all along the document.

[16]Like International Criticality Safety Benchmark Evaluation Project.

50s, a Zero-Power-Reactor (ZPR-3) configuration had been initiated in the Argonne National Laboratory to be used as a fast reactor benchmark. This design has been adapted afterwards to serve as a criticality safety benchmark in the intermediate energy range, which is the present IEU-MET-FAST-016 benchmark. These benchmarks from the ICSBEP are well-known standard experiments, well described in the literature. They are very interesting to validate the processing of ^{238}U, a crucial isotope of the nuclear industry.

The TEX experiments for ^{239}Pu

The TEX program [86], as *Thermal/Epithermal eXperiments*, is a recent series of experiments issued from an on-going work at Lawrence Livermore National Laboratory in collaboration with several institutes in the world, among which IRSN. The objective of this series is to provide experiments sensitive in the intermediate spectrum range, under-represented until now in the ICSBEP database. These benchmarks have been recently submitted to the ICSBEP, and should be accepted for the 2020 edition of the handbook [83].

The TEX experiments of interest in this work are composed of superposed plutonium metal plates, with plates composed of an aluminum-polyethylene alloy between them to serve as moderator. A thin polyethylene reflector has been added to the ensemble to get close to criticality. The benchmark reference name as submitted to the ICSBEP is PU-MET-MIXED-002 (like Plutonium Metal Mixed n.2). As it is often the case in this sort of experiments, several configurations have been used which correspond to various thicknesses of the polyethylene plates. This enables to tune the neutron spectrum to be sensitive to various energy ranges. For the PU-MET-MIXED-002 experiment five configurations have been developed. All five configurations are presented in reference [87], and can be used as benchmarks. In this thesis, only the first and the second ones have been found to be sensitive to the ^{239}Pu probability tables and thus retained. They are referred in the following as PU-MET-MIXED-002-1 and PU-MET-MIXED-002-2.

These two set-ups have been used in this PhD to test the probability tables of ^{239}Pu which presents the interest to be a fissile element, especially important in the nuclear industry.

Artificial assemblies Pu-Mo for ^{96}Mo

In the journey to investigate the quality of the implementation of the probability tables treatment in the IRSN Monte-Carlo code MORET-5.D in 2015, the need for dedicated benchmarks very sensitive to the probability tables emerged. As mentioned, not so many benchmarks are available and most of them are not sensitive enough to display very huge discrepancies in case the probability tables are modified. In order to get rid of this issue, a set of artificial benchmarks have been designed at IRSN [82]. These benchmarks are named Pu-Mo-type1, Pu-Mo-type2, Pu-Mo-type3, and UPuMoZr-type1. Each of them comes in three variants, which makes up to a total of 12 benchmarks. The fissile material is plutonium, and the probability tables of interest are mainly the molybdenum ones. These benchmarks are representative of some process of the French facilities at La Hague, which is the main center for fuel recycle operations in France. The benchmarks remain theoretical though. In particular they model infinite medium. This is non-physical but enables to highlight the effect of the probability tables. As will be presented, the effect of the probability tables is of the order of several thousands of pcm.

The use of these benchmarks has been carried out in this work to test the probability tables of ^{96}Mo, an intermediate-sized nuclide quite present in the nuclear industry.

6.2.2 Direct sampling comparison with NJOY

In the following, the aforementioned benchmarks will be used to estimate the impact of the processing methods. The nuclides will thus be processed by GAIA-2, NJOY, and a combination of the two codes. Then the resulting ACE files will serve as input nuclear data files in the same benchmark configurations. In the definition of the benchmark configurations many materials are

involved in the fissile volumes, the moderators, the reflectors, etc. For instance, in the Pu-Mo experiments, the main reflector is composed of natural molybdenum, which involves both ^{95}Mo and ^{96}Mo. However, in order to get a clear view of the impact of the different processings, only a single nuclide is reprocessed with different methods for each benchmark family: ^{238}U for IEU-MET-FAST benchmarks, ^{239}Pu for PU-MET-MIXED-002 benchmarks, and ^{96}Mo for Pu-Mo ensembles. All the other nuclides defined in the benchmarks rely on the same processed files[17]. Resulting differences between the benchmark outputs are then expected to be due to the different processings of each nuclide only[18].

Before dealing with the benchmarking results, it is of high interest to have a first glance at these three nuclides. Indeed, a first cross-checking can be performed to compare the probability tables produced by the module PURR from NJOY and the ones from the module TOP of GAIA-2. One may even look at the sampled cross section distributions of both codes.

Figure 6.3: Cross section distributions of ^{238}U at 40 keV and T=293.6K, sampled by NJOY (PURR module), and GAIA-2 (TOP module), for total, elastic and capture reactions. The cumulative probability tables produced by both modules have been represented too. For partial reactions these tables are conditional probabilities to the total reaction.

Figure 6.3 displays the PURR and TOP sampled cross sections of ^{238}U at 40 keV and 293.6K for total, elastic, and capture reactions, along with their respective probability tables. Figure 6.4 displays the distributions for ^{239}Pu at 29.5 keV and 293.6K, for elastic, capture and fission reactions. The fission has been represented rather than the total because ^{239}Pu is a fissile nuclide. Finally, Figure 6.5 represents ^{96}Mo at 20 keV and 300K. The temperature slightly differs in this latter case, because the corresponding benchmark calculations have been performed at this temperature.

The case of ^{96}Mo is rather interesting, as the sampled distribution is rather skewed on the right. According to the discussions in Chapter 5, a difference between the diverse probability tables construction methods is more likely to be observed for such cases. This will be confirmed in the benchmarks results in Section 6.3.

The probability tables in TOP have been built with the NJOY-like method. In all cases, the sampled cross sections in TOP have been produced with 300 pairs of uncorrelated resonances, and 100 000 Monte-Carlo iterations. Considering the ratios $\overline{\Gamma}/\overline{D}$ for the spingroups of the diverse isotopes, these numbers are coherent with the developments presented in Chapter 3. Table 6.1

---

[17]They come from the JEFF-3.2 library processed by NJOY-2012.
[18]Except for the Monte-Carlo statistical uncertainty.
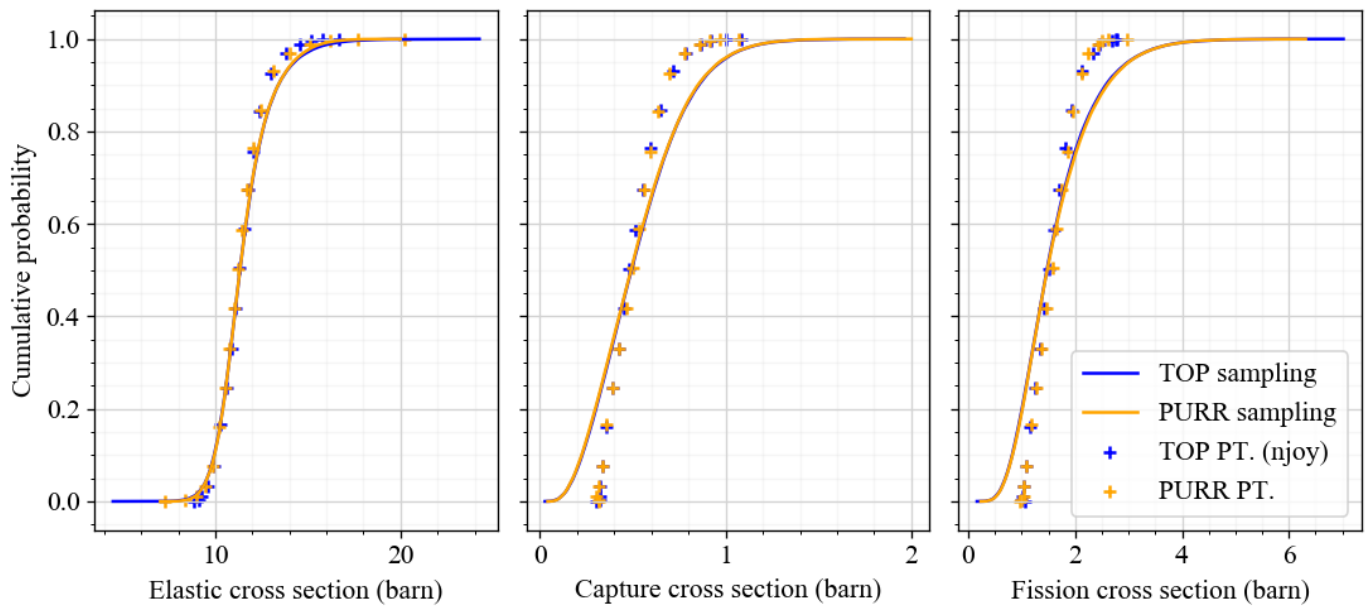
Figure 6.4: Cross section distributions of ^{239}Pu at 29.5 keV and T=293.6K, sampled by NJOY (PURR module), and GAIA-2 (TOP module), for elastic, capture and fission reactions. The cumulative probability tables produced by both modules have been represented too. For partial reactions these tables are conditional probabilities to the total reaction.
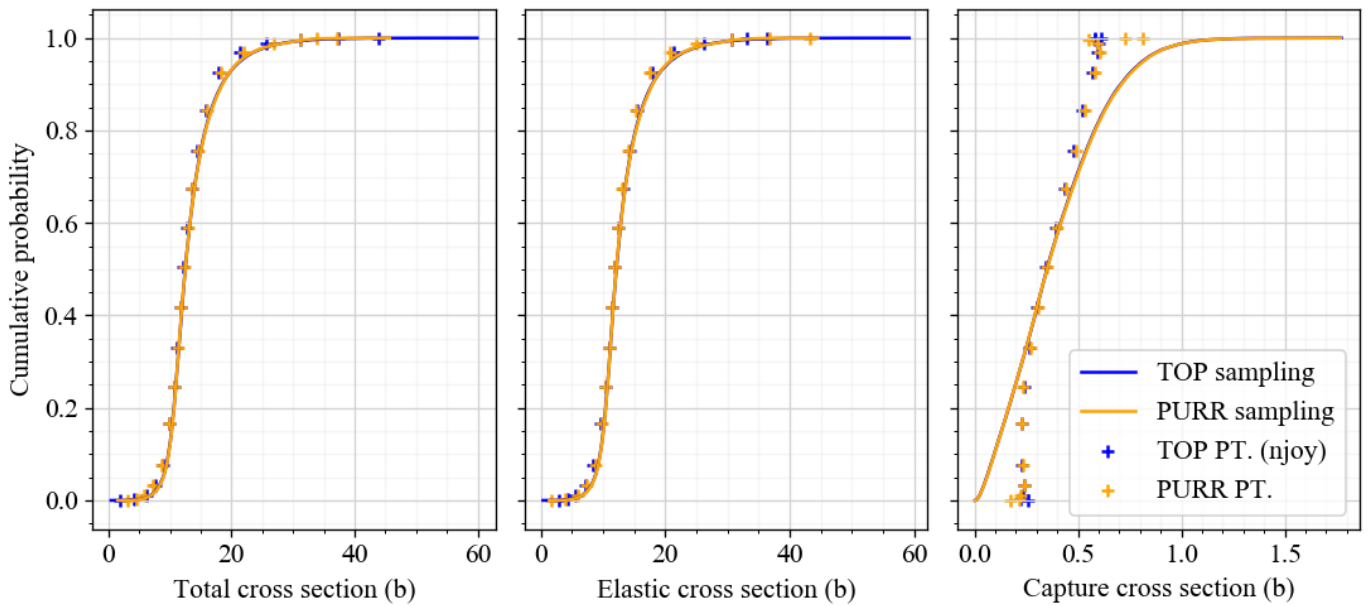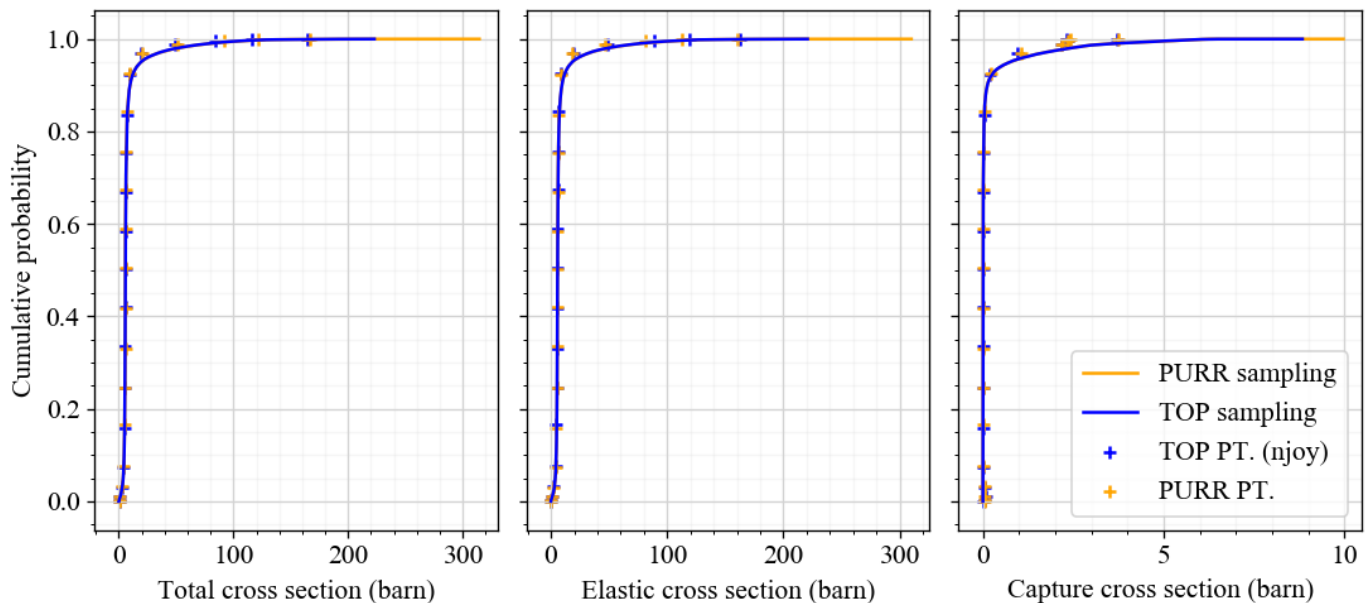

Figure 6.5: Cross section distributions of ^{96}Mo at 20 keV and T=300K, sampled by NJOY (PURR module), and GAIA-2 (TOP module), for total, elastic and capture reactions. The cumulative probability tables produced by both modules have been represented too. For partial reactions, these tables are conditional probabilities to the total reaction. The TOP sampling has been superimposed to PURR's for readability, because it yielded less extreme values in that case.

shows these $\overline{\Gamma}/\overline{D}$ values of the first spingroup[19] ($l = 0$) for all nuclides at the selected reference energy, along with the estimated required number of pairs of resonances for the Kolmogorov-Smirnov distance to be close to at least 1% of the 500-pairs distribution.

The sampled cross sections seem to match very well between the two codes in all cases. This

---

[19]This spingroup has the main weight in the final computations

Nuclide	$\overline{\Gamma}/\overline{D}$	Required number of pairs of resonance in the ladders
^{238}U	0.019521	242
^{239}Pu	0.063240	231
^{96}Mo	0.005386	11

Table 6.1: $\overline{\Gamma}/\overline{D}$ ratios for the first spingroup ($l = 0$) of the three nuclides at the considered reference energy represented on Figures 6.3–6.5. The corresponding estimated number of required pairs of resonances in the ladders computed in Chapter 3 has been indicated.

close agreement indicates that both methods of cross sections reconstruction – at a reference energy, or over a whole range – provide similar results. Let us underline that this constitutes a result in itself. The main difference between both codes seems to lie in the tails of the sampled distributions. For ^{238}U and ^{239}Pu, the TOP sampling seems to provide more extreme values than PURR. However, for ^{96}Mo, the opposite situation is observed. A more complete study of the impact of cross sections reconstruction procedures in the ladder method would have been necessary to draw a conclusion about this slight discrepancy.

6.2.3   Reference benchmark calculations

The benchmarks described in Section 6.2.1 have been modeled with the IRSN Monte-Carlo code MORET-5.D. For each set of benchmarks, the effective multiplication factor k_{eff} has been calculated with a statistical uncertainty of 5 pcm. The nuclear data files have been processed with GAIA-2, NJOY, and a combination of both codes, in order to highlight and validate the probability tables implementation in GAIA-2 compared to NJOY. Only a single nuclide is processed differently in each benchmark: ^{238}U is processed for IEU-MET-FAST benchmarks, ^{239}Pu for PU-MET-MIXED-002 benchmarks, and ^{96}Mo for Pu-Mo benchmarks. The initial evaluation files come from the JEFF-3.2 library, and when NJOY was required[20], the version used was NJOY-2016.35. For all the other nuclides present in the benchmarks, processed files available at IRSN have been utilized. These files had been obtained from the JEFF-3.2 library processed with NJOY-2012.

Actually, the aforementioned nuclides have been reprocessed from five different manners. First, the processing has been carried out with NJOY and GAIA-2, relying on their respective modules in the resolved and unresolved resonance ranges. The NJOY processing is thus done by calling RECONR and BROADR modules, and then PURR. The GAIA-2 processing is done with the successive use of modules DOP and TOP. The computed values are stored in Table 6.2 and Table 6.3, along with the experimental measured k_{eff} when available. The absolute differences in pcm from NJOY or the experimental values have also been indicated.

At first sight, the results between the GAIA-2 and NJOY codes seem to match. In order to observe the discrepancies between the codes only due to the resolved resonance range processing, the nuclides of interest have been processed again by each code, without probability tables in the unresolved resonance range. This means PURR and TOP modules have not been included. The k_{eff} results are stored in Table 6.4 and Table 6.5. The absolute differences between these two cases have been displayed, as well as the absolute difference with the NJOY or GAIA-2 results.

Two important conclusions may be drawn from the results of Table 6.4 and Table 6.5. First, the results yielded by the resolved resonance processing of GAIA-2 and NJOY are very similar as the most disagreeing benchmark is PuMo-type2-c2, with only a 23 pcm difference. Secondly, the considered benchmarks are indeed sensitive to the probability tables in the unresolved resonance

---

[20]Note that the ACER module is always required.

Benchmark	IMF-003	IMF-007	IMF-016	PMM-002-1	PMM-002-2
EXP	1.0000	1.00490	1.00130	1.00090	1.00082
Experimental uncertainty	± 0.00170	± 0.00010	± 0.00080	± 0.00120	± 0.00010
NJOY	1.00227	1.00420	0.99658	1.00029	0.99621
pcm / EXP	227	-70	-472	-61	-461
GAIA-2	1.00225	1.00388	0.99638	1.00017	0.9963
pcm / EXP	225	-102	-492	-73	-452
pcm / NJOY	-2	-32	-20	-12	9

Table 6.2: k_{eff} calculations performed with the IRSN Monte-Carlo code MORET-5.D for several ICSBEP benchmarks at T=293.6K. IMF is an abbreviation for IEU-MET-FAST, and PMM for PU-MET-MIXED, which are part of the TEX experiments. Here, ^{238}U and ^{239}Pu from JEFF-3.2 have been processed by NJOY-2016.35 (modules RECONR, BROADR, and PURR) and GAIA-2 (modules DOP and TOP). Other nuclides come from JEFF-3.2 processed by NJOY-2012.

Benchmark	PuMo-1.1	PuMo-1.2	PuMo-1.3	PuMo-2.1	PuMo-2.2	PuMo-2.3
NJOY	1.26253	1.20384	1.18172	0.54499	0.56957	0.74542
GAIA-2	1.26266	1.20382	1.18171	0.54519	0.56972	0.74541
pcm / NJOY	13	-2	-1	20	15	-1
Benchmark	PuMo-3.1	PuMo-3.2	PuMo-3.3	PuMoZr.1	PuMoZr.2	PuMoZr.3
NJOY	0.30536	0.32337	0.47588	0.14322	0.1647	0.33278
GAIA-2	0.30560	0.32339	0.47589	0.14335	0.16474	0.33271
pcm / NJOY	24	2	1	13	4	-7

Table 6.3: k_{eff} calculations performed with the IRSN Monte-Carlo code MORET-5.D for several fictitious benchmarks representative of La Hague operations at T=300K. Here, ^{96}Mo from JEFF-3.2 has been processed by NJOY-2016.35 (modules RECONR, BROADR, and PURR) and GAIA-2 (modules DOP and TOP). Other nuclides come from JEFF-3.2 processed by NJOY-2012.

Benchmark	IMF-003	IMF-007	IMF-016	PMM-002-1	PMM-002-2
NJOY_NOPT	1.00283	0.99999	0.99316	1.00079	0.99649
pcm / NJOY	56	-421	-342	50	28
GAIA-2_NOPT	1.00295	1.00008	0.99302	1.0008	0.99653
pcm / GAIA-2	70	-380	-336	63	23
pcm / NJOY_NOPT	12	9	-14	1	4

Table 6.4: k_{eff} calculations performed with the IRSN Monte-Carlo code MORET-5.D for several ICSBEP benchmarks at T=293.6K. IMF is an abbreviation for IEU-MET-FAST, and PMM for PU-MET-MIXED, which are part of the TEX experiments. Here, ^{238}U and ^{239}Pu from JEFF-3.2 have been processed by NJOY-2016.35 without probability tables (modules RECONR and BROADR) and GAIA-2 without probability tables (module DOP). Other nuclides come from JEFF-3.2 processed by NJOY-2012.

Benchmark	PuMo-1.1	PuMo-1.2	PuMo-1.3	PuMo-2.1	PuMo-2.2	PuMo-2.3
NJOY_NOPT	1.23747	1.1998	1.18001	0.50571	0.53854	0.73330
pcm / NJOY	-2506	-404	-171	-3928	-3103	-1212
GAIA-2_NOPT	1.2373	1.19977	1.17994	0.50564	0.53831	0.73331
pcm / GAIA-2	-2353	-380	-164	-3575	-2889	-1139
pcm / NJOY_NOPT	-17	-3	-7	-7	-23	1
Benchmark	PuMo-3.1	PuMo-3.2	PuMo-3.3	PuMoZr.1	PuMoZr.2	PuMoZr.3
NJOY_NOPT	0.27832	0.29899	0.46132	0.13198	0.15422	0.32635
pcm / NJOY	-2704	-2438	-1456	-1124	-1048	-643
GAIA-2_NOPT	0.27831	0.29898	0.46139	0.13189	0.15425	0.32618
pcm / GAIA-2	-2466	-2244	-1376	-1034	-973	-638
pcm / NJOY_NOPT	-1	-1	7	-9	3	-17

Table 6.5: k_{eff} calculations performed with the IRSN Monte-Carlo code MORET-5.D for several fictitious benchmarks representative of La Hague operations at T=300K. Here, ^{96}Mo from JEFF-3.2 has been processed by NJOY-2016.35 without probability tables (modules RECONR, BROADR) and GAIA-2 without probability tables (module DOP). Other nuclides come from JEFF-3.2 processed by NJOY-2012.

range[21], as the differences with the complete NJOY and GAIA-2 cases are very important, especially for the Pu-Mo series. In order to get a better understanding of the effect of the unresolved resonance range processing, the probability tables of GAIA-2 have been used in replacement of the NJOY ones in the NJOY processing path, and benchmarks calculations performed. Results are stored in Table 6.6 and Table 6.7.

Benchmark	IMF-003	IMF-007	IMF-016	PMM-002-1	PMM-002-2
NJOY + PT_GAIA-2	1.00228	1.00408	0.99643	1.00034	0.99617
pcm / NJOY	1	-12	-15	5	-4

Table 6.6: k_{eff} calculations performed with the IRSN Monte-Carlo code MORET-5.D for several ICSBEP benchmarks at T=293.6K. IMF is an abbreviation for IEU-MET-FAST, and PMM for PU-MET-MIXED which are part of the TEX experiments. Here, ^{238}U and ^{239}Pu from JEFF-3.2 have been processed by a combination of NJOY-2016.35 with the probability tables of GAIA-2 (modules RECONR, BROADR and TOP). Other nuclides come from JEFF-3.2 processed by NJOY-2012.

It appears that the k_{eff} values do not change significantly when the tables of GAIA-2 are used in place of the NJOY tables in the NJOY flow. This is an important result, as it appears that the tables produced by GAIA-2 are close to the NJOY ones, and constitutes a reference validation for the calculation results that will be presented later.

The absolute differences with NJOY for all processings have been represented on Figure 6.6. In these figures, the actual computed k_{eff} values have been represented on the bottom right.

It is thus considered that the calculation of the reference tables in TOP and their integration in place of PURR's in the workflow of NJOY is validated. This bring two conclusions. First, the

---

[21]Actually, they have been selected for this reason.
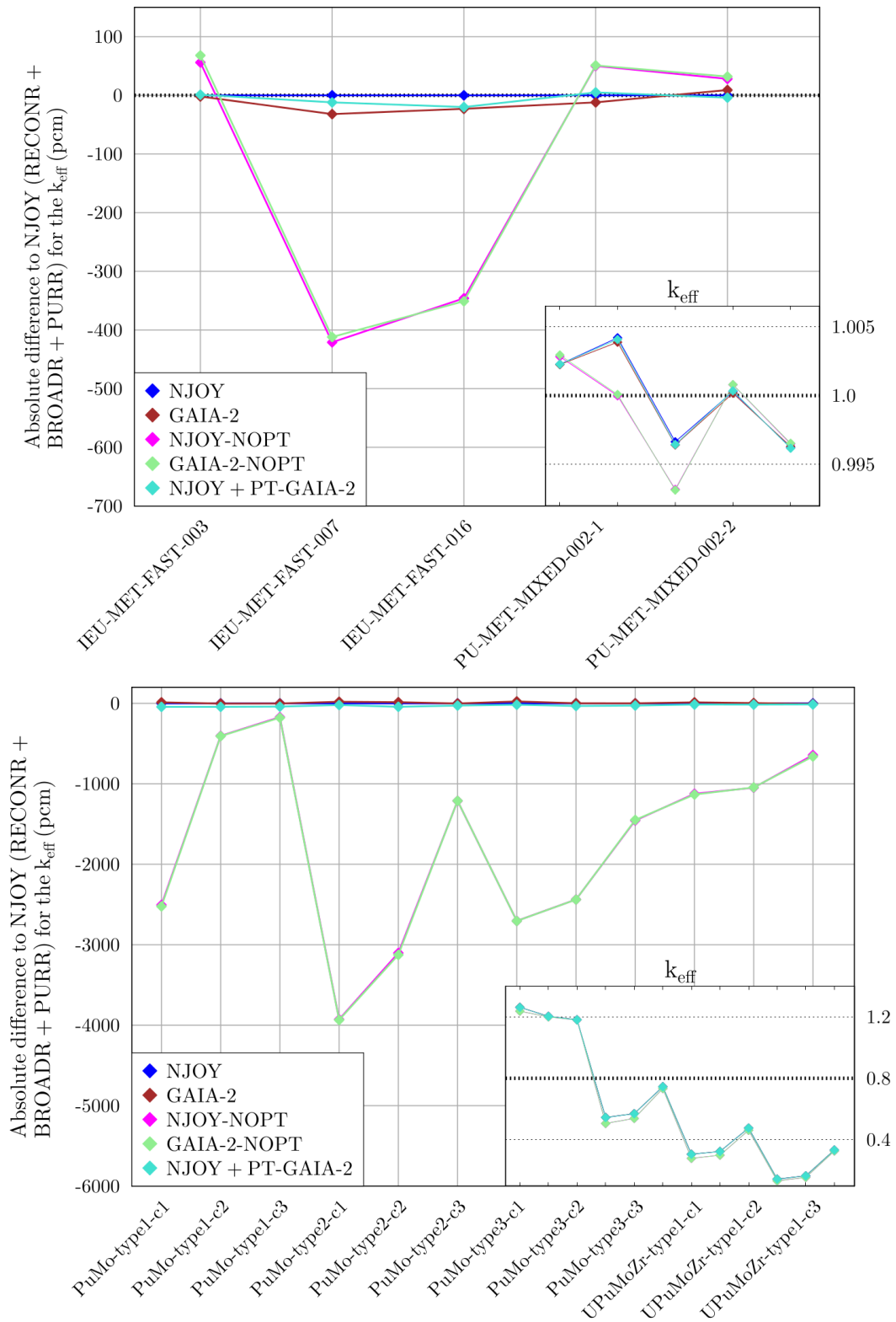
Figure 6.6: Absolute difference for the k_{eff} computed with MORET-5 for several processing of ^{238}U (IEU-MET-FAST benchmarks), ^{239}Pu (PU-MET-MIXED benchmarks) or ^{96}Mo (Pu-Mo series), between a full NJOY processing (RECONR + BROADR + PURR) and other processing paths. Figures on the bottom right display the raw k_{eff} values obtained for the benchmarks.

Benchmark	PuMo-1.1	PuMo-1.2	PuMo-1.3	PuMo-2.1	PuMo-2.2	PuMo-2.3
NJOY + PT_GAIA-2	1.2621	1.20341	1.18132	0.54479	0.56915	0.74515
pcm / NJOY	-43	-43	-40	-20	-42	-27
Benchmark	PuMo-3.1	PuMo-3.2	PuMo-3.3	PuMoZr.1	PuMoZr.2	PuMoZr.3
NJOY + PT_GAIA-2	0.30519	0.32305	0.47561	0.14308	0.16455	0.33265
pcm / NJOY	-17	-32	-27	-14	-15	-13

Table 6.7: k_{eff} calculations performed with the IRSN Monte-Carlo code MORET-5.D for several fictitious benchmarks representative of La Hague operations at T=300K. Here, ^{96}Mo from JEFF-3.2 has been processed by a combination of NJOY-2016.35 with the probability tables of GAIA-2 (modules RECONR, BROADR and TOP). Other nuclides come from JEFF-3.2 processed by NJOY-2012.

coupling is successful and can be used as a basis to test the impact in integral calculations of the several new procedures in the unresolved resonance range developed in this work. The second conclusion is related to the impact of the cross sections reconstruction in the ladder method. As a reminder, the only difference between NJOY and TOP implementations in this section lies during the reconstruction of cross sections step, just after the resonance ladder sampling. TOP only produces a single cross section value for each sampled ladder, whereas PURR computes each time a whole punctual cross section function on a grid around the reference energy as described in Listing 5.1, and stores all the calculated cross sections. As both cross section distributions match and integral calculations too, this seems to indicate that both methods provide the same results.

In the following, the probability tables will be computed with TOP, relying on several methods developed in this thesis which differ from the reference implementation. They will be included in the NJOY processing in order to investigate a potential impact on the k_{eff} integral calculations.

6.3 Modified procedures in the unresolved resonance range

6.3.1 Probability tables construction

The first investigated modified procedure in the unresolved resonance range is related to the form of the produced probability tables. For the nuclides ^{238}U, ^{239}Pu, and ^{96}Mo, the probability tables of GAIA-2 have been computed according to the several methods presented in Chapter 5, and integrated in the NJOY-processed files (obtained after the use of RECONR + BROADR modules). The considered methods of probability tables construction are equiprobable, k-means, k-medians, NJOY-like, and logarithmic. All the tables have been built with 20 bins. In order to get a reference to compare the calculations results, equiprobable tables with 1000 bins have been also produced. These latter tables fit the cross section distributions with more points, and we believe they may constitute a more accurate result than all the other methods.

The same set of benchmarks as in the previous subsection has been used with MORET to compute k_{eff} values with a statistical uncertainty of 5 pcm. The different computed values have been stored in Table 6.8 and Table 6.9 along with the difference (in pcm) with the results obtained with the use of 1000-bins equiprobable tables. The k_{eff} variations have also been represented on Figure 6.7 for all benchmarks.

Several comments can be made about these results. One of the most important features is

Benchmark	IMF-003	IMF-007	IMF-016	PMM-002-1	PMM-002-2
Equip.-1000	1.00227	1.00415	0.99649	1.00032	0.99625
NJOY-like	1.00228	1.00408	0.99644	1.00034	0.99617
pcm / Equip-1000	1	-7	-5	2	-8
Equip.	1.00223	1.00412	0.99650	1.00024	0.99618
pcm / Equip-1000	-4	-3	1	-8	-7
K-means	1.00218	1.00455	0.99703	1.00016	0.99614
pcm / Equip-1000	-9	40	54	-16	-11
K-medians	1.00234	1.00446	0.99693	1.00033	0.99628
pcm / Equip-1000	7	31	44	1	3
Logarithmic	1.00229	1.00210	0.99457	1.00024	0.99616
pcm / Equip-1000	2	-205	-192	-8	-9

Table 6.8: k_{eff} for ICSBEP benchmarks with Monte-Carlo code MORET-5.D, for several methods of probability tables construction.

that the k-means and k-medians methods provide higher k_{eff} values than all the other ones[22], except logarithmic which is known to be the less precise. On the other hand, the smallest k_{eff} are obtained with NJOY-like probability tables. Equiprobable tables stand in-between. The 1000 bins and 20 bins outcomes remain close to each other, even if adding bins in the equiprobable tables seems to slightly reduce the computed k_{eff} values. Taking the 1000-bins equiprobable outcome as a reference yields the very symmetrical aspect of Figure 6.7. Let us mention that all these remarks are true for all the considered benchmarks, except for the PU-MET-MIXED-002 series and IEU-MET-FAST-003. For these latter ones, the differences between the computed k_{eff} remain in the statistical uncertainty of the Monte-Carlo calculations which is 5 pcm. Actually, these benchmarks were already the less sensitive to probability tables as shown in previous subsection. As a consequence, conclusions cannot be drawn for these benchmarks from the probability tables construction aspect, and all comments made in this subsection do not apply to them.

The diverse methods of probability tables construction yield increasing k_{eff} values in next order: NJOY-like, equiprobable, k-medians, and k-means tables. This observation is only true for the benchmarks considered, but it seems an important issue. In particular, it may seem surprising that the NJOY and k-clustering tables display an opposite behavior compared to the equiprobable table, according to the reasons detailed in the previous chapter. It has been mentioned that both methods well describe the cumulative and in particular the right tail, at least better than the equiprobable method does. The main difference is that more points are provided to describe the left tail of the cumulative with the NJOY method. This latter reason could maybe explain the difference between the methods. Indeed the k-means method and the k-medians method – even if it is less marked – do not deal with the left tail of the cross section distributions accurately, and dedicate more attention to the bins with the higher variance. These methods do not treat mre consistently the left part of skewed distributions (like ^{156}Eu in previous chapter, and ^{96}Mo in the present case) than an equiprobable binning does. This fact might explain the higher k_{eff} values found with the k-medians and k-means methods.

To support this idea, one may note that the introduction of additional bins in the equiprobable tables systematically reduces the k_{eff}. Incidentally, more bins result in a better fit of the left tail. Moreover, for IEU-MET-FAST-007 and IEU-MET-FAST-016, the 1000-bins equiprobable

---

[22]To be slightly more precise the k-means method provides even greater values.

Benchmark	PuMo-1.1	PuMo-1.2	PuMo-1.3	PuMo-2.1	PuMo-2.2	PuMo-2.3
Equip.-1000	1.26350	1.20405	1.18178	0.54622	0.57056	0.74577
NJOY-like	1.26210	1.20341	1.18132	0.54479	0.56915	0.74515
pcm / Equip-1000	-140	-64	-46	-143	-141	-62
Equip.	1.26352	1.20416	1.18184	0.54639	0.57075	0.74601
pcm / Equip-1000	2	11	6	17	19	24
K-means	1.2645	1.20426	1.18193	0.54787	0.57173	0.74628
pcm / Equip-1000	100	21	15	165	117	51
K-medians	1.26405	1.20412	1.18193	0.54702	0.57128	0.74615
pcm / Equip-1000	55	7	15	80	72	38
Logarithmic	1.26484	1.20446	1.18211	0.54827	0.57214	0.74654
pcm / Equip-1000	134	41	33	205	158	77
Benchmark	PuMo-3.1	PuMo-3.2	PuMo-3.3	PuMoZr.1	PuMoZr.2	PuMoZr.3
Equip.-1000	0.30624	0.32422	0.47641	0.14367	0.16511	0.33305
NJOY-like	0.30519	0.32305	0.47561	0.14308	0.16455	0.33265
pcm / Equip-1000	-105	-117	-80	-59	-56	-40
Equip.	0.30627	0.32426	0.47661	0.14372	0.16521	0.3332
pcm / Equip-1000	3	4	20	5	10	15
K-means	0.30729	0.32496	0.47683	0.14404	0.16549	0.33336
pcm / Equip-1000	105	74	42	37	38	31
K-medians	0.30682	0.32449	0.4768	0.14389	0.1653	0.3332
pcm / Equip-1000	58	27	39	22	19	15
Logarithmic	0.30777	0.32535	0.47708	0.14425	0.16569	0.33343
pcm / Equip-1000	153	113	67	58	58	38

Table 6.9: k_{eff} for Pu-Mo benchmarks with Monte-Carlo code MORET-5.D, for several methods of probability tables construction.

tables provide smaller k_{eff} values than the NJOY binning. Actually, for a non-skewed case such as ^{238}U, an equiprobable binning with many points may better explore the left tail than the NJOY binning, which could explain this result.

It appears on these examples that more bins in the left tail of the cross section distributions might provide smallest values of the k_{eff}. The NJOY-like tables provide a good exploration of this zone. However, the comparison with the 1000-bins equiprobable tables, seen as a "reference" calculation, seems to indicate that the k_{eff} values computed from NJOY-like tables are underestimated for the Pu-Mo series. This is an issue in particular from a criticality safety point of view. In fact the k-medians method yields results closer to the reference 1000-bins equiprobable outcome, and should maybe be preferred. Taking this approach, the equiprobable tables seem even better.

The main issue with this whole analysis is probably that it is only performed on the k_{eff} while other quantities could be relevant. In particular, considering the neutron flux would be interesting, as it is directly related to the reaction rates. k_{eff} remains a crucial quantity in criticality safety analysis though, and it seems natural to calibrate tables according to it. In
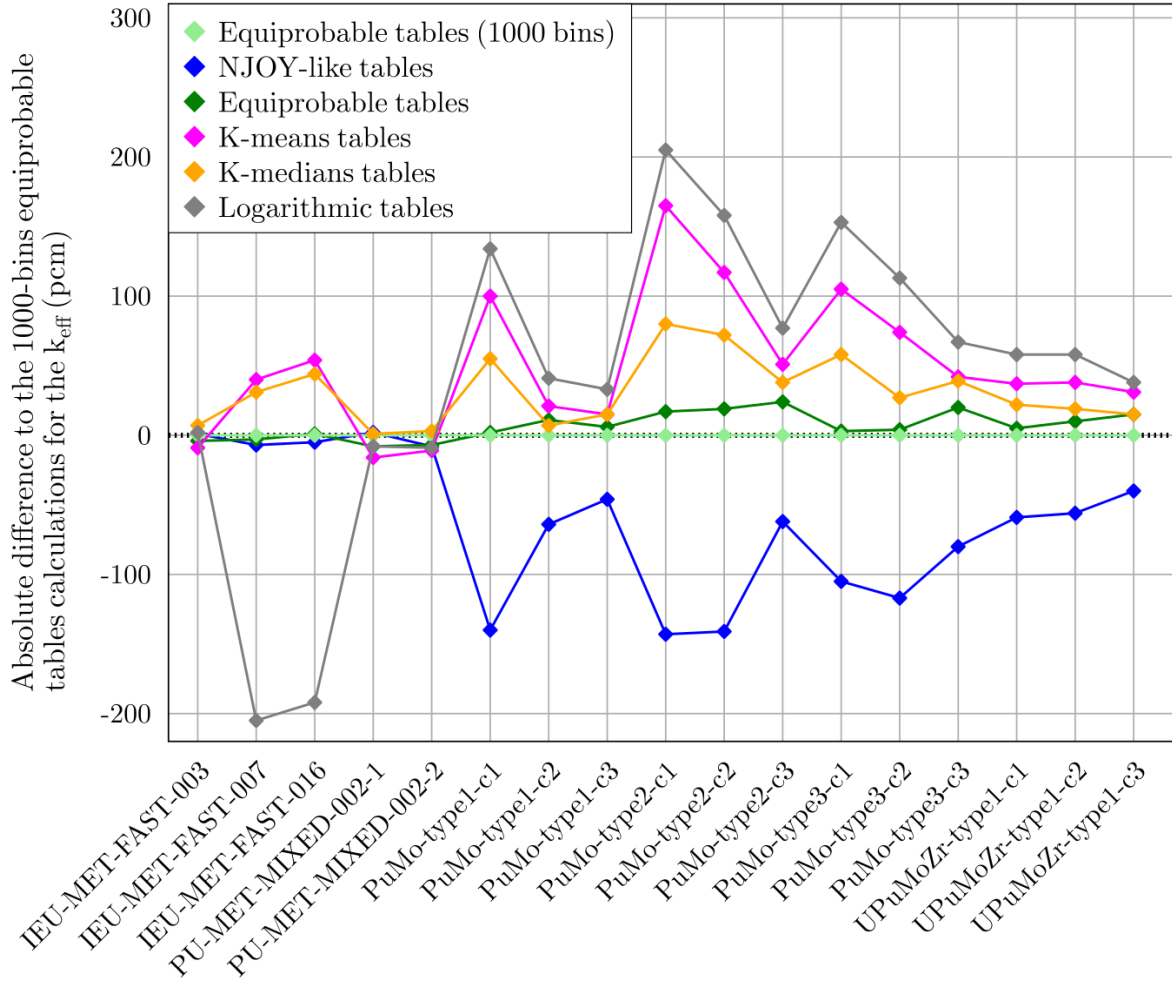
Figure 6.7: Absolute difference for the k_{eff} computed with MORET-5 for the benchmarks of interest when probability tables are computed with a 1000-bins equiprobable method, or other methods with only 20 bins. The results are provided for the 3 IEU-MET-FAST benchmarks (reprocessing of ^{238}U), the 2 benchmarks of the PM-MET-MIXED series (reprocessing of ^{239}Pu), and the 12 benchmarks of the Pu-Mo series (reprocessing of ^{96}Mo).

particular, all the previous considerations should force us to revise the conclusions of the previous chapter about the best choices of the tables.

Indeed, devoting more or less attention to the diverse parts of the cross section distribution seems to have a direct influence on the k_{eff}. In such conditions, the best option would probably be to dedicate the same level of attention everywhere, and the simplest option to reach this goal is to raise the number of bins in the probability tables. This constitutes a major change compared to the prerequisites of the previous chapter, where the number of bins was fixed to 20 not to slow down the Monte-Carlo computations. The integral calculations performed, and the manifest disagreements between the methods seem to prove that the number of bins has to be increased.

If the number of bins is increased however, the default method could become the equiprobable binning. Indeed, with this method, the Monte-Carlo codes could avoid implementing a comparison routine at the bin selection step, and thus get faster. As a consequence, the increase in the number of bins would not result in a major loss in speed calculations.

All theses discussions about the form of the probability tables will be tackled once more in the paragraph about the choice of the reference energy mesh, in Section 6.3.3. Let us now focus on another point of interest, namely the influence of correlating the resonance spacings during

the sampling of resonance ladders.

6.3.2   Correlated resonance spacings

Benchmark calculations have been used in this work to estimate the influence of the resonance spacings correlations in the ladder method. GAIA-2 probability tables for each nuclide have been produced using ladders composed of correlated resonance spacings from the GOE, before being integrated in the NJOY processed files (issued from RECONR + BROADR). Several processings have been performed. GOE eigenvalues have been unfolded using the exact tabulated method introduced in this work in Section 4.2.1 and with the more conventional asymptotic method that relies on the cumulative of the Wigner semi-circle law. Both methods have been used to produce NJOY-like and 1000-bins equiprobable tables. K-medians probability tables relying on correlated resonance spacings with an exact tabulated unfolding have been produced too. The computed k_{eff} for the benchmarks used until now are shown in Table 6.10 and Table 6.11. The difference (in pcm) with an equivalent processing but using uncorrelated resonance spacings is presented in Figure 6.8.

Benchmark	IMF-003	IMF-007	IMF-016	PMM-002-1	PMM-002-2
Tabulated exact unfolded – NJOY tables	1.00224	1.00392	0.99634	1.00028	0.99624
pcm / Uncorrelated	-4	-16	-10	-6	7
Asymptotic unfolded – NJOY tables	1.00225	1.00391	0.99639	1.00031	0.99629
pcm / Uncorrelated	-3	-17	-5	-3	12
pcm / Tab. ex. unfolded	1	-1	5	3	5
Tabulated exact unfolded – Equiprobable-1000 tables	1.00226	1.00416	0.99647	1.00026	0.99623
pcm / Uncorrelated	-1	1	-2	-6	-2
Asymptotic unfolded – Equiprobable-1000 tables	1.00225	1.00400	0.99650	1.00028	0.99622
pcm / Uncorrelated	-2	-15	1	-4	-3
pcm / Tab. ex. unfolded	-1	-16	3	2	-1
Tabulated exact unfolded – k-medians tables	1.00235	1.00431	0.99663	1.00037	0.99620
pcm / Uncorrelated	1	-15	-30	4	-8

Table 6.10: k_{eff} for ICSBEP benchmarks with Monte-Carlo code MORET-5.D, in case the resonance spacings are or not correlated. Three methods of probability tables construction have been considered, and for NJOY-like and 1000-bins equiprobable tables, two methods of eigenvalues unfolding (cf. Section 4.2.1).

Several comments can be made from these results. First of all, correlating the resonance spacings seems to have a small impact for the computed k_{eff} for IEU-MET-FAST and PU-MET-MIXED-002 benchmarks. In most cases, the k_{eff} seems to be reduced compared to the uncorrelated case. On the other hand, the impact is much bigger for the Pu-Mo series[23], and correlated spacings tend to produce higher k_{eff}.

The most significant observed fact is the weaker variation from the uncorrelated case when probability tables are built from the k-medians or 1000-bins method rather than the NJOY

---

[23]Again, this is mainly due to the fact that these benchmarks are more sensitive to the probability tables.

Benchmark	PuMo-1.1	PuMo-1.2	PuMo-1.3	PuMo-2.1	PuMo-2.2	PuMo-2.3
Tabulated exact unfolded – NJOY tables	1.26342	1.20408	1.18189	0.54621	0.57049	0.74582
pcm / Uncorrelated	132	67	57	142	134	67
Asymptotic unfolded – NJOY tables	1.26353	1.20411	1.18184	0.54639	0.57076	0.74593
pcm / Uncorrelated	143	70	52	160	161	78
pcm / Tab. ex. unfolded	11	3	-5	18	27	11
Tabulated exact unfolded – Equiprobable-1000 tables	1.26368	1.20412	1.18188	0.54647	0.57081	0.74594
pcm / Uncorrelated	18	7	10	25	25	17
Asymptotic unfolded – Equiprobable-1000 tables	1.26392	1.20412	1.18191	0.54684	0.57109	0.74610
pcm / Uncorrelated	42	7	13	62	53	33
pcm / Tab. ex. unfolded	24	0	3	37	28	16
Tabulated exact unfolded – k-medians tables	1.26448	1.20417	1.18194	0.54743	0.57153	0.74651
pcm / Uncorrelated	43	5	1	41	25	36
Benchmark	PuMo-3.1	PuMo-3.2	PuMo-3.3	PuMoZr.1	PuMoZr.2	PuMoZr.3
Tabulated exact unfolded – NJOY tables	0.30626	0.32409	0.47646	0.14353	0.16509	0.33305
pcm / Uncorrelated	107	104	85	45	54	40
Asymptotic unfolded – NJOY tables	0.30633	0.32426	0.47643	0.14361	0.16513	0.33309
pcm / Uncorrelated	114	121	82	53	58	44
pcm / Tab. ex. unfolded	7	17	-3	8	4	4
Tabulated exact unfolded – Equiprobable-1000 tables	0.30662	0.32436	0.47656	0.14364	0.16506	0.33314
pcm / Uncorrelated	38	14	15	-3	-5	9
Asymptotic unfolded – Equiprobable-1000 tables	0.30683	0.32458	0.47678	0.14378	0.16531	0.33323
pcm / Uncorrelated	42	7	13	62	53	33
pcm / Tab. ex. unfolded	21	22	22	14	25	9
Tabulated exact unfolded – k-medians tables	0.30721	0.32497	0.47721	0.14397	0.16537	0.33338
pcm / Uncorrelated 59	36	37	11	20	18	

Table 6.11: k_{eff} for Pu-Mo benchmarks with Monte-Carlo code MORET, in case the resonance spacings are or not correlated. Three methods of probability tables construction have been considered, and for NJOY-like and 1000-bins equiprobable tables, two methods of eigenvalues unfolding (cf. Section 4.2.1).

method. According to what has been said in Chapter 4, the variance of the distribution is slightly reduced by taking into account the resonance correlations. Tails are thus less extreme.
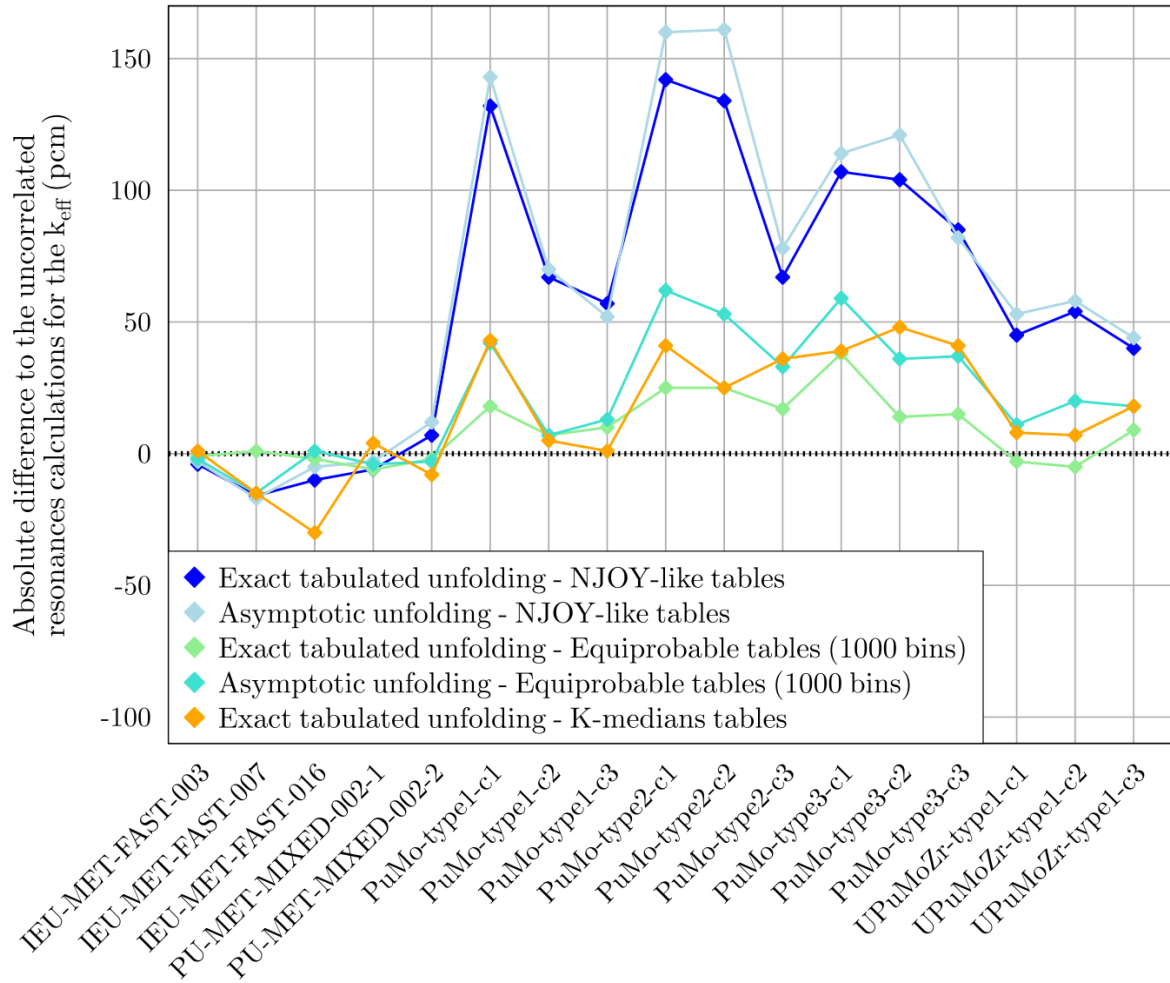
Figure 6.8: Absolute difference for the k_{eff} computed with MORET-5.D for the benchmarks of interest when resonance spacings are or not correlated. The results are displayed when probability tables are built according to the NJOY, 1000-bins equiprobable or k-medians method. In the former cases, the results for two methods of unfolding are shown. The results are provided for the 3 IEU-MET-FAST benchmarks (reprocessing of ^{238}U), the 2 benchmarks of the PM-MET-MIXED series (reprocessing of ^{239}Pu), and the 12 benchmarks of the Pu-Mo series (reprocessing of ^{96}Mo).

As k-medians tables less describe the tails of the distributions than the NJOY-like tables, they are actually less sensitive to the changes induced in the cross sections distributions. This remark seems true for all the benchmarks of the Pu-Mo series, and thus for the relatively skewed isotope ^{96}Mo. In any case, correlating the resonance spacings seems to have an impact on the integral calculations. As more physics is embedded in these latter ones, systematically correlating the resonance spacings appears like the way to go.

The other most interesting feature of Figure 6.8 is the close agreement between the outcomes obtained with the asymptotic or tabulated exact unfolding. The maximum of disagreement is of 37 pcm only in case of 1000-bins equiprobable tables, for PuMo-type2-c1 benchmark, which is the most sensitive to the probability tables. As a consequence it looks like the use of the tabulated exact unfolding method developed in Section 4.2.1 is still preferable, but relying on the cumulative of the Wigner semi-circle law appears reasonable.

6.3.3 Choice of the reference energy grid

The last point tackled in this section concerns the choice of the reference energy mesh across the unresolved resonance range. Three possible choices have been presented in Section 6.1.2: keeping the initial ENDF energy mesh, adopting the NJOY approach by adding several pretabulated energies, or computing the probability tables on an averaged-linearized grid. This latter method relies on the Hauser-Feschbach formalism to create the reference energy grid. The resulting meshes are usually thinner than the NJOY or ENDF ones, and more coherent with the average cross section values provided in the MF3 part of the PENDF file. In order to investigate the impact of the reference energy grid the processing of the nuclides of interest has been performed with the NJOY code (use of RECONR + BROADR), and probability tables from TOP have been added to the files, like in previous analyses about the probability tables form and resonances correlations. These tables have been produced on the averaged-linearized energy grid. Several probability tables construction methods have been used. Then, ACE files have been produced with the ACER module from NJOY, and k_{eff} computed with MORET-5.D with a statistical uncertainty of 5 pcm for all benchmarks presented in Section 6.2.1. These k_{eff} values are shown in Table 6.12 and Table 6.13. The differences with the k_{eff} obtained on the NJOY reference energy mesh (each time comparing probability tables built with the same method) have been displayed on Figure 6.9.

Benchmark	IMF-003	IMF-007	IMF-016	PMM-002-1	PMM-002-2
Linearized mesh NJOY tables	1.00224	1.00408	0.99638	1.00038	0.99627
pcm / NJOY mesh	-4	0	-6	4	10
Linearized mesh Equip. tables	1.00227	1.00428	0.99661	1.00034	0.99623
pcm / NJOY mesh	4	16	11	10	5
Linearized mesh Equip. tables (1000 bins)	1.00221	1.00414	0.99657	1.00031	0.99627
pcm / NJOY mesh	-6	-1	8	-1	2
Linearized mesh K-medians tables	1.00222	1.00427	0.99680	1.00028	0.99634
pcm / NJOY mesh	-12	-19	-13	-5	6

Table 6.12: k_{eff} for ICSBEP benchmarks computed with the Monte-Carlo code MORET-5.D when the reference energy mesh in the URR is a linearized grid.

Let us note that an impact due to the choice of the reference energy mesh is quite visible for the Pu-Mo series – and thus for the processing of ^{96}Mo – and not much for the ICSBEP benchmarks. Moreover, and as in the previous discussion about resonance spacings correlations, the results seem to highly depend on the method employed to build the probability tables. Indeed, they do not change much when equiprobable probability tables are used. On the other hand, providing a thinner reference energy mesh yields a consequent variation for the computed k_{eff} when k-medians or NJOY-like probability tables are used.

A very important feature is the fact that k-medians-yielded k_{eff} are lowered by using a thinner mesh, while NJOY ones are increased, and equiprobable ones remain constant. Considering Figure 6.9 the resulting k_{eff} produced by different probability tables methods seem to get closer when the reference energy mesh gets thinner. These results are displayed on Figure 6.10, which is exactly the same as[24] Figure 6.7[25] except that the calculations have been performed on an averaged-linearized reference energy mesh rather than on the usual NJOY-like mesh [26].

---

[24]Except for the k-means and logarithmic methods which are not displayed.
[25]Which compared to the 1000-bins equiprobable tables the outcomes of the other methods of construction.
[26]The same scale has even been kept on the y-axis for both figures.

Benchmark	PuMo-1.1	PuMo-1.2	PuMo-1.3	PuMo-2.1	PuMo-2.2	PuMo-2.3
Linearized mesh NJOY tables	1.26333	1.20394	1.18190	0.54562	0.57019	0.74568
pcm / NJOY mesh	123	53	58	83	104	53
Linearized mesh Equip. tables	1.26377	1.20404	1.18185	0.54618	0.57086	0.74606
pcm / NJOY mesh	25	-12	1	-21	11	5
Linearized mesh Equip. tables (1000 bins)	1.26337	1.20402	1.18180	0.54619	0.57056	0.74587
pcm / NJOY mesh	-13	-3	2	-3	0	10
Linearized mesh K-medians tables	1.26365	1.20413	1.18196	0.54638	0.57073	0.74593
pcm / NJOY mesh	-40	1	3	-64	-55	-22
Benchmark	**PuMo-3.1**	**PuMo-3.2**	**PuMo-3.3**	**PuMoZr.1**	**PuMoZr.2**	**PuMoZr.3**
Linearized mesh NJOY tables	0.30599	0.32383	0.47620	0.14345	0.16509	0.33299
pcm / NJOY mesh	80	78	59	37	54	34
Linearized mesh Equip. tables	0.30640	0.32437	0.47668	0.14371	0.16517	0.33322
pcm / NJOY mesh	13	11	7	-1	-4	2
Linearized mesh Equip. tables (1000 bins)	0.30636	0.32417	0.47652	0.14363	0.16515	0.33302
pcm / NJOY mesh	12	-5	11	-4	4	-3
Linearized mesh K-medians tables	0.30635	0.32421	0.47647	0.14368	0.16518	0.33321
pcm / NJOY mesh	-47	-28	-33	-21	-12	1

Table 6.13: k_{eff} for Pu-Mo benchmarks computed with the Monte-Carlo code MORET-5.D when the reference energy mesh in the URR is a linearized grid.

It turns out that providing a thinner mesh effectively reduces the discrepancies between the several methods of probability table computations. The overall behavior of the diverse methods remains true, as NJOY-like tables still provide smaller k_{eff} than the other methods, and k-medians tables still issue higher k_{eff} values than the 1000-bins equiprobable reference. However, all results are closer to the equiprobable results, which remain close to the results obtained on the NJOY-like reference energy mesh.

This substantial difference between the NJOY-like mesh and the averaged-linearized one is only due to the addition of reference energies at which probability tables are computed to describe the cross sections across the unresolved resonance range. Let us underline that these tables are built on the basis of the provided evaluated average resonance parameters, interpolated at the said energies. As a consequence, providing such additional probability tables in the unresolved resonance range cannot deteriorate the quality of the results[27]. As a consequence, the present results on the linearized grid should be considered more accurate than the ones using the NJOY grid. This is corroborated by the fact all probability tables methods provide more equivalent results.

From this analysis, a conclusion and a sketch of explanation can be drawn. First, it seems useful to provide probability tables on an extended number of reference energies – relying on the interpolation of average resonance parameters – to simply get better results. It even seems

---

[27]The question is rather related to performance, and usefulness of computing additional probability tables in the unresolved resonance range.
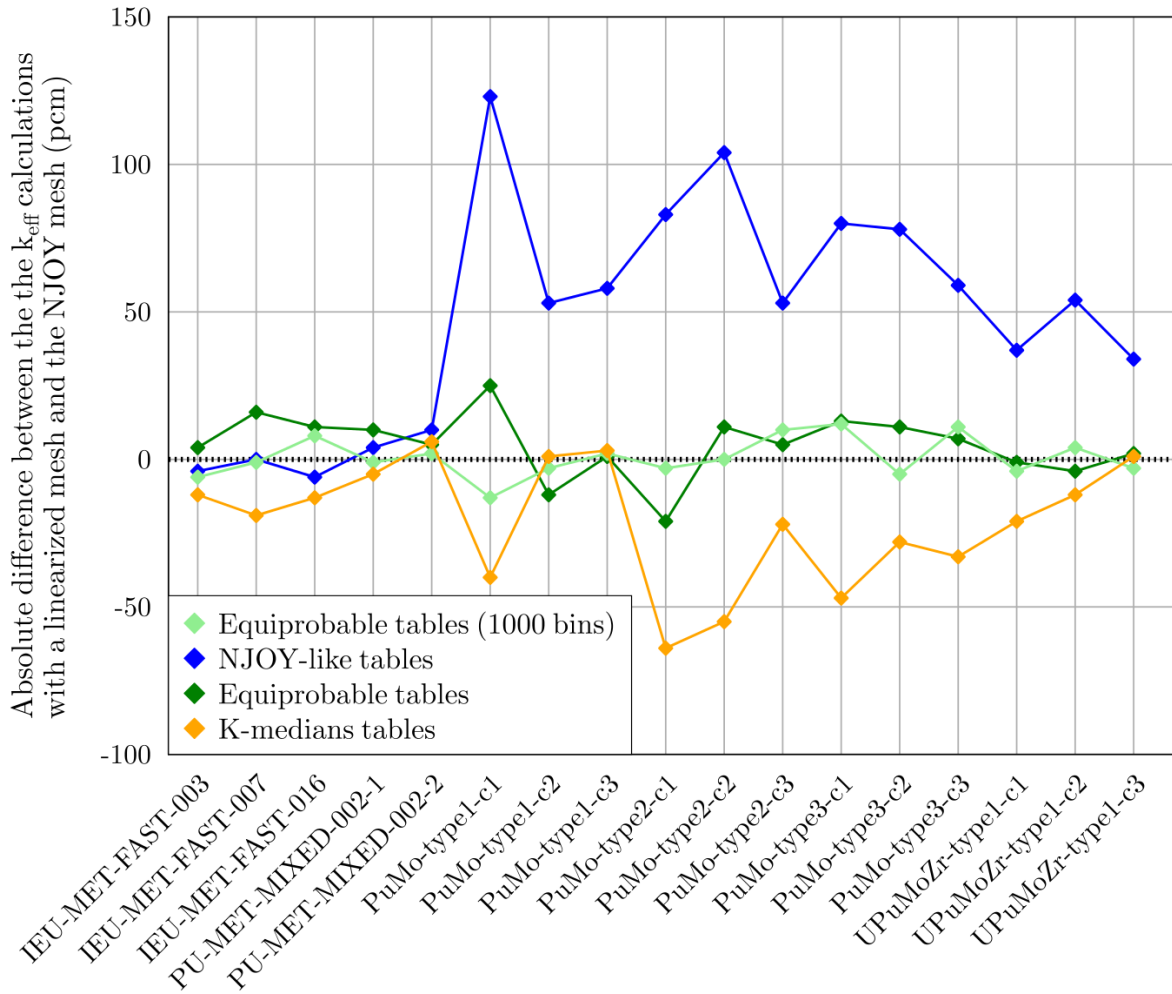
Figure 6.9: Absolute variation of the k_{eff} computed with MORET-5 for the benchmarks of interest when the reference energy mesh is linearized rather than following the NJOY method. The results are displayed when probability tables are built according to the several methods of probability table construction. The results are provided for the 3 IEU-MET-FAST benchmarks (reprocessing of ^{238}U), the 2 benchmarks of the PU-MET-MIXED series (reprocessing of ^{239}Pu), and the 12 benchmarks of the Pu-Mo series (reprocessing of ^{96}Mo).

that the few energies added by NJOY are not enough, and the linearization of the average cross sections looks like a better approach. Secondly, the poorer results observed on the NJOY mesh must be related to the interpolation of probability tables when a cross section value is required between two provided tables. As said in Section 6.1.2, the interpolation of cross sections bins relies on the assumption that the cross section distributions are slowly-varying function of the energy, so that tables are actually close to each other. From the integral results performed, it looks like this assumption does not hold especially for methods that dedicate much attention to the tails of the distributions like the NJOY and k-medians methods.

Let us finally highlight that the equiprobable probability tables are the less impacted by the choice of the reference mesh, mainly because all the central values are not high-variance zones. This fact seems to be a determinant argument to drop the 20-bins NJOY-like and k-clustering tables in favor of large (and even very large) equiprobable tables, that Monte-Carlo can use to directly sample cross section values.
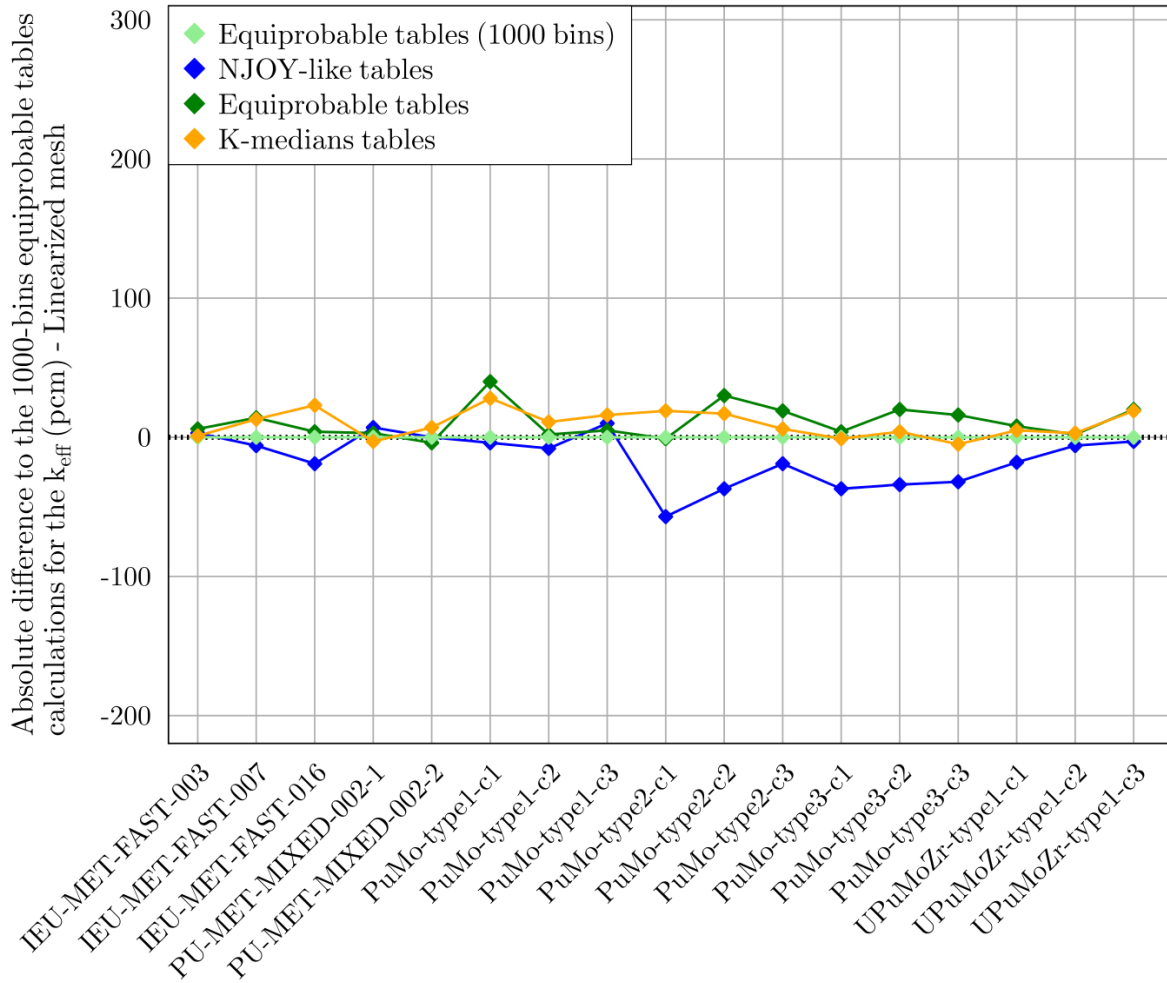
Figure 6.10: Absolute difference for the k_{eff} computed with MORET-5.D for several benchmarks, between 1000-bins equiprobable probability tables and the other methods of construction with 20 bins. The reference energy mesh is linearized across the URR, contrary to the results of Figure 6.7 which used a NJOY-like energy mesh.

Conclusion of the chapter

This chapter aimed at describing the integration of the methods developed in the precedent chapters to treat the unresolved resonance range into the workflow of the processing codes. Our current practice is to embed the computed probability tables in a PENDF file which contains the linearized broadened cross sections. Then, the NJOY module ACER is utilized to convert this PENDF file into an ACE file usable by Monte-Carlo codes MORET-5.D and MCNP-6.2 for neutronics applications. All the developments have been integrated in an independent C++ module named TOP which is now part of the IRSN processing system GAIA-2. All methods and parameters of the probability tables construction, among which the nature of the tables, the number of Monte-Carlo iterations or resonances to consider in the ladders, the possibility to correlate the resonances spacings during the ladders construction and the unfolding techniques to apply, are controlled from a single YAML-formatted input text file. Moreover, the current use of PENDF files between the modules enables an easy connection with NJOY, useful to cross check the results of the several methods. All the methods are thus easily understandable and usable by a third-party user that would wish to use the GAIA-2 probability tables produced by the TOP module. It must be underlined that this development part remains an important element of this PhD work. The integration of the TOP module in the GAIA-2 system has been

tested by cross-checking the obtained results with NJOY on integral calculations. To do so, a set of benchmarks was retained, among which three benchmarks of the IEU-MET-FAST series of the international criticality benchmarks reference ICSBEP, two of the recent TEX experiments which have been submitted to the ICSBEP under the denomination PU-MET-MIXED-002, and twelve benchmarks from the "Pu-Mo series". These latter ones are artificial benchmarks developed at IRSN some years ago to be sensitive to the probability tables, and are representative of some facilities of the French La Hague recycling plant. These benchmarks have been modeled with the IRSN Monte-Carlo code MORET-5.D to compute k_{eff} with a statistical uncertainty of 5 pcm. The input ACE files for each nuclide have been processed by NJOY, GAIA-2, and a combination of both codes for cross-checking purposes. The considered nuclides are ^{238}U, ^{239}Pu, and ^{96}Mo, quite used in the nuclear industry.

In a first step of validation, the TOP probability tables have been constructed to mimic the NJOY ones. The ladder method has been adjusted on the basis of the work carried in Chapter 3 to produce ladders large enough to provide correct cross section distributions. The resonances were uncorrelated, and the tables have been built according to the NJOY method. At this stage, the only important difference between the two methods took place at the cross section calculation step. TOP only computes a single cross section value for each resonance ladder, whereas NJOY reconstructs a complete punctual cross section in the vicinity of the reference energy on a relatively large energy grid, and stores all values. A direct comparison between the TOP and NJOY cross section sampled distributions and probability tables showed a good agreement between both implementations. One must underline that this constitutes an important result actually. As all steps of the methods are the same except the cross sections reconstruction, this indicates that computing a punctual cross section around the reference energy like NJOY does is a legitimate way of proceeding.

The produced tables have been integrated in the NJOY processed files containing the linearized broadened cross sections (use of modules RECONR + BROADR), and the corresponding files processed by GAIA-2 (use of module DOP). Tables issued from a complete NJOY processing have also been produced. This operation has been performed for all three selected nuclides. The aforementioned benchmarks have been run with MORET-5.D, and corresponding k_{eff} values retrieved. The results showed a good agreement, which constituted a first step of validation of the probability table implementation in TOP.

Once the probability tables implementation in the processing codes was proved successful, modified tables have been produced by TOP to estimate the impact of the new methods developed in this thesis on integral calculations. The choice has been made to integrate TOP probability tables in the NJOY processing flow. The first comparison aimed at estimating the impact of the method of probability tables construction. Thus, 20-bins tables have been built according to the methods developed in Chapter 5, and compared to a reference calculation made with 1000-bins equiprobable tables. These latter are supposed to be more precise because the number of bins is increased and thus detail more accurately the distributions. On most benchmarks, and especially the ones from the Pu-Mo series, the NJOY-like tables seem to provide much smaller k_{eff} than the equiprobable reference. In the same time, k-means and k-medians tables provide overestimated values for the k_{eff}. NJOY and k-clustering methods have thus opposite behavior compared to the equiprobable reference. A potential explanation is that the left tail of the distribution is poorly represented in the k-clustering methods. In the meantime, the NJOY tables provide too small values. As a consequence, the same amount of detail should probably be dedicated to all parts of the distribution, and it seems nor the k-clustering nor the NJOY empirical methods provide sufficiently good results with only 20 bins. In that context, the best option is probably to increase the number of bins in the tables. In order not to slow down the Monte-Carlo computations – which was the main objective of keeping a number of bins rather low – we highly suggest that the Monte-Carlo codes adapt their implementations to use large sized equiprobable tables, and take advantage of the direct access to bin values provided by the equiprobable binning. This idea is even supported by the fact memory storage is not a

real issue anymore, and large tables can be efficiently stored in the cache of recent computers.

The second development tested in this chapter concerned the use of correlated resonance spacings. The benchmark integral calculations seemed to provide two relevant conclusions. First of all, the two unfolding methods presented in Chapter 4 provide roughly equivalent results. If the exact tabulated method seems to be the way to go, the usual use of the cumulative of the asymptotic Wigner semi-circle law for the unfolding may remain acceptable. Secondly, the effect of the correlation seemed more marked for NJOY-like tables than k-medians and 1000-bins equiprobable tables. As the former better describe the tails of the distribution, the impact of the resonance spacings correlation is actually significant in these parts. This is in agreement with the conclusions of Chapter 4. As the resonance ladders using correlated spacings are more physical, it is believed correlating the resonances should be used systematically in the framework of the ladder method.

Finally, a last question has been treated in the chapter, which appeared to be of particular importance. This is the problem of the reference energy mesh on which probability tables have to be computed, and provided to the Monte-Carlo codes. The considered codes actually rely on the interpolation of cross section values from the probability tables around the energy for which they need a cross section. This interpolation should be handled carefully, and necessarily introduces an error. This error is supposed to be negligible if the tables only slightly differ across the unresolved resonance range. In fact, as average resonance parameters can be interpolated at any energy in the unresolved resonance range from the evaluated resonance parameters, probability tables can be computed at any energy in the range. In any case, it seems more physical to interpolate resonance parameters rather than cross sections, and the choice of the output reference energy mesh can be discussed. Three possibilities have been dealt with in this work: the initial ENDF reference energies, the NJOY mesh as the code actually adds some pre-tabulated reference energies under some conditions, and an *averaged-linearized* grid in the unresolved resonance range. For this latter, the idea is to provide a linearized grid for the cross sections in the unresolved resonance range, like in the resolved resonance range. The grid is computed there for the average cross sections, calculated with the Hauser-Feschbach formalism. The technique to compute such a mesh is a simple linearization algorithm, which can be adapted from the resolved range practices. These meshes are thinner than the ENDF and NJOY ones, and more coherent with the usual produced average cross sections in the MF3 section of the PENDF file.

k_{eff} computations with MORET-5.D have been performed for the several probability tables construction methods. The results compared to the NJOY mesh indicates a change for the NJOY and k-clustering tables, while equiprobable results remain roughly the same. A closer look reveals however that using a thinner reference energy mesh shifted the results for all probability tables construction method closer to the reference many-bins equiprobable calculations. In other words, the results match much better between all probability tables construction methods when the reference energy mesh is thinner. This constitutes a strong result, as it seems to indicate that the discrepancies between the several probability tables methods are due to interpolation errors. In other words, the assumption that cross section distributions and probability tables are slowly varying quantities as a function of the energy does not hold. The use of a thin reference energy mesh seems thus preferable. Moreover, as the equiprobable tables can be used smartly in Monte-Carlo codes, this reinforces the idea that these tables are the more adapted, if enough bins are considered.

Conclusion

In this document, the numerical methods implemented in the IRSN processing code GAIA-2 to treat the nuclear data in the unresolved resonance range have been presented. The main objective of this thesis was to establish a clear methodology to handle nuclear data in the unresolved resonance range, develop improved methods for data processing, and cross-check the processed data with the outcomes of the existing current in-use software. The nature of the evaluated nuclear data in the ENDF evaluations only enables the computation of cross sections as average values (potentially self-shielded), or probability tables. On the basis of the Hauser-Feschbach theory, average cross sections values can be computed directly from the average resonance parameters. Using the ladder method, probability distributions of the cross section values at particular reference energies can be sampled, and probability tables derived. Finally, self-shielded average cross sections can be retrieved from the probability tables. These issues have been addressed, and a piece of software named TOP has been developed and included in the nuclear data processing code GAIA-2. A great majority of the aspects of the average cross sections and probability tables calculation in the unresolved resonance range has been investigated in the present work, summarized in this document, and tested against the NJOY code. The impact of the diverse methods has been estimated in integral benchmarks. As a result, a complete methodology for the unresolved resonance range has been proposed, which was the initial objective of this thesis. In the course towards the establishment of this methodology, several interesting questions and conclusions arose which may have applications in other fields than the sole unresolved resonance range processing. They will be summarized in this conclusion as well.

After a detailed background presentation of the topic in the first part of this document, the real starting point of this work was to list all the hypotheses usually made at each step of the ladder method. These issues could be simple practical details of implementation, or more complex physical assumptions. Subsequently, the resulting structure of the document followed the steps of the ladder method. The second part of this thesis focused on the statistical sampling of resonances, which constitutes the backbone of the ladder method. The third part focused on the construction of probability tables from a practical point of view, and their use in neutronics applications. In this thesis, we have chosen to leap over the questions related to the reconstruction of cross sections in the context of the ladder method. Several questions could have been tackled, such as the impact of using another formalism than SLBW in the unresolved resonance range (although this issue has been addressed by A. Holcomb in a previous PhD dissertation) or the differences induced by reconstructing a whole punctual cross sections in the vicinity of the reference energies rather than on a single point. These questions have not been dealt with in this PhD, although some insights could be provided. Relying on the simplest and more conservative assumptions for the cross sections calculations (SLBW formalism and computations of cross sections values at the reference energies only), a complete methodology has been developed.

The most critical step of the ladder method is the resonance sampling. From the work carried, it is recommended to rely on random matrices of the GOE to sample the resonance energies. The idea is to choose matrices from the GOE, or more judiciously from equivalent tridiagonal matrices, with a size equivalent to the number of resonances to be sampled. Once obtained, the eigenvalues should be unfolded with the suggested exact tabulated method described in this document, and their fluctuations retrieved. Resonance energies can then be placed successively, starting with the leftmost one to avoid the bus waiting time paradox. In this work, the resonance widths are sampled from χ^2 distributions with an appropriate number of degrees of freedom, but it should be possible to correlate them in a similar manner as that used for the resonance energies sampling. The method is not straightforward, and has not been explored in this work. In order to know the appropriate size of the matrix to sample, we recommend to consider for each particular spingroup the ratio $\overline{\Gamma}/\overline{D}$ between the spingroup average total width and average resonance spacing, evaluated at the considered energy. Cases with large ratios require larger resonance ladders. Providing a quantitative estimation for both parameters requires to establish a criterion for the convergence of the sampled cross sections probability distribution, which is very delicate. This is however mandatory for practical applications, and we suggest to compare the $\overline{\Gamma}/\overline{D}$ value to 10^{-2}. Below this value, 100 pairs of resonance around the reference energy provide accurate results. Above, the number of resonances has to be increased. In the meantime, 100 000 Monte-Carlo iterations looks like a minimal number to perform, which should maybe be raised if the $\overline{\Gamma}/\overline{D}$ ratio is small. Once the resonance ladders have been sampled, this work only considered the calculations of cross sections at the single reference energy, even if strong insights seem to indicate that calculating a whole punctual cross section around the reference energy for each ladder is legitimate. The details of such a construction have not been investigated in this document. The final step of the ladder method consists to build probability tables from the cross sections sampling. In this document several approaches have been mentioned and two new methods have been proposed based on a k-clustering algorithm, called k-means and k-medians. These tables aimed at minimizing the variance of the mean cross section values in all the bins. Several considerations on particular nuclides have shown that these tables, and especially the k-medians ones behave well. However, further considerations based on benchmarks calculations showed that the number of bins should probably be raised to an amount superior to the usual value of 20, whatever the form of the tables. In fact, it is even believed that the best option is to stick to very large equiprobable probability tables, with for instance 1000 bins. This assumption is motivated by several facts. First of all, computer memory has become a less impacting issue than speed for Monte-Carlo calculations. This paves the way for larger, more precise tables. Secondly, larger tables might slightly decrease the speed of current Monte-Carlo codes which rely on a search routine to select the probability tables bins. However, using equiprobable bins, this search step can be omitted so that larger tables do not slow down the Monte-Carlo codes. Finally, equiprobable tables make the energy interpolation of the probability tables unambiguous and reduce the interpolation errors. This latter point has been proved important in several cases. At last, the choice of the energy mesh on which probability tables are provided to the Monte-Carlo codes is questionable. We propose the processing codes to provide them on an averaged-linearized grid to be coherent with the doing of the MF3 PENDF file, which is usually thinner than the initial reference energy mesh from the evaluations.

In this work, the unresolved resonance parameters have also been exploited to compute average cross sections according to the Hauser-Feschbach formalism. This theory relies on the calculation of a width fluctuation correction factor (WFCF), which can be accomplished from several manners. In this work, the usual Moldauer method for the computations of the WFCF has been implemented, as well as a more complex method referred to as the GOE method. This latter includes GOE fluctuations of the resonance parameters whereas the former assumes the resonance widths follow independent χ^2 distributions, which is an asymptotic result only. In order to compute the average cross sections with the GOE method from the resonance parameters given in the ENDF formalism, two additional hypotheses were made. The first one relates

the parameters to the transmission ratios following a classical practice, and the second one divides the reaction widths provided with a degree of freedom greater than 1 into as many reaction channels with equal widths. Following these hypotheses, average cross sections have been computed for all *elementary spingroups* of JEFF-3.2 according to both methods. The results closely match for spingroups with a low $\overline{\Gamma}/\overline{D}$ ratio, and progressively disagree when the ratio increases until it reaches a 30% disagreement. This huge outcome is not fully explained yet, but could be due to the fact the relation between the transmission ratios and the resonance parameters does not hold anymore. At the same time, the average cross sections derived from the ladder method samplings have been compared for all these spingroups with the Hauser-Feschbach values. Results match when the WFCF is computed with the Moldauer method. Note that this is also true when resonance spacings are correlated according to the GOE in the ladder method. This result should probably be investigated more in detail when the resonances widths are correlated in the ladder method sampling step, which has not been carried out in this thesis.

It is useful to underline some aspects of the work performed here which are of interest in other fields. In particular, a common methodology has been developed in this work to derive meaningful results, based on the decomposition of the evaluations content in the unresolved resonance range into *elementary spingroups*. These elementary spingroups correspond to sets of 16 scalar input parameters that play a role in the unresolved resonance range calculations, for a particular spingroup of a given isotope at a single reference energy. All calculations performed in the unresolved resonance range can be decomposed into the sum of sub-calculations performed for these elementary spingroups. Their main interest is directly related to their scalar nature, which enables to perform detailed calculations to estimate the weight of each parameter in the final results. This allows to identify the more critical cases for an output of interest. This has been used successfully to identify spingroups of the nuclides of JEFF-3.2 which needed the larger ladders or the more Monte-Carlo iterations at the resonance sampling step. It has also been used to estimate the most sensitive cases to the resonance correlations, and for which the width fluctuation correction factor differed between the Moldauer and GOE approaches. Finally, it has been used to identify a nuclide with a very skewed probability distribution, ^{156}Eu, for which accurate probability tables are very difficult to build. It is believed this decomposition of the evaluations content in elementary spingroups could actually be a relevant approach for other purposes, such as a real sensitivity analysis of the resonance parameters in the unresolved resonance range. This latter point has not been investigated in this work, but seems promising.

Considering the work carried out in this thesis, future perspectives look numerous and challenging, as they concern evaluators, processing codes developers, and neutronics codes users. To begin with, the correlation of reaction widths in the Monte-Carlo sampling of resonances based on the random matrix theory should be investigated. It is indeed probable that the influence of the widths correlation bring out significant changes. In particular, the calculations of the average cross sections should be inspected, and compared to the GOE variant of the Hauser-Feschbach problem. Such an implementation would require to match the R-Matrix theory with the GOE eigenvectors structure, and is not trivial. Secondly, we strongly suggest to design the new generation of neutronics Monte-Carlo codes – currently in development under the name HPC[28] – to be able to handle large equiprobable probability tables, which are likely to behave well for these computations. In parallel, it is advised to get prepared for a more sophisticated representation of cross section distributions, using parametric estimators notably. More tests are however required to find a relevant form of such an estimator. Considering the proper development of GAIA-2, it could be very interesting to achieve the implementation of a Nuclear Data Handler and an ACE file parser to get rid of the ENDF limitations, and of any use of NJOY. This is an urgent topic as the GNDS is about to become the dominant format for newly released evaluated nuclear data files in the upcoming years. Finally, it seems relevant to perform benchmarks sensitive to the

---

[28]High Performance Computing.

unresolved resonance range of several nuclides of interest for the nuclear industry, and sensitive to the many nuclides for which not a single benchmark has been ever designed. This latter point is a complex topic though, but could help to provide more information about the dynamic of the statistical properties of the nuclear levels, and to determine the situations in which multigroup or probability tables approaches are the more informative. All these issues are believed to be extremely useful for both nuclear physics and engineering points of view.

Bibliography

[1] G. Ferran. *Nouvelles méthodes numériques pour le traitement des sections efficaces nucléaires.* PhD thesis, École doctorale de l'École Polytechnique, September 2014.

[2] CSEWG working group. *ENDF-6 Formats Manual, Data Formats and Procedures for the Evaluated Nuclear Data Files ENDF/B-VI and ENDF/B-VII*, 2012.

[3] A. Hébert. *Applied Reactor Physics.* Presses Internationales Polytechnique, 2009.

[4] A.J. Koning and J.M. Akkermans. Pre-equilibrium nuclear reactions: an introduction to classical and quantum-mechanical models. In *Nuclear reaction data and nuclear reactors*, pages 143–158. The Abdus Salam International Center for Theoretical Physics, 1999.

[5] G. Noguere. Contributions to the study of the unresolved resonance range of neutron-induced reactions. HDR, Université Bordeaux-1, 2014.

[6] M.C. Moxon and et al. Report AERE-R7864. Technical report, Harwell Laboratory, 1974.

[7] T. Freiman. *Méthode multipôle pour l'évaluation au vol de la dépendance en température des sections efficaces nucléaires.* PhD thesis, CEA, Université Paris-Saclay, PHENIICS, January 2020.

[8] C. Josey, P. Ducru, B. Forget, and K. Smith. Windowed multipole for cross section Doppler broadening. *Journal of Computational Physics*, 307:715–727, 2016.

[9] L.B Levitt. The probability table method for treating unresolved neutron resonances in Monte-Carlo applications. *Nuclear Science and Engineering*, 49:450–457, 1972.

[10] R.E. MacFarlane and A.C. Kahler. *The NJOY Nuclear Data Processing System, Version 2016*, 2016. LA-UR-17-20093.

[11] L. Leal, G. de Saussure, and R.B. Perez. *URR Computer Code: A code to calculate resonance neutron cross-section probability tables, Bondarenko self-shielding factors, and self-indication ratios for fissile and fertile nuclides*, 1990.

[12] D.E. Cullen. *Program GROUPIE (version 79-1): calculation of Bondarenko self-shielded neutron cross sections and multiband parameters from data in the ENDF/B format*, 1980.

[13] A. Nasri. *Microscopic non-local potentials for the study of scattering observables of nucleons within the coupled channel framework.* PhD thesis, Université Paris-Saclay, PHENIICS, September 2018.

[14] H.A. Bethe. Theory of disintegration of nuclei by neutrons. *Phys. Rev.*, 47:747–759, 1935.

[15] A.J. Koning and D. Rochman. Modern nuclear data evaluation with the TALYS code system. *Nuclear Data Sheets*, 113:2841–2934, 2012.

[16] Peter Schillebeeckx. Neutron time-of-flight measurements and transmission measurement. Workshop on the Evaluation of Nuclear Reaction Data for Applications, October 2017.

[17] Nancy M. Larson. *Updated users guide for SAMMY: multilevel R-Matrix fits to neutron data using Bayes equations*, 2008. ENDF-364/R2.

[18] L. Clouvel. *Quantification de l'incertitude du flux neutronique rapide reçu par la cuve d'un réacteur à eau pressurisée*. PhD thesis, CEA, Université Paris-Saclay, October 2019.

[19] D. Brown. Detailed requirements for a next generation nuclear data structure. Technical report, OECD/NEA/WPEC Subgroup 38, 2016.

[20] D.E. Cullen and C.R. Weisbin. Exact Doppler broadening of tabulated cross sections. *Nuclear Science Engineering*, 60:199, 1976.

[21] V. Jaiswal. *Theoretical and experimental approach towards generation of thermal scattering law for light water*. PhD thesis, IRSN, Université de Lille, October 2018.

[22] A.M. Lane and R.G. Thomas. R-Matrix Theory of nuclear reactions. *Review of Modern Physics*, 257, 1958.

[23] E.P. Wigner and L. Eisenbud. Higher angular momenta and long range interaction in resonance reactions. *Phys Rev*, 72:29, 1947.

[24] L. Leal. Brief review of the R-Matrix theory. Technical report, Oak Ridge National Laboratory, 2009. MIT Course.

[25] C.W. Reich and M.S. Moore. Multilevel formula for the fission process. *Phys Rev*, 111:929, 1958.

[26] A.W. Solbrig. Doppler effect in neutron absorption resonances. *American Journal of Physics*, 29:257, 1961.

[27] W.E. Lamb. Capture of neutrons by atoms in a crystal. *Physical Review*, 55:55, 1939.

[28] H.A. Bethe. A new method for the doppler broadening of the Solbrig's kernel using a Fourier transform. *Nuclear Science and Engineering*, 179:285–301, 2015.

[29] D.G. Cacuci. *Handbook of nuclear engineering*. Springer, Springer Reference edition, 2010.

[30] F.H. Fröhner. *Evaluation and analysis of nuclear resonance data*. Nuclear Energy Agency, JEFF Report 18, 2009.

[31] E.P. Wigner. Conference on neutron physics by time-of-flight. Technical report, ORNL, 1956. National Laboratory Report.

[32] C.E. Porter and R.G. Thomas. Fluctuations of nuclear reaction widths. *Physical Review*, 104:483, 1956.

[33] J.E. Lynn. *The theory of neutron resonance reactions*. Clarendon Press, 1958.

[34] D.E. Cullen. A short history of ENDF/B unresolved resonance parameters. Technical report, Lawrence Livermore National Laboratory, 2010.

[35] M. Gyulassy and T. Perkins. Relationships between experimental and theoretical parameters in unresolved resonance theory. *Nuclear Science and Engineering*, 53:482–486, 1974.

[36] F. Gunsing. Resonances in neutron-induced reactions. *Eur. Phys. J. Plus*, 133:440, 1964.

[37] P.A. Moldauer. Statistical theory of nuclear collision cross sections. *Physical Review*, 135, 1964.

[38] S. Hilaire, Ch. Lagrange, and A.J. Koning. Comparisons between various width fluctuation correction factors for compound nucleus reactions. *Annals of Physics*, 306:209–231, 2003.

[39] A.J Koning, S. Hilaire, and M. Duijvestijn. *TALYS-1.2: A nuclear reaction program*, 2009.

[40] A.R. DiDonato and A.H. Morris. Computation of the incomplete gamma function ratios and their inverse. *ACM Transactions on Mathematical Software*, 12:377–393, 1986.

[41] A.M. Holcomb. *A new unresolved resonance region methodology.* PhD thesis, Georgia Institute of Technology, November 2015.

[42] L. F. Cugliandolo. Advanced statistical physics: Random matrices. Course given at the Paris-VI University, 2018.

[43] J-F. Laprise. *Matrices aléatoires et billards classiques: universalité dans les mesures statistiques sur les trajectoires.* PhD thesis, Université Laval, Québec, 2010.

[44] H. J. Montgomery. The pair correlation of zeros of the zeta function. *Analytic number theory, Proc. Sympos. Pure Math., XXIV, Providence, R.I.: American Mathematical Society*, pages 181–193, 1973.

[45] L. Lalou, P. Cizeau, M. Potters, and J-F. Bouchaud. Random matrix theory and financial correlation. World Scientific Publishing Company.

[46] L. Erdos. Universality of Wigner random matrices: a survey of recent results, 2010.

[47] G. Ben Arous and A. Guionnet. Wigner matrices. In *The Oxford Handbook of Random Matrix Theory.* Oxford Library, 2015.

[48] G. Livan, M. Novaes, and P. Vivo. Introduction to random matrices theory and practice, 2017.

[49] Y.V. Fyodorov. Introduction to the random matrix theory: Gaussian unitary ensemble and beyond, 2004. https://arxiv.org/pdf/math-ph/0412017.pdf.

[50] M.L. Mehta. *Random matrices, 3th edition.* Pure and Applied Mathematics Series 142. Elsevier, 2004.

[51] A. Abul-Magd S. Abuelenin. Effect of unfolding on the spectral statistics of adjacency matrices of complex networks. *Procedia Computer Science*, 12:69–74, 2012.

[52] O. Bohigas and MJ. Giannoni. Chaotic motion and random matrix theory. *Mathematical and Computational Methods in Nuclear Physics*, 1984.

[53] M. Gaudin. Sur la loi limite de l'espacement des valeurs propres d'une matrice aléatoire. *Nuclear Physics*, 25:447–458, 1961.

[54] F.J. Dyson and M.L. Mehta. Statistical theory of the energy levels of complex systems (IV). *Journal of Mathematical Physics*, 4:701, 1963.

[55] L. Leal and N. M. Larson. SAMDIST: A computer code for calculating statistical distributions for R-Matrix resonance parameters, 1995. ORNL/TM-13092.

[56] D. Mulhall, Z. Huard, and V. Zelevinsky. Ergodicity of the Δ_3 statistic and purity of neutron resonance data. *Physical Review C*, 76, 2007.

[57] Alan Edelman and Per-Olof Persson. Numerical methods for eigenvalue distributions of random matrices, 2005.

[58] I. Dumitriu and A. Edelman. Matrix models for β-ensembles. *Journal of Mathematical Physics*, 11:5830–5847, 2002.

[59] E.S. Coakley and V. Rokhlin. A fast divide-and-conquer algorithm for computing the spectra of real symmetric tridiagonal matrices. *Applied and Computational Harmonic Analysis*, 34:379–414, 2013.

[60] F. Haake. *Quantum signatures of chaos.* Springer, 4th edition edition, 2018.

[61] D. Brown. A tale of two tools: mcres.py, a stochastic resonance generator, and grokres.py, a resonance quality assurance tool, 2018. BNL-209313-2018-INRE.

[62] A.N. Pettitt. A two-sample Anderson-Darling rank statistic. *Biometrika*, 63:161–168, 1976.

[63] J.J.M. Verbaarschot, H.A. WeidenMüller, and M.R. Zirnbauer. Grassmann integration in stochastic quantum physics: The case of compound-nucleus scattering. *Physics Report*, 129:367–438, 1985.

[64] J.J.M. Verbaarschot. Investigation of the formula for the average of two S-Matrix elements in compound nucleus reactions. *Annals of Physics*, 168:368–386, 1986.

[65] H.L Hartney, E.G Lanza, and P. Pereyra. On a class of integrals appearing in the theory of statistical nuclear reactions. *Annals of Physics*, 176:140–144, 1987.

[66] R. Piessens, E. De Doncker-Kapenga, and C.W. Überhuber. *QUADPACK: a subroutine package for automatic integration.* Springer, 1983.

[67] M. Coste-Delclaux. *Modélisation du phénomène d'autoprotection dans le code de transport multigroupe APOLLO2.* PhD thesis, CEA, 2006. CEA-R-6114.

[68] L. Mao, I. Zmijarevic, and R. Sanchez. Resonance self-shielding methods for fast reactor calculations—comparison of a new Tone's method with the subgroup method in APOLLO3. *Nuclear Science and Engineering*, 188:1–18, 2017.

[69] L.L Carter, R.C. Little, J.S. Hendricks, and R.E. MacFarlane. New probability table treatment in MCNP for unresolved resonances, 1998. Report LA-UR-98-26.

[70] T.M. Sutton and F.B. Brown. *Implementation of the probability table method in a continuous-energy Monte-Carlo code system*, 1998.

[71] P. Ribon and JM. Maillard. Les tables de probabilités: application au traitement des sections efficaces pour la neutronique, 1986. Note CEA-N-2485.

[72] A. Hébert and M. Coste-Delclaux. Computing moment-based probability tables for self-shielding calculations in lattice codes. *Nuclear Science and Engineering*, 142:245–257, 2002.

[73] K.H. Knuth. Optimal data-based binning for histograms and histogram-based probability density models. *Digital Signal Processing*, 95, 2019.

[74] G.F. Jenks. The data model concept in statistical mapping. *International Yearbook of Cartography*, 7:186–190, 1967.

[75] H. Wang and M. Song. Ckmeans.1d.dp: Optimal k-means clustering in one dimension by dynamic programming. *The R Journal*, 3/2, 2011.

[76] M. Song and H Zhong. Efficient weighted univariate clustering maps outstanding dysregulated genomic zones in human cancers. *Bioinformatics*, btaa613, 2020. Supplementary Note N5.

[77] C. Sugar and G. James. Finding the number of clusters in a dataset. *Journal of the American Statistical Association*, 98:750–763, 2003.

[78] C.J. Werner. *MCNP User's Manual - Code Version 6.2*, 2018. LA-UR-17-29981.

[79] B. Cochet and A. Jinaphanh. *MORET User's Manual - Version 5.D.1*, 2017. IRSN PSN-EXP/SNC/2017-282.

[80] J.L Conlin. A compact ENDF (ACE) format specification. LA-UR-19-29016.

[81] O. Ben-Kiki, C. Evans, and I. döt Net. YAML ain't markup language. `https://yaml.org/spec/1.2/spec.html`, 2009. Accessed: 2020-08-10.

[82] A. Jinaphanh. Probability tables treatment. Technical report, IRSN, 2015. Rapport PSN-EXP/SNC/2015-285.

[83] International handbook of evaluated criticality safety benchmark experiments, 2006.

[84] J. Sapir, B. Krohn, and R. Mosteller. Big Ten: A large, mixed-uranium-metal cylindrical core with 10% average ^{235}U enrichment, surrounded by a thick ^{238}U reflector. Technical report, Los Alamos National Laboratory, 1995. Report LA-UR-11-04640.

[85] R.M. Lell. ZPR-3 Assembly 11: A cylindrical assembly of highly enriched uranium and depleted uranium with an average ^{235}U enrichment of 12% and a depleted uranium reflector. Technical report, Argonne National Laboratory, 1995. NEA/NSC/DOC(95)03/III, Volume III.

[86] C. Percher, A. J. Nelson, W. J. Zyweic, S.S. Kim, and D.P. Heinrichs. Thermal Epithermal Experiments (TEX): Test bed assemblies for efficient generation of integral benchmarks. Technical report, Lawrence Livermore National Laboratory, 2019. Report LLNL-CONF-776306.

[87] C. Percher and J. Norris. TEX plutonium baseline assemblies: plutonium/aluminum metal alloy plates with varying thicknesses of polyethylene moderator and a thin polyethylene moderator. Technical report, Lawrence Livermore National Laboratory, 2020. Draft of the submitted paper to ICSBEP.

[88] J.F. Delmas. *Introduction au calcul des probabilités et à la statistique. Deuxième édition*. Les presses de l'ENSTA, 2013.

[89] J. VanderPlas. The waiting time paradox, or, why is my bus always late? `http://jakevdp.github.io/blog/2018/09/13/waiting-time-paradox/`, 2018. Accessed: 2020-01-30.

Appendix A: Central spacing distribution in the bus waiting time paradox

The aim of this appendix is to establish the distribution of the central spacing between resonances around the reference energy in the ladder method. It has been pushed forward in Section 3.1 that the situation can be closely related to a well-known paradox, the so-called *bus waiting time paradox*, which states that someone randomly walking by a bus stop is highly likely to wait more than (half) the mean time between the buses. To be consistent with the problem in the literature, this appendix aims at establishing the statistical waiting time of a pedestrian standing at a bus stop. Afterwards, the situation can be directly translated to the problematic of nuclear resonances sampling. The proof presented here has been taken from [88], and only requires a small mathematical background. We then present some convergence results for the Poisson and Wigner spacing case.

Proof of the central spacing distribution

Over a day, successive buses reach a bus stop at times modeled with a sequence of random variables T_k ($k \geq 2$), all independent and following the same law T, in order to take into account the randomness of traffic conditions. At time $t = 0$, the first bus leaves the bus stop[29], and we introduce $S_k = \sum_{i=1}^{k} T_i$ the time at which the kth bus reaches the bus stop. Let us consider a finite number of buses over the day, namely n buses, so that the last bus reaches the bus stop at time $t = S_n$. A pedestrian walk by the bus stop at random before the end of the day. Let us call T_n^* the time elapsed between the departure of the previous bus (let us define its number as N_n^*) and the arrival of the next one. The objective here is to detail the law of T_n^* and it's asymptotical behavior (which corresponds to the case where there is an infinity of buses).

First of all, let us remark that T_n^* (nor its limit T^*) is unlikely to follow the same law T which models the times between the buses. Indeed, T_n^* depends on the arrival of the pedestrian at the bus stop. However, he is more likely to reach the bus stop while the time between the buses is, actually, long. The fact that the distribution of T_n^* differs from T results in the waiting time paradox. Figure 11 pictures the situation.

Let g be a measurable bounded function. As it is common, we will try to establish an expression for $E[g(T_n^*)]$, before taking $g(x) = e^{iux}$ to establish an equality in law through the use of the characteristic functions. Breaking down T_n^* over the various values of N_n^*, next relationship holds:

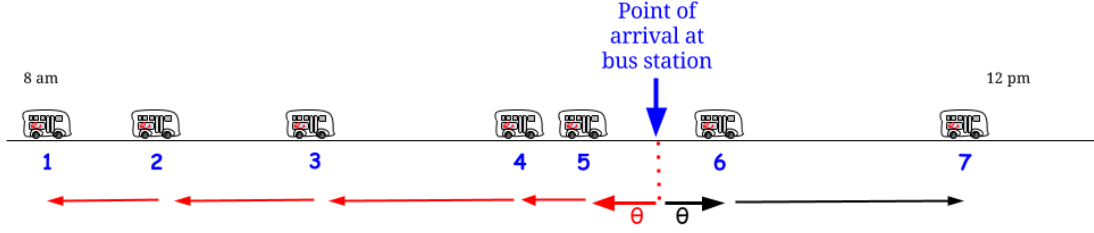[29]Of course, we neglect the time spent by buses at the bus stop to pick up travelers.

Figure 11: The waiting time bus paradox: the pedestrian is more likely to reach the bus stop while buses are far from each other [89]

$$\mathbb{E}\left[g\left(T_n^*\right)\right] = \sum_{k=1}^{n} \mathbb{E}\left[\mathbb{1}_{\{N_n^*=k\}} g\left(T_k\right)\right] \tag{1}$$

The pedestrian coming at the bus stop can be modeled with a random variable, which follows US_n, U being the uniform law over $[0,1]$[30]. Subsequently, $\{N_n^* = k\} = \left\{U \in \left]\frac{S_{k-1}}{S_n}, \frac{S_k}{S_n}\right]\right\}$. There, introducing the next lemma is useful:

Lemma. *For a random variable Z independent from U, and any bounded measurable function ϕ:*

$$\mathbb{E}[\phi(U,Z)] = \mathbb{E}\left[\int_0^1 \phi(u,Z)\, du\right] \tag{2}$$

It is thus straightforward to rewrite the the probability for the immediate bus to be the k-th one:

$$\mathbb{P}\left(N_n^* = k\right) = \mathbb{E}\left[\mathbb{1}_{\left\{U \in \left]\frac{S_{k-1}}{S_n}, \frac{S_k}{S_n}\right]\right\}}\right] = \mathbb{E}\left[\frac{S_k}{S_n} - \frac{S_{k-1}}{S_n}\right] = \mathbb{E}\left[\frac{T_k}{S_n}\right] \tag{3}$$

There, we can notice that all $\dfrac{T_k}{S_n}$ follow the same law. As a consequence,

$$1 = \mathbb{E}\left[\frac{\sum_{k=1}^{n} T_k}{S_n}\right] = \sum_{k=1}^{n} \mathbb{E}\left[\frac{T_k}{S_n}\right] = \sum_{k=1}^{n} \mathbb{E}\left[\frac{T_1}{S_n}\right] = n\mathbb{E}\left[\frac{T_1}{S_n}\right] = n\mathbb{E}\left[\frac{T_k}{S_n}\right] \tag{4}$$

And thus $\mathbb{P}\left(N_n^* = k\right) = \frac{1}{n}$, and N_n^* follows a uniform law over $\{1, \ldots, n\}$. We can now jump back to the decomposition of the expected value of $g(T_n^*)$ in Equation (1), and make use of the proposed lemma once again:

$$\mathbb{E}\left[g\left(T_n^*\right)\right] = \sum_{k=1}^{n} \mathbb{E}\left[\mathbb{1}_{\{N_n^*=k\}} g\left(T_k\right)\right] = \sum_{k=1}^{n} \mathbb{E}\left[\mathbb{1}_{\left\{U \in \left]\frac{S_{k-1}}{S_n}, \frac{S_k}{S_n}\right]\right\}} g(T_k)\right] \tag{5}$$

$$= \sum_{k=1}^{n} \mathbb{E}\left[\frac{T_k}{S_n} g(T_k)\right] \tag{6}$$

$$= \mathbb{E}\left[\frac{nT_1}{S_n} g(T_1)\right] \tag{7}$$

Let us now try to obtain the asymptotic distribution followed by T_n^*, when $n \to \infty$. Let us first define the random variable $X_n = \frac{nT_1}{S_n}$. Using the fact that $S_n/n \xrightarrow{n\infty} \mu$ and the continuity of the application $x \mapsto T_1/x$ in μ, the variable X_n converges almost surely toward the random variable $X = T_1/\mu$.

---

[30]This comes from the fact that the elapsed time between the first and last bus is S_n.

It is now relevant to use the linearity of the expected value, to get

$$E[g(T_n^*)] = E[X_n g(T_1)] = E[Xg(T_1)] + E[(X_n - X)g(T_1)] \tag{8}$$

Using the triangular inequality and the fact that g is bounded:

$$|E[(X_n - X)g(T_1)]| \leq E[|X_n - X||g(T_1)|] \leq ||g||_\infty E[|X_n - X|] \tag{9}$$

Let us briefly prove that $X_n \xrightarrow{n\infty} X$ implies $E[|X_n - X|] \xrightarrow{n\infty} 0$. Such a demonstration makes use of Lebesgue's dominated convergence theorem to pass the limit into the expectation. There, we can introduce the (continuous) function $\psi_+ : x \mapsto \max(x, 0)$, so that for $x \geq 0$, $y \geq 0$, $\psi_+(x - y) \leq x$. Introducing $Y_n = \psi_+(X - X_n)$, we are able to use Lebesgue's dominated convergence theorem, as
- ψ_+ is continuous so $Y_n \to 0$
- $|Y_n| \leq X$
- X is integrable

and we can prove that $\lim_{n\infty} \mathbb{E}[Y_n] = \mathbb{E}[\lim_{n\infty} Y_n] = 0$.

Connecting $|.|$ and ψ_+ is straightforward, as for $x \geq 0$, $|x| = -x + 2\psi_+(x)$, and we can finally conclude that $\mathbb{E}[|X_n - X|] = \mathbb{E}[-X + X_n + 2\psi_+(X - X_n)] = 2\mathbb{E}[\psi_+(X - X_n)] \xrightarrow{n\infty} 0$ almost surely.

Returning back to Equations (8) and (9),

$$\lim_{n\infty} \mathbb{E}[g(T_n^*)] = \mathbb{E}[Xg(T_1)] = \frac{1}{\mu}\mathbb{E}[Tg(T)] \tag{10}$$

As this equation is true for any bounded measurable function g, we can conclude that $(T_n^*, n \geq 1)$ converges to a variable $T*$, whose density is $f^* : t \mapsto \frac{t}{\mu}f(t)$, where f is the density of T, and μ is the expected value of T.

This proves the bus waiting time paradox. In our case, the expected value of the Wigner law equals 1, and the central spacing follows a Maxwell-Boltzmann distribution with parameter $\sqrt{\frac{2}{\pi}}$, in the asymptotic case of many resonances in the ladder.

Study of the convergence to the asymptotic limit

It is of interest to study the convergence of $(T_n^*, n \geq 1)$ to its asymptotic limit T^*. Let us remind that n is the number of buses in a day, or alternatively, the number of resonances in a ladder for the problem tackled in this thesis. Carrying out this study is useful for the original problem of resonance ladders sampling, especially when the ladder is built starting with the leftmost resonance (NJOY-like method). More precisely, if the ladder has too few resonances, the central spacing is likely not to follow the asymptotic distribution T^*. Instinctively, this may be understood as follows: enough resonances must be sampled so that the influence of the starting point does not intervene anymore.

Let us come back to the buses, keeping in mind that the results are easily transportable to the resonance ladders problem. We will simulate the waiting time of pedestrians according to the number of buses in a day. In order to achieve this goal, we will simulate the arrival times of n buses over a day, and then randomly sample the arrival time of a pedestrian between the first and the last bus, and store the interval of time elapsed between the previous and next bus. Then, we will repeat this operation over many days to obtain a valid statistic of the central spacing. A slightly simplified version of the algorithm (where buses comes at random time, thus following a Poisson process) can be found for instance in [89]. In Python, the algorithm using a Wigner law for the spacing between the buses can the be written as:

```
def simulate_days(ndays = 10000, nbus_day = 100):
    span_times= []
    rand = np.random.RandomState()
    for ii in range(ndays):
        spacing_buses = rayleigh.rvs(size=nbus_day-1, scale=np.sqrt(2./np.pi))
        arrival_times = np.zeros(nbus_day)
        for jj in range(1, nbus_day):
            arrival_times[jj] = arrival_times[jj-1] + spacing_buses[jj-1]
        passenger_time = arrival_times.min() + (arrival_times.max() -
arrival_times.min()) * rand.rand(1)
        i = bisect.bisect_left(arrival_times, passenger_time)
        span_times.append(arrival_times[i] - arrival_times[i-1])
    return span_times
```

An usual practice is to suppose that the arrival of a bus does not depend on the arrival time of previous buses, [31] so that they actually follow a Poisson process and are not correlated. In this case, the law of spacing between them is an exponential law $E(x) = e^{-x}$, and the corresponding asymptotic limit for $T*$ is a Gamma law of parameter 2, $E^*(x) = xe^{-x}$.

Figure 12 displays the convergence of the distribution of the spacing between buses at the pedestrian arrival time, according to the number of buses in the day. It appears that the convergence to the the limit T^* is slightly faster for the Wigner distribution. Anyway, the asymptotic limit seems to be reached quite fast.
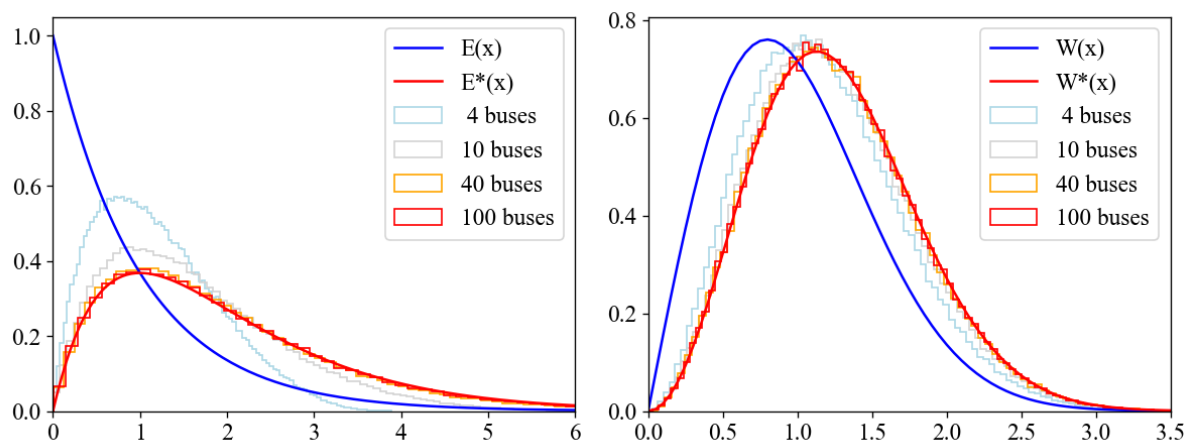

Figure 12: Convergence of the distribution of the interval between buses at a pedestrian arrival as a function of the number of buses per day. On the left, when buses are uncorrelated (Poisson process), on the right when the spacing between buses follows a Wigner distribution.

---

[31] Which is of course not the case, as buses have a time schedule, and are often able to adapt their journey to maintain a more regular space between them.

Appendix B: Materials related to the size of ladders

Present appendix refers to the work carried out in Section 3.3.1 which investigated the required number of resonances to sample in the ladder method.

First, the convergence plots – equivalent to Figures 3.6–3.8 – are plotted when cross sections have been Doppler-broadened at T=293.6K. Several statistics representative of cross sections sets (from which probability tables will be derived) obtained from ladders of different sizes are compared to asymptotic values obtained from cross sections derived from large ladders of resonances, composed of 500 pairs. For each statistics, the relative difference (in %) with the 500-pairs result are plotted on Figures 13–15. Each set of figures corresponds to a particular reaction, and each figure corresponds to a particular statistics. On each figure, each line corresponds to a particular elementary spingroup from JEFF-3.2, defined in Section 3.2.1. The red line is the less converged case. All calculations have been carried out with set of 100 000 cross section values, corresponding to 100 000 ladders.

The results do not differ significantly from the behavior observed at T=0K, even if the number of pairs to sample seems rather more important. This issue is discussed in the main body of the present thesis.

In a second time, scatter plots equivalent to Figures 3.15–3.15 display the minimum number of pairs of resonances to sample using a weaker criterion.
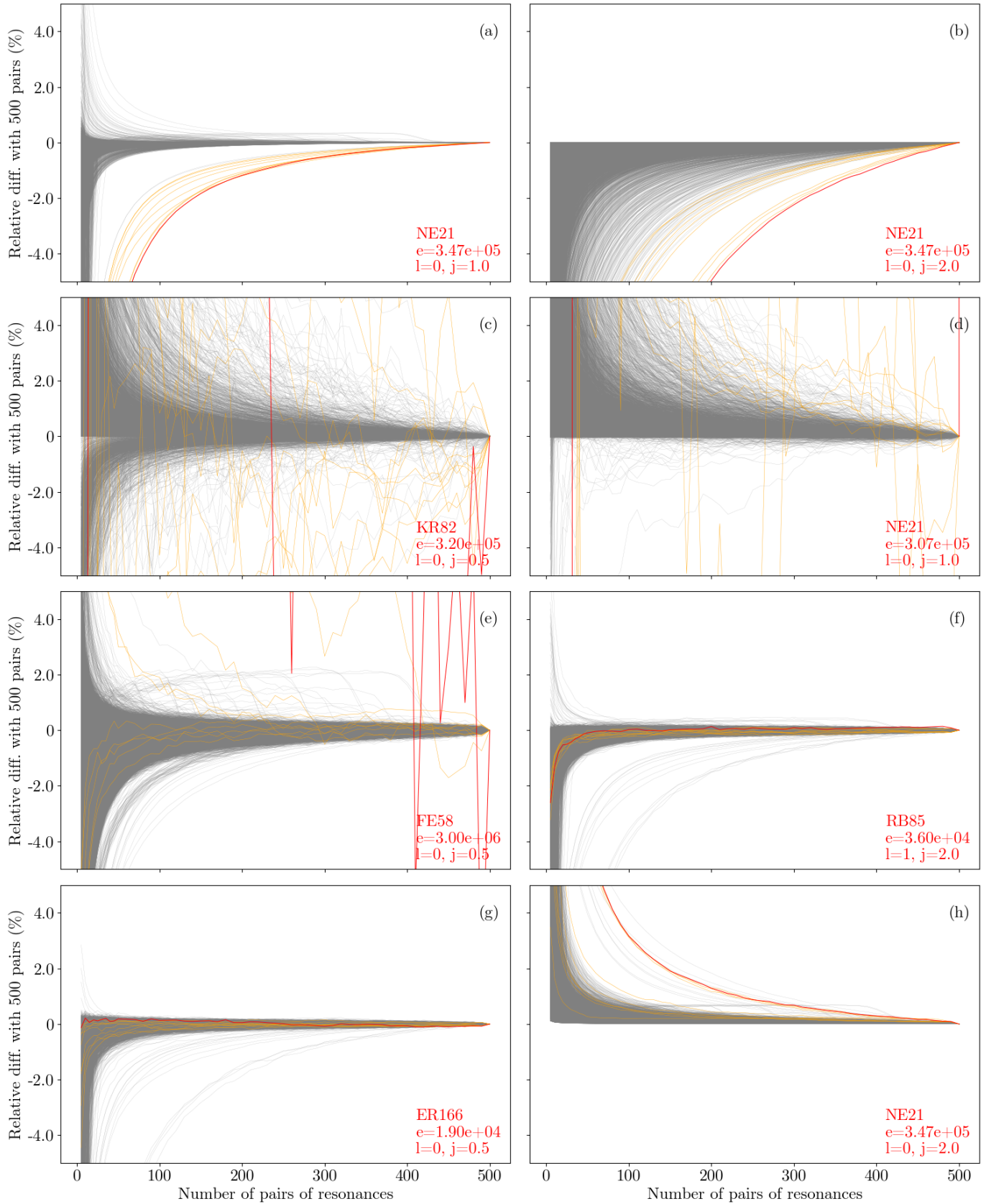
Figure 13: Convergence of various statistics of the elastic sampled cross sections set toward the reference (500 pairs of resonances) at T=293.6K. (a) mean, (b) variance, (c) skewness, (d) kurtosis, (e) first quartile, (f) fourth quartile, (g) 95th percentile, (h) Kolmogorov-Smirnov distance.
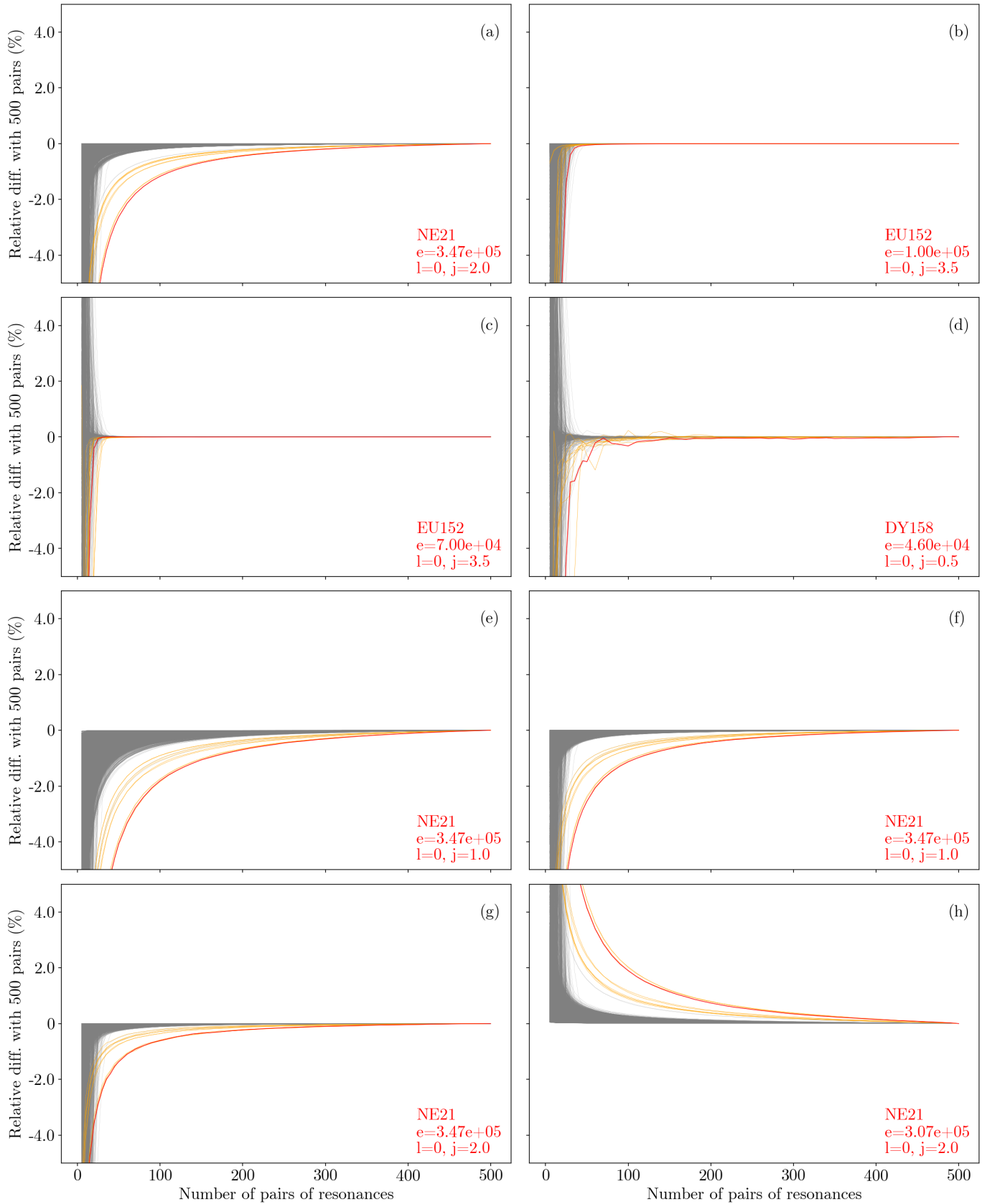
Figure 14: Convergence of various statistics of the capture sampled cross sections set toward the reference (500 pairs of resonances) at T=293.6K. (a) mean, (b) variance, (c) skewness, (d) kurtosis, (e) first quartile, (f) fourth quartile, (g) 95th percentile, (h) Kolmogorov-Smirnov distance.
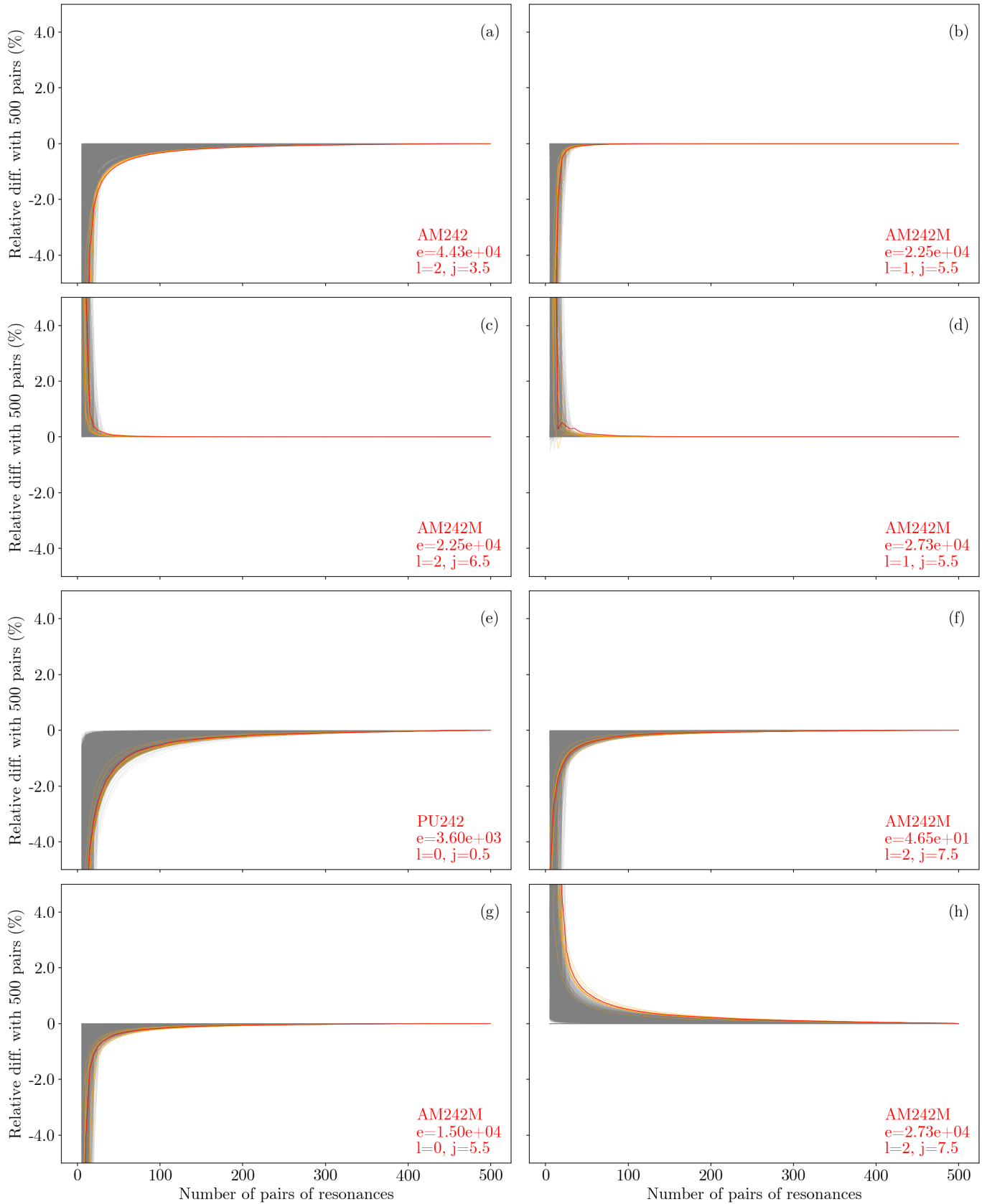
Figure 15: Convergence of various statistics of the fission sampled cross sections set toward the reference (500 pairs of resonances) at T=293.6K. (a) mean, (b) variance, (c) skewness, (d) kurtosis, (e) first quartile, (f) fourth quartile, (g) 95th percentile, (h) Kolmogorov-Smirnov distance.

Figure 16: Required number of resonances to reach close to 1% of the 500-pairs values for each spingroup, plotted against their $\overline{\Gamma}/\overline{D}$ value, at T=0K. Each figure corresponds to a statistics of interest: (a) mean, (b) variance, (c) skewness, (d) kurtosis, (e) first quartile, (f) fourth quartile, (g) 95th percentile, (h) Kolmogorov-Smirnov distance.
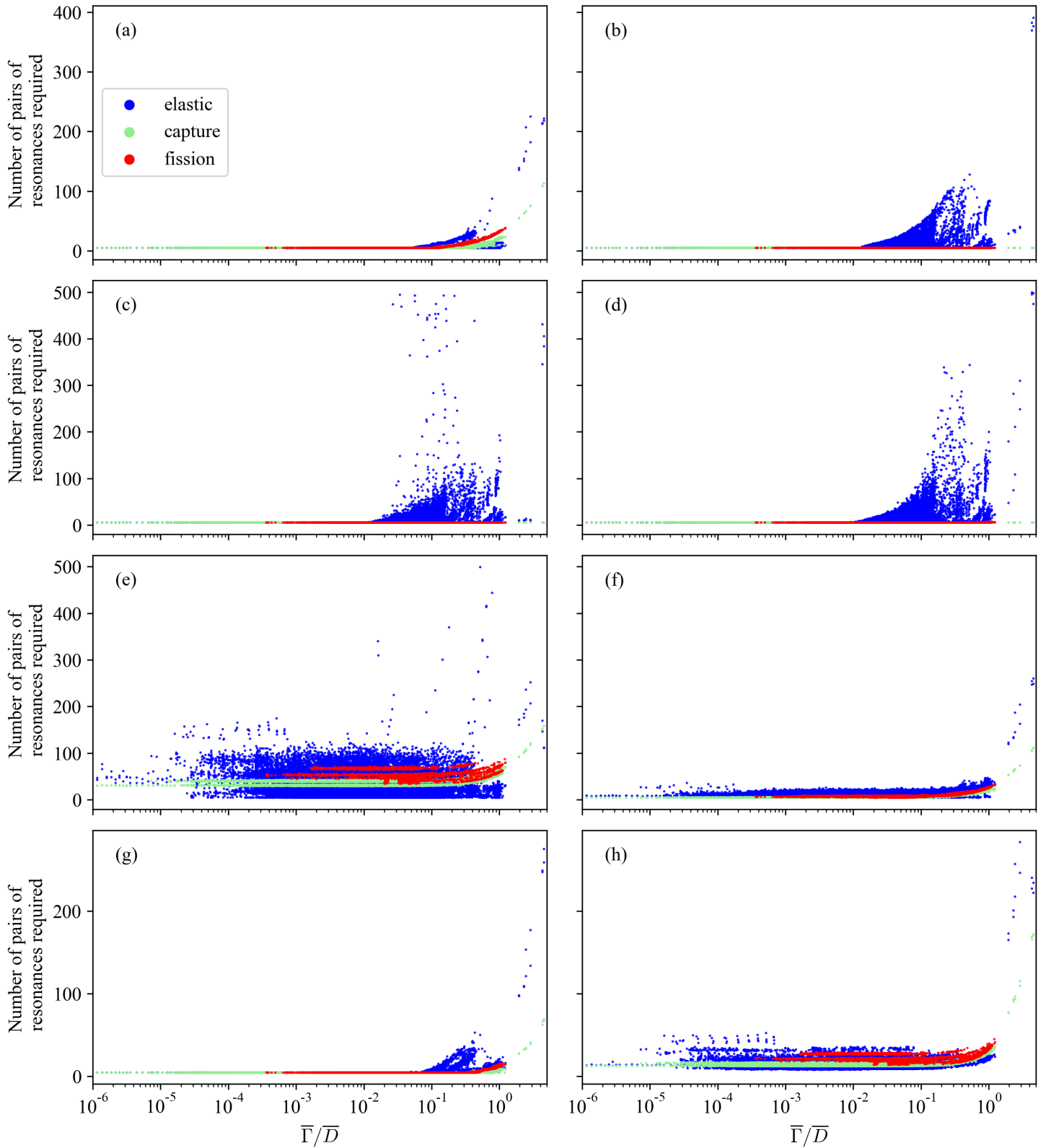
Figure 17: Required number of resonances to reach close to 1% of the 500-pairs values for each spingroup, plotted against their $\overline{\Gamma}/\overline{D}$ value, at T=293.6K. Each figure corresponds to a statistics of interest: (a) mean, (b) variance, (c) skewness, (d) kurtosis, (e) first quartile, (f) fourth quartile, (g) 95th percentile, (h) Kolmogorov-Smirnov distance.
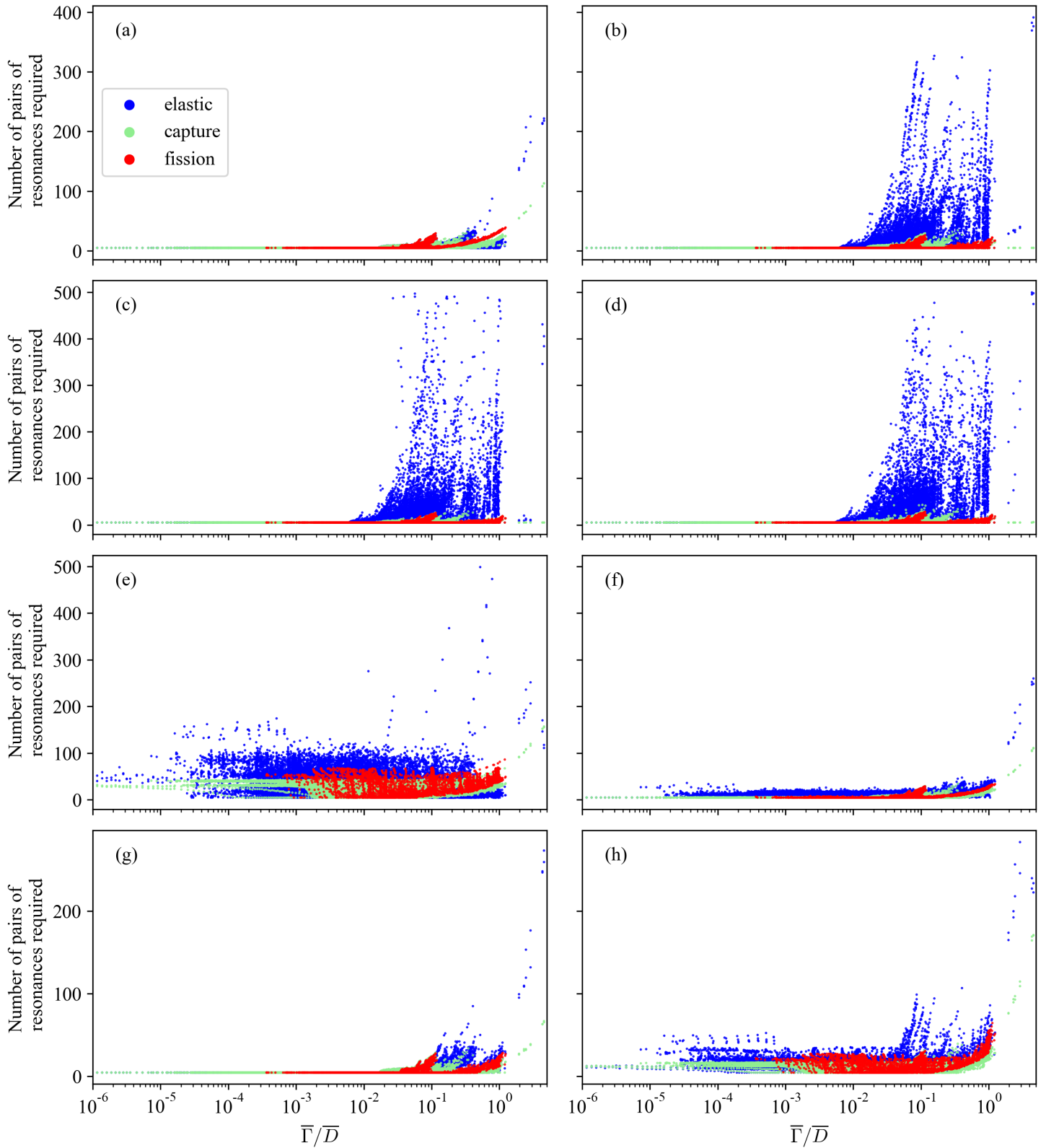
Appendix C: Statistics of cross sections obtained from correlated spacings

The random matrix theory has been adapted to produce resonance ladders with correlated spacings in Chapter 4. For all 41 486 elementary spingroups of JEFF-3.2 defined in Section 3.2.1, cross sections sets have been computed with this method. Due to the huge amount of time required, only 20 000 Monte-Carlo iterations were performed with ladders of size 1000, to be compared to the 200 000 iterations performed in Chapter 3 with uncorrelated spacings. The next moment and quantile statistics have been computed for cross sections sets issued from both methods: mean, variance, skewness, kurtosis, first and fourth quartile, and 95th percentile. The percentage difference between each statistics computed from the two sets (Wigner - 200 000 iterations) and (GOE - 20 000 iterations) have been performed, and displayed in this Appendix on Figure 18 for T = 293.6K. On this figure, the x-axis is an index on which spingroup cases have been ranged and sorted in ascending $\overline{\Gamma}/\overline{D}$ ratios.

Note that the Kolmogorov-Smirnov statistics widely used in Chapter 3 has not been computed between these two ensembles of cross sections, because it requires to store all the elements, which was too complex from a storage point of view. This statistics has been computed however when both sets of cross sections are only composed of 20 000 elements, and displayed in the body of this thesis. It notably served as a basis for a strict hypothesis test.

The lack of iterations and the apparently small impact of the spacings correlation on the cross sections distributions makes the real impact of the method hard to separate from the Monte-Carlo fluctuations. It seems like the variance is still slightly impacted by the change of method in some cases, at high $\overline{\Gamma}/\overline{D}$.
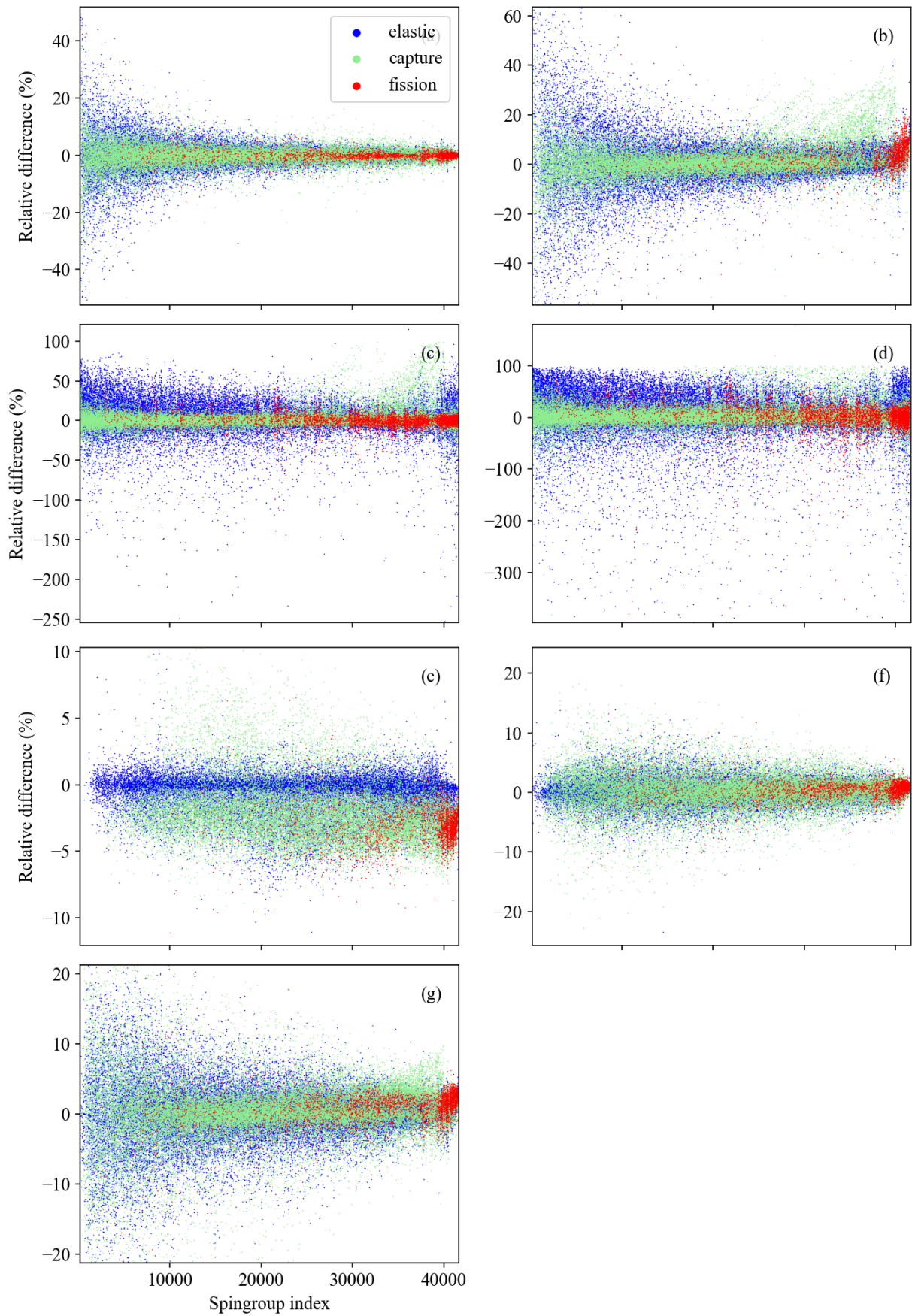
Figure 18: Relative difference between several scalar statistics ((a) mean, (b) variance, (c) skewness, (d) kurtosis, (e) first quartile, (f) fourth quartile, (g) 95th percentile) of cross sections sets obtained with correlated spacings (20 000 iterations) and uncorrelated ones (200 000) iterations, at T=0K. Computations have been performed for all input parameters from JEFF-3.2, sorted in ascending $\overline{\Gamma}/\overline{D}$.

Résumé en français

L'Institut de Radioprotection et de Sûreté Nucléaire (IRSN) est l'organisme public chargé de l'estimation et de la prévention des risques liés au nucléaire en France. Il est à ce compte chargé d'études de sûreté, qui s'appuient sur des simulations numériques afin d'évaluer les risques présents dans les installations nucléaires. Une discipline intervenant dans ces études est la neutronique, qui s'intéresse au cheminement des neutrons dans la matière. Les logiciels de neutronique modélisent de manière déterministe ou stochastique le transport des neutrons à l'aide de l'équation de Boltzmann, qui fait intervenir les sections efficaces de réaction, grandeurs décrivant la probabilité pour une réaction nucléaire particulière de se produire en fonction de l'énergie des neutrons. Les sections efficaces font partie intégrante de l'ensemble des données utilisées à l'interface entre la physique et l'ingénierie nucléaire, appelées données nucléaires.

Le calcul des sections efficaces est réalisé par des codes de traitement de données nucléaires, dont le représentant le plus connu est le logiciel NJOY développé au Los Alamos National Laboratory, aux Etats-Unis. Récemment, l'IRSN a engagé le développement d'un code équivalent, GAIA-2, afin d'implémenter des méthodes indépendantes de traitement des données nucléaires. L'objectif est de s'assurer de la qualité des données utilisées par les codes de neutronique au cours des études de sûreté nucléaire. Les développements réalisés au cours de la présente thèse ont visé à estimer la qualité des modèles existants pour traiter les sections efficaces dans un domaine d'énergie particulier, appelé domaine des résonances non résolues, et à proposer de nouvelles méthodes de traitement des données nucléaires. Ces dernières ont été mises en œuvre dans le logiciel GAIA-2. Ce travail a été réalisé en collaboration avec le Commissariat à l'Energie Atomique et aux Energies Alternatives (CEA) à Saclay, qui possède une expertise manifeste dans le domaine et développe également un logiciel de traitement des données nucléaires, GALILLE-1.

Pour un type de noyau atomique donné, les sections efficaces sont des fonctions de l'énergie du neutron incident. En réalité, trois plages énergétiques peuvent être distinguées. A faible énergie, le couplage entre l'énergie du neutron incident et les niveaux d'énergie discrets du noyau cible crée un phénomène de résonance, qui structure la section efficace. Celle-ci présente alors des pics bien espacés ; il s'agit du domaine des résonances résolues. Au fur et à mesure que l'énergie du neutron augmente, les résonances se rapprochent jusqu'à devenir indiscernables expérimentalement. On parle alors du domaine des résonances non résolues. Enfin, à haute énergie, les niveaux d'énergie se superposent et le phénomène de résonance disparaît, ce qui définit le domaine du continuum. La présente thèse s'intéresse au calcul des sections efficaces dans le domaine des résonances non résolues. Dans ce domaine, seules les valeurs moyennes des paramètres expérimentaux depuis lesquels les sections efficaces sont calculées sont accessibles. En conséquence, seules les valeurs moyennes des sections efficaces peuvent être calculées grâce à un formalisme théorique dit de Hauser-Feschbach, ainsi que leurs distributions de probabilité à des valeurs d'énergie tabulées, à l'aide d'une méthode Monte-Carlo appelée la *méthode des ladders*. Cette dernière représentation est généralement exploitée sous forme discrète (on parle alors de tables de probabilité) dans les codes neutroniques stochastiques.

Au cours de cette thèse, une méthodologie complète de calcul des tables de probabilité dans le domaine des résonances non résolues a été établie. La quasi-totalité des questions liées à la mise en œuvre de la méthode a été abordée, et dans la plupart des cas des éléments de réponse ont été apportés.

La première partie de ce document est composée de deux chapitres, qui constituent une introduction détaillée aux problématiques de la thèse. Le premier chapitre débute avec un rappel du modèle du noyau composé en usage pour décrire le phénomène de résonance dans la théorie des réactions nucléaires induites par les neutrons. La notion de section efficace est présentée, ainsi que sa représentation sous forme de tables de probabilité. Ces dernières sont une forme discrète de la distribution de probabilité de la section efficace sur un intervalle énergétique. Cette représentation est notamment utile car elle permet de prendre en compte lors des calculs neutroniques le phénomène d'autoprotection, qui résulte de l'interaction entre le flux neutronique et les inflexions résonantes des sections efficaces. Une présentation du cadre mathématique, appelé théorie de la matrice R, permettant le calcul des sections efficaces depuis les paramètres de résonance mesurés expérimentalement conclut ce premier chapitre.

Le second chapitre est dédié aux méthodes de traitement des données nucléaires dans le domaine des résonances non résolues. Le format ENDF des évaluations de données nucléaires est décrit. Les évaluations contiennent les paramètres de résonance moyens du domaine non résolu, à savoir l'espacement moyen entre les résonances, et les valeurs moyennes des largeurs de réaction auxquelles sont attribués des degrés de liberté. Ces paramètres sont fournis à des énergies tabulées de référence dans le domaine non résolu, et pour plusieurs groupes de spin correspondant aux états quantiques possibles de l'interaction neutron-noyau. Les deux voies de travail qui permettent d'exploiter ces paramètres sont ensuite présentées. La première est la théorie de Hauser-Feschbach, qui permet de calculer les sections efficaces moyennes depuis les paramètres moyens directement. Celle-ci repose sur le calcul d'un facteur de correction de fluctuations des largeurs (WFCF), qui repose habituellement sur une approximation de Moldauer supposant que les largeurs de réaction suivent une loi statistique du χ^2. La seconde approche est ladite *méthode des ladders*. Le principe est d'exploiter les paramètres de résonance moyens fournis pour échantillonner des jeux de résonances résolues statistiquement acceptables (appelés *ladders*) au voisinage des énergies de référence. Un tel échantillonnage exploite les lois statistiques théoriques des paramètres de résonance, à savoir la loi de Wigner pour l'espacement, et la loi du χ^2 pour les largeurs de réaction. Une fois les résonances échantillonnées, des valeurs de sections efficaces peuvent être calculées à l'énergie de référence à l'aide des formules de la matrice R. En répétant cette opération, un échantillonnage statistique Monte-Carlo de valeurs possibles des sections efficaces est obtenu, à l'issue duquel une table de probabilité peut être dérivée. La méthode des ladders se décompose en trois phases distinctes. La première est l'échantillonnage des résonances. La seconde est le calcul des sections. La troisième est la dérivation d'une table de probabilité discrète depuis l'échantillonnage des valeurs de sections efficaces. Au cours de cette thèse, seules la première et la troisième phase ont été étudiées. Le calcul des sections efficaces suit les pratiques usuelles. En particulier, les sections sont calculées avec le formalisme Single-Level Breit-Wigner de la théorie de la matrice R à l'énergie de référence uniquement, et les sections élargies par effet Doppler $\psi - \chi$ pour prendre en compte l'effet de la température.

La seconde partie de cette thèse se concentre sur l'échantillonnage statistique de résonances dans le domaine non résolu. Dans le troisième chapitre, l'approche classique fondée sur l'utilisation des lois de Wigner et du χ^2 est conservée. L'objectif du chapitre est d'étudier les modalités de l'échantillonnage. Dans un premier temps, deux méthodes de la littérature sont présentées, qui correspondent aux pratiques des codes NJOY (Los Alamos National Laboratory) et AMPX (Oak Ridge National Laboratory). Dans le premier cas, une première résonance est placée à bonne distance de l'énergie de référence. Dans le second cas, un espacement central est tiré afin de placer les deux résonances les plus proches de l'énergie de référence. Dans cette thèse, il a été montré que les deux approches étaient équivalentes, à condition de tirer l'espacement

central dans la loi de Wigner biaisée par la taille. Cela permet d'éviter un biais dû à une application originale du paradoxe de l'autobus. Dans un second temps, cette thèse s'est intéressée au nombre minimal de résonances et d'itérations Monte-Carlo à tirer. L'idée est de reformuler le problème en fonction des paramètres de résonances qui interviennent en pratique dans le traitement du domaine non résolu. En réalité, les calculs dans le domaine réalisé lors du traitement de bibliothèques de données nucléaires se décomposent en sous-calculs pour chaque noyau, chaque énergie et chaque groupe de spin particulier. Les bibliothèques de données nucléaires peuvent être transformées en *groupes de spin élémentaires*, jeux de 16 paramètres scalaires d'entrée de la méthode des ladders. La conversion de JEFF-3.2 engendre ainsi 41 486 groupes de spin élémentaires, qui constituent une base de cas-tests pertinente. Afin d'estimer le nombre nécessaire de résonances pour chacun des 41 486 cas, un calcul de référence est fait avec des ladders comportant 500 paires de résonances, et des troncatures successives de celui-ci. Les échantillons de sections efficaces obtenus avec différents nombres de résonances sont alors comparés avec la distribution issue du calcul prenant en compte 500 paires de résonance, sur la base de diverses statistiques (moments, quantiles, et distance de Kolmogorov-Smirnov), pour tous les groupes de spin élémentaires. Un exercice similaire a été réalisé pour étudier l'influence des paramètres de résonance sur le nombre minimal d'itérations Monte-Carlo requis. L'interprétation simultanée des résultats pour ces deux études a permis de mettre en lumière le rôle pivot du ratio $\overline{\Gamma}/\overline{D}$ entre la largeur moyenne de réaction totale et l'espacement moyen entre les résonances évalué à l'énergie de référence. Lorsque ce ratio est grand, plus de résonances et moins d'itérations Monte-Carlo sont nécessaires pour le groupe de spin élémentaire concerné. Il est par ailleurs suggéré de prendre au moins 100 000 itérations Monte-Carlo et 100 paires de résonances, et de comparer le ratio $\overline{\Gamma}/\overline{D}$ à 10^{-2} pour savoir quel critère augmenter.

Dans le quatrième chapitre, la loi de Wigner pour l'espacement a été remplacée par une approche plus proche de la physique, qui fait intervenir la théorie des matrices aléatoires. L'idée, due à Wigner dans les années 50, consiste à remplacer le Hamiltonien inconnu du système par une matrice aléatoire ayant les mêmes symétries, et d'étudier la distribution statistique des valeurs propres. Ces dernières correspondent aux niveaux d'énergie du noyau composé, et donc aux énergies de résonance. Afin de prendre en compte le grand nombre de résonances du Hamiltonien, la matrice aléatoire doit être étudiée lorsque sa taille tend vers l'infini. Les matrices ayant les bonnes symétries sont les matrices de l'ensemble Gaussien Orthogonal (GOE) ; la loi de Wigner correspond notamment à l'espacement entre les valeurs propres d'une matrice du GOE de taille 2×2 seulement. En pratique, il est intéressant d'échantillonner toutes les énergies de résonance en utilisant des matrices de grande taille, afin de prendre en compte les corrélations entre les énergies de résonance. Dans cette thèse, les matrices du GOE ont été remplacées par des matrices tridiagonales ayant les mêmes distributions de valeurs propres, en suivant une recommandation de la littérature. Cette pratique permet d'accélérer les calculs. Une fois obtenues, les valeurs propres doivent être déployées pour pouvoir récupérer leurs fluctuations. Ce déploiement corrige la non-uniformité de leur densité. Deux méthodes sont proposées dans cette thèse pour réaliser cette étape. La première consiste à utiliser la fonction de répartition de la loi du demi-cercle de Wigner, forme asymptotique de la distribution des valeurs propres de matrices du GOE de taille infinie. En pratique, les matrices échantillonnées ont des tailles finies (de l'ordre de 10^2), et la densité de leurs valeurs propres ne suit pas la loi exacte du demi-cercle de Wigner, mais une expression plus complexe dans laquelle des polynômes de Hilbert interviennent. La deuxième méthode de déploiement proposée dans cette thèse est dite « tabulée exacte », et repose sur le calcul numérique sur une grille fine de la densité exacte des valeurs propres échantillonnées depuis des matrices du GOE de taille finie. Il a été montré que cette méthode permet un meilleur déploiement des valeurs propres. Les jeux de résonances obtenus en corrélant l'espacement diffèrent légèrement du cas non-corrélé. La loi de l'espacement est différente de 2%, et les espacements sont autocorrélés négativement : un grand espacement entre les résonances est plus susceptible d'être suivi par un petit. Les ladders obtenus sont ainsi plus rigides, ce qui est mesuré par la statistique du Δ_3. En pratique, la comparaison des résultats avec

le cas non-corrélé sur les 41 486 groupes de spin élémentaires de JEFF-3.2 montre que l'impact de la corrélation des espacements est faible. Une ouverture est faite au cours de ce chapitre sur le calcul de Hauser-Feschbach utilisant une méthode de calcul du WFCF prenant en compte les fluctuations du GOE. La comparaison avec les valeurs de sections efficaces moyennes calculées avec l'approximation de Moldauer montre un bon accord pour les cas ayant un faible ratio $\overline{\Gamma}/\overline{D}$. Le désaccord augmente avec cette grandeur. La comparaison avec les valeurs moyennes tirées de l'échantillonnage corrélé ou non montre un accord avec l'approximation de Moldauer. Il serait cependant intéressant de corréler les largeurs de réaction, afin d'estimer l'impact possible sur les valeurs moyennes. Ce calcul n'a pas été réalisé au cours de cette thèse.

La dernière partie de la thèse s'intéresse au couplage avec les codes de neutronique stochastiques (appelés également Monte-Carlo). Ceux-ci utilisent des tables de probabilité à 20 paliers, version discrète des distributions de probabilité des sections efficaces approchées par l'échantillonnage statistique de la méthode des ladders. Cette conversion, qui n'est pas unique, fait l'objet du cinquième chapitre de cette thèse. Plusieurs méthodes existantes sont présentées : linéaire, logarithmique, équiprobable, moments, et la méthode empirique de NJOY. Deux autres méthodes sont introduites : k-means et k-medians, toutes deux fondées sur un algorithme de k-clustering. L'objectif de ces méthodes est de trouver le découpage de l'échantillon de section efficace qui minimise la variance des paliers, c'est-à-dire la somme des distances entre les éléments de chaque palier de la table à la valeur moyenne (ou médiane) des paliers. Ces méthodes se fondent sur un algorithme de programmation dynamique implémenté dans le package Ckmeans.1d.dp du logiciel de statistique R. Comparées sur des cas typiques du domaine non résolu, comme ^{235}U ou ^{238}U, ces méthodes se comportent très bien. En particulier, elles représentent avec précision la queue de la distribution et les zones d'inflexion. Afin de tester ces méthodes sur des cas plus exotiques, les 41 486 groupes de spin élémentaires de JEFF-3.2 ont été mis à profit de nouveau. Pour chacun d'entre eux, la somme des distances des éléments de l'échantillonnage à la valeur moyenne du palier auquel ils appartiennent a été calculée. Le cas où cette grandeur est la plus élevée est un groupe de spin de ^{156}Eu à 1 eV, pour lequel la distribution de probabilité de la section efficace est très asymétrique. En ce cas précis, les tables k-means échouent à représenter les premiers 95% de la distribution de la section efficace. Les autres méthodes ont également des difficultés importantes pour s'ajuster à la distribution avec 20 paliers seulement.

Le sixième chapitre est un chapitre de validation des tables de probabilité échantillonnées par la méthode des ladders dans des calculs intégraux appelés benchmarks. La production des tables dans le domaine non résolu est intégrée dans le code de traitement de données nucléaires GAIA-2, au sein d'un module appelée TOP (*Table Of Probabilities*). Trois séries de benchmarks de criticité sont retenues, pour tester trois isotopes différents : ^{238}U, ^{239}Pu, et ^{96}Mo. Une première série de calcul du facteur de multiplication neutronique k_{eff} à l'aide du code Monte-Carlo MORET-5.D a été réalisée, en utilisant les fichiers de données nucléaires de JEFF-3.2 traités par NJOY, GAIA2, NJOY sans tables de probabilité, GAIA-2 sans tables de probabilité, et NJOY avec les tables de GAIA-2 ; les tables de probabilité de GAIA-2 visant à ressembler au maximum à celles de NJOY. Les résultats montrent un très bon accord, ce qui permet d'estimer le poids des méthodes de traitement des tables lorsque les procédures sont modifiées. Ainsi, la forme des tables, l'impact des corrélations des espacements entre les résonances, et le choix du maillage énergétique sur lequel les tables sont fournies aux codes Monte-Carlo sont explorés. Concernant ce dernier point, trois maillages sont considérés : le maillage initial des fichiers ENDF, une procédure empirique de NJOY permettant d'ajouter des énergies de référence prédéfinies, et un maillage dit *moyenné-linéarisé*, qui adapte une pratique du domaine résolu visant à fournir un maillage permettant l'interpolation linéaire des sections efficaces avec moins de 0.1% d'erreur. Les résultats indiquent clairement que l'erreur d'interpolation des tables est diminuée en ce dernier cas. Par ailleurs, il est suggéré d'utiliser des tables de probabilité ayant un plus grand nombre de paliers que 20, au vu des résultats divergents entre les méthodes équiprobables, NJOY, et k-medians. En conséquence, la solution la plus pertinente est d'adapter les codes Monte-Carlo afin qu'ils utilisent des tables équiprobables de grande taille (1000 paliers sont

suggérés). En effet, les limitations liées à la mémoire des ordinateurs qui justifiaient l'utilisation de tables de petite taille ne sont plus d'actualité, et l'utilisation de tables équiprobables permet, grâce à leurs propriétés mathématiques, de se passer d'une routine de recherche de palier dans les codes Monte-Carlo. Ces derniers ne seraient alors pas ralentis par l'utilisation de tables de grande taille. Il est ainsi fortement suggéré que la nouvelle génération de codes neutroniques stochastiques dite *High Performance Computing* se prépare à l'utilisation de telles tables de probabilité.

Le travail réalisé au cours de cette thèse a ainsi permis de mettre en place une méthodologie pour le traitement des sections efficaces dans le domaine non résolu. Les recommandations faites au cours de cette thèse ont un impact pour les évaluateurs, les développeurs de codes de traitement de données nucléaires, et les développeurs de codes neutroniques. Les développements réalisés ont également été implémentés dans le code de traitement de données nucléaires de l'IRSN, GAIA-2, au sein d'un module indépendant. Une validation sur une base de tests plus large est néanmoins requise pour valider l'ensemble des résultats obtenus.

Titre : Développement d'une méthodologie pour exploiter les données nucléaires dans le domaine des résonances non-résolues, et impact sur la criticité et la physique des réacteurs

Mots clés : Données nucléaires, sections efficaces, résonances non-résolues, processing, tables de probabilité

Résumé : Les calculs neutroniques réalisés notamment pour assurer l'exploitation et la sûreté des installations nucléaires sont très dépendants des données nucléaires, qui décrivent les interactions neutron-matière. En particulier, la connaissance des sections efficaces, qui définissent la probabilité d'occurrence des réactions nucléaires en fonction de l'énergie du neutron, est primordiale. Dans la plage d'énergies du neutron incident qualifiée de domaine des résonances non résolues, une structure résonante caractérise les sections efficaces mais les résonances ne peuvent être différenciées expérimentalement. Seules les valeurs moyennes des sections efficaces peuvent alors être calculées à partir de paramètres moyens mesurés expérimentalement, ainsi que leurs distributions de probabilité à l'aide d'une méthode Monte-Carlo appelée « la méthode des ladders ». En ce dernier cas, une représentation discrète est alors privilégiée, fondée sur l'utilisation de tables de probabilité.
Cette thèse développe une méthodologie précise pour traiter les sections efficaces dans le domaine des résonances non résolues. Le travail réalisé porte notamment sur les méthodes d'échantillonnage statistique de résonances dans le cadre de la méthode des ladders. Plusieurs points sont traités parmi lesquels l'influence du nombre de résonances échantillonnées sur le calcul des sections efficaces, ou le nombre minimal d'itérations Monte-Carlo à réaliser. Ces questions sont reformulées en fonction des paramètres de résonance fournis, et une relation est établie avec le ratio entre l'espacement moyen entre les résonances et la largeur moyenne de réaction totale. Les calculs sont réalisés sur des bibliothèques entières de données nucléaires, ce qui constitue un point fort de cette thèse. La théorie des matrices aléatoires est ensuite introduite pour échantillonner des jeux de résonances en meilleur accord avec la physique sous-jacente du problème traité. La mise en œuvre de cette théorie permet ici de corréler les espacements entre les résonances échantillonnées. L'ensemble des calculs est comparé à la théorie de Hauser-Feschbach pour le calcul des valeurs moyennes, avec des résultats probants lorsque cette dernière utilise l'approximation de Moldauer. Plusieurs méthodes de construction de tables de probabilité sont également étudiées, et deux nouvelles méthodes fondées sur des algorithmes de k-clustering sont introduites. Des calculs de benchmarks à l'aide de codes neutroniques permettent de compléter les résultats obtenus, et d'établir une série de recommandations pour le traitement des sections efficaces dans le domaine des résonances non-résolues.

Title: Development of a methodology to exploit nuclear data in the unresolved resonance range and the impact on criticality safety and reactor applications

Keywords: Nuclear data, cross sections, processing, unresolved resonance range, probability tables

Abstract: Neutronics computations are widely used in reactor physics and criticality calculations to ensure the safety and the exploitation of nuclear facilities. They rely on nuclear data which describe neutron-matter interactions. Among them, cross sections are fundamental data that express the probability for a particular reaction to occur as a function of the incident neutron energy. At the intermediate to high energy range, cross section shapes are no longer distinguished, which defines the so-called unresolved resonance range. There, cross sections can only be computed as average values from average experimentally-determined parameters, as well as probability tables. These latter are a discretized form of the cross section probability distributions, determined from a Monte-Carlo-based technique called the ladder method.
This thesis aims at proposing a robust methodology to process cross sections in the unresolved resonance range. In particular, the work carried out deals with statistical sampling of resonances in the framework of the ladder method. Several issues are tackled, among which the impact of the number of sampled resonances on cross section calculations, as well as the number of Monte-Carlo iterations performed. A relation is established between these quantities and values of the input resonance parameters, namely the ratio of the average resonance spacing and the average total reaction width. Calculations are done for constituents of entire nuclear data libraries, which is an advantage of this work. Then, the random matrix theory is introduced to produce more physical sets of resonances that take into account correlations between the resonance spacings. All calculations are compared to the outcomes of the Hauser-Feschbach formalism for the calculation of average cross sections. When these latter ones are computed using the Moldauer assumption, results significantly match. Several probability table construction methods are then studied. Two innovative methods are introduced, based on a k-clustering algorithm. Benchmarks calculations using neutronics codes complete the results, and enable to formulate a detailed methodology for the nuclear data processing in the unresolved resonance range.